VOLUME 75 OCTOBER 28, 1971 NUMBER 22

JPCHAx

THE JOURNAL OF PHYSICAL CHEMISTRY

PUBLISHED BIWEEKLY BY THE AMERICAN CHEMICAL SOCIETY

THE JOURNAL OF

PHYSICAL CHEMISTRY

BRYCE CRAWFORD, Jr., *Editor*
STEPHEN PRAGER, *Associate Editor*
ROBERT W. CARR, Jr., FREDERIC A. VAN-CATLEDGE, *Assistant Editors*

EDITORIAL BOARD: A. O. ALLEN (1970–1974), R. BERSOHN (1967–1971), J. R. BOLTON (1971–1975), S. BRUNAUER (1967–1971), M. FIXMAN (1970–1974), H. S. FRANK (1970–1974), J. R. HUIZENGA (1969–1973), M. KASHA (1967–1971), W. J. KAUZMANN (1969–1973), W. R. KRIGBAUM (1969–1973), R. A. MARCUS (1968–1972), W. J. MOORE (1969–1973), J. A. POPLE (1971–1975), B. S. RABINOVITCH (1971–1975), H. REISS (1970–1974), S. A. RICE (1969–1975), R. E. RICHARDS (1967–1971), F. S. ROWLAND (1968–1972), R. L. SCOTT (1968–1972), R. SEIFERT (1968–1972)

CHARLES R. BERTSCH, *Manager, Editorial Production*

AMERICAN CHEMICAL SOCIETY, *1155 Sixteenth St., N.W., Washington, D. C. 20036*
FREDERICK T. WALL, *Executive Director*

Books and Journals Division
JOHN K CRUM, *Director (Acting)*
JOSEPH H. KUNEY, *Head, Business Operations Department*
RUTH REYNARD, *Assistant to the Director*

©Copyright, 1971, by the American Chemical Society. Published biweekly by the American Chemical Society at 20th and Northampton Sts., Easton, Pa. 18042. Second-class postage paid at Washington, D. C., and at additional mailing offices.

All manuscripts should be sent to *The Journal of Physical Chemistry*, Department of Chemistry, University of Minnesota, Minneapolis, Minn. 55455.

Additions and Corrections are published once yearly in the final issue. See Volume 74, Number 26 for the proper form.

Extensive or unusual alterations in an article after it has been set in type are made at the author's expense, and it is understood that by requesting such alterations the author agrees to defray the cost thereof.

The American Chemical Society and the Editor of *The Journal of Physical Chemistry* assume no responsibility for the statements and opinions advanced by contributors.

Correspondence regarding accepted copy, proofs, and reprints should be directed to Editorial Production Office, American Chemical Society, 20th and Northampton Sts., Easton, Pa. 18042. Manager: CHARLES R. BERTSCH. Assistant Editor: EDWARD A. BORGER. Editorial Assistant: EVELYN J. UHLER.

Advertising Office: Century Communications Corporation, 142 East Avenue, Norwalk, Conn. 06851.

Business and Subscription Information

Remittances and orders for subscriptions and for single copies, notices of changes of address and new professional connections, and claims for missing numbers should be sent to the Subscription Service Department, American Chemical Society, 1155 Sixteenth St., N.W., Washington, D. C. 20036. Allow 4 weeks for changes of address. Please include an old address label with the notification.

Claims for missing numbers will not be allowed (1) if received more than sixty days from date of issue, (2) if loss was due to failure of notice of change of address to be received before the date specified in the preceding paragraph, or (3) if the reason for the claim is "missing from files."

Subscription rates (1971): members of the American Chemical Society, $20.00 for 1 year; to nonmembers, $40.00 for 1 year. Those interested in becoming members should write to the Admissions Department, American Chemical Society, 1155 Sixteenth St., N.W., Washington, D. C. 20036. Postage to Canada and countries in the Pan-American Union, $4.00; all other countries, $5.00. Single copies for current year: $2.00. Rates for back issues from Volume 56 to date are available from the Special Issues Sales Department, 1155 Sixteenth St., N.W., Washington, D. C. 20036.

This publication and the other ACS periodical publications are now available on microfilm. For information write to: MICROFILM, Special Issues Sales Department, 1155 Sixteenth St., N.W., Washington, D. C. 20036.

Notice to Authors last printed in the issue of June 10, 1971

THE JOURNAL OF
PHYSICAL CHEMISTRY

Volume 75, Number 22 October 28, 1971

The Second Symposium on Electron Spin Resonance Spectroscopy, The University of Georgia, December 7–9, 1970

AUTHOR INDEX

In papers with more than one author the name of the author to whom inquires about the paper should be addressed is marked with an asterisk in the by-line.

ANNOUNCEMENT

Single copies of this issue are available for $2.00 from the Special Issues Sales Department, American Chemical Society, 1155 Sixteenth St., N. W., Washington, D. C. 20036.

THE JOURNAL OF
PHYSICAL CHEMISTRY
Registered in U. S. Patent Office © Copyright, 1971, by the American Chemical Society

VOLUME 75, NUMBER 22 OCTOBER 28, 1971

The Second Symposium on Electron Spin Resonance Spectroscopy

THE UNIVERSITY OF GEORGIA, ATHENS, GEORGIA

DECEMBER 7–9, 1970

Introductory Remarks

by Edward G. Janzen

Department of Chemistry, University of Georgia, Athens, Georgia

and Ralph Livingston

Chemistry Division, Oak Ridge National Laboratory, Oak Ridge, Tennessee

In 1966 a major conference covering various applications of electron spin resonance in chemistry was held at Michigan State University, and the collection of papers along with discussion was published in this Journal [*J. Phys. Chem.*, **71**, 1 (1967)]. The pace of research in this area has accelerated rapidly, and the subject has become of ever increasing importance to the chemist. With a lapse of four years since the initial conference, it was highly appropriate to hold a second symposium in order to summarize many of the new developments in electron spin resonance spectroscopy. The second symposium, like the first, was sponsored by the Division of Physical Chemistry of the American Chemical Society.

The conference was divided into six sessions with each containing major talks setting the theme of the sessions. These were followed by shorter contributions focusing on more detailed research areas. All participants, especially those giving major talks, were urged to prepare written accounts of their work so that they could be published together. This collection is the result, truly a gratifying response. Ample time was allowed for discussion at the meeting, and participants were invited to prepare written accounts of their comments. Some of the papers are followed by these comments. In planning the meeting, we were aware of the great diversity of topics in electron spin resonance and tried to have a number of areas represented that are of special interest to the chemist. We did not include work on semiconductors but did include such areas as spin labels and selected problems of biological interest because of the attention they have

attracted for the chemist. With this diversity of coverage, we found that the meeting provided much stimulation for the participants and feel that collecting this material for publication will provide a useful addition to the esr literature.

We wish to thank all of those who participated in the symposium and particularly those who prepared manuscripts so that this collection would be possible. A special word of thanks is due Professor F. A. VanCatledge of *The Journal of Physical Chemistry* for his editorial help.

EDITOR'S NOTE. For diverse reasons, not all of the invited papers at the Second Symposium on Electron Spin Resonance are included in this symposium issue. We will attempt however, insofar as it is possible, to provide leading references to the materials upon which these talks were based. We hope that this effort will, in some small way, compensate for their absence from this issue.

"Magnetic Resonance in Near-Degenerate Molecules: Benzene and Ion Radicals and Myoglobin" by M. Karplus:

D. Purins and M. Karplus, *J. Chem. Phys.*, **50,** 214 (1969).

R. G. Shulman, S. H. Glarum, and M. Karplus, *J. Mol. Biol.*, **57,** 93 (1971).

D. Purins and M. Karplus, *J. Chem. Phys.*, to be published.

"Optically Detected Magnetic Resonance in Zero Field and Optical Phase Procession in Phosphorescent Triplets" by C. B. Harris:

C. B. Harris, D. S. Tinti, M. A. El-Sayed, and A. H. Maki, *Chem. Phys. Lett.*, **4,** 409 (1969).

M. J. Buckley, C. B. Harris, and A. H. Maki, *ibid.*, **4,** 269 (1969).

M. J. Buckley and C. B. Harris, *ibid.*, **5,** 205 (1970).

C. B. Harris, *J. Chem. Phys.*, **54,** 972 (1971).

C. B. Harris, Proceedings of the 5th Molecular Crystals Symposium, Philadelphia, Pa., 1970.

Electron Spin Resonance Line Shapes and Saturation in the Slow Motional Region[1a]

by Jack H. Freed,*[1b] Gerald V. Bruno,[1c] and Carl F. Polnaszek[1d]

Department of Chemistry, Cornell University, Ithaca, New York 14850 *(Received November 25, 1970)*

Publication costs borne completely by The Journal of Physical Chemistry

The stochastic Liouville method is developed and applied in a manner appropriate to analyze the problem of esr line shapes and saturation in the slow-motional region with particular emphasis on rotational diffusion. Detailed unsaturated line shape solutions are obtained for axial and asymmetric g tensors and axial dipolar tensors. These line shapes are compared to the predicted rigid-solid spectral shapes. In particular, it is shown that the pseudo-secular dipolar terms make significant contributions to the slow tumbling line shapes expected for ^{14}N-containing radicals such as nitroxides and may not be neglected in such cases. Saturation effects are analyzed for a two-jump model, as well as for rotational diffusion of the g tensor. It is found that even in the slow-motional region, a fundamental role is played by the T_1's that are obtained from the spin-relaxation theories. One finds that the significant line shape changes resulting from saturation are dependent on the rotational diffusion rates.

I. Introduction

There has recently been a growing interest in the character of esr line shapes in the region of slow tumbling where the earlier relaxation theories[2] are no longer adequate. The cause of the slow tumbling may be due to the use of a viscous solvent, a radical attached to a macromolecule, or a particularly large anisotropic term in the spin-Hamiltonian (*e.g.*, for triplets and other spins of higher multiplicity). In these cases, the condition $|\mathcal{H}_1(t)|\ \tau_R \ll 1$ required for the relaxation theories may no longer be fulfilled. Here $\mathcal{H}_1(t)$ is the rotationally dependent perturbation in the spin-Hamiltonian and τ_R is the rotational correlation time.

Kubo has called attention to the stochastic Liouville method, in recent work,[3,4] as a general method for calculating spectral line shapes even when the conditions for motional narrowing are no longer fulfilled. The method is, in principle, applicable to any stochastic modulation of $\mathcal{H}_1(t)$ provided only that the stochastic process is assumed to be Markoffian. In Kubo's recent work it was also assumed that the processes were Gaussian, but this is not necessary for the method and not the case for rotational diffusion.

This method seems simpler and more general than the recent work on viscous media by Itzkowitz[5] using a model of randoms jumps with Monte Carlo techniques as well as the work of Korst and Lazarev,[6] which like the present work is based on the diffusion equation.

Of related interest is the straightforward manner in which we are able to include nonsecular effects in order to see to what extent they may be important for line shapes and saturation. Our rigorous analysis of nonsecular effects is based upon an approach utilizing fast motional spin states unlike the slow-motional "adiabatic" approximation used by Itzkowitz[5] and Korst and Lazarev.[6] We note that recent work by Sillescu and Kivelson[7] and Freed[8] represent generalized solutions which can readily include nonsecular effects, but the detailed analyses given remained essentially perturbative in technique.[9] Also, in related work on triplets by Norris and Weissman,[10] only secular terms were needed.

Kubo's treatment of line shapes is based on linear response theory (the autocorrelation function) and is therefore not applicable for saturation phenomena. We have modified the approach, by starting from the density matrix equations of motion, so that the radiation field is included explicitly and saturation effects may be studied. The method is readily seen to be a generalization to a continuous range of the random

(1) (a) Supported in part by the Advanced Research Projects Agency and by a grant from the National Science Foundation (Grant No. GP-13780). (b) This work was begun while J. H. F. was visiting the Department of Physics, Tokyo University, sponsored by a grant from the United States–Japan Co-operative Science Program (National Science Foundation). (c) American Chemical Society–Petroleum Research Fund Fellow 1969–1970. (d) National Institutes of Health Predoctoral Fellow, 1969–1971.

(2) (a) J. H. Freed and G. K. Fraenkel, *J. Chem. Phys.*, **39**, 326 (1963); (b) D. Kivelson, *ibid.*, **33**, 1094 (1960).

(3) R. Kubo, "Stochastic Processes in Chemical Physics, Advances in Chemical Physics," Vol. XVI, K. E. Shuler, Ed., Wiley, New York, N. Y., 1969, p 101.

(4) R. Kubo, *J. Phys. Soc. Jap. Suppl*, **26**, 1 (1969).

(5) M. S. Itzkowitz, *J. Chem. Phys.*, **46**, 3048 (1967).

(6) (a) N. N. Korst and A. V. Lazarev, *Mol. Phys.*, **17**, 481 (1969); (b) I. V. Alexandrov, A. N. Ivanova, N. N. Korst, A. V. Lazarev, A. I. Prikhozhenko, and V. B. Stryukov, *ibid.*, **18**, 681 (1970).

(7) H. Sillescu and D. Kivelson, *J. Chem. Phys.*, **48**, 3493 (1968).

(8) J. H. Freed, *ibid.*, **49**, 376 (1968).

(9) R. G. Gordon (private communication) has developed a useful approach based on finite difference techniques.

(10) J. R. Norris and S. I. Weissman, *J. Phys. Chem.*, **73**, 3119 (1969).

variable of earlier and well-known techniques for handling relaxation resulting from jump phenomena occurring between a finite number of sites. The correspondence with a two-jump model (as well as the nature of the approximations for saturation) are shown in Appendix B.

II. General Method

The density-matrix equation of motion due to the random Hamiltonian $\mathcal{H}(t)$ is given by

$$\frac{\partial \rho}{\partial t} = -i[\mathcal{H}(t),\rho] \tag{1}$$

It is now assumed that there are a complete set of random variables Ω, which suffice to describe the random behavior of $\mathcal{H}(t)$ and which is described by a Markoff process. Thus

$$\frac{\partial}{\partial t}P(\Omega,t) = -\Gamma_\Omega P(\Omega,t) \tag{2}$$

where $P(\Omega,t)$ is the probability of finding Ω at the particular state at time t. The process is assumed to be stationary, so that Γ is a time-independent Markoff operator, and also that the process has a unique equilibrium distribution, $P_0(\Omega)$, characterized by

$$\Gamma P_0(\Omega) = 0 \tag{3}$$

Kubo[4] shows that eq 1-3 lead to the equation of motion

$$\frac{\partial}{\partial t}\rho(\Omega,t) = -i[\mathcal{H}(\Omega),\rho(\Omega,t)] - \Gamma_\Omega\rho(\Omega,t) \tag{4}$$

where, however, $\rho(\Omega,t)$ is now understood to be an average ρ [defined by $\int\rho P(\Omega,\rho,t)d\rho$] associated with a particular value of Ω for the bath, hence a particular value of $\mathcal{H}(\Omega)$.

The steady-state spectrum in the presence of a single rotating radiofrequency field is determined by the power absorbed from this field. One finds for the λth (multiple) hyperfine line at "orientation" specified by Ω[11]

$$\mathcal{P}_\lambda(\Omega) = 2\mathfrak{N}\hbar\omega\sum_j d_{\lambda_j}Z_{\lambda_j}{}^{(1)\prime\prime}(\Omega) \tag{5}$$

where $\mathcal{P}_\lambda$ is the power absorbed, $\mathfrak{N}$, the concentration of electron spins, and $Z_{\lambda_j}{}^{(1)\prime\prime}$ is defined by the series of equations

$$(\rho - \rho_0)_{\lambda_j} \equiv \chi_{\lambda_j} \tag{6}$$

$$\chi_{\lambda_j} = \sum_{n=-\infty}^{\infty} e^{in\omega t}Z_{\lambda_j}{}^{(n)} \tag{7}$$

and

$$Z_{\lambda_j}{}^{(n)} = Z_{\lambda_j}{}^{(n)\prime} + iZ_{\lambda_j}{}^{(n)\prime\prime} \tag{8}$$

In eq 6, $\rho_0(\Omega)$ is the equilibrium spin density matrix whose Ω dependence is such that $\Gamma_\Omega\rho_0 = 0$. In eq 7, the steady-state solution χ_{λ_j} has been expanded in a Fourier series with time-independent coefficients $Z_{\lambda_j}{}^{(n)}$. Thus $\rho_0(\Omega) = \rho_0{}^{(0)}$. Equation 5 displays the fact that it is the $n = 1$ harmonic which is directly observed. (We will also use $\chi_a{}^{(0)}$ as the zeroth harmonic for the diagonal element corresponding to state a.)

In the above notation ρ_{λ_j} means the matrix element of ρ

$$\rho_{\lambda_j} \equiv \langle\lambda_{j-}|\rho|\lambda_{j+}\rangle \tag{9}$$

where λ_{j-} and λ_{j+} are the two levels between which the λ_jth transition occurs, and a "raising convention" is implied. This notation is discussed elsewhere.[11] Equivalent definitions apply to other operator matrix elements.

Also in eq 5 $d_{\lambda_j} = {}^1/_2\gamma_e B_1$ for all allowed esr transitions induced by the radiofrequency field, and is otherwise zero.

The total absorption is then obtained as an equilibrium average of eq 5 over all Ω. Thus we introduce averages such as

$$\bar{Z}_{\lambda_j}{}^{(n)} = \int d\Omega P_0(\Omega)Z_{\lambda_j}{}^{(n)}(\Omega) \tag{10}$$

so that

$$\mathcal{P}_\lambda = 2\mathfrak{N}\hbar\omega\sum_j d_{\lambda_j}\bar{Z}_{\lambda_j}{}^{(1)\prime\prime} \tag{11}$$

where we have taken d_{λ_j} essentially independent of orientation.[12] We now separate $\mathcal{H}$ into three components

$$\mathcal{H} = \mathcal{H}_0 + \mathcal{H}_1(\Omega) + \epsilon(t) \tag{12}$$

where in the high-field approximation

$$\hbar\mathcal{H}_0 = \bar{g}_s\beta_e B_0 S_z - \hbar\sum_i\gamma_i I_{z_i}B_0 - \hbar\gamma_e\sum_i\bar{a}_i S_z I_{z_i} \tag{13}$$

yields the zero-order energy levels and transition frequencies

$$\mathcal{H}_1(\Omega) = \sum_{L,m,\mu,i} F'_{\mu,i}{}^{(L,m)}(\Omega)A'_{\mu,i}{}^{(L,-m)} \tag{14}$$

is the perturbation depending on orientation angles Ω expressed in the notation of Freed and Fraenkel,[2a] and

$$\hbar\epsilon_1(t) = {}^1/_2\hbar\gamma_e B_1[S_+\exp(-i\omega t) + S_-\exp(i\omega t)] \tag{15}$$

is the interaction with the radiation field.

When one takes the $\langle\lambda_{j-}|\ |\lambda_{j+}\rangle$ matrix elements of eq 4 and utilizes eq 6-8, the steady-state equation for $Z_{\lambda_j}{}^{(1)}$ is found to be

$$\Delta\omega_\lambda Z_{\lambda_j}{}^{(1)} + [\mathcal{H}_1(\Omega),Z^{(1)}(\Omega)]_{\lambda_j} - i[\Gamma_\Omega Z^{(1)}(\Omega)]_{\lambda_j} + d_{\lambda_j}(\chi_{\lambda_j}{}^{+(0)} - \chi_{\lambda_j}{}^{-(0)}) = q\omega_\lambda d_{\lambda_j} \tag{16}$$

Here $\chi_{\lambda_j}{}^{+(0)}$ and $\chi_{\lambda_j}{}^{-(0)}$ represent the deviations from

(11) J. H. Freed, *J. Chem. Phys.*, **43**, 2312 (1965).

(12) This is reasonable for free radicals with small Δg values. For large Δg values the orientation dependence of γ_e must be considered (*cf.* B. Bleaney, *Proc. Phys. Soc. (London)*, **A75**, 621 (1960)).

spin equilibrium of the upper (+) and lower (−) electron spin states associated with the λ_jth transition, and $\Delta\omega_\lambda = \omega - \omega_\lambda$, where $\hbar\omega_\lambda = E_{\lambda_j+} - E_{\lambda_j-}$. The $Z^{(1)}(\Omega)$ are matrices defined by eq 6 and 8. Also $q = \hbar/kT(1/N)$ where N = number of spin eigenstates and the high-temperature approximation has been assumed. The equation for $\bar{Z}_{\lambda_j}{}^{(1)}$ then becomes

$$\Delta\omega_\lambda \bar{Z}_{\lambda_j}{}^{(1)} + \int d\Omega P_0(\Omega)[\mathcal{K}_1(\Omega), Z^{(1)}(\Omega)]_{\lambda_j} - i\int d\Omega P_0(\Omega)[\Gamma Z^{(1)}(\Omega)]_{\lambda_j} + d_{\lambda_j}(\bar{\chi}_{\lambda_j+}{}^{(0)} - \bar{\chi}_{\lambda_j-}{}^{(0)}) = q\omega_\lambda d_{\lambda_j} \quad (17)$$

To perform the integrations over Ω in eq 17 we expand the matrix element $Z(\Omega)_{\lambda_j}{}^{(n)}$ in a complete set of orthogonal eigenfunctions of Γ_Ω, call them $G_m(\Omega)$, with eigenvalues E_m

$$Z(\Omega,\omega)_{\lambda_j}{}^{(n)} = \sum_m [C_m{}^{(n)}(\omega)]_{\lambda_j} G_m(\Omega) \quad (18)$$

or in operator notation

$$Z(\Omega)^{(n)} = \sum_m C_m{}^{(n)}(\omega) G_m(\Omega) \quad (18a)$$

where $C_m{}^{(n)}$ is still an operator in spin space and is a function of ω, but is independent of Ω. Then eq 17 becomes

$$\Delta\omega_\lambda \bar{Z}_{\lambda_j}{}^{(1)} + \sum_m \int d\Omega P_0(\Omega) G_m(\Omega) \times [\mathcal{K}_1(\Omega), C_m{}^{(1)}]_{\lambda_j} + d_{\lambda_j}(\bar{\chi}_{\lambda_j+}{}^{(0)} - \bar{\chi}_{\lambda_j-}{}^{(0)}) = q\omega_\lambda d_{\lambda_j} \quad (19)$$

In obtaining eq 19 we have assumed that $P_0(\Omega)$ gives an isotropic distribution of orientations. Thus $P_0 \propto G_0(\Omega)$ with eigenvalue $E_0 = 0$. Since $G_0(\Omega) \equiv 1$ is orthogonal to all $G_m(\Omega)$ with $m \neq 0$ in the Hilbert space of Ω, it then follows that the third term on the left-hand side of eq 17 vanishes upon averaging.

Note also that

$$\bar{Z}_{\lambda_j}{}^{(n)} = [C_0{}^{(n)}]_{\lambda_j} \quad (20)$$

from the definitions of eq 10 and 18. Thus the absorption (eq 11) depends only on the $[C_0{}^{(1)}]_{\lambda_j}$ for all allowed transitions λ_j.

When we premultiply eq 16 by $G_m{}^*(\Omega)$ and integrate over Ω, we obtain for $[C_m{}^{(1)}]$

$$N_{m'}(\Delta\omega_\lambda - iE_{m'})[C_{m'}{}^{(1)}]_{\lambda_j} + \sum_m \int d\Omega G_{m'}{}^*(\Omega) G_m(\Omega)[\mathcal{K}_1(\Omega), C_m{}^{(1)}]_{\lambda_j} + N_{m'} d_{\lambda_j}([C_{m'}{}^{(0)}]_{\lambda_j+} - [C_{m'}{}^{(0)}]_{\lambda_j-}) = q\omega_\lambda d_{\lambda_j}\delta(m',0)N_{m'} \quad (21)$$

Here $N_{m'}$ is a normalizing factor

$$N_m = \int d\Omega G_m{}^*(\Omega) G_m(\Omega) \quad (22)$$

Thus the coupling to the Markovian relaxation process of Γ_Ω comes about only if the perturbation $\mathcal{K}_1(\Omega)$ can couple $[C_0{}^{(1)}]_{\lambda_j}$ to some coefficient $C_m{}^{(1)}$ where $m \neq 0$.

A form of eq 21, but written for the diagonal elements $[C_m{}^{(n)}]_{\lambda_j\pm}$, is needed in problems involving a nonsecular $\mathcal{K}_1$ which induces electron spin flips. It is given in section IIIB on saturation.

The above approach, hence eq 21, is valid for any Markovian or diffusive process. Equation 21 will yield coupled algebraic equations for the coefficients $[C_m{}^{(n)}]_{\lambda_j}$, and one attempts to solve for the $[C_0{}^{(1)}]_{\lambda_j}$ utilizing only a finite number of such coefficients. The convergence depends essentially on the ratio $|\mathcal{K}_1(\Omega)|/E_{m'}$. The larger the value of this ratio the more terms $[C_m{}^{(1)}]_{\lambda_j}$ are needed. The results obtained by second-order relaxation theory are recovered when only one order beyond $[C_0{}^{(1)}]_{\lambda_j}$ is included.

When we apply the method to rotational modulation, then Ω refers to the values of the Euler angles for a tumbling molecular axis with respect to a fixed laboratory axis system. Thus we have for isotropic rotational diffusion

$$\Gamma_\Omega \longrightarrow R\nabla_\Omega{}^2 \quad (23)$$

where $\nabla_\Omega{}^2$ is the rotational diffusion operator and R is the diffusion coefficient. Although the method is fully applicable to problems involving anisotropic rotational diffusion, we have assumed isotropic diffusion for simplicity in obtaining and illustrating typical results. A complete set of eigenfunctions of Γ_Ω for eq 23 are then the Wigner rotation matrices $\mathfrak{D}^L{}_{KM}(\Omega)$ with eigenvalues $E_m = E_{L,K,M} = RL(L+1)$.[13] We now express eq 14 as

$$\mathcal{K}_1(t) = \sum_{L,m,m',\mu,i} \mathfrak{D}_{-m,m'}{}^L(\Omega) F'_{\mu,i}{}^{(L,m)} A_{\mu,i}{}^{(L,m')} \quad (24)$$

where both the $F'_{\mu,i}{}^{(L,m)}$ and the $A_{\mu,i}{}^{(L,m')}$ are irreducible tensor components of rank L and component m and m'. The F' in eq 24 are expressed in molecule-fixed coordinates, while A is a spin operator quantized in space-fixed axes. The $\mathfrak{D}_{-m,m'}{}^{(L)}(\Omega)$ terms include the transformation from space-fixed to molecule-fixed axes. It follows from the orthogonality relation[14] of the $\mathfrak{D}_{KM}{}^L$'s that

$$N_{KM}{}^L = \frac{8\pi^2}{2L+1} \quad (25)$$

and

$$P_0(\Omega) = \frac{1}{8\pi^2} = \frac{1}{8\pi^2}\mathfrak{D}_{0,0}{}^0(\Omega) \quad (26)$$

The evaluation of the integral on the left-hand side of eq 21 is obtained utilizing[14]

$$\int d\Omega \mathfrak{D}_{m_1m_1'}{}^{L_1}(\Omega)\mathfrak{D}_{m_2m_2'}{}^{L_2}(\Omega)\mathfrak{D}_{m_3m_3'}{}^{L_3}(\Omega) = 8\pi^2 \begin{pmatrix} L_1 & L_2 & L_3 \\ m_1 & m_2 & m_3 \end{pmatrix} \begin{pmatrix} L_1 & L_2 & L_3 \\ m_1' & m_2' & m_3' \end{pmatrix} \quad (27)$$

(13) J. H. Freed, *J. Chem. Phys.*, **41**, 2077 (1964).

(14) A. R. Edmonds, "Angular Momentum in Quantum Mechanics," Princeton University Press, Princeton, N. J., 1957.

Table I: Line Shape Deviations from Lorentzian as $|\mathfrak{F}|/R$ Increases, for Single Line Broadened by Axial g Tensor

$\|\mathfrak{F}\|/R$	Relative $1/_2$–$1/_2$ width[d]	Relative abs heights	I_{abs}[a]	Relative deriv width	Relative deriv height	I_{deriv}[b]	Derivative asymmetry[c]
0.2	1.00	1.000	1.00	1.00	1.000	1.00	1.000
1.0	2.57	0.393	1.01	2.59	0.154	1.03	1.000
2.5	5.50	0.188	1.034	5.62	0.034	1.074	1.008
5.0	10.4	0.107	1.11	10.75	0.0103	1.20	1.11
8.0	14.55	0.0815	1.185	13.9	0.0059	1.14	1.52

[a] $I_{abs} \equiv$ relative $1/_2$–$1/_2$ width $\times$ relative absorption height; $I_{abs} = 1$ for a Lorentzian. [b] $I_{deriv} \equiv$ (relative derivative width)$^2 \times$ relative derivative height; $I_{deriv} = 1$ for a Lorentzian. [c] Derivative asymmetry is the ratio of the height of the low-field derivative extremem to the height of the high-field derivative extremum. Note $(g_{||} - g_\perp)$ is taken as negative. [d] Rotationally invariant width component of 0.61 is included.

where the terms in parentheses in eq 27 are the $3j$ symbols; also

$$\mathfrak{D}_{m,m'}{}^{L*} = (-)^{m-m'}\mathfrak{D}_{-m,-m'}{}^{L} \tag{28}$$

III. Applications

A. No Saturation. The case of no saturation is achieved by setting $\chi_{\lambda_i^+} = \chi_{\lambda_i^-} = 0$, so the last term on the left-hand side of eq 21 is zero.

1. Axially Symmetric Secular g Tensor. A particularly simple example of the above formulation is for a one-line esr spectrum broadened mainly by the secular anisotropic g-tensor term, for which $g_x = g_y = g_\perp$ and $g_z = g_{||}$. When $\omega_0^2\tau_R^2 \gg 1$, the nonsecular term will make a negligible contribution compared to the secular term.

For this case eq 24 is

$$\mathfrak{K}_1(t) = \mathfrak{D}_{0,0}{}^2(\Omega)^2/_3\hbar^{-1}\beta_e B_0(g_{||} - g_\perp)S_z \equiv \mathfrak{D}_{0,0}{}^{(2)}(\Omega)\mathfrak{F}S_z \tag{29}$$

We have

$$-[S_z, C_m{}^{(1)}]_{\lambda_i} = [C_m{}^{(1)}]_{\lambda_i} \tag{30}$$

for a doublet state. When eq 29 and 30 are substituted into eq 21 (for no saturation), and eq 25–28 are utilized, then one obtains

$$[(\omega - \omega_0) - iRL(L+1)][C_{0,0}{}^L(\omega)]_{\lambda_i} - (2L+1)\mathfrak{F}\sum_{L'}\begin{pmatrix} L & 2 & L' \\ 0 & 0 & 0 \end{pmatrix}^2 [C_{0,0}{}^{L'}(\omega)]_{\lambda_i} = q\omega_\lambda d_{\lambda_i}\delta(L,0) \tag{31}$$

Now from eq 11 the absorption is proportional to

$$\pi \cdot \bar{Z}_{\lambda_i}{}^{(1)''} = Im[C_{0,0}{}^{0(1)}]_{\lambda_i} \tag{32}$$

Equation 31 defines an infinite set of coupled algebraic equations for the complex coefficients $C_{0,0}{}^L(\omega)$ (where we have dropped the superscript (1) for simplicity). The triangle property of the $3j$ symbols means, however, that the Lth equation is coupled only to the $L \pm 2$th equations, so only even L values appear. Approximations to the complete solution may be obtained by terminating the coupled equations at some finite limit by letting $C_{0,0}{}^L = 0$ for $L > n$ where $r = (n/2) + 1$ gives the order of the equations. The order r needed to obtain a satisfactory solution depends on the ratio $|\mathfrak{F}/R|$; the larger this ratio, the greater the value of n needed. A crude discussion of the convergence problem for this case appears in Appendix A, and it utilizes the fact that the present simple case has a continued fraction representation. We have found the convergence to be very rapid. Thus for $|\mathfrak{F}/R| \leqq 10$, $r \lessapprox 4$ is sufficient, for $|\mathfrak{F}/R| \sim 100$, $r \approx 7$, while for $|\mathfrak{F}/R| \leqq 1000$, $r \approx 10$ is needed (when $T_2|\mathfrak{F}| \approx 75$). (Note that the validity of relaxation theory[2] requires $|\mathfrak{F}/6R| \ll 1$ since the rotational correlation time in this case is $[L(L+1)R]^{-1}$ with $L = 2$.)

The results, given as both absorptions and first derivatives, in Table I and Figure 1, show the expected trends. As $|\mathfrak{F}/R|$ increases to unity (the region where relaxation theory applies), the main effect of the line shape is a broadening (*cf.* Table I). In the region $|\mathfrak{F}/R|$ of 1 to 10 the resonance peak shifts downfield, and the shape becomes markedly asymmetric. Between 10 and 100 a new high-field peak appears, and at 1000 the solidlike spectrum is sharpening up (one is observing a decrease of "motional broadening") as it clearly is approaching the powder spectrum given in Figures 1C and D. The powder spectrum was computed from the expressions given by Lefebvre and Maruani.[15]

The effect of including a rotationally invariant Lorentzian line width, T_2^{-1}, by letting $\omega_0 \rightarrow \omega_0 + iT_2^{-1}$ in eq 31 is shown in Figure 2. The effect of increasing T_2^{-1} is to smooth out the appearance of a solidlike spectrum.

2. Asymmetric Secular g Tensor. If now we let $g_x \neq g_y$, then

$$\mathfrak{K}_1(\Omega) = \mathfrak{F}_0\mathfrak{D}_{0,0}{}^2S_z + \mathfrak{F}_2S_z[\mathfrak{D}_{-2,0}{}^2 + \mathfrak{D}_{2,0}{}^2] \tag{33}$$

where

(15) R. Lefebvre and J. Maruani, *J. Chem. Phys.*, 42, 1480 (1965). Their formulas were first converted into units of gauss from reciprocal seconds.

$$\mathfrak{F}_0 = {}^2/_3[g_z - {}^1/_2(g_x + g_y)]\hbar^{-1}\beta_e B_0 \qquad (34a)$$

and

$$\mathfrak{F}_2 = \frac{1}{\sqrt{6}}(g_x - g_y)\hbar^{-1}\beta_e B_0 \qquad (34b)$$

The relevant coupled equations are given by

$$(2L + 1)^{-1}[(\omega - \omega_0) - iT_2^{-1} - iRL(L + 1)]\bar{C}_{K,0}{}^L - \mathfrak{F}_0\sum_{L'}\begin{pmatrix} L & 2 & L' \\ K & 0 & -K \end{pmatrix}\begin{pmatrix} L & 2 & L' \\ 0 & 0 & 0 \end{pmatrix}\bar{C}_{K,0}{}^{L'} - \mathfrak{F}_2\sum_{L'}\begin{pmatrix} L & 2 & L' \\ 0 & 0 & 0 \end{pmatrix}\left[\begin{pmatrix} L & 2 & L' \\ K & -2 & -(K-2) \end{pmatrix}\bar{C}_{K-2,0}{}^{L'} + \begin{pmatrix} L & 2 & L' \\ K & 2 & -(K+2) \end{pmatrix}\bar{C}_{K+2,0}{}^{L'}\right] = q\omega_\lambda d_{\lambda_j}\delta_{L,0}\delta_{K,0} \qquad (35)$$

where K is positive, and eq 32 as well as the triangle rule requiring $L' = L \pm 2$ or L still holds. Also one must have $K \leqq L$, etc. The superbars in eq 35 imply the following symmetrization

$$\bar{C}_{K,0}{}^L = {}^1/_2(C_{K,0}{}^L + C_{-K,0}{}^L) \qquad (36a)$$

and

$$\bar{C}_{0,0}{}^L = C_{0,0}{}^L \qquad (36b)$$

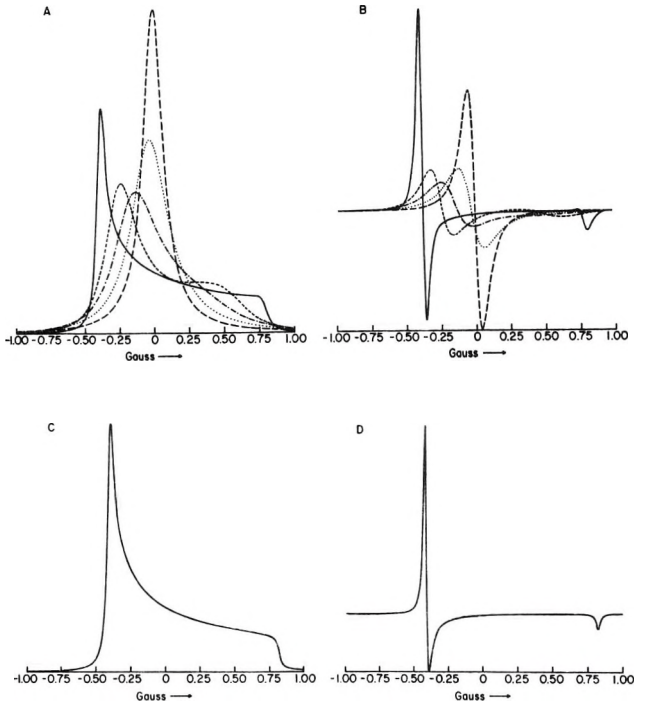

Figure 1. Line shapes for an axially symmetric g tensor as a function of $|\mathfrak{F}|/R$: A, absorption line shapes; B, first derivative. The different $|\mathfrak{F}|/R$ values are — —, 2.5; ····, 5; -·-·, 10; ---, 25; ——, 1000; C and D, rigid limit absorption and derivative line shapes. All correspond to $(g_{||} - g_\perp) = -7.50 \times 10^{-4}$, $\bar{g} = 2.00285$ and are centered about $\hbar\omega_0/\bar{g}\beta_e \equiv B_0 = 3300$ G and a rotationally invariant $(2/\sqrt{3})T_2^{-1}/|\gamma_e| = 0.02$ G.

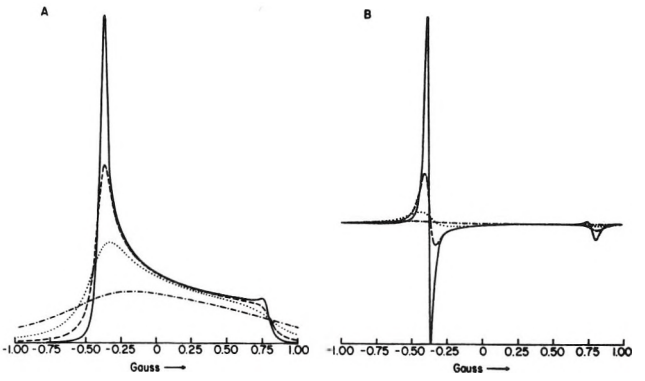

Figure 2. Line shapes for an axially symmetric g tensor as a function of the rotationally invariant component T_2^{-1}: A, absorption; B, derivative. The different values of $(2/\sqrt{3})T_2^{-1}/|\gamma_e|$ are ——, 0.01 G; —, 0.05 G; ····, 0.150 G, -·-, 0.500 G. In all cases $|\mathfrak{F}|/R = 1000$.

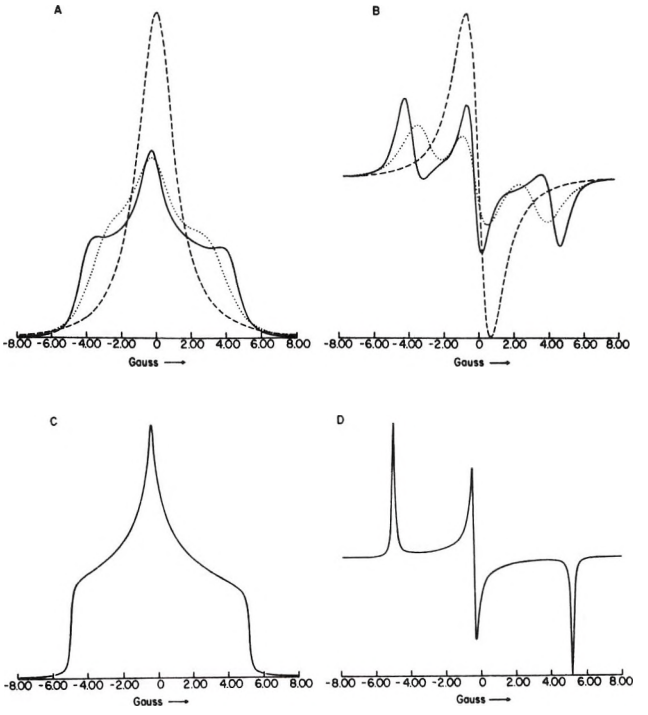

Figure 3. Line shapes for an asymmetric g tensor as a function of $|\mathfrak{F}_0|/R$; A, absorption; B, derivative. The different $|\mathfrak{F}_0|/R$ values are ---, 5; ····, 25; ——, 100. C and D, rigid limit absorption and derivative line shapes. All correspond to $g(x) = 2.00890$, $g(y) = 2.00610$, $g(z) = 2.00270$ and are centered about $B_0 = 3300$ G, with a rotationally invariant $(2/\sqrt{3})T_2^{-1}/|\gamma_e| = 0.1$ G.

The order of the equations, when one terminates for $L > n$ is now $1 + n(n + 6/8)$. However the proper value of n, again depends on $|\mathfrak{F}_0/R|$ for $|\mathfrak{F}_0| > |\mathfrak{F}_2|$, and values of n equivalent to those of case 1 are again applicable.

The progress of the line shapes, as $|\mathfrak{F}_0/R|$ increases, is seen from Figure 3 to be similar to case 1, but in the region of 10 to 100 three peaks now appear. The limiting powder spectrum appears in Figure 3c, and

although there still is appreciable motion for $|\mathfrak{F}_0/R| = 100$, this case is seen to be beginning to approach the powder spectrum (note that intensities of separately computed viscous liquid and powder spectra are arbitrary).

3. g Tensor plus END Tensor Including Pseudo-Secular Terms. The power of the method is exemplified in this case, where the pseudo-secular ($S_zI_\pm$) terms, which can cause nuclear spin flips, can be comparable in importance to the secular terms when ω_n, the nuclear spin Larmour frequency is small.[2] The retention of the pseudo-secular terms results in $[\mathcal{H}_1, \mathcal{H}_0] \neq 0$, unlike the previous cases.

a. One Nuclear Spin of $I = 1/2$. This is the simplest case for illustrating the method. The labeling of the energy levels and relevant transitions is given in Figure 4a. The resonance frequencies for the two allowed transitions (1 and 2) and the two forbidden transitions (3 and 4) are

$$\begin{aligned} \omega_1 &= \omega_{aa'} = \omega_e - {}^1/_2\gamma_e\bar{a} \longrightarrow -a' \\ \omega_2 &= \omega_{bb'} = \omega_e + {}^1/_2\gamma_e\bar{a} \longrightarrow a' \\ \omega_3 &= \omega_{ba'} = \omega_e + \omega_n \longrightarrow \omega_n \\ \omega_4 &= \omega_{ab'} = \omega_e - \omega_n \longrightarrow -\omega_n \end{aligned} \tag{37}$$

The resonant frequencies become $\pm a' = \pm\gamma_e\bar{a}/2$ and $\pm\omega_n$ when ω_e is taken as the origin of the spectrum for convenience.

For simplicity we again assume axial symmetry for the g tensor and the dipolar tensor. Then

$$\mathcal{H}_1(\Omega) = \mathfrak{D}_{0,0}^2 S_z[\mathfrak{F} + D'I_z] + (\mathfrak{D}_{0,1}^2 I_+ S_z - \mathfrak{D}_{0,-1}^2 I_- S_z)D \tag{38}$$

where

$$D = -2\pi\xi_i D_i^0 \tag{39a}$$

with $\xi_i = {}^1/_2\pi|\gamma_e|\gamma_i\hbar$ and D_i^0 is discussed elsewhere.[16] Also

$$D' = -({}^8/_3)^{1/2}D \tag{39b}$$

If we write $[\mathcal{H},\rho] \equiv \mathcal{H}^\times\rho$,[8] then one has

$$[\mathcal{H}_1^\times]_{\alpha\alpha'\beta\beta'} = [\mathcal{H}_{1_{\alpha\beta}}\delta_{\alpha'\beta'} - \mathcal{H}_{1_{\beta'\alpha'}}\delta_{\alpha\beta}] \tag{40}$$

where α, α', β, and β' are eigenstates of $\mathcal{H}_0$. $\mathcal{H}_1^\times$ may be represented as a simple Hermitian matrix in the space of transitions 1–4

$$\mathcal{H}_1^\times(\Omega) = \begin{pmatrix} 1 & 2 & 3 & 4 \\ \mathfrak{D}_{0,0}^2(\mathfrak{F} + {}^1/_2D') & 0 & s & s^* \\ 0 & \mathfrak{D}_{0,0}^2(\mathfrak{F} - {}^1/_2D') & s & s^* \\ s^* & s^* & \mathfrak{D}_{0,0}^2\mathfrak{F} & 0 \\ s & s & 0 & \mathfrak{D}_{0,0}^2\mathfrak{F} \end{pmatrix} \tag{41}$$

where $s = {}^1/_2\mathfrak{D}_{0,1}^2 D$. One must now develop eq 21 for nondegenerate transitions $\lambda = 1, 2, 3$, and 4. We shall represent the appropriate coefficients as $C_{K,M}{}^L(\lambda)$. Then we obtain

$$\begin{aligned} &(2L+1)^{-1}[(\omega + a') - i\{T_2^{-1} + RL(L+1)\}]C_{0,0}{}^L(1) - \\ &(\mathfrak{F} + {}^1/_2D')\sum_{L'}\begin{pmatrix} L & 2 & L' \\ 0 & 0 & 0 \end{pmatrix}^2 C_{0,0}{}^{L'}(1) + \\ &{}^1/_2D\sum_{L'\neq 0}\begin{pmatrix} L & 2 & L' \\ 0 & 0 & 0 \end{pmatrix}\begin{pmatrix} L & 2 & L' \\ 0 & 1 & -1 \end{pmatrix}[C_{0,1}{}^{L'}(3) - \\ &C_{0,-1}{}^{L'}(4)] = q\omega_1 d_1\delta_{L,0} \end{aligned} \tag{42a}$$

$$\begin{aligned} &(2L+1)^{-1}[(\omega - a') - i\{T_2^{-1} + RL(L+1)\}] \times \\ &C_{0,0}{}^L(2) - (\mathfrak{F} - {}^1/_2D')\sum_{L'}\begin{pmatrix} L' & 2 & L \\ 0 & 0 & 0 \end{pmatrix}^2 C_{0,0}{}^{L'}(2) + \\ &{}^1/_2D\sum_{L'\neq 0}\begin{pmatrix} L & 2 & L' \\ 0 & 0 & 0 \end{pmatrix}\begin{pmatrix} L & 2 & L' \\ 0 & 1 & -1 \end{pmatrix}[C_{0,1}{}^{L'}(3) - \\ &C_{0,-1}{}^{L'}(4)] = q\omega_2 d_2\delta_{L,0} \end{aligned} \tag{42b}$$

$$\begin{aligned} &\frac{D}{2}\sum_{L'}\begin{pmatrix} L & 2 & L' \\ 0 & 0 & 0 \end{pmatrix}\begin{pmatrix} L & 2 & L' \\ 1 & -1 & 0 \end{pmatrix}[C_{0,0}{}^{L'}(1) + \\ &C_{0,0}{}^{L'}(2)] + (2L+1)^{-1}[(\omega - \omega_n) - \\ &i\{T_2^{-1} + RL(L+1)\}]C_{0,1}{}^L(3) + \\ &\mathfrak{F}\sum_{L'\neq 0}\begin{pmatrix} L & 2 & L' \\ 0 & 0 & 0 \end{pmatrix}\begin{pmatrix} L & 2 & L' \\ 1 & 0 & -1 \end{pmatrix}C_{0,1}{}^{L'}(3) = 0 \end{aligned} \tag{42c}$$

$$\begin{aligned} &-\frac{D}{2}\sum_{L'}\begin{pmatrix} L & 2 & L' \\ 0 & 0 & 0 \end{pmatrix}\begin{pmatrix} L & 2 & L' \\ -1 & 1 & 0 \end{pmatrix}[C_{0,0}{}^L(1) + \\ &C_{0,0}{}^L(2)] + (2L+1)^{-1}[(\omega + \omega_n) - \\ &i\{T_2^{-1} + RL(L+1)\}]C_{0,-1}{}^L(4) + \\ &\mathfrak{F}\sum_{L'\neq 0}\begin{pmatrix} L & 2 & L' \\ 0 & 0 & 0 \end{pmatrix}\begin{pmatrix} L & 2 & L' \\ -1 & 0 & 1 \end{pmatrix}C_{0,-1}{}^{L'}(4) = 0 \end{aligned} \tag{42d}$$

While eq 42a and b are applicable for $L = 0$, eq 42c and d require $L, L' > 0$, and in all cases L and L' must be even and $L' = L \pm 2$ or L. Equations 42 represent four infinite sets of coupled equations (*i.e.*, expansions in L) which are then coupled among each other due to the pseudo-secular contribution from the END term.

The absorption is proportional to

$$Z_1'' + Z_2'' = Im[C_{0,0}{}^0(1) + C_{0,0}{}^0(2)]\pi^{-1} \tag{43}$$

When the series of eq 42 are terminated for $L > n$, the coupled algebraic equations are of order $r = 2(n+1)$ (the coefficients $C_{0,0}{}^0(3)$ and $C_{0,0}{}^0(4)$ are not needed to

(16) G. K .Fraenkel, *J. Phys. Chem.*, **71**, 139 (1967). Specifically for an axially symmetric hyperfine tensor we have $A_\parallel = \bar{a} + \frac{2\sqrt{6}}{3}\xi_i D_i^{(0)}$ and $A_\perp = \bar{a} - \frac{\sqrt{6}}{3}\xi_i D_i^{(0)}$ where the A's are in $\sec^{-1}$ and $D_i^{(0)}$ is in cm^{-3}.

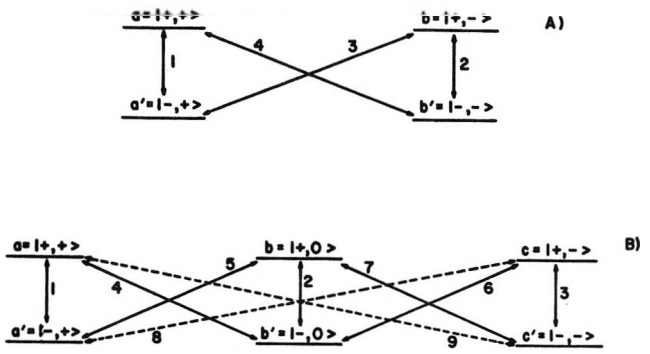

Figure 4. Energy levels and transitions for A, $S = {}^1/_2$, $I = {}^1/_2$ case; B, $S = {}^1/_2$, $I = 1$ case. The notation is $|M_S,M_I\rangle$.

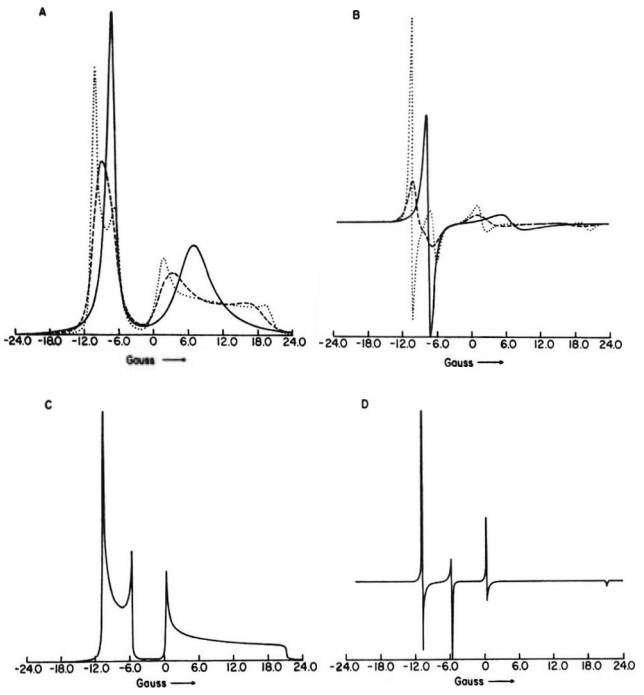

Figure 5. Line shapes for $S = {}^1/_2$, $I = {}^1/_2$ with axially symmetric g tensor and hyperfine tensor and small ω_n: A, absorption; B, derivative. The different $\mathfrak{F}/R$ values are ——, 2; – –, 15; ···, 100. C and D, rigid limit absorption and derivative line shapes. All correspond to $g_{||} = 2.00270$, $g_\perp = 2.00750$, $A_{||} = 32$ G, $A_\perp = 6$ G, $|\omega_n/\gamma_e| = 0.36$ G, $(2/\sqrt{3})T_2^{-1}/|\gamma_e| = 0.1$ G, and are centered about $B_0 = 3300$ G.

obtain the spectrum from eq 43). When $|D| \ll |a \pm \omega_n|$, then it is possible to use a perturbation technique to uncouple the coefficients for $\lambda = 1$ and 2 from those for $\lambda = 3$ and 4. (This technique is discussed in some detail in section B2.)

The solutions to eq 42 and 43 for the case of a small ω_n are given in Figure 5. This is a situation wherein a perturbation approach is not applicable. The parameters utilized for Figure 5 are appropriate for a nitroxide,[17] except that here $I = {}^1/_2$. (An ^{15}N nucleus is thus moderately well represented.) One again sees the gradual transition from liquidlike to solidlike line shapes as $|\mathfrak{F}|/R$ is increased, and even at $|\mathfrak{F}|/R = 100$ the correspondence to the rigid limit (Figure 5C) is clear.

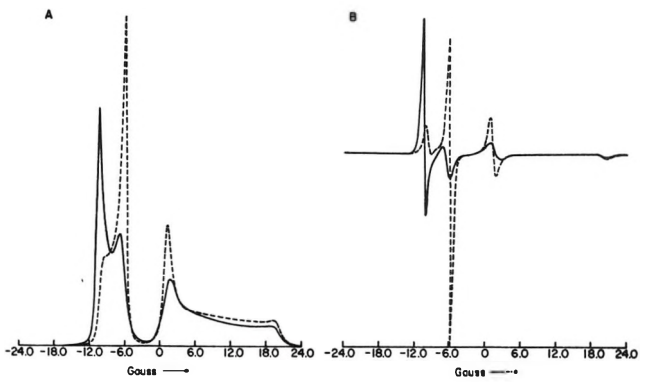

Figure 6. Comparison for $S = {}^1/_2$, $I = {}^1/_2$ of line shapes which include pseudo-secular contributions to line shapes for which they are omitted, when ω_n is small; $|\mathfrak{F}|/R = 100$. All other parameters as in Figure 5: A, absorption; B, derivative. —— corresponds to inclusion of pseudo-secular terms; – – corresponds to their omission.

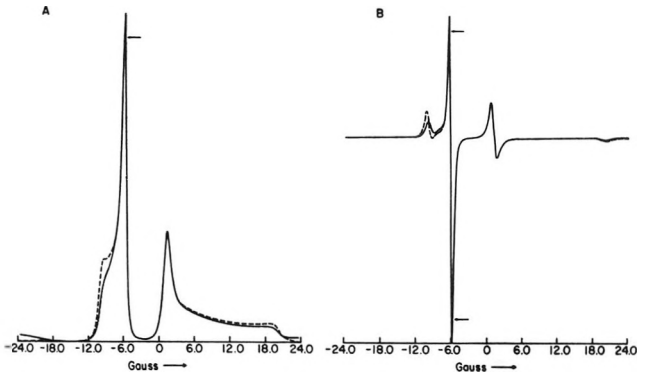

Figure 7. Comparison for $S = {}^1/_2$, $I = {}^1/_2$ of line shapes which include pseudo-secular contributions to line shapes for which they are omitted, when ω_n is large; $|\mathfrak{F}|/R = 100$. $|\omega_n/\gamma_e| = 23.0$ G. All other parameters as in Figure 5: A, absorption; B, derivative. —— corresponds to inclusion of pseudo-secular terms; – – corresponds to their omission. [Spin parameters $(g_{||} - g_\perp)$, $|\omega_n/\gamma_e|$, $A_{||}$, $A_\perp$, and the abscissas of graph scale to a typical ring proton case when divided by 4.6.]

Figures 6 and 7 show the results of a study to determine the importance of the pseudo-secular contributions. Figure 6 corresponds to the same parameters as Figure 5 with $|\mathfrak{F}|/R = 100$, but the complete solution is compared to the simplified solution obtained by the neglect of the pseudo-secular terms (*i.e.*, the terms in eq 42a and b which couple in forbidden transitions 3 and 4). There is no question but that the absorption and derivative line shapes are significantly altered by the presence of pseudo-secular terms. In Figure 7, a similar comparison was made, but here ω_n was increased by a factor of 65 while all other parameters were kept constant. With this choice of ω_n, the relevant spin parameters scale reasonably well to those for a typical aromatic

(17) O. H. Griffith, D. W. Cornell, and H. M. McConnell, *J. Chem. Phys.*, **43**, 2909 (1965); T. J. Stone, T. Buckman, P. L. Nordio, and H. M. McConnell, *Proc. Nat. Acad. Sci. U. S.*, **54**, 1010 (1965).

ring proton when one divides them by 4.6. In this case it is seen that the pseudo-secular terms make only a minor contribution to the line shapes, as expected, since $|D| \ll |a' \pm \omega_n|$. Such small effects can be accounted for by perturbation techniques. Similar results are obtained at lower values of $|\mathfrak{F}|/R$, although for $|\mathfrak{F}|/R = 10$ the primary effect of the pseudo-secular terms is to further broaden and shift the peaks rather than to change the spectral shapes markedly.

b. One Nuclear Spin of $I = 1$ (^{14}N). The energy levels and three allowed and six forbidden transitions are shown in Figure 4B for this case. We again assume axially symmetric tensors, and following a procedure similar to that used in part a for $I = {}^1/_2$, we obtain sets of equations which couple all nine transitions and are of order $r = (9/2)n + 3$. They can be summarized as follows.

$$(2L+1)^{-1}\{[\omega + (2-\lambda)2a'] - i[T_2^{-1} + RL(L+1)]\}C_{0,0}{}^{L}(\lambda) - [\mathfrak{F} + (2-\lambda)D'\sum_{L'}\begin{pmatrix} L & 2 & L' \\ 0 & 0 & 0 \end{pmatrix}^2 \times C_{0,0}{}^{L'}(\lambda) + \frac{\sqrt{2}}{2}D\sum_{L'}\begin{pmatrix} L & 2 & L' \\ 0 & 0 & 0 \end{pmatrix}\begin{pmatrix} L & 2 & L' \\ 0 & 1 & -1 \end{pmatrix}\mathrm{f}(L',\lambda) = q\omega_\lambda d_\lambda \delta_{L,0} \text{ (for } \lambda = 1, 2, \text{ or } 3) \quad (44)$$

where

$$\mathrm{f}(L',1) = C_{0,1}{}^{L'}(4) - C_{0,-1}{}^{L'}(5) \quad (44a)$$

$$\mathrm{f}(L',3) = C_{0,1}{}^{L'}(6) - C_{0,-1}{}^{L'}(7) \quad (44b)$$

$$\mathrm{f}(L',2) = \mathrm{f}(L',1) + \mathrm{f}(L',3) \quad (44c)$$

$$(2L+1)^{-1}\{[\omega - (-1)^\lambda\omega_n + \nu a'] - i[T_2^{-1} + RL(L+1)]\}C_{0,-1}{}^{L}\lambda(\lambda) + (\mathfrak{F} + \nu^1/_2 D') \times \sum_{L'\neq 0}\begin{pmatrix} L & 2 & L' \\ 0 & 0 & 0 \end{pmatrix}\begin{pmatrix} L & 2 & L' \\ 1 & 0 & -1 \end{pmatrix}C_{0,-1}{}^{\lambda L'}(\lambda) + (-1)^\lambda\frac{\sqrt{2}}{2}D\sum_{L'}\begin{pmatrix} L & 2 & L' \\ 0 & 0 & 0 \end{pmatrix}\begin{pmatrix} L & 2 & L' \\ 1 & -1 & 0 \end{pmatrix} \times [C_{0,0}{}^{L'}(\epsilon) + C_{0,0}{}^{L'}(2)] - (-1)^\lambda\frac{\sqrt{2}}{2}D \times \sum_{L'\neq 0}\begin{pmatrix} L & 2 & L' \\ 0 & 0 & 0 \end{pmatrix}\begin{pmatrix} L & 2 & L' \\ 1 & 1 & -2 \end{pmatrix}C_{0,2(-1)^\lambda L'}(\nu') = 0 \text{ (for } \lambda = 4, 5, 6, \text{ or } 7) \quad (45)$$

where $\nu = +1$ and $\epsilon = 1$ when $\lambda = 4$ or 5 and $\nu = -1$ and $\epsilon = 3$ when $\lambda = 6$ or 7; also $\nu' = 8$ for $\lambda = 4$ or 6 and $\nu' = 9$ for $\lambda = 5$ or 7. Also

$$(2L+1)^{-1}\{[(\omega - (-)^\lambda 2\omega_n] - i[T_2^{-1} + RL(L+1)]\}C_{0,2(-)^\lambda L}(\lambda) - \mathfrak{F}\sum_{L'\neq 0}\begin{pmatrix} L & 2 & L' \\ 0 & 0 & 0 \end{pmatrix}\begin{pmatrix} L & 2 & L' \\ 2 & 0 & -2 \end{pmatrix}C_{0,2(-1)^\lambda L'(\lambda)} - (-)^\lambda\frac{\sqrt{2}}{2}D\sum_{L'\neq 0}\begin{pmatrix} L & 2 & L' \\ 0 & 0 & 0 \end{pmatrix}\begin{pmatrix} L' & 2 & L \\ 2 & -1 & -1 \end{pmatrix}\mathrm{f}(L',\lambda) = 0 \text{ (for } \lambda = 8 \text{ or } 9) \quad (46)$$

where

$$\mathrm{f}(L',8) = C_{0,1}{}^{L'}(4) + C_{0,1}{}^{L'}(6) \quad (46a)$$

$$\mathrm{f}(L',9) = C_{0,-1}{}^{L'}(5) + C_{0,-1}{}^{L'}(7) \quad (46b)$$

The above equations are valid for even L and L'. Finally

$$I(\omega) = \frac{1}{\pi}Im[C_{0,0}{}^{0}(1) + C_{0,0}{}^{0}(2) + C_{0,0}{}^{0}(3)] \quad (47)$$

Computer simulations of these equations for the nitroxidelike values employed in part a are given in Figures 8 and 9. In Figure 8 results for a range of $|\mathfrak{F}|/R$ values are given, and they show the progress from liquidlike to solidlike spectra. In Figure 9 a comparison is made between line shapes obtained (for $|\mathfrak{F}|/R = 100$) when pseudo-secular terms are both included and omitted. Again it is clear that these terms make important contributions. Also shown in Figure 9 is a comparison of the rigid limit spectra predicted for the two cases when pseudo-secular terms are either included or omitted, and the difference is significant.

B. Saturation. To describe a saturated spectrum, one needs, according to eq 21, expressions for the $[C_m{}^{(0)}]_{\lambda_j\pm}$. These may be obtained by taking the $\langle\lambda_j\pm|-|\lambda_j\pm\rangle$ matrix elements of eq 4 and performing a derivation like that which leads to eq 21. We obtain

$$N_m(in\omega + E_m')[C_{m'}{}^{(n)}]_{\lambda_j\pm} = \mp id_{\lambda_j}N_{m'}([C_{m'}{}^{(n+1)}]_{\lambda_j\rightarrow} - [C_{m'}{}^{(n-1)}]_{\lambda_j\leftarrow}) - i\sum_m\int d\Omega G_{m'}{}^*(\Omega)G_m(\Omega)[\mathfrak{K}_1{}^{(\text{nonsec})}, C_m{}^{(n)}]_{\lambda_j\pm,\lambda_j\pm} \quad (48)$$

(Here, the subscript $\lambda_{j\rightarrow} \equiv \lambda_j$ refers to the $\langle\lambda_j-|-|\lambda_j+\rangle$ matrix element, while $\lambda_{j\leftarrow}$ refers to the $\langle\lambda_j+|-|\lambda_j-\rangle$ matrix element.) The superscript (nonsec) refers to the fact that only the nonsecular part of $\mathfrak{K}_1$ need be retained. Equation 48 is also needed for problems involving no saturation, but a nonsecular $\mathfrak{K}_1$ which induces electron spin flips.

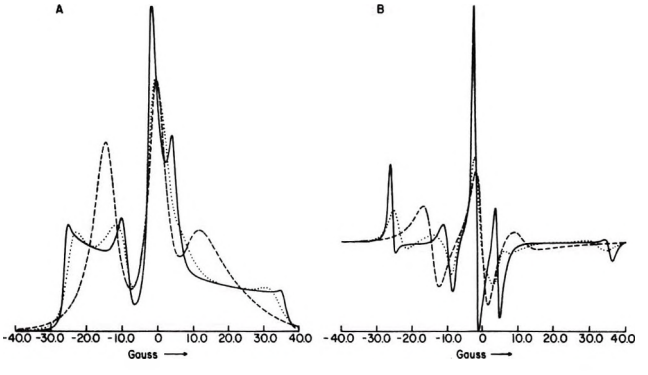

Figure 8. Line shapes for $S = {}^1/_2$, $I = 1$ (^{14}N nucleus) with axially symmetric g tensor, hyperfine tensor, and small ω_n: A, absorption; B, derivative. Parameters same as in Figure 5 except $(2/\sqrt{3})T_2^{-1}/|\gamma_e| = 0.3$ G. The $|\mathfrak{F}|/R$ values are ---, 2; ...., 15; ——, 100.

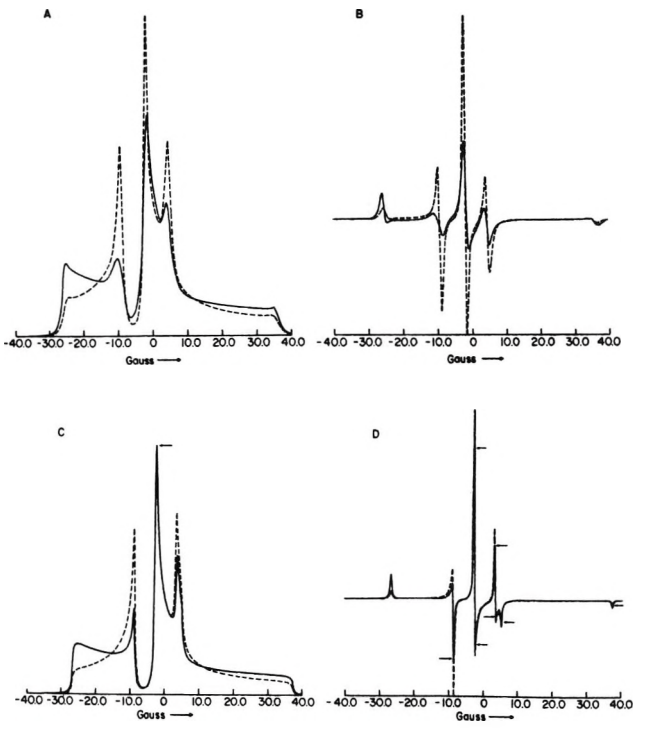

Figure 9. Comparison for $S = {}^1/_2$, $I = 1$ (^{14}N nucleus) of line shapes which include pseudo-secular contributions to line shapes for which they are omitted, when ω_n is small; $|\mathfrak{F}|/R = 100$. All other parameters as in Figure 5: A, absorption; B, derivative; C and D, rigid limit. —— corresponds to inclusion of pseudo-secular terms; — corresponds to their omission. Arrows are used to locate derivative extrema in D when otherwise unclear. Note that in A and B the shapes are normalized to a common integrated intensity, while in C and D they are normalized to the same total height.

It is often convenient to look at the difference

$$[b_{m'}{}^{(n)}]_{\lambda_i} \equiv [C_{m'}{}^{(n)}]_{\lambda_i +} - [C_{m'}{}^{(n)}]_{\lambda_i -} \quad (49)$$

which is found, from eq 48, to obey the equation

$$N_{m'}(in\omega + E_{m'})[b_{m'}{}^{(n)}]_{\lambda_i} = -i2d_{\lambda_i}N_{m'}([C_{m'}{}^{(n+1)}]_{\lambda_i \rightarrow} - C_{m'}{}^{(n-1)}]_{\lambda_i \leftarrow}) - i\sum_m \int d\Omega G_{m'}{}^*(\Omega)G_m(\Omega)([\mathcal{H}_1{}^{(\text{nonsec})}, C_m{}^{(n)}]_{\lambda_i + \lambda_i +} - [\mathcal{H}_1{}^{(\text{nonsec})}, C_m{}^{(n)}]_{\lambda_i - \lambda_i -}) \quad (50)$$

It follows from the Hermitian properties of ρ and ρ_0 as well as eq 6, 7, and 18 that

$$N_{m'}[C_{m'}{}^{(n)}]_{ab} = \sum_m [C_m{}^{(-n)}]_{ba}{}^* \int G_{m'}{}^*(\Omega)G_m{}^*(\Omega)d\Omega \quad (51)$$

Equation 51 also applies for $b = a$. Thus in eq 48

$$[C_{m'}{}^{(n-1)}]_{\lambda_i \leftarrow} = N_{m'}{}^{-1}\sum_m [C_m{}^{(-n+1)}]_{\lambda_i \rightarrow}{}^* \times \int G_{m'}{}^*(\Omega)G_m{}^*(\Omega)d\Omega \quad (52)$$

A form of eq 21 generalized to any n (not just $n = 1$) is sometimes needed. It is

$$N_{m'}[(n\omega - \omega_\lambda) - iE_{m'}] \times [C_{m'}{}^{(n)}]_{\lambda_i} + \sum_m \int d\Omega G_{m'}{}^*(\Omega)G_m(\Omega) \times [\mathcal{H}_1(\Omega), C_m{}^{(n)}]_{\lambda_i} + d_{\lambda_i}N_{m'}[b_{m'}{}^{(n-1)}]_{\lambda_i} = q\omega_\lambda d_{\lambda_i}\delta(m',0)\delta(n,1) \quad (53)$$

In eq 48 (or 50) and 53, one sees that it is only through effects of the radiation field, where the strength of interaction with the spins is given by $d_{\lambda_i} \equiv {}^1/_2\omega_1$, that the nth harmonics $[C_{m'}{}^{(n)}]$ are coupled to harmonics $[C_m{}^{(n\pm1)}]$. An analysis of these equations (which is given in more detail for the simple two-jump case in Appendix B) leads to the result that the extent of coupling depends essentially on the ratio ω_1/ω_0, which is very small in the presence of large applied dc fields. Hence, it is sufficient for high-field saturation cases to retain only the $n = 1$ terms (which include $[C_0{}^{(1)}]_{\lambda_i}$, the observed signal) and the $n = 0$ terms (which include $[b_0{}^{(0)}]_{\lambda_i}$, the dc population differences). Higher harmonics become important in a variety of multiple resonance schemes or experiments done at lower dc fields.

1. Rotationally Invariant T_1. We consider a simple case of saturation. The unsaturated line shape is assumed to be due mainly to the secular part of an axially symmetric g tensor just as in section IIIA1, while there is a rotationally invariant $T_1 = (2W_e)^{-1}$, where W_e is the lattice-induced electron spin flip process. This is introduced by replacing in eq 50 $E_{m'} \rightarrow E_{m'} + 2W_e$. We also include a rotationally invariant $T_2 \leqq T_1$ by letting $iE_{m'} \rightarrow i(E_{m'} + T_2{}^{-1})$ in eq 53.

For the secular perturbation of eq 29, it is only necessary to consider $[C_{0,0}{}^{L(1)}]_{\lambda_i}$ and $[b_{0,0}{}^{L(0)}]_{\lambda_i}$, and one obtains from eq 50 and 53

$$[(\omega - \omega_0) - iRL(L+1) - iT_2{}^{-1}][C_{0,0}{}^{L(1)}]_{\lambda_i} - (2L+1)\mathfrak{F}\sum_{L'}\begin{pmatrix} L & 2 & L' \\ 0 & 0 & 0 \end{pmatrix}^2 \times [C_{0,0}{}^{L'(1)}]_{\lambda_i} + \frac{4|d_{\lambda_i}|^2}{RL(L+1) + 2W_e} \times Im[C_{0,0}{}^{L(1)}]_{\lambda_i} = q\omega_\lambda d_{\lambda_i}\delta(L,0) \quad (54)$$

Equation 54 with eq 32 then determines the saturated spectrum. Note that the saturation term (*viz.* the last term on the left-hand side of eq 54) for $L = 0$ is unaffected by the rotational motion; while for $L > 0$ we find $W_e \rightarrow W_e + {}^1/_2RL(L+1)$, *i.e.*, the rotational motion aids the spin relaxation by spreading the spins over all orientations, which, due to $\mathcal{H}_1(\Omega)$ have different "static" resonant frequencies.

The computer solution to eq 54 is conveniently developed after the real and imaginary parts have been separated. The results for $|\mathfrak{F}|/R = 10$ and 100 are given, respectively, in Figures 10 and 11. Each figure shows curves corresponding to values of B_1 covering a

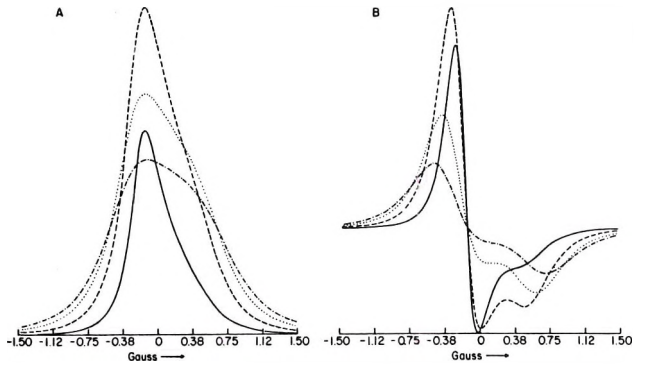

Figure 10. Saturation of single line with rotationally invariant T_1, as a function of B_1 for $|\mathfrak{F}|/R = 10$: $g_{||} = 2.00235$, $g_\perp = 2.00310$, $T_2 = T_1 = (2W_e)^{-1}$ and $(2/\sqrt{3})T_2^{-1}/|\gamma_e| = 0.02$ G. The different values of $(1/2)B_1$ are ——, 0.01 G; — —, 0.0333 G; ····, 0.0667 G; -·-·-, 0.100 G. These correspond to intensity factors of 1418, 913, 481, and 280, respectively. A, absorption; B, derivative.

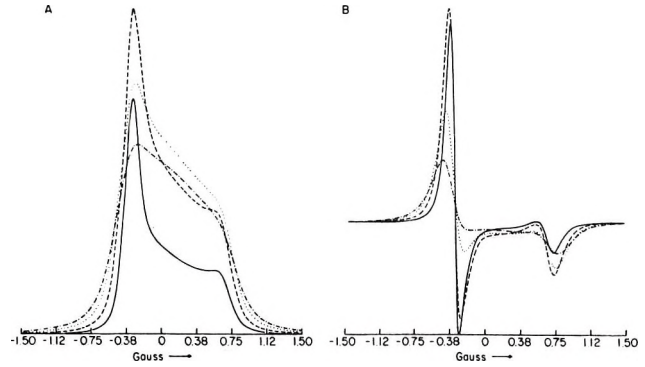

Figure 11. Saturation of single line with rotationally invariant T_1, as a function of B_1 for $|\mathfrak{F}|/R = 100$. The different values of $(1/2)B_1$ are ——, 0.01 G; - - -, 0.025 G; ····, 0.050 G; -·-, 0.075 G. These correspond to intensity factors of 1414, 1052, 580, and 352, respectively. All other parameters as in Figure 10: A, absorption; B, derivative.

range in which saturation is important. A measure of the extent of saturation of a particular line shape is given by the integrated area under the absorption curve. These are given as intensity factors in relative units in the figure captions. They aid cross-comparisons between the different figures. Thus we note that roughly the same degree of saturation is achieved for a given B_1 in both figures. In general, one sees that the effect of the saturation on the line shape is to broaden out the spectrum while acting to "wash out" the asymmetric appearance. This is similar to the effect of increasing T_2^{-1} for the unsaturated spectrum (*cf.* Figure 2) (except for the reduction of intensity in the case of saturation).

2. g Tensor (Axially Symmetric). We now include the nonsecular portion of the g tensor to give

$$\mathcal{H}_1 = \mathfrak{F}[\mathfrak{D}_{0,0}{}^2S_z - (^3/_8)^{1/2}(\mathfrak{D}_{0,1}{}^2S_+ - \mathfrak{D}_{0,-1}{}^2S_-)] \quad (55)$$

Equation 55 substituted into eq 53 and 50, respectively, leads to

$$(-)^{K-M}[n\omega - \omega_0 - iT_2^{-1} - iRL(L+1)] \times [C_{-K,-M}{}^{L(n)}]_{\lambda_i} - (2L+1)\mathfrak{F}\sum_{L',K',M'}\begin{pmatrix} L & 2 & L' \\ K & 0 & K' \end{pmatrix} \times \begin{pmatrix} L & 2 & L' \\ M & 0 & M' \end{pmatrix}[C_{K',M'}{}^{L'(n)}]_{\lambda_i} + (-)^{K-M}d_{\lambda_i} \times [b_{-K,-M}{}^{L(n-1)}] + (2L+1)(^3/_8)^{1/2}\mathfrak{F} \times \sum_{L',K',M'}\begin{pmatrix} L & 2 & L' \\ K & 0 & K' \end{pmatrix}\begin{pmatrix} L & 2 & L' \\ M & -1 & M' \end{pmatrix}[b_{K',M'}{}^{L'(n)}]_{\lambda_i} - q\omega_0\delta(n,0)\delta_{K,0}\delta_{M,1}(^3/_8)^{1/2}\mathfrak{F} = q\omega_\lambda d_{\lambda_i}\delta_{L',0}\delta_{n,1} \quad (56)$$

and

$$(-)^{K-M}[(^1/_2)in\omega + (^1/_2)RL(L+1) + W_e] \times [b_{-K,-M}{}^{L(n)}]_{\lambda_i} = -id_{\lambda_i}(-)^{K-M} \times ([C_{-K,-M}{}^{L(n+1)}]_{\lambda_i\rightarrow} - [C_{-K,-M}{}^{L(n-1)}]_{\lambda_i\leftarrow}) + i(2L+1)(^3/_8)^{1/2}\mathfrak{F}\sum_{L',K',M'}\begin{pmatrix} L & 2 & L' \\ K & 0 & K' \end{pmatrix}\left\{\begin{pmatrix} L & 2 & L' \\ M & 1 & M' \end{pmatrix} \times [C_{K'M'}{}^{L'(n)}]_{\lambda_i\rightarrow} + \begin{pmatrix} L & 2 & L' \\ M & -1 & M' \end{pmatrix}[C_{K'M'}{}^{L'(n)}]_{\lambda_i\leftarrow}\right\} \quad (57)$$

We find from eq 25, 28, and 51 that

$$[C_{-K,-M}{}^{L(n)}]_{\lambda_i\leftarrow} = (-)^{K-M}[C_{K,M}{}^{L(-n)^*}]_{\lambda_i\rightarrow} \quad (58a)$$

and

$$[b_{-K,-M}{}^{L(n)}]_{\lambda_i} = (-)^{K-M}[b_{K,M}{}^{L(-n)^*}]_{\lambda_i} \quad (58b)$$

so $[b_{0,0}{}^{L(0)}]_{\lambda_i}$ is real, and eq 57 can be more conveniently rewritten.

We now employ the high-field, moderate saturation approximations (*i.e.*, $|\omega_1/\omega_0| \ll 1$, where $\omega_1 = 2d_{\lambda_i}$ and $|\mathfrak{F}/\omega_0| \ll 1$), as well as the *ad hoc* relaxation to thermal equilibrium assumption, which are discussed in Appendix B. This leads to simplified coupled equations between the coefficients $C_{0,0}{}^{L(1)}$ and $b_{0,0}{}^{L(1)}$ and between $C_{0,0}{}^{L(0)}$ and $b_{0,0}{}^{L(0)}$ as a result of the nonsecular part of eq 55, while $C_{0,0}{}^{L(1)}$ and $b_{0,0}{}^{L(0)}$ are coupled *via* the saturating microwave field. However, the assumption that $|\mathfrak{F}/\omega_0| \ll 1$ further allows one to employ second-order perturbation theory and decouple $C_{0,0}{}^{L(1)}$ from $b_{0,0}{}^{L(1)}$ and $b_{0,0}{}^{L(0)}$ from $C_{0,0}{}^{L(0)}$. The resulting equations are

$$\{(\omega - \omega_0) - i[T_2^{-1} + RL(L+1)]\}C_{0,0}{}^{L(1)} - (2L+1)\mathfrak{F}\sum_{L'}\begin{pmatrix} L & 2 & L' \\ 0 & 0 & 0 \end{pmatrix}^2 C_{0,0}{}^{L'(1)} + d_{\lambda_i}b_{0,0}{}^{L(0)} + \left[\text{terms in } C_{0,0}{}^{L''(1)} \text{ of order } \frac{\mathfrak{F}^2}{-\omega_0 + iRL(L+1)}\right] = q\omega_\lambda d_\lambda\delta_{(L,0)} \quad (59)$$

and

$$\left[\frac{RL(L+1)}{2} + W_e\right] b_{0,0}{}^{L(0)} - 2d_{\lambda_i} Im C_{0,0}{}^{L(1)} -$$

$$(3/8)(2L+1)\mathfrak{F}^2 \sum_{L',L''} \begin{pmatrix} L & 2 & L' \\ 0 & 0 & 0 \end{pmatrix} \begin{pmatrix} L & 2 & L' \\ 0 & 1 & -1 \end{pmatrix} \times$$

$$\begin{pmatrix} L' & 2 & L'' \\ 0 & 0 & 0 \end{pmatrix} \begin{pmatrix} L' & 2 & L'' \\ 1 & -1 & 0 \end{pmatrix} \left[\frac{(2L+1)V(L,L')}{V(L,L')^2 + \left(\frac{2L+1}{2L'+1}\omega_0\right)^2} + \right.$$

$$\left. \frac{(2L''+1)V(L'',L')}{V(L'',L')^2 + \left(\frac{2L''+1}{2L'+1}\omega_0\right)^2} \right] b_{0,0}{}^{L''(0)} = 0 \quad (60)$$

where

$$V(L,L') = {}^1/_2 RL(L+1) + W_e - \left(\frac{2L+1}{2L'+1}\right)[RL'(L'+1) + T_2{}^{-1}] \quad (60a)$$

In eq 59 we are neglecting terms of order $\mathfrak{F}^2 C_{0,0}{}^{L''(1)}/[-\omega_0 + iRL(L+1)]$ since when $RL(L+1) \ll |\omega_0|$, as is the case for slow tumbling, then these nonsecular terms are of order $|\mathfrak{F}/\omega_0|$ smaller than the secular terms in $\mathfrak{F}$; *i.e.*, we are neglecting the nonsecular contributions to the unsaturated line widths as compared to the secular contributions for slow tumbling (*cf.* section A1). These nonsecular terms must, however, be included in eq 60 since this equation predicts the T_1-type behavior and is not explicitly affected by the secular terms in $\mathfrak{F}$. Note that for $RL(L+1) \ll |\omega_0|$, then $|V(L,L')|, |V(L'',L')| \ll \omega_0{}^2$ and the terms in V^2 in the denominators of the last terms on the left-hand side of eq 60 may be omitted. Furthermore, in this limit a perturbation analysis of the coupling of $b_{0,0}{}^{L(0)}$ to $b_{0,0}{}^{L''(0)}$ in equation 60 shows that it is sufficient to restrict the summation over L'' in this equation to just $L'' = L$. This, then, just leaves the terms diagonal in $b_{0,0}{}^{L(0)}$ in eq 60. However, these diagonal corrections are of order of magnitude $|\mathfrak{F}/\omega_0|^2 R$ and are thus negligibly small compared to ${}^1/_2 RL(L+1)$. *Thus, the contribution of the nonsecular terms in eq 60 is negligible in our approximation except for the diagonal term for $L = 0$!* This contribution to $L = 0$ is readily calculated, and is

$$W_e{}^{(G)} = (9/10)(\mathfrak{F}/\omega_0)^2 R \quad (61)$$

which is just the result obtained from relaxation theory for $|R/\omega_0| \ll 1$,[2a,11] even though we are now allowing for slow tumbling: $|\mathfrak{F}/R| > 1$ (cf. Appendix B). The net conclusion is that for $|\mathfrak{F}|, R, \ll |\omega_0|$, the solution to the present case is just given by eq 54 for the rotationally invariant T_1, but with $W_e \rightarrow W_e + W_e{}^{(G)}\delta_{L,0}$ in that equation, where $W_e{}^{(G)}$ is given by eq 61.

The solutions for different $\omega_1 = \gamma_e B_1$ in the region of saturation are given in Figures 12 and 13 for values of $|\mathfrak{F}|/R = 10$ and 100, respectively. One notes, from the intensity factors given in these figures, that roughly the same degree of saturation is achieved for cases $|\mathfrak{F}|/R = 10$ and 100 when B_1 is only about three times weaker for the latter case. One again finds that the effect of saturation is to broaden out and to tend to reduce the asymmetry of the spectrum.

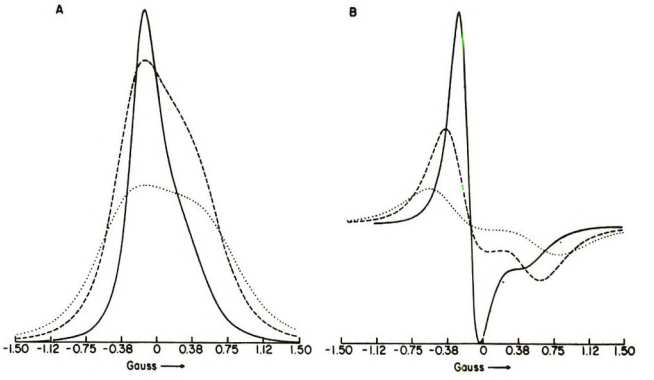

Figure 12. Saturation of single line with g-tensor relaxation as a function of B_1 for $|\mathfrak{F}|/R = 10$; $g_{||} = 2.00235$, $g_\perp = 2.00310$; $W_e = T_2{}^{-1} = 0$. The different values of $(1/2)B_1$ are ——, 1×10^{-5} G; ---, 5×10^{-1} G; ····, 1×10^{-4} G. Corresponding to intensity factors of 1053 342, 139, respectively. A, absorption; B, derivative.

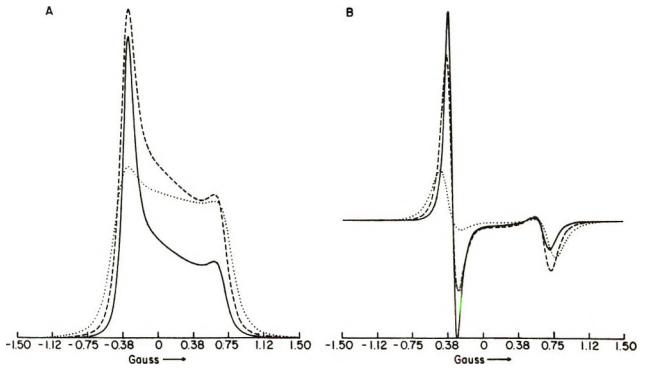

Figure 13. Saturation of single line with g tensor relaxation as a function of B_1 for $|\mathfrak{F}|/R = 100$. The different values of $(1/2) \times B_1$ are ——, 3×10^{-6} G; ---, 7.5×10^{-6} G; ····, 2×10^{-5} G. These correspond to intensity factors of 1382, 914, 308, respectively. All other parameters as in Figure 12.

The rather surprisingly weak dependence of the intensity factors as a function of B_1 for the different $|\mathfrak{F}|/R$ values in the slow tumbling region is most likely due to the fact that different portions of the spectrum are found to saturate to a different extent. This is most clearly seen in Figures 11 and 13 for the cases of $|\mathfrak{F}|/R = 100$. What should be an equivalent point of view is suggested by the nature of the coupled eq 54 (also as modified by inclusion of eq 61). We note that as $|\mathfrak{F}|/R$ becomes larger, coefficients $C_{0,0}{}^{L(1)}$ for the larger L values play a greater role in the coupled equations. But these terms have "effective" T_1's of $[2W_e + RL(L+1)]^{-1}$ in eq 54, so that while R may become smaller, $L(L+1)R$ for the contributing terms is not decreasing as fast. Similar comments apply to the width com-

ponents where T_2^{-1} replaced by $RL(L + 1) + T_2^{-1}$ (although here their relative value compared to $\mathfrak{F}$ becomes important). The components of higher L value are therefore not as easily saturated as the components of lower L value, and the latter are expected to make the major contribution to an unsaturated spectrum. This, one would expect, is the reason for the significant line shape changes obtained as a resulting of saturation.

A comparison of Figures 10 and 11 for a rotationally invariant T_1 and Figures 12 and 13 for the g-tensor contribution suggests that appropriate experimental studies might distinguish between such cases. The differences are clearer from the absorption plots. Thus in Figure 13A the line shape appears to be "squaring-up" more than in Figure 11A, for comparable intensity factors.

IV. Conclusions

It has been shown that the stochastic Liouville method may be successfully applied to obtain rapidly convergent solutions for a wide variety of esr line shape problems in the slow tumbling region. These included esr line shapes in the presence of g tensor and dipolar perturbations as well as the effects of saturation on the slow tumbling line shapes. The method may also be readily applied to include other relaxation effects (*e.g.*, nuclear quadrupolar terms), to spins of higher multiplicity, and to multiple resonance effects. Further, Markovian processes other than isotropic rotational diffusion could be incorporated.

Our results on unsaturated line shapes have clearly demonstrated the importance of the pseudo-secular dipolar terms in determining the line shapes in the slow tumbling region. The criterion for when they have major effects is $D \gtrsim |a' \pm \omega_n|$; *i.e.*, the anisotropic dipolar terms are comparable to or larger than the pure nuclear-spin transition frequencies. This is the usual case for ^{14}N nuclei in nitroxide compounds but not for typical ring protons. No recourse had to be made in our work to the "adiabatic" approximation used by earlier workers[5,6] which is valid in the near rigid limit, but begins to break down as the tumbling becomes faster due to "pseudo-secular" contributions.[7]

Our results on the effects of saturation have shown that rather significant line shape changes are predicted to be induced as a function of the saturating fields (Figures 10–13). This suggests that experimental saturation studies, in which the line shape changes are monitored, could be useful in extracting out spin relaxation information in the slow tumbling region. Also, our analysis of both a simple two-jump case (Appendix B) and a rotational diffusion case show that, even in the slow motional region, a fundamental role is played by the T_1's that are obtained from the spin relaxation theories (where $|\mathfrak{IC}_1\tau_c| \ll 1$ is assumed).

Acknowledgment. One of us (J. H. F.) wishes to thank Professor R. Kubo for his kind hospitality at the University of Tokyo, where this work was begun, and for calling the stochastic Liouville method to his attention.

Appendix A

On the Convergence of the Solutions. We examine some aspects of the convergence of the simplest case: section IIIA1, the axially symmetric g tensor. This solution is of the form (in matrix notation)

$$(\mathbf{A} + k\mathbf{1})(\mathbf{C}) = (\mathbf{U}) \tag{A1}$$

where $\mathbf{A}$ is a complex continuant matrix with diagonal elements $A_{LL} = -iRL(L + 1) - (2L + 1)\mathfrak{F}\begin{pmatrix} L & 2 & L \\ 0 & 0 & 0 \end{pmatrix}^2$ and the only off-diagonal elements, $A_{L,L\pm2} = -(2L + 1)\mathfrak{F}\begin{pmatrix} L & 2 & L\pm2 \\ 0 & 0 & 0 \end{pmatrix}^2$, $A_{L\pm2,L} = -[2(L + 2) + 1]\mathfrak{F}\begin{pmatrix} L & 2 & L\pm2 \\ 0 & 0 & 0 \end{pmatrix}^2$. The unit matrix of eq A1 is multiplied by $k = (\omega - \omega_0) - iT_2^{-1}$; $\mathbf{C}$ is a column vector of the coefficients $C_{0,0}{}^L$, and $\mathbf{U}$ is a column vector where $U_L = \delta(L,0)$. Let us partition $\mathbf{A}$ as

$$\mathbf{A} = \begin{pmatrix} A_{0,0} & \mathbf{A}^{0,P} \\ \mathbf{A}^{P,0} & \mathbf{A}^{P} \end{pmatrix} \tag{A2}$$

where $A_{0,0}$ is the first diagonal element of $\mathbf{A}$. Then let $\mathbf{t}$ define the transformation which diagonalizes $\mathbf{A}^P$; $\mathbf{t}^{-1}\mathbf{A}^P\mathbf{t} = a$. Note that $\mathbf{A}^P$ is symmetrized by the similarity transformation

$$\mathbf{S}^{-1}\mathbf{A}^P\,\mathbf{S} = \hat{\mathbf{A}}^P \tag{A3}$$

where $\mathbf{S}$ is a diagonal matrix with elements $S_{L,L} = [2L + 1]^{1/2}$. Specifically $\hat{A}_{L,L\pm2} = [(2L + 1)^{-1} \times (2[L \pm 2] + 1)]^{1/2}A_{L,L\pm2}$ while $\hat{A}_{L,L} = A_{L,L}$. Then we may write $\mathbf{t} = \mathbf{SO}$ where $\mathbf{O}$ is the complex orthogonal transformation (*i.e.*, $\mathbf{O}^{-1} = \mathbf{O}^{tr}$) which diagonalizes $\hat{\mathbf{A}}^P$. If we define $\mathbf{T}$ as partitioned according to eq A2 by

$$\mathbf{T} \equiv \begin{pmatrix} 1 & 0 \\ 0 & \mathbf{t} \end{pmatrix} \tag{A4}$$

then by transforming eq A1 by $\mathbf{T}$ and solving for $C_{0,0}{}^0$ we obtain

$$C_{0,0}{}^0 = [(A_{0,0} + k) - A_{0,2}A_{2,0}\sum_{L>0}^{n} O_{2,L}(a_L + k)^{-1}O^{-1}{}_{L,2}]^{-1} \tag{A5}$$

Note that if $|A_{n,n} - A_{n-2,n-2}| \gg |\hat{A}_{n,n-2}|$, then in the diagonalization by $\mathbf{O}$, the nth coefficient $C_{0,0}{}^n$ will mix in very weakly with $C_{0,0}{}^2$, so that $O_{2,n}$ and $O_{n,2}{}^{-1}$ are very small. Thus unless $(a_n + k)^{-1}$ is unusually large (*e.g.*, a resonance) we can neglect its contribution to $C_{0,0}{}^0$ compared to the other terms in eq A6. Since, $A_{L,L} > A_{L-2,L-2}$ for both the real and imaginary parts, we expect that $a_n > a_{n-2}$. We can then terminate the expansion with reasonable confidence when the above inequality is fulfilled. This is undoubtedly too strong

a condition, because we have not considered the chain whereby $C_{0,0}^{n}$ couples *via* $C_{0,0}^{n-2}$, $C_{0,0}^{n-4}$, ... to $C_{0,0}^{2}$, which further reduces the magnitude of $O_{2,n}$.

Now

$$A_L - A_{L+2} = +iR(4L + 6) + \mathfrak{F}(2L + 3)^{-1}\left[\frac{(L + 2)(L + 3)}{(2L + 7)} - \frac{L(L + 1)}{(2L - 1)}\right]$$

while $\hat{A}_{L,L+2} = \mathfrak{F}[(2L + 1)(2L + 5)]^{1/2}\begin{pmatrix} L+2 & L & 2 \\ 0 & 0 & 0 \end{pmatrix}^2$. It is sufficient to consider just $+Im(A_L - A_{L+2})$ in place of $|A_L - A_{L+2}|$. Thus we want

$$\frac{|\mathfrak{F}|}{R} < \frac{4n + 6}{[(2n + 1)(2n + 5)]^{1/2}}\begin{pmatrix} n+2 & n & 2 \\ 0 & 0 & 0 \end{pmatrix}^{-2} \xrightarrow{n \text{ large}} \frac{8}{3}(4n + 6) \quad \text{(A6)}$$

(*e.g.*, for $n = 12$ we have $|\mathfrak{F}|/R < 143$) as a reasonable guide to convergence. We have found from the computer simulations that for $|\mathfrak{F}|/R = 100$ a value of $n = 12$ is sufficient. Also, these criteria are found to carry over into the more complex cases studied.

When a rotationally invariant T_2^{-1} is introduced, it both increases the value of $(A_{0,0} + k)$ in eq A6 while reducing *all* values of $(a_L + k)^{-1}$ in the summation term of this equation. It thus reduces the importance of each term in the summation by the factor $A_{0,0}a_L/(A_{0,0} + k)\cdot(a_L + k)$. Finally as ω (or ω_0 in a field sweep) is swept away from resonance, thus increasing k, one again gets a suppression of the summation terms, *except for resonances* that appear for $Im(a_L + k) = 0$ (as well as coupled resonances of these terms with the $(A_{0,0} + k)$ term). The effect of these resonances is found to yield spurious "local peaks" when the cut-off value, n is too small for a good approximation.

We note that if the above diagonalization scheme is applied to the *full* **A** matrix, one then obtains solutions of $C_{0,0}^{0}$ in the form of a superposition of Lorentzians

$$Im(C_{0,0}^{0}) = Im\sum_{L=0}^{n}(O_{0,L})^2(a_{LL} + k)^{-1} \quad \text{(A7)}$$

where the terms in eq A7 are defined as before but now as applied to **O** diagonalizing the full **A**. This procedure (for the case of only secular terms) is similar to the approach of Korst and Lazarev.[6] Similar diagonalizations should be appropriate for the more complex cases. (Note that to the extent $O_{0,L}$ is complex, there will be "dispersion-shaped" components in the absorption.)

Appendix B

The Two-Jump Case and Saturation. A two-jump modulation of $\mathcal{H}_1$ is assumed, such that

$$\mathcal{H}_1(i) = \mathfrak{F}(i)[S_z + {}^1/_2(S_+ + S_-)] \quad \text{(B1)}$$

where $\mathfrak{F}(1) = -\mathfrak{F}(2) = \mathfrak{F}$ a real quantity. A simple two-level esr transition is considered.

In the space of the two jumps

$$\Gamma = \begin{pmatrix} +\omega_J & -\omega_J \\ -\omega_J & +\omega_J \end{pmatrix} \quad \text{(B2)}$$

where ω_J is the mean jump rate between the two sites, and clearly $P_0(1) = P_0(2) = {}^1/_2$. We now write eq 53 and 50 for this case, but in the form appropriate *before the substitution* of eq 18 is made (*cf.* eq 16)

$$(n\omega - \omega_0 + (-)^i\mathfrak{F} - i\omega_J)Z^{(n)}(i) + i\omega_e Z^{(n)}(j) + dY^{(n-1)}(i) - (-)^{i1}/_2\mathfrak{F}[Y^n(i) - q\omega_0\delta(n,0)] = {}^1/_2q\omega_0 d\delta(n,1) \qquad (i \neq j) \quad \text{(B3)}$$

and

$$({}^1/_2n\omega - {}^1/_2i\omega_J - iW_e)Y^n(i) + {}^1/_2i\omega_J Y^n(j) = d(Z^{(n+1)}(i) - Z^{(1-n)*}(i)) + (-)^{i1}/_2\mathfrak{F}(Z^{(n)}(i) - Z^{(-n)*}(i)) \qquad (i \neq j) \quad \text{(B4)}$$

Note that we have let $Y^{(n)}(i) \equiv \chi_{\lambda^+}{}^{(n)} - \chi_{\lambda^-}{}^{(n)}$, and we have dropped the λ_j and $\lambda_{j\pm}$ subscripts for this single transition. A rotationally invariant electron spin flip rate, W_e has been introduced.

The eigenfunctions of eq B2 are just the sum and difference of the two-jump sites with eigenvalues of zero and $-2\omega_J$, respectively. Thus we introduce the sum and difference modes

$$Z^{(n)}(\pm) = Z^{(n)}(1) \pm Z^{(n)}(2) \quad \text{(B5a)}$$

$$Y^{(n)}(\pm) = Y^{(n)}(1) \pm Y^{(n)}(2) \quad \text{(B5b)}$$

and rewrite eq B3 and B4 as

$$(n\omega - \omega_0)Z^{(n)}(+) - \mathfrak{F}Z^{(n)}(-) + dY^{(n-1)}(+) + {}^1/_2\mathfrak{F}Y^{(n)}(-) = q\omega_0 d\delta(n,1)$$

$$(n\omega - \omega_0 - 2i\omega_J)Z^{(n)}(-) - \mathfrak{F}Z^{(n)}(+) + dY^{(n-1)}(-) + {}^1/_2\mathfrak{F}Y^{(n)}(+) = -\mathfrak{F}q\omega_0\delta(n,0)$$

and

$$({}^1/_2n\omega - iW_e)Y^n(+) = -d(Z^{(n+1)}(+) - Z^{(-n+1)*}(+)) - {}^1/_2\mathfrak{F}(Z^{(n)}(-) - Z^{(-n)*}(-)) \quad \text{(B6a)}$$

$$({}^1/_2n\omega - i\omega - iW_e)Y^n(-) = -d(Z^{(n+1)}(-) - Z^{(-n+1)*}(-)) - {}^1/_2\mathfrak{F}(Z^{(n)}(+) - Z^{(-n)*}(+)) \quad \text{(B6b)}$$

The spectrum is given by $ImZ^{(1)}(+)$. In the absence of saturation, the secular term in $\mathcal{H}_1$ (proportional to $\mathfrak{F}$ in eq B5) couple $Z^{(n)}(+)$ with $Z^{(n)}(-)$, and the extent of coupling depends on the ratio $|\mathfrak{F}/2\omega_J|$. (This is seen by comparing the off-diagonal elements with the differences in diagonal elements for the matrix of the coupled equations of B5 and B6.) The non-secular terms (proportional to $\mathfrak{F}/2$ in eq B5 and B6)

couple the $Z^{(n)}(\pm)$ with the $Y^{(n)}(\pm)$ by eq B5, while the $Y^{(n)}(\mp)$ are coupled to both $Z^{(n)}(\pm)$ and $Z^{(-n)*}(\pm)$ by eq A6b. The extent of these latter couplings depends essentially on the ratios $\mathfrak{F}/|n\omega + 2ik\omega_J|$ and $\mathfrak{F}/|3n\omega + 2ik\omega_J|$, respectively (with $k = 1$ or 2 depending on whether one has $Z^{(n)}(+)$ or $Z^{(n)}(-)$), where we want $\omega \sim \omega_0$. For small values of $\mathfrak{F}/2\omega_J$, relaxation theory suffices.

In the presence of saturation, the interaction with the radiation term leads to a coupling of $Z^{(n)}(\pm)$ to $Y^{(n-1)}(\pm)$ (*via* eq B5), and the $Y^{(n-1)}(\pm)$ are coupled to $Z^{(n)}(\pm)$ and $Z^{(-n+2)*}(\pm)$ *via* eq B6. Here the extent of coupling depends on the ratios $|\omega_1|/|(n+1)\omega - 2\omega_0 + 2iW_e|$ and $|\omega_1|/|(-n+3)\omega - 2\omega_0 - 2iW_e|$, respectively, for the plus signs (with $W_e \rightarrow W_e - \omega_J$ for the minus signs), and we have taken W_e to be small. Thus in the high-field saturation case where $|\omega_1/\omega_0| \ll 1$, the $Z^{(1)}(\pm)$ and $Y^{(0)}(\pm)$ terms are dominant. The $Z^{(0)}(\pm)$ and $Y^{(1)}(\pm)$ terms coupled in by $\mathfrak{IC}_1$ must also be considered. Also we are neglecting $Z^{(-1)*}(\pm)$, since $|\mathfrak{F}/3\omega_0|$ is assumed small.

1. Neglect of Nonsecular Terms, but $W_e \neq 0$. Equations B5 and B6 need only be written for $Z^{(1)}(\pm)$ and $Y^0(\pm)$ for this case. The solution for $Z^{(1)}(+)$ is given by

$$\left[(\omega - \omega_0)\left(1 - \frac{\mathfrak{F}^2}{S}\right) - i2\omega_J\mathfrak{F}^2/S\right]Z^{(1)}(+) + 2d^2\left[\frac{1}{W_e} + \frac{\mathfrak{F}^2}{S}\frac{1}{\omega_J + W_e}\right]Z^{(1)}(+)'' = q\omega_0 d \quad \text{(B7)}$$

where

$$S = (\omega - \omega_0)^2 + 4\omega_J{}^2[1 + d^2/\omega_J(\omega_J + W_e)] \quad \text{(B7a)}$$

The resonance frequenci(es) and width(s) are obtained from the coefficient of $Z^{(1)}(+)$ in eq B7, while the saturation parameter or T_1 appears in the coefficient of $Z^{(1)}(+)''$. In the motional narrowing region, where $\mathfrak{F}^2/\omega_J{}^2 \ll 1$, we have $\mathfrak{F}^2/S \ll 1$, and we may set $(\omega - \omega_0)^2 \approx 0$ in eq B7a for S for the region of resonance. We then get a single line at $\omega = \omega_0$; with

$$T_2{}^{-1} = \mathfrak{F}^2/\{2\omega_J[1 + d^2/\omega_J(\omega_J + W_e)]\} \quad \text{(B8a)}$$

and

$$T_1{}^{-1} = (2W_e) \quad \text{(B8b)}$$

Thus T_2 can be affected by the strength of the radio-frequency field. The slow motional region ($\mathfrak{F}^2/\omega_J{}^2 \gg 1$) is recovered by first letting $\omega_J = 0$, and solving for the zeroes in the coefficient of $Z^{(1)}(+)$ which are, of course, $\omega - \omega_0 = \pm\mathfrak{F}$. Then we let $(\omega - \omega_0)^2 = \mathfrak{F}^2$ in eq B7a. This yields, for each of the two distinct resonance lines

$$T_2{}^{-1} = 2\omega_J[1 + 4d^2\omega_J/\mathfrak{F}^2(\omega_J + W_e)]^{-1} \quad \text{(B9a)}$$

$$T_1 = (2W_e)^{-1}\left[1 + \left(\frac{W_e}{\omega_J + W_e}\right) \times \left(1 + \frac{4d^2\omega_J}{\mathfrak{F}^2(\omega_J + W_e)}\right)^{-1}\right] \quad \text{(B9b)}$$

Again it is possible for a large d^2 to affect the relaxation times. Note that for $W_e \gg \omega_J$ (and small enough d^2), $T_1 = W_e{}^{-1}$ and is thus twice as long as the motional narrowing result of eq B8b.

2. Nonsecular Terms Included and $W_e = 0$. We now must include contributions from $Z^{(1)}(\pm)$, $Y^{(0)}(\pm)$, $Z^{(0)}(\pm)$, and $Y^{(1)}(\pm)$, and we neglect all other harmonics. It is useful to employ the other high-field condition: $\mathfrak{F}^2/\omega_0{}^2 \ll 1$, to facilitate the solution, which after some algebra (and an important assumption; see below) is

$$\left[\Delta\omega_0'' - \frac{\mathfrak{F}^2}{S}\Delta\omega_0' - ia_\omega - 2i\omega_J\frac{\mathfrak{F}^2}{S}\right]Z^{(1)}(+) + 2d^2\left[\frac{\mathfrak{F}^2}{\omega_J S} + a(\omega_0)^{-1}\right]Z^{(1)}(+)'' = q\omega_0 d \quad \text{(B10)}$$

where

$$a(\omega_0) = \frac{\mathfrak{F}^2\omega_J}{\omega_0{}^2 + 4\omega_J{}^2} \quad \text{(B10a)}$$

$$S = \Delta\omega_0'{}^2 + 4\omega_J{}^2(1 + d^2/\omega_J{}^2) \quad \text{(B10b)}$$

$\Delta\omega_0' = \omega - \omega_0 - \mathfrak{F}^2/2\omega$, and $\Delta\omega_0'' = \omega_0 - \omega_0 - (\omega/2\omega_J)\cdot a(\omega)$. The imaginary term $ia(\omega)$ in the coefficient of $Z^{(1)}(+)$ in eq B10 gives the nonsecular contribution to the width according to eq B10a (for $\omega \sim \omega_0$). This is a well-known result from relaxation theory, but it is obtained in the present case *without any assumptions regarding the magnitude* of $\mathfrak{F}^2/\omega_J{}^2$. This is also true for the T_1 contribution of $^1/_2a(\omega_0)^{-1}$ in the coefficient of $Z^{(1)}(+)''$ (but see below). The associated dynamic frequency shift is $(\omega/2\omega_J)a(\omega)$. The terms in eq B10 shown explicitly with $\mathfrak{F}^2$ all arise from the secular contribution (compare eq B7). The motional narrowing result, wherein we have $\mathfrak{F}^2/\omega_J{}^2 \ll 1$, and $\mathfrak{F}^2/S \ll 1$ is obtained as in case 1, and we neglect the small dynamic frequency shifts. Then we have for the single line at $\omega \cong \omega_0$

$$T_2{}^{-1} = \mathfrak{F}^2/\{2\omega_J[1 + d^2/\omega_J{}^2]\} + a(\omega_0) \quad \text{(B11a)}$$

and

$$T_1{}^{-1} = 2a(\omega_0) \quad \text{(B11b)}$$

The dependence of T_2 on the strength of the saturating field is equivalent to the result discussed by Abragam[18] and Bloch[19] for the case of a "viscous liquid" where $\mathfrak{F}^2/4\omega_J{}^2 \ll 1$, but $d^2/\omega_J{}^2 \gtrsim 1$. The methods of this paper (including rotational diffusion) allow for solu-

(18) A. Abragam, "The Principles of Nuclear Magnetism," Oxford University Press, London, 1961, Chapter XII.

(19) F. Bloch, *Phys. Rev.*, **105**, 1206 (1957).

tions even when $\mathfrak{F}^2/4\omega_J^2$ is not small. When $\mathfrak{F}^2/4\omega_J^2 \gg 1$, *i.e.*, slow motion (and we let $d^2/\mathfrak{F}^2 \ll 1$), then one has two lines at $\Delta\omega_0' = \pm\mathfrak{F}$ each having $T_2^{-1} = 2\omega_J$ and $T_1^{-1} = 2a(\omega_0)$ with $T_1 \gg T_2$. Thus T_1 is given by the second-order relaxation theory result even though the condition for validity of the theory no longer applies.

An important assumption was made in the above in order to guarantee relaxation to equilibrium. The nature of this assumption can more clearly be seen by writing the solution for the case where the secular terms have been omitted with $W_e \neq 0$, but small. Then one has

$$[\Delta\omega_0'' - ia(\omega)]Z^{(1)}(+) + dY^{(0)}(+) = q\omega_0 d \quad \text{(B12a)}$$

and

$$dZ^{(1)}(+)'' = {}^1/_2a(\omega_0)[Y^{(0)}(+) - q\omega_0] + {}^1/_2W_eY^{(0)}(+) \quad \text{(B12b)}$$

In eq B12b we see that $a(\omega_0)$ plays a role identical with W_e in causing spin relaxation except for the term in $q\omega_0 = (P_b)_0 - (P_a)_0$ (the difference in spin populations at equilibrium). That is, $Y^{(0)}(+) - q\omega_0 = \rho_{aa} - \rho_{bb}$ and the effect of $a(\omega_0)$ in eq B12b is to tend to relax the spins to infinite temperature (where $(P_b)_0 = (P_a)_0$) rather than to the proper thermal distribution. This is the well-known fundamental difficulty in semiclassical relaxation theories, which in the present method may be overcome in a manner analogous to those theories by letting $Y^{(0)}(+) + q\omega_0 \rightarrow Y^{(0)}(+)$ for such terms (where we are assuming a high temperature approximation) and the equivalent has also been done in section IIIB. The question remains of a rigorous justification for such an *ad hoc* assumption for small ω_J (hence small $a(\omega_0)$) when a rigorous spin relaxation theory approach is no longer applicable.[20] We note, however, that should the extra term in $q\omega_0$ be included, it would affect an unsaturated as well as a saturated line shape equally and merely in their *absolute* intensities. That is from eq B12 one has

$$[\Delta\omega'' - ia(\omega)]Z^{(1)}(+) + \frac{2d^2}{a(\omega_0) + W_e}Z^{(1)}(+)'' = q\omega_0 d\left[1 - \frac{a(\omega_0)}{a(\omega_0) + W_e}\right]$$

so the *relative* intensity changes due to the onset of saturation are unaffected by the assumption, and for small enough $a(\omega_0) \ll W_e$, even the absolute effects become negligible.

Discussion

J. HARRIMAN. Can you handle anisotropic rotation? What will the effect be?

J. FREED. Yes. Let me illustrate with the case of axially symmetric rotational diffusion. For this case the eigenfunctions for eq 23 are still the Wigner rotation matrices: $D_{KM}^{L}(\Omega)$ but now with eigenvalues

$$E_m = E_{L,K,M} = R_xL(L+1) + (R_z - R_x)K^2$$

with $R_x = R_y$ and R_z the principal values of the diffusion tensor and the molecular z axis as the axis of symmetry. If the z axis also corresponds to a principal axis of the g and dipolar tensors, then it is an almost trivial matter to correct the equations in our paper for effects of such diffusion. One then sees that the K-dependent term in $E_{L,K,M}$ will only affect the spectrum if $g_x \neq g_y$ and/or the dipolar terms $D_i^{(\pm 2)} \neq 0$.

When the rotational diffusion is asymmetric, the proper eigenfunctions for eq 23 become linear combinations of spherical harmonics (see J. H. Freed, *J. Chem. Phys.*, **41**, 2077 (1964), for further details), and while the method applies, the equations constituting a solution to the spectrum become more complex though tractable.

We might note that a situation like $R_z \gg R_x$, or the reverse inequality, allows for the interesting possibility that there is fast tumbling about one axis, while there is slow tumbling about another.

O. H. GRIFFITH. In your calculations of rotational correlation times, are there any other parameters in addition to the intrinsic line width and the principal values of the hyperfine and g tensors?

J. FREED. No. A particular calculated spectrum is determined solely by the rotational diffusion coefficient R, an intrinsic line width, and the principal values and axes of the hyperfine and g tensors.

In our experimental studies (S. Goldman, G. Bruno, C. Polnaszek, and J. H. Freed, *J. Chem. Phys.*, in press) we find that the intrinsic line widths needed to get good agreement between the computed and experimental spectra are temperature dependent, *e.g.*, essentially zero in the faster tumbling regions to a few gauss in the near-rigid and rigid regions.

D. LENIART. Since the esr line shape depends critically upon the pseudo-secular contribution of the dipolar interaction, do you feel that it would be advantageous to study these slow tumbling systems by multiple resonance techniques such as Electron-Electron Double Resonance (Eldor) to extract more *explicit experimental* data?

J. FREED. I think our predicted spectra showing effects of saturation on slow tumbling line shapes encourages one to think that useful information may be obtained by saturation studies. J. S. Hyde has independently come to similar conclusions from his experimental work. Eldor would certainly be a means of extending such studies, and we plan to develop appropriate solutions utilizing the approach given in our paper.

D. E. WOOD. How much computer time is required to fit a series of spectra from slow to fast limit, for say a nitroxide radical?

J. FREED. The following are typical computer times for the nitroxidelike spectra, $I = 1$, $S = {}^1/_2$, given in our paper: 575, 350, and 200 sec for F/R values of 100, 15, and 3, respectively. The computer is an IBM 360/65 and the Gaussian elimination method was used. We anticipate order of magnitude reductions in computer time when we have converted our method of solution to diagonalization by the QR transform method, since only one diagonalization per F/R value is required to obtain the whole spectrum. Further reductions in time may be possible by utilizing more modern iterative computer methods.

(20) That $a(\omega_0)$ still represents a relaxation mechanism resulting from modulation of the nonsecular terms even by a small ω_J, can be illustrated in a manner analogous to that discussed by Abragam for scalar relaxation of the second kind (ref 18, p 312). For the present case one may formally let $\mathfrak{F} = 2AI_z(t)$ where $I = {}^1/_2$ and assume $I_z(t)$ is rapidly equilibrated. The process modulating $I_z(t)$ must have a white spectrum up through frequencies of the order of ω_0 in order to recover eq B10a.

Spin-Restricted SCF–CI Theory and Calculations of Contact Hyperfine Splittings[1]

by Gershon Vincow[2]

Department of Chemistry, University of Washington, Seattle, Washington 98105 *(Received January 25, 1971)*

Publication costs assisted by the Petroleum Research Fund and the National Science Foundation

The nonempirical spin-restricted SCF–CI method is applied to π-electron free radicals. Calculation of the coefficients of the configurations using Rayleigh–Schrodinger perturbation theory leads to a general expression for the spin density at a magnetic nucleus. The expression to second order is discussed. The quantitative validity of the related semiempirical equations, such as the McConnell equation, is also discussed. Variational calculations using a variety of STO basis sets were performed for $CH_3\cdot$ and $CH\cdot$. The results for the ^1H and ^{13}C contact hyperfine splittings are discussed. Comparison is made with the semiempirical INDO method for the calculation of hyperfine splittings.

I. Introduction

This paper concerns nonempirical calculations of ^1H and ^{13}C contact hyperfine splittings of π-electron free radicals. These calculations were motivated by an interest in the following questions. (1) What is the nature of the wave function required for an accurate calculation of the hyperfine splittings? (2) Can nonempirical calculations serve as a useful check on semiempirical results? (3) What is the quantitative validity of those relationships, such as the McConnell equation and the Karplus–Fraenkel equation, which have established the nuclear hyperfine splittings as experimental probes of the π-electron spin distribution?

II. General Theory

The Fermi contact hyperfine splitting of nucleus N can be calculated from

$$a^N = \frac{8\pi}{3} g_e g_N \beta_e \beta_N \gamma(\mathbf{r}_N) \qquad (1)$$

where g_e and g_N are the electron and nuclear g factors, β_e and β_N are the Bohr and nuclear magnetons, and $\gamma(\mathbf{r}_N)$, the spin density at the nucleus, is given by[3]

$$\gamma(\mathbf{r}_N) = \left\langle \psi \middle| \sum_k (S_z)^{-1} \mathbf{S}_{zk} \delta(\mathbf{r}_k - \mathbf{r}_N) \middle| \psi \right\rangle \qquad (2)$$

In eq 2 ψ denotes the exact ground-state wave function, $\mathbf{S}_{zk}$ is the spin operator acting on electron k, $\mathbf{r}_k$ and $\mathbf{r}_N$ denote the electron and nuclear positions, and the summation is over all electrons. Physically, $\gamma(\mathbf{r}_N)$ is just the net density of electron spin at a position in space $\mathbf{r}_N$, *i.e.*, the number of electrons/(Bohr)^3 with spin α minus the number of electrons/(Bohr)^3 with spin β.

To calculate splittings suitable for comparison with experiment, one must include in eq 2 statistical averaging over the thermally populated vibronic states.[4] In this paper we will consider only the electronic part of the wave function, ψ_{el}, in the Born–Oppenheimer scheme. Experimental splittings will be "corrected," if necessary, to extract the electronic contribution for comparison with the calculations.

There are many approaches to the calculation of ψ_{el}. Here the spin-restricted nonrelativistic SCF plus configuration-interaction (CI) method will be employed. The coefficients of the various configurations can readily be calculated for a particular molecule using the variation method. This method was employed for the calculations of $CH_3\cdot$ and $CH\cdot$ discussed in section IV.

III. Perturbation Theory

A general expression for the hyperfine splitting can be obtained using perturbation theory to calculate the coefficients of the configurations. Rayleigh–Schrodinger double perturbation theory[5] using the Epstein–Nesbet partitioning[6] has been previously employed to calculate $\gamma(\mathbf{r}_N)$, a first-order property, to first[7] and second[8] orders in the electron–electron repulsion perturbation.

A. First Order. We begin with the first-order expression in order to introduce the relationships between splittings and π-electron spin distribution.

The dominant term in the wave function is the restricted SCF determinant

(1) Acknowledgment is made to the donors of the Petroleum Research Fund of the American Chemical Society and to the National Science Foundation for partial support of this research.

(2) This paper was written, in part, while the author was an NSF Senior Postdoctoral Fellow at Harvard University. The hospitality of Professor Martin Karplus is gratefully acknowledged.

(3) The δ function form for the spin density operator is an approximation; see S. M. Blinder, *Advan. Quantum Chem.*, **2**, 47 (1965), and references cited therein for a discussion of this point.

(4) S. Y. Chang, E. R. Davidson, and G. Vincow, *J. Chem. Phys.*, **52**, 5596 (1970).

(5) J. O. Hirschfelder, W. B. Brown, and S. T. Epstein, *Advan. Quantum Chem.*, **1**, 255 (1964).

(6) P. Claverie, S. Diner, and J. P. Malrieu, *Int. J. Quantum Chem.*, **1**, 751 (1967).

(7) (a) H. M. McConnell and D. B. Chesnut, *J. Chem. Phys.*, **28**, 107 (1958); (b) A. D. McLachlan, H. H. Dearman, and R. Lefebvre, *ibid.*, **33**, 65 (1960); (c) S. Y. Chang, E. R. Davidson, and G. Vincow, *ibid.*, **49**, 528 (1968).

(8) J.-P. Malrieu, *ibid.*, **46**, 1654 (1967).

$$\psi^{(0)} = |\phi_1(1)\bar{\phi}_1(2)\cdots\phi_{k-1}(2k-3)\times \bar{\phi}_{k-1}(2k-2)\phi_k(2k-1)| \quad (3)$$

where $\{\phi_j\}_{j=1}^{k-1}$ denote the doubly occupied molecular orbitals, ϕ_k is the singly occupied SCFMO, and $\{g_m\}_{m=k+1}^{\infty}$ are a set of functions which taken with the $\{\phi_i\}_{i=1}^{k}$ form a complete orthonormal set. The most convenient choice for the g_m are the virtual SCFMO's.

In the first order only configurations arising from single replacements $\phi_j \rightarrow g_m$ will contribute to the hyperfine splitting. Two such doublets can be formed. The conventional choice of spin functions for the $\phi_j g_m \phi_k$ portion of these configurations is

$$[2]^{-1/2}(\alpha\beta\alpha - \beta\alpha\alpha) \quad (4)$$

and

$$[6]^{-1/2}(\alpha\beta\alpha + \beta\alpha\alpha - 2\alpha\alpha\beta) \quad (5)$$

We have extended the previous derivations[7a,b] by removing the restriction of σ–π separability and considering an arbitrary choice of spin eigenfunctions.[7c] The configurations are described by

$$\psi_{pjm} = [2(1+\mu_p+\mu_p^2)]^{-1/2}(|a\rangle - \mu_p|b\rangle) \quad (p = 1, 2) \quad (6)$$

where

$$|a\rangle = |\phi_1(1)\bar{\phi}_1(2)\cdots\phi_j(2j-1)\bar{g}_m(2j)\cdots \phi_k(2k-1)| - |\phi_1(1)\bar{\phi}_1(2)\cdots \bar{\phi}_j(2j-1)g_m(2j)\cdots\phi_k(2k-1)| \quad (7)$$

$$|b\rangle = |\phi_1(1)\bar{\phi}_1(2)\cdots\bar{\phi}_j(2j-1)g_m(2j)\cdots \phi_k(2k-1)| - |\phi_1(1)\bar{\phi}_1(2)\cdots \phi_j(2j-1)g_m(2j)\cdots\bar{\phi}_k(2k-1)| \quad (8)$$

$$\mu_2 = -(\mu_1+2)/(2\mu_1+1) \quad (9)$$

so that

$$\langle\psi_{1jm}|\psi_{2jm}\rangle = 0 \quad (10)$$

Using first-order perturbation theory to compute the coefficients of the configurations ψ_{pjm}, the spin density at a magnetic nucleus is

$$\gamma(\mathbf{r}_N) = \phi_k^2(\mathbf{r}_N) + \sum_{m,j}\left\{\sum_p 3\mu_p^2/4(1+\mu_p+\mu_p^2)\Delta E_{pjm}\right\}\times [g_m\phi_k|\phi_k\phi_j]\phi_j(\mathbf{r}_N)g_m(\mathbf{r}_N) \quad (11)$$

where the SCFMO's are assumed real, the expression in square brackets is a conventional exchange integral and

$$\Delta E_{pjm} = \langle\psi_{pjm}|\mathcal{H}|\psi_{pjm}\rangle - \langle\psi^{(0)}|\mathcal{H}|\psi^{(0)}\rangle \quad (12)$$

Equation 11 is applicable to any free radical, *e.g.*, both "π" and "σ" types. The first term is the SCF contribution which is zero for planar π-electron radicals. In the remainder of this paper we will restrict ourselves to this case. The second term then has nonzero contributions only from excitations of the type $\sigma \rightarrow \sigma^*$.

The dependence of $\gamma(\mathbf{r}_N)$ on μ_p has been investigated by nonempirical calculations of ·CH fragment using a minimum basis set of Slater-type orbitals.[7c] A maximum variation of about 10% in the proton hyperfine splitting is found. This sensitivity, absent if a variational calculation is performed, is reduced by an order of magnitude if the calculation is carried out to second order. For the conventional choice of spin eigenfunctions ($\mu_1 = 0$, $\mu_2 = -2$) the second order and variation method results are essentially the same as those obtained using the first-order expression.

We therefore choose to simplify eq 11 using the choice of spin doublets given in eq 4 and 5. The contribution of ψ_{1jm} to the splitting is zero. For a planar π-electron radical

$$\gamma(\mathbf{r}_N) = \sum_{m,j}\frac{2[g_m\phi_k|\phi_k\phi_j]}{\Delta E_{2jm}}\phi_j(\mathbf{r}_N)g_m(\mathbf{r}_N) \quad (13)$$

There is no restriction in eq 13 as to the nature or completeness of the basis set used to expand the SCFMO's.

A connection between the first-order spin density at a magnetic nucleus and the zero-order (*i.e.*, SCF) spin distribution can readily be established.

The singly occupied SCFMO is expanded in an atomic orbital representation, $\{\chi_t\}$

$$\phi_k = \sum_t c_{tk}\chi_t \quad (14)$$

Then the zero-order spin density function is

$$\gamma^{(0)}(\mathbf{r}) = \phi_k^2(\mathbf{r}) = \sum_{t,t'}\gamma_{t,t'}^{(0)}\chi_t(\mathbf{r})\chi_{t'}^*(\mathbf{r}) \quad (15)$$

where

$$\gamma_{tt'}^{(0)} = c_{tk}c_{t'k} \quad (16)$$

are the elements of the spin density coefficient matrix.

Substituting eq 14 and 16 into eq 13 and multiplying by the appropriate constants given in eq 1

$$a^N = \sum_{t,t'}\frac{8\pi}{3}g_e\beta_e g_N\beta_N\sum_{m,j}\left\{\frac{2[g_m\chi_{t'}|\chi_t\phi_j]}{\Delta E_{2jm}}\times \phi_j(\mathbf{r}_N)g_m(\mathbf{r}_N)\right\}\gamma_{tt'}^{(0)} \quad (17)$$

$$= \sum_{tt'}G_{t't}^{N}\gamma_{tt'}^{(0)} = tr(\mathbf{G}^N\boldsymbol{\gamma}^{(0)}) \quad (18)$$

1. Proton Hyperfine Splitting: McConnell Equation. An important and useful equation was proposed by McConnell for the case of proton hyperfine splitting of π-electron radicals. This can be viewed as a simplification of eq 17.

It is assumed that the π electrons are described using a minimum basis set. A particular proton (denoted p) is bonded to the carbon atom bearing the 2p–π atomic orbital χ_p. All terms in the double sum of eq 18 are neglected relative to $G_{pp}^{H}\gamma_{pp}^{(0)}$. It is further assumed

that G_{pp}^{H} is essentially a transferable constant among all positions in the molecule and among all hydrocarbon radicals. Using a semiempirical estimate, Q, for this constant we obtain

$$a_p^{H} = Q\gamma_{pp}^{(0)} = Qc_{pp}^{2} \tag{19}$$

or, in the conventional notation

$$a_p^{H} = Q\rho_{pp}^{\pi} \tag{20}$$

To the extent that the McConnell equation is valid, proton hyperfine splittings are an *experimental probe* of π "spin densities," $\gamma_{pp}^{(0)}$. Values of $\gamma_{pp}^{(0)}$ obtained from eq 19 should be compared with theoretical values readily computed from nonempirical minimum-basis SCF wave functions. These have not been available. Comparisons have instead been made using a variety of semiempirical π-electron theories (HMO, PPP–MO, McLachlan–MO, UHF–MO, VB). The concordance obtained in many cases has been interpreted as a critical test of the accuracy of these semiempirical theories.

A vast amount of esr data has been correlated using the McConnell proportionality. Therefore an interesting and important question to pose is the extent of its quantitative validity. This depends on (1) the validity of using a minimum basis set for the π electrons, (2) the size of the errors made in neglecting the various terms $G_{kk'}^{H}\gamma_{k'k}^{(0)}$ $(k \neq k')$ and in assuming the constancy of G_{pp}^{H}, and (3) the size of the error made in treating the splitting only to first order. These factors will be discussed in succeeding sections. It should be noted that such errors are partially compensated by the use of a semiempirical estimate for Q.

2. Other Nuclei. Relationships similar to the McConnell proportionality have also been developed for other nuclei such as ^{13}C, ^{14}N, and ^{17}O.[9-11] Thus the corresponding splittings have also been used as experimental probes of the spin distribution in π-electron radicals. For example, the Karplus–Fraenkel equation expresses the ^{13}C splitting on carbon p in terms of π spin densities on atom p and its nearest neighbors and on semiempirical constants. This equation can be viewed as corresponding to the following simplification of eq 18

$$a_p^{C} = G_{pp}^{C}\gamma_{pp}^{(0)} + \sum_i G_{ii}^{C}\gamma_{ii}^{(0)} \tag{21}$$

where i denotes the neighboring carbon atoms.

B. Second Order. Malrieu has extended the perturbation theory of the σ spin density to second order for the case of a planar π radical.[8] The σ part of the electronic wave function is limited to a single bonding (σ) and antibonding (σ^*) orbital localized on a CH bond. Thus this treatment should yield the main features of the results for proton splittings but must be extended to account for splittings of other nuclei.

The theory is developed in the space of all determinants with correct space symmetry and $M_s = +1/2$, rather than in terms of configurations which are S^2 eigenfunctions. The author states that this should introduce only a third-order error in the results. The unperturbed energies of all determinants with the same spatial configuration and different spin functions are taken to be the same.

That part of the wave function required for a calculation of $\gamma(\mathbf{r}_N)$ to second order is

$$\Psi_{el} = \psi^{(0)} + (C_{\sigma\to\sigma^*}^{(1)} + C_{\sigma\to\sigma^*}^{(2)})\psi_{\sigma\to\sigma^*} + C_{\pi\to\pi^*}^{(1)}\psi_{\pi\to\pi^*} + C_{\substack{\sigma\to\sigma^*\\ \sigma\to\sigma^*}}^{(1)}\psi_{\substack{\sigma\to\sigma^*\\ \sigma\to\sigma^*}} + C_{\substack{\sigma\to\sigma^*\\ \pi\to\pi^*}}^{(1)}\psi_{\substack{\sigma\to\sigma^*\\ \pi\to\pi^*}} \tag{22}$$

where $\psi^{(0)}$ is again a spin-restricted SCF determinant with orbitals of σ and π symmetry

$$\psi^{(0)} = |\sigma\bar{\sigma}\pi_1\bar{\pi}_1\cdots\pi_i\bar{\pi}_i\cdots\pi_0| \tag{23}$$

and the other terms symbolically represent the sum over all "excited" determinants of the various types. These are single replacements of σ and π orbitals, double replacement of σ orbitals, and a double replacement, $\sigma \to \sigma^*$ and $\pi \to \pi^*$. The coefficients of the determinants are designated $C^{(i)}$ where i is the order of pertubation theory employed in their calculation.

Results of Malrieu's second-order perturbation theory calculation for the spin density at a point $\mathbf{r}_N$ in the molecular plane are given below.[8] The first-order term is

$$2C_{\sigma\to\sigma^*}^{(1)}\langle\psi^{(0)}|\gamma|\psi_{\sigma\to\sigma^*}\rangle = 2\frac{[\sigma\pi_0|\pi_0\sigma^*]}{E(\sigma|\sigma^*)}\sigma(\mathbf{r}_N)\sigma^*(\mathbf{r}_N) \tag{24}$$

This is a special case of eq 13, where γ is the spin-density operator defined in eq 2 and where $E(\sigma|\sigma^*)$ denotes an unperturbed energy difference assumed equal for the three determinants with space part $\sigma\sigma^*\cdots\pi_i\pi_i\cdots\pi_0$. There are six second-order terms which are denoted by Roman numerals.

$$\text{(I)}\quad (C_{\sigma\to\sigma^*}^{(1)})^2\langle\psi_{\sigma\to\sigma^*}|\gamma|\psi_{\sigma\to\sigma^*}\rangle = \left[\frac{[\sigma\pi_0|\pi_0\sigma^*]}{E(\sigma|\sigma^*)}\right]^2[\sigma^2(\mathbf{r}_N) + \sigma^{*2}(\mathbf{r}_N)] \tag{25}$$

$$\text{(II)}\quad (C_{\substack{\sigma\to\sigma^*\\ \sigma\to\sigma^*}}^{(1)})^2\langle\psi_{\substack{\sigma\to\sigma^*\\ \sigma\to\sigma^*}}|\gamma|\psi_{\substack{\sigma\to\sigma^*\\ \sigma\to\sigma^*}}\rangle = 0 \tag{26}$$

$$\text{(III)}\quad 2(C_{\sigma\to\sigma^*}^{(1)})(C_{\substack{\sigma\to\sigma^*\\ \sigma\to\sigma^*}}^{(1)})\langle\psi_{\sigma\to\sigma^*}|\gamma|\psi_{\substack{\sigma\to\sigma^*\\ \sigma\to\sigma^*}}\rangle = 2\left[\frac{[\sigma\pi_0|\pi_0\sigma^*]}{E(\sigma|\sigma^*)}\right]\left[\frac{[\sigma\sigma|\sigma^*\sigma^*]}{E\begin{pmatrix}\sigma|\sigma^*\\ \sigma|\sigma^*\end{pmatrix}}\right]\sigma(\mathbf{r}_N)\sigma^*(\mathbf{r}_N) \tag{27}$$

(9) M. Karplus and G. K. Fraenkel, *J. Chem. Phys.*, **35**, 1312 (1961).

(10) T. Yonezawa, T. Kawamura, and H. Kato, *ibid.*, **50**, 3482 (1969), and references cited therein.

(11) M. Broze and Z. Luz, *ibid.*, **51**, 738 (1969).

$$\text{(IV)}\quad [C^{(1)}_{\substack{\sigma\to\sigma^*\\ \pi\to\pi^*}}]^2\langle\psi_{\substack{\sigma\to\sigma^*\\ \pi\to\pi^*}}|\gamma|\psi_{\substack{\sigma\to\sigma^*\\ \pi\to\pi^*}}\rangle =$$

$$\sum_{\pi_j^*}\Bigg[2\left\{\frac{[\sigma\pi_0|\pi_j^*\sigma^*]}{E\begin{pmatrix}\sigma & \sigma^*\\ \pi_0 & \pi_j^*\end{pmatrix}}\right\}^2\sigma^{*2}(\mathbf{r}_N) + 2\frac{[\sigma\pi_0|\pi_j^*\sigma^*][\sigma\pi_0|\sigma^*\pi_j^*]}{\left\{E\begin{pmatrix}\sigma & \sigma^*\\ \pi_0 & \pi_j^*\end{pmatrix}\right\}^2}(\sigma^2(\mathbf{r}_N) - \sigma^{*2}(\mathbf{r}_N))\Bigg] +$$

$$\sum_{\pi_i}\Bigg[2\left\{\frac{[\sigma\pi_i|\pi_0\sigma^*]}{E\begin{pmatrix}\sigma & \sigma^*\\ \pi_i & \pi_0\end{pmatrix}}\right\}^2\sigma^2(\mathbf{r}_N) - 2\frac{[\sigma\pi_i|\pi_0\sigma^*][\sigma\pi_i|\sigma^*\pi_0]}{\left\{E\begin{pmatrix}\sigma & \sigma^*\\ \pi_i & \pi_0\end{pmatrix}\right\}^2}(\sigma^2(\mathbf{r}_N) - \sigma^{*2}(\mathbf{r}_N))\Bigg] \quad (28)$$

Here π_j^* denotes the virtual SCFMO's of π symmetry. The terms summing over the π_j^* give the contribution from "excitations" of the type $\sigma \to \sigma^*$, $\pi_0 \to \pi_j^*$ while those summing over π_i represent the contribution from $\sigma \to \sigma^*$, $\pi_i \to \pi_0$ "excitations."

$$\text{(V)}\quad 2(C^{(1)}_{\substack{\pi\to\pi^*}})(C^{(1)}_{\substack{\sigma\to\sigma^*\\ \pi\to\pi^*}})\langle\psi_{\substack{\pi\to\pi^*}}|\gamma|\psi_{\substack{\sigma\to\sigma^*\\ \pi\to\pi^*}}\rangle =$$

$$\sum_{\pi_i}\sum_{\pi_j^*}2\left[\frac{[\pi_i\pi_0|\pi_0\pi_j^*]}{E(\pi_i|\pi_j^*)}\right]\left[\frac{[\sigma\pi_i|\pi_j^*\sigma^*]}{E\begin{pmatrix}\sigma & \sigma^*\\ \pi_i & \pi_j^*\end{pmatrix}}\right]\sigma(\mathbf{r}_N)\sigma^*(\mathbf{r}_N) \quad (29)$$

$$\text{(VI)}\quad 2(C^{(2)}_{\sigma\to\sigma^*})\langle\psi^{(0)}|\gamma|\psi_{\sigma\to\sigma^*}\rangle =$$

$$\sum_{\pi_i}\sum_{\pi_j^*}2\Bigg[\frac{[\sigma^*\pi_i|\pi_j^*\sigma][\pi_i\pi_0|\pi_0\pi_j^*]}{E(\sigma|\sigma^*)}\times\left\{[E(\pi_i|\pi_j^*)]^{-1} + \left[E\begin{pmatrix}\sigma & \sigma^*\\ \pi_i & \pi_j^*\end{pmatrix}\right]^{-1}\right\}\sigma(\mathbf{r}_N)\sigma^*(\mathbf{r}_N) +$$

$$\sum_{\pi_i}\sum_{\pi_j^*}2\frac{[\sigma\pi_0|\pi_0\sigma^*]}{E(\sigma|\sigma^*)}\sigma(\mathbf{r}_N)\sigma^*(\mathbf{r}_N)\Bigg[\frac{[\sigma\sigma|\sigma^*\sigma^*]}{E\begin{pmatrix}\sigma & \sigma^*\\ \sigma & \sigma^*\end{pmatrix}} + \frac{[\sigma\sigma^*|\sigma^*\sigma]}{E(\sigma|\sigma^*)} - \frac{\{[\sigma\pi_0|\pi_0\sigma] + [\sigma^*\pi_0|\pi_0\sigma^*]\}}{2E(\sigma|\sigma^*)}\Bigg] +$$

$$\sum_{\pi_j^*}2\Bigg[\frac{\{[\sigma\pi_0|\pi_j^*\sigma] - [\sigma^*\pi_0|\pi_j^*\sigma^*]\}}{E(\sigma|\sigma^*)}\times\left(\frac{[\sigma\pi_0|\sigma^*\pi_j^*]}{E\begin{pmatrix}\sigma & \sigma^*\\ \pi_0 & \pi_j^*\end{pmatrix}} - \frac{[\sigma\pi_0|\pi_j^*\sigma^*]}{E(\sigma|\sigma^*)}\right)\times\frac{\{2[\sigma\pi_0|\pi_j^*\sigma] + [\sigma^*\pi_0|\sigma^*\pi_j] - [\sigma\pi_0|\sigma\pi_j^*]\}}{E\begin{pmatrix}\sigma & \sigma^*\\ \pi_0 & \pi_j^*\end{pmatrix}}\Bigg]\times\sigma(\mathbf{r}_N)\sigma^*(\mathbf{r}_N) +$$

$$\sum_{\pi_i}2\Bigg[\frac{\{[\sigma^*\pi_0|\pi_i\sigma^*] - [\sigma\pi_0|\pi_i\sigma]\}}{E(\sigma|\sigma^*)}\times\left(\frac{[\sigma^*\pi_0|\sigma\pi_i]}{E\begin{pmatrix}\sigma & \sigma^*\\ \pi_i & \pi_0\end{pmatrix}} - \frac{[\sigma\pi_0|\pi_i\sigma^*]}{E(\sigma|\sigma^*)}\right)\times\frac{\{2[\sigma^*\pi_0|\pi_i\sigma^*] + [\sigma\pi_0|\sigma\pi_i] - [\sigma^*\pi_i|\sigma^*\pi_0]\}}{E\begin{pmatrix}\sigma & \sigma^*\\ \pi_i & \pi_0\end{pmatrix}}\Bigg]\times$$

$$\sigma(\mathbf{r}_N)\sigma^*(\mathbf{r}_N) \quad (30)$$

Thus to second order $\gamma(\mathbf{r}_N)$ is given by the sum of eq 24–30.

C. Discussion. 1. First-Order Contribution. It is quite clear from numerous estimates that the term $G_{pp}{}^H\gamma_{pp}{}^{(0)}$, which corresponds to the McConnell relationship, is typically the leading term in the first-order contribution to $\gamma(\mathbf{r}_H)$. Impetus for refinement of the McConnell equation has come from the data for even-alternant hydrocarbon cation and anion radicals.[12] Cation splittings are usually about 10–20% larger than those at corresponding ring positions in the anions. (A consistent exception occurs at the 2 position in the linear polyacenes where the anion splittings are larger. No theory has been proposed to date which accounts for these data.) Semiempirical π-electron theories predict equal values of $\gamma_{pp}{}^{(0)}$ for cation and anion (pairing theorem). Using the McConnell relationship and these theories one thus fails to account for the experimental differences in splitting.

Two extensions of the McConnell relationship have been proposed and have gained currency. The Colpa–Bolton (CB) relationship[13,14]

$$a_p{}^H = (Q_0 + K\epsilon_p{}^\pi)\rho_{pp}{}^\pi \quad (31)$$

corresponds to the elimination of the assumption that $G_{pp}{}^H$ is a constant.

A different proportionality factor $(Q_0 + K\epsilon_p{}^\pi)$ is used for each carbon p. This factor depends on the excess π charge density on that atom, $\epsilon_p{}^\pi \equiv 1 - q_p{}^\pi$ ($q_p{}^\pi$ is the total π-electron charge density on carbon p). The use of HMO theory, for which $\epsilon_p{}^\pi = \pm\rho_{pp}{}^\pi$ for cations and anions, and semiempirical parameters $Q_0 = -27$ G and $K = -12$ G lead to an improved concordance of theory with experiment.

Another two-parameter relationship which leads to improved results for the hydrocarbon ions is the Giacometti, Nordio, and Pavan (GNP) equation[15]

$$a_p{}^H = Q_0\rho_{pp}{}^\pi + Q_1(\rho_{p,p+1}{}^\pi + \rho_{p,p-1}{}^\pi) \quad (32)$$

This relationship corresponds to the inclusion of the nearest-neighbor "bond spin density" terms,

(12) G. Vincow, "Radical Ions," E. T. Kaiser and L. Kevan, Ed., Wiley, New York, N. Y., 1968, Chapter 4.

(13) J. R. Bolton, *J. Chem. Phys.*, **43**, 309 (1965).

(14) J. P. Colpa and J. R. Bolton, *Mol. Phys.*, **6**, 273 (1963); J. Higuchi, *J. Chem. Phys.*, **39**, 3455 (1963); K. G. Kay and H. J. Silverstone, *ibid.*, **46**, 2854 (1967).

(15) G. Giacometti, P. L. Nordio, and M. V. Pavan, *Theor. Chim. Acta*, **1**, 404 (1963).

$\sum_{p,p'} G_{pp'}{}^{H}\gamma_{p'p}{}^{(0)}$, subject to the simplification $G_{p,p\pm1} = G_{p\pm1,p}(Q_1 \sim 2G_{p,p+1})$. Using HMO theory $\rho_{p,p\pm1}{}^{\pi} = c_{0,p}c_{0,p\pm1}$, which are equal in magnitude and opposite in sign for cation and anion; the cations have the positive values. Thus provided $Q_1 < 0$, as is reasonable to expect, the GNP equation predicts the cation to have the larger splittings. Suggested semiempirical values of the parameters are $Q_0 = -31.5$ G and $Q_1 = -7.0$ G or $Q_0 = -27$ G and $Q_1 = -6.3$ G.

Moss and Fraenkel have made an in-depth assessment of the CB and GNP equations.[16] Using *HMO theory for* $\rho_{pp}{}^{\pi}$ *throughout*, these investigators find that (1) statistical analysis of the fit to the available experimental data shows that the CB correlation is to be preferred; (2) the GNP equation reduces to a simple form

$$a_p{}^{H} = (Q_0 + Q_1\lambda)\rho_{pp}{}^{\pi} \tag{33}$$

where $E = \alpha + \lambda\beta$ is the HMO orbital energy for the unpaired electron; thus this relationship between splittings and spin densities lacks an explicit dependence on off-diagonal elements of the spin density coefficient matrix; and (3) fitting the experimental data to the form of each equation in turn yields $K/Q_0{}^2 = -0.0168$ G^{-1} for the CB relation (*vs.* $-12/(27)^2 = -0.0165$) and $Q_1/Q_0 = 0.196$ (*vs.* $(7)/(31.5) = 0.222$ and $(6.3)/(27) = (0.233)$).

To justify the use of the CB or GNP relationship it is not sufficient to show that either alone or even both together lead to a better fit of theory and experiment. Calculations must be performed which demonstrate that the effects represented are indeed quantitatively significant.

Bolton[13] has rationalized the CB equation as expressing the influence of excess π charge density on the exponents of the 2p and 2s orbitals on carbon. He has attempted to assess this effect quantitatively by a calculation of the CH fragment. The 2s- and 2p-orbital exponents on carbon for an ion radical, ζ, are related to those for a neutral radical, ζ_0, by the semiempirical equation

$$\zeta = \zeta_0 + 0.225\epsilon^{\pi} \tag{34}$$

The exponent ζ_0 is taken as the conventional value used for Slater-type orbitals.

For a minimum basis set calculation of the CH fragment the leading term in the proton splitting is

$$\frac{16\pi}{3} g_e\beta_e g_N\beta_N \frac{[\sigma_B\pi_0|\pi_0\sigma_A]}{\Delta E_{2BA}}\sigma_B(\mathbf{r}_H)\sigma_A(\mathbf{r}_H) \tag{35}$$

where σ_B, σ_A are the CH bonding and antibonding orbitals. Assuming that the only effect of nonzero excess charge density is to modify the 2s- and 2p-orbital exponents in the exchange integral $[\sigma_B\pi_0|\pi_0\sigma_A]$ and neglecting all overlap integrals, Bolton obtained an equation of the desired form with Q_0 and K both negative and $Q_0/K = 3.4$. Since the Slater 2s orbital on carbon which was employed is not orthogonal to 1s on carbon, Bolton suggested a correction to the evaluation of the integral and obtained $Q_0/K = 2.24$. This ratio is in very good agreement with the result of the semiempirical fit $Q_0/K = 2.25$.

We have performed a CH fragment calculation similar to Bolton's, but incorporating a number of improvements, namely the inclusion of atomic orbital overlap, consideration of the dependence of ΔE_2 on exponents, and use of a properly orthogonalized 2s orbital on carbon.[7c] The result is $Q/K = 27$ or $K = -1$ G, a value for this parameter which is an order of magnitude smaller than obtained by Bolton. Our calculation thus suggests that the difference in proton splittings between cations and anions is not principally due to the effect of excess π charge density of the exponents of the 2s and 2p orbitals.

A similar conclusion regarding the magnitude of the excess charge density effect has been reached by Melchior.[17] This investigator has performed an interesting calculation of the ^1H and ^{13}C splittings of $CH_3\cdot$ and $C_2H_4^{\pm}$. A set of orthonormal σ MO's is constructed for substitution in the first-order expression (eq 13). The central feature of the calculation is that the MO's are built from localized orbitals. These are minimum basis two-center bonding and antibonding orbitals and inner shell atomic orbitals. The sets of bonding and antibonding localized orbitals are separately orthogonalized using a Lowdin transformation. Then the transformed antibonding orbitals are orthogonalized to the transformed bonding orbitals which are kept fixed. The energy differences ΔE_{2jm} are treated as semiempirical parameters. Predictions are made for the $\mathbf{G}^H$ and $\mathbf{G}^C$ matrices of $CH_3\cdot$ and $C_2H_4^{\pm}$.

The importance of including overlap is stressed. If this is done the McConnell Q parameter, $G_{pp}{}^{H}$, is found to be particularly insensitive to effects such as variations in bond length, atomic orbital hybridization, formal charge, and bond polarity. Also $G_{pp}{}^{C}$ is shown to be virtually independent of substituents. These are encouraging results which support the validity of the McConnell and Karplus–Fraenkel equations.

Giacometti and coworkers have attempted to estimate the magnitude of the "near-neighbor" effect using a 3-carbon atom π-radical fragment.[15] Assuming a single (σ, σ^*) pair of localized CH orbitals one can write

$$\frac{Q_1}{Q_0} = \frac{2[\sigma\chi_p|\chi_{p+1}\sigma^*]}{[\sigma\chi_p|\chi_p\sigma^*]} \tag{36}$$

where χ_p is a 2p–π atomic orbital on carbon atom p. The C_pH_p bonding orbital, σ, is proportional to $(\lambda t + h)$, where t is an sp^2 hybrid, h is a 1s orbital on hydrogen, and λ is a bond polarity parameter. Estimating these

(16) R. E. Moss and G. K. Fraenkel, *J. Chem. Phys.*, **50**, 252 (1969).
(17) M. T. Melchior, *ibid.*, **50**, 511 (1969).

integrals ($\lambda = 1$) GNP obtained $Q_1/Q_0 = {}^1/_2$ which is quite large. We have calculated these integrals using conventional Slater orbital exponents, $\lambda = 0.9$, and $r_{CC} = 1.40$ Å. The result is $Q_1/Q_0 = 0.083$, which is much smaller and is a factor of 3 less even than the semiempirical ratio.

Melchior has obtained a similar result using two-center σ molecular orbitals. Transformation to sets of orthogonalized molecular orbitals leads to a larger effect. For the case of ethylene cation and anion ($C_2H_4^{\pm}$), both assumed planar, Melchior obtains $G_{pp}{}^H = -27.2 \pm 1.8$ G, $G_{p,p+1}{}^H = G_{p+1,p}{}^H = -3.0 \pm 0.3$ G, $G_{p+1,p+1}{}^H = +1.8 \pm 0.2$ G. Then $Q_1 \sim 2G_{CC'}{}^H = 6$ G in quite good agreement with the semiempirical results.

Actually Melchior's results do not lead to a larger splitting for the cation radical provided one includes atomic orbital overlap in the calculation of $\gamma_{pq}{}^{(0)}$. The singly occupied SCFMO's of $C_2H_4^{\pm}$ are symmetry orbitals, namely

$$\pi_0^{\pm} = [2(1 \pm S_{12})]^{-1/2}(\chi_1 \pm \chi_2) \tag{37}$$

where $S_{12} = \langle\chi_1|\chi_2\rangle \approx {}^1/_4$. Then

$$\gamma_+{}^{(0)} = \begin{bmatrix} {}^2/_5 & {}^2/_5 \\ {}^2/_5 & {}^2/_5 \end{bmatrix} \tag{38}$$

and

$$\gamma_-{}^{(0)} = \begin{bmatrix} {}^2/_3 & -{}^2/_3 \\ -{}^2/_3 & {}^2/_3 \end{bmatrix} \tag{39}$$

Using $\mathbf{G}$ as quoted above, $a_+{}^H = -12.6$ G and $a_-{}^H = -12.9$ G which are equal within the error limits. The bond spin density effect is cancelled by the fact that the diagonal spin density $\gamma_{pp}{}^{(0)}$ is much larger for the anion.

This section has dealt with extensions of the McConnell equation introduced to explain the larger experimental splittings for hydrocarbon cation radicals. Neither the excess charge density effect nor the bond spin density effect has been shown theoretically to be the leading correction to the McConnell equation. Further work is needed. A likely possibility for investigation is the difference in the energy denominators ΔE_{2jm}.[8] Another possibility is that important contributions will be found among the second-order terms.

Before leaving the subject of the first-order contributions to $\gamma(\mathbf{r}_H)$ we present the following interesting speculation. Experimental proton splittings divided by the McConnell equation Q may be a better probe of diagonal spin densities in an orthogonalized Lowdin basis, λ, than in the conventional nonorthogonalized atomic orbital basis, χ.

Semiempirical π-electron theories employed to compute $\rho_{pp}{}^{\pi}$ usually invoke the zero differential overlap approximation. For such theories the preferred interpretation is that the implicit basis consists of Lowdin orbitals.[18] These are symmetrically orthogonalized according to the prescription

$$\lambda = \mathbf{S}^{-1/2}\chi \tag{40}$$

where $\mathbf{S}$ is the overlap matrix in the χ basis. Returning to the general first-order equation for $\gamma(\mathbf{r}_H)$ (eq 13) and expanding the singly occupied SCFMO in the λ, one obtains

$$a^H = \sum_{p,q}(G_{qp}{}^H)^{\lambda}(\gamma_{pq}{}^{(0)})^{\lambda} \tag{41}$$

where superscript λ denotes the Lowdin basis and

$$(G_{qp}{}^H)^{\lambda} = \sum_u \sum_v (\mathbf{S}^{-1/2})_{pu}(\mathbf{S}^{-1/2})_{qv}(G_{vu}{}^H)^{\chi} \tag{42}$$

Our claim, then, is that $(G_{p,p\pm1}{}^H)^{\lambda} \ll (G_{p,p\pm1}{}^H)^{\chi}$, *i.e.*, the effect of bond spin density is smaller using the Lowdin basis and consequently the McConnell equation is made a better approximation.

To support this idea we again consider $C_2H_4^{\pm}$ and expand the singly occupied SCFMO in terms of Lowdin orbitals[19]

$$\pi_0^{\pm} = \frac{1}{\sqrt{2}}(\lambda_1 \pm \lambda_2) \tag{43}$$

$$\lambda_1 = [{}^1/_2(1+S)^{-1/2} + {}^1/_2(1-S)^{-1/2}]\chi_1 + [{}^1/_2(1+S)^{-1/2} - {}^1/_2(1-S)^{-1/2}]\chi_2 \tag{44}$$

$$\lambda_2 = [{}^1/_2(1+S)^{-1/2} - {}^1/_2(1-S)^{-1/2}]\chi_1 + [{}^1/_2(1+S)^{-1/2} + {}^1/_2(1-S)^{-1/2}]\chi_2 \tag{45}$$

Since $\pi_0^{\pm}$ are symmetry orbitals, eq 43 is identical with eq 37 and is formally identical with the result of HMO theory without overlap. Straightforward substitution in eq 42 using Melchior's $\mathbf{G}^{\chi}$ and a power series expansion for $\mathbf{S}^{-1/2}$ yields $(G_{12}{}^H)^{\lambda} = -0.2 \pm 0.4$ G, zero within the assigned uncertainties (*cf.* $(G_{12}{}^H)^{\chi} = -3.0 \pm 0.3$ G). Also, the leading term in $\mathbf{G}$ changes only a few per cent, $(G_{11}{}^H)^{\lambda} = -27.7$ G whereas $(G_{11}{}^H)^{\chi} = -27.2 \pm 1.8$ G.

2. Second-Order Contributions. Two questions are posed. How large are the second-order contributions to $\gamma(\mathbf{r}_N)$? How do they modify the first-order relationship between splittings and π spin densities?

Malrieu estimated that the second-order terms contribute to the Q constant ($G_{pp}{}^H$) by at least about one-fourth of the first-order contribution and are thus quite important.[8] He expanded π_0 as a linear combination of the χ_p and examined those terms proportional to $\gamma_{pp}{}^{(0)}$. That part of term III (eq 27) is then

$$Q\left\{\frac{[\sigma\sigma|\sigma^*\sigma^*]}{E\begin{pmatrix}\sigma & |\sigma^*\\ \sigma & |\sigma^*\end{pmatrix}}\right\}$$

which is estimated to be *ca.* ${}^1/_8Q$. The same quantity is found in term VI.

We can also estimate the quantitative importance of

(18) K. Jug, *Theor. Chim. Acta*, **14**, 91 (1969), and references cited therein.

(19) R. G. Parr, *J. Chem. Phys.*, **33**, 1184 (1960).

the second-order contributions and some first-order contributions omitted by Malrieu by a consideration of our minimum-basis variational calculations of $CH_3\cdot$ (*cf.* section IV). This is a particularly simple case since $\gamma^{(0)} = \gamma_{11}{}^{(0)} \approx 1$. Further, there are no $\pi \rightarrow \pi^*$ excitations, and hence terms IV, V, and most of VI equal zero.

A variational SCF–CI(S + D) calculation was performed using STO's with Slater rules orbital exponents and "equivalent" bonding and antibonding σ orbitals (B_i, A_i).[20] That part of the wave function which is of interest is represented symbolically as

$$\psi = a_0\psi_0 + a_i\psi_{B_i\rightarrow A_i} + b_i\psi_{B_j\rightarrow A_i} + c_i\psi_{B_i{}^2\rightarrow A_i{}^2} + \ldots \quad (46)$$

The overall result of this calculation is $a^{H_1} = -33.1$ G. The first-order variational contribution from the excitation $B_1 \rightarrow A_1$ ($2a_0a_1\langle\psi_0|\gamma(\mathbf{r}_1)|\psi_{B_1\rightarrow A_1}\rangle$) is -33.5 G. First-order perturbation theory for the $B_1 \rightarrow A_1$ excitation gives -34.8 G in very good agreement with the variational result.

Variational counterparts to the second-order terms I and III are $a_1{}^2\langle\psi_{B_1\rightarrow A_1}|\gamma|\psi_{B_1\rightarrow A_1}\rangle = +1.2$ G (-4%) and $2a_1c_1\langle\psi_{B_1\rightarrow A_1}|\gamma|\psi_{B_1{}^2\rightarrow A_1{}^2}\rangle = -2.9$ G (9%). The latter is close to Malrieu's estimate (12%) of the corresponding perturbation term.

Omitted by Malrieu are (1) the $B_j \rightarrow A_i$ excitations whose first-order contribution to the splitting is $+2.1$ G (-6%), and (2) the inner-shell excitation $1a_1 \rightarrow A_1$ which gives a negligible contribution (2×10^{-3} G) to the proton splitting (but not to the ^{13}C splitting).

The importance of including excitations $B_k \rightarrow A_1$ is even greater for ^{13}C hyperfine splitting. For the minimum-basis calculation of $CH_3\cdot$ the splitting, to a good approximation, is proportional to $6\bar{\gamma}_{B_1A_1}B_1(\mathbf{r}_C) \times A_1(\mathbf{r}_C) + 12\bar{\gamma}_{B_1A_2}B_1(\mathbf{r}_C)A_2(\mathbf{r}_C)$. ($\bar{\gamma}$ denotes the spin density coefficient matrix in an MO representation.) Since $A_2(\mathbf{r}_C) = A_1(\mathbf{r}_C)$ and $\bar{\gamma}_{B_1A_2} \approx {}^1/_5\bar{\gamma}_{B_1A_1}$, the second term is 40% of the conventional leading term.

Malrieu has made an important point with regard to the effect of the second-order contribution on the general correlation of proton splitting and π spin distribution. He has shown that from the sum of term V, the first line in (VI) and the first-order contribution (subject to the approximation $E\begin{pmatrix}\sigma & \sigma^*\\ \pi_i & \pi_j^*\end{pmatrix} = E(\sigma|\sigma^*) + E(\pi_i|\pi_j^*)$) one can derive a new McConnell-type term $G_{pp}{}^H\gamma_{pp}{}^{(1)}$. Here $\gamma_{pp}{}^{(1)}$ is calculated using first-order perturbation theory applied to ψ_0 *plus* all single $\pi \rightarrow \pi^*$ excitations. This is a qualitative justification for using the McConnell equation with spin densities calculated by various semiempirical π-electron theories which are in a sense equivalent to restricted SCFMO plus CI, *e.g.*, UHF–MO and McLachlan–MO. Quantitatively, the use of an unrestricted SCF wave function leads to a more complex term.[8,21,22]

IV. Variational Calculations

A. SCF–CI. The ground-state electronic wave functions of the simplest π-electron radicals, $CH_3\cdot$ and $CH\cdot$, were calculated using the nonempirical spin-restricted SCF method plus limited configuration interaction.[20,23] Configurations were formed by replacing occupied SCF–MO's with virtual SCF–MO's, multiplying these space-orbital products by appropriate spin eigenfunctions, and antisymmetrizing. The SCFMO's were expanded in terms of Slater-type orbitals (STO's).

Variational calculations using only single replacements of space orbitals are denoted SCF–CI(S). Calculations including all singly and doubly "excited" configurations are labeled SCF–CI(S+D).

B. Proton Hyperfine Splittings. 1. Minimum Basis Sets. What is our rationale for performing *ab initio* minimum basis set calculations of hyperfine splittings? The McConnell relation for proton splittings (and its extensions), the Karplus–Fraenkel equation for ^{13}C splittings, and similar equations for ^{14}N and ^{17}O are all given in terms of minimum basis π spin densities. Also the semiempirical INDO theory utilizes a minimum basis set. Nonempirical minimum basis calculations should be performed to help explore the validity of these useful relationships and of this semiempirical theory.

Three minimum basis sets of STO's were employed for $CH_3\cdot$ and $CH\cdot$. Orbital exponents are given in Table I. The exponents of the Slater set were chosen using Slater's rules. Those of the BMMO set were optimized values obtained by minimization of the SCF energy. The third set, denoted hybrid, is an *ad hoc* basis, with BMMO exponents on carbon and the Slater value on hydrogen ($\zeta_h = 1.0$).

Table I: Orbital Exponents of STO's for Minimum Basis Set Calculations

	ζ_h	ζ_{1s_C}	ζ_{2s_C}	ζ_{2p_σ}	ζ_{2p_π}
Slater basis	1.00	5.70	1.625	1.625	1.625
BMMO basis ($CH_3\cdot$)	1.19	5.68	1.75	1.80	1.46
BMMO basis ($CH\cdot$)	1.215	5.675	1.615	1.664	1.538

The calculated proton splittings are given in Table II. For methyl radical the hybrid basis gives good agreement with experiment (20% deviation), the Slater basis leads to fairly good agreement (44%), but the fully optimized BMMO wave function yields a splitting which is almost 100% larger than experiment.

(20) S. Y. Chang, E. R. Davidson, and G. Vincow, *J. Chem. Phys.*, **52**, 1740 (1970).

(21) G. Orlandi and G. Giacometti, *ibid.*, **48**, 2830 (1968).

(22) J. P. Malrieu, *ibid.*, **48**, 2831 (1968).

(23) S. M. Poling, E. R. Davidson, and G. Vincow, to be published.

Similar trends are noted for CH·. In this case there is no measured value of the splitting. Comparison is made with the best calculation, which involves the 24 STO near-Hartree–Fock basis of Cade and Huo.[24] The Slater and hybrid bases give very similar results, −22 and −21 G, and these are quite close to the calculated CH-24 (cusp) splitting, −20.4 G. The BMMO result (−34.5 G) is about 75% larger.

Table II: Proton Hyperfine Splittings of CH_3· and CH· Calculated Using Various Basis Sets

	CH_3·		CH·	
	Exptl			
	−23.04 G[a]			
	SCF-CI(S)	SCF-CI(S + D)	SCF-CI(S)	SCF-CI(S + D)
	A. Minimum Basis Sets			
Slater	−29.15	−33.12		−22.06
Hybrid		−27.5		−21.20
BMMO	−38.85	−43.79	−31.44	−34.55
	B. Extended Basis Sets			
Double ζ	−36.14[b]	−38.21[b]	−29.04[c]	−29.81[c]
	−25.31[d]			
CH-14			−19.89	−18.77
CH-24			−21.45	
CH-24 (Cusp)			−22.08	−20.39[e]

[a] The vibrational contribution to this splitting is only a few per cent. We neglect this and directly compare our calculations based on the electronic wave function. [b] The carbon exponents are Clementi's optimized DZ set and those on hydrogen are 1.0, 1.26. [c] The carbon exponents are generally similar to Clementi's set[23] and those on hydrogen are 0.97, 1.23. [d] The carbon exponents are Clementi's optimized DZ set and those on hydrogen are 1.26, 2.52. [e] Not all double excitations were included. Those 1827 spin-adapted configurations which make the largest contribution to the energy (as estimated using second-order perturbation theory) were used.

We interpret these results for the case of CH_3·. Quantitative analysis of the calculated splittings is simplified if the spin density is expanded in the Slater atomic orbital representation

$$\gamma(\mathbf{r}_H) = \sum_{i,j} \gamma_{ij} \phi_i^*(\mathbf{r}_H) \phi_j(\mathbf{r}_H) \qquad (47)$$

The leading term is $\gamma_{hh} h^2(r_H)$ which is more than 95% of $\gamma(\mathbf{r}_H)$. Values of γ_{hh} and $h^2(r_H)$ for the minimum basis calculations are

Basis	γ_{hh} SCF-CI(S)	γ_{hh} SCF-CI(S + D)	$h^2(r_H)$ $(\zeta_h^3 \pi^{-1})$
Slater	−0.0562	−0.0646	π^{-1}
BMMO	−0.0452	−0.0513	$1.68\pi^{-1}$
Hybrid	...	−0.056	π^{-1}

Variations among the γ_{hh} are not as large as the variations of $h^2(r_H)$. The value of the hydrogen orbital at the nucleus is proportional to the orbital exponent cubed. Thus the magnitude of the splitting depends strongly on the choice of ζ_h.

We offer the following explanation of why the BMMO set gives a much worse splitting than the Slater basis. The Slater set uses $\zeta_h = 1.0$ which is likely the correct value to give a local solution of the Hartree–Fock equation near the nucleus. But the exponents on carbon are not optimized, and this probably leads to a worse value of γ_{hh} than that predicted by the BMMO set. The optimization of the hydrogen exponent in the BMMO basis, however, yields $\zeta_h = 1.2$ and thus much too large a value for $h^2(r_H)$ and the splitting.

As an *ad hoc* alternative we propose the hybrid basis. It combines the advantages of using the optimized basis on carbon and the intuitive value for $h^2(r_H)$. Indeed the hybrid set value for γ_{hh} is much closer to the BMMO result than to the Slater value. Quantitatively, the hybrid basis results for CH_3· and CH· are quite good and offer promise for the eventual success of minimum basis calculations on large free radicals. Also, these results support the validity of the use of a minimum basis for the π electrons, as in McConnell's equation.

Another interesting *ad hoc* procedure is not to calculate $h^2(r_H)$ at all but to set it equal to π^{-1}. Then using the BMMO value $\gamma_{hh} = -0.0513$, the leading term in the splitting equals −26.0 G in excellent agreement with experiment.

The use of this intuitive choice for $h^2(r_H)$ has also been considered by Meyer.[25] This author has made an investigation using Gaussian function basis sets for the calculation of hyperfine splittings. The problem here is that the "weak" Gaussian functions adequately describing the valence regions are nearly constant in the neighborhood of the nucleus. In contrast STO's have cusps at the nucleus. Meyer's proposal is to prepare the basis by putting the "hardest" Gaussian functions into a group with fixed coefficients so that the orbital "will take the correct value at the nucleus" (Z^3/π).

A promising semiempirical approach for the calculation of spin densities at the nucleus, $\gamma(\mathbf{r}_N)$, is the INDO method of Pople, Beveridge, and Dobosh.[26] In brief this method consists of computing a spin-unrestricted SCF determinant using a minimum basis set limited to the valence shell electrons. Various approximations are involved in the calculation of the matrix elements of the Fock operator (F_{uv}). None of the disposable parameters involved in F_{uv} are chosen on the basis of experimental hyperfine constants. Differential overlap is neglected except for the one-center integrals.

The hyperfine splitting of nucleus N is approximated by the term proportional to $\gamma_{S_N S_N} S_N^2(r_N)$ where S_N is the s-type valence atomic orbital on nucleus N. All

(24) P. E. Cade and W. M. Huo, *J. Chem. Phys.*, **47**, 614 (1967).

(25) W. Meyer, *ibid.*, **51**, 5149 (1969).

(26) J. A. Pople, D. L. Beveridge, and P. A. Dobosh, *J. Amer. Chem. Soc.*, **90**, 4201 (1968).

other terms in the atomic orbital expansion of $\gamma(\mathbf{r}_N)$ are neglected. Then, in gauss

$$a^N = \left[\frac{8\pi}{3} g_N \beta_N S_N^2(r_N)\right] \gamma_{S_N S_N} \qquad (48)$$

The quantity in brackets is assumed to be a constant for all radicals involving hyperfine splitting with nucleus N. Again, there is the question of the appropriate value to use for $S_N^2(r_N)$. This is solved by plotting experimental a^N *vs.* calculated $\gamma_{S_N S_N}$ for a large number of radicals and selecting the value of the quantity in brackets as that slope which gives the best linear relation in a least-squares sense.

The INDO spin-unrestricted result for $CH_3\cdot$ is $\gamma_{hh} = -0.0405$ in good agreement with the nonempirical SCF–CI(S) values, *ca.* −0.05. The INDO wave function, however, is not an eigenfunction of S^2. Beveridge and Dobosh[27] have considered the effect of the spin contamination. Spin annihilation (in which the quartet contribution is projected out of the wave function) yields $\gamma_{hh} = -0.0133$ in poor agreement with our results. Similarly, the INDO values for $\gamma_{2s_c 2s_c}$ are 0.0542 and 0.0184 before and after spin annihilation, respectively. The SCF–CI(S) results are closer to the spin-unrestricted values, namely 0.1637 and 0.1105, for the Slater and BMMO bases. These comparisons for $CH_3\cdot$ indicate that the spin-unrestricted results are to be preferred.

Beveridge and Dobosh arrive at the same conclusion. Although the spin-annihilated results for ^1H, ^{13}C, and ^{14}N give a somewhat better linear regression of a^H *vs.* $\gamma_{S_N S_N}$, the slope yields a value of $S_N^2(r_N)$ which is considerably further from the result of atomic SCF functions than does the spin-unrestricted slope.

The slope for the spin-unrestricted calculations of proton splittings is 539.86 G (standard deviation 7.29 G) or $S_N^2(r_N) = 0.338$ au^{-3}. This is quite close to our intuitive value $\pi^{-1} = 0.318$.

Finally, we note that the neglect of the inner shell in the INDO method is well justified for proton splittings. For $CH_3\cdot$ and $CH\cdot$, the contributions of inner-shell excitations to the proton splittings are $\approx 10^{-3}$ and $\approx 10^{-2}$ G, respectively.

2. Extended Basis Sets. At the double-ζ (DZ) level of basis set, optimization of hydrogen exponents still leads to a proton hyperfine splitting which is too large (*cf.* Table II). For $CH_3\cdot$ we used Clementi's optimized DZ set on carbon and varied the hydrogen exponents. The SCF energy minimum was obtained using exponents close to $\zeta_h = 1.0, 1.26$. The corresponding SCF–CI(S+D) calculation yielded −38.21 G, a 66% deviation from experiment. For $CH\cdot$, using a similar set of exponents (with $\zeta_h = 0.97, 1.23$) we obtained −29.81 G (SCF–CI(S+D)). This value is 50% larger than the CH-24 (Cusp) result.

We have found a DZ set on hydrogen, for use in extended basis calculations, which appears to yield good values for a^H. These 1s hydrogen exponents, $\zeta_h = 1.34, 2.90$ are taken from the CH-24 near-Hartree–Fock basis of Cade and Huo. Dropping ten basis functions, those with the lowest coefficients in the occupied CH-24 SCFMO's, yields the CH-14 basis which retains the above DZ set on hydrogen. The proton splitting varies only slightly (<10%) from the CH-24 results. We did not perform a true DZ (CH-10) calculation using these hydrogen exponents. However, we did perform CH-13 calculations dropping the four appropriate orbitals one at a time from the CH-14 basis. The resultant proton splittings differed from the CI–S value for CH-14 by small amounts ($\lesssim 0.6$ G) which sum to zero. Hence we would expect a CH-10 calculation with $\zeta_h = 1.34, 2.90$ to give a proton splitting close to the CH-24 value. We have performed a DZ calculation for $CH_3\cdot$ using similar hydrogen exponents, $\zeta_h = 1.26, 2.52$. The SCF–CI-(S + D) calculation yielded $a^H = -25.31$ G in excellent agreement with experiment. Finally, we performed a slightly extended minimum basis calculation of $CH\cdot$, using the BMMO exponents on carbon and the DZ set proposed above for hydrogen. The SCF–CI(S+D) splitting is −23.5 G, in fairly good agreement with the CH-24 calculation.

We have performed $CH\cdot$ calculations at the 24 STO basis level (labeled CH-24 (Cusp)) in which the CI wave function has been constrained to satisfy electron-nuclear coalescence cusp conditions at both nuclei.[23] The proton splitting is essentially the same with and without the restriction. This is evidence that the CH-24 basis set is reasonably complete in the neighborhood of hydrogen, which, in turn, supports the use of the CH-24 splitting as the standard of comparison in lieu of an experimental result.

C. ^{13}C Hyperfine Splittings. The results of the ^{13}C hyperfine splitting calculations are shown in Table III. Both minimum basis sets give splittings of *ca.* 140 G for planar $CH_3\cdot$. These are in very poor agreement with the experimental result, *ca.* 28 G (electronic contribution).[28] The Slater basis SCF–CI(S) result, +133.6 G, can be broken down into a −15.4-G first-order contribution due to inner-shell polarization,[29] a + 140 G first-order contribution associated with valence shell polarization and +9.0 G from second-order terms.

The DZ $CH_3\cdot$ calculations lead to much smaller splittings, *e.g.*, +25.7 G (SCF–CI(S+D)), in considerably improved agreement with experiment. The close quantitative concordance is likely fortuitous as indi-

(27) D. L. Beveridge and P. A. Dobosh, *J. Chem. Phys.*, **48**, 5532 (1968).

(28) R. W. Fessenden [*J. Phys. Chem.*, **71**, 74 (1967)] analyzed the experimental ^{13}C splittings of $^{13}CH_3\cdot$ and $^{13}CD_3\cdot$ (85°K) in terms of the average of an expression $a^C = a_0 + a_2\theta^2$ over the thermally populated vibrational states involving the out-of-plane bending motion. He obtained $a_0 = 28.3$ G.

(29) The term inner-shell polarization denotes the contribution to the spin density arising from "excited" configurations involving replacement of the inner-shell SCFMO.

Table III: ^{13}C Hyperfine Splittings of $CH_3\cdot$ and $CH\cdot$ Calculated Using Various Basis Sets

	$CH_3\cdot$		$CH\cdot$	
	Exptl			
	+38.34 G		...	
	Electronic contribution			
	+28 G[a]		...	
	SCF–CI(S)	SCF–CI(S+D)	SCF–CI(S)	SCF–CI(S+D)
	A. Minimum Basis Sets			
Slater	133.6	142.4	...	35.91
BMMO	132.3	140.5	32.99	30.43
Hybrid				31.52
	B. Extended Basis Sets			
Double ζ	23.04	25.68	−3.82	−2.83
CH-14			3.64	0.46
CH-24			24.48	...
CH-24 (Cusp)			5.86	−1.19[b]

[a] See ref 28. [b] Not all double excitations were included. Those 1827 spin-adapted configurations which make the largest contribution to the energy were used.

cated by our results for $CH\cdot$ (see below). Analysis of the SCF–CI(S) splitting, +23.0 G, yields −51.1 G from first-order contributions of inner-shell polarization, +70.1 G from first-order contributions of valence-shell excitations and +4.0 G from second-order terms. The inner- and valence-shell contributions tend to cancel each other, thus yielding the improved splitting.

Similar cancellation is found in the work of Chung,[30] who performed a nonempirical one-center expansion SCF calculation of $^{13}CH_3\cdot$ with an extended STO basis. A second-order perturbation theory CI calculation yielded $a^C = +2.7$ G. First-order inner- and valence-shell contributions were −46.3 and +43.4 G, respectively (second-order terms equaled +5.7 G). The close concordance of the inner-shell result with this work is a reflection of the fact that Chung also used a DZ $1s_c$ basis and chose exponents similar to ours.

We tentatively conclude that a minimum basis calculation of ^{13}C hyperfine splitting (and, by analogy, also ^{14}N and ^{17}O splitting) is inadequate for quantitative accuracy. For $^{13}CH_3\cdot$ the valence-shell terms are overestimated while the reverse is true for inner-shell polarization.

The latter result can be understood as follows. In the minimum basis calculations all of the virtual orbitals are *valence-shell* antibonding orbitals. Excitations to these orbitals from the inner-shell SCFMO yield small contributions to the splittings (*ca.* −15 G for $CH_3\cdot$ and −3.5 G for $CH\cdot$). For extended basis sets such as the DZ set there are much larger inner-shell contributions, namely from excitations to virtual (correlation) orbitals which are essentially localized in the *same* region of space (crudely, $(1s_c + 1s_c') \rightarrow (1s_c - 1s_c')$).

The difficulty of computing an accurate ^{13}C splitting is confirmed by the results for $CH\cdot$. For this molecule the situation is probably aggravated by the occurrence of a very small magnitude of a^C. As in the case of $CH_3\cdot$ the minimum basis splittings, +30–35 G, are considerably larger than the DZ result, −3 G. For the extended basis there appears to be almost quantitative cancellation of inner- and valence-shell contributions. The CH-14 SCF–CI(S + D) splitting, +0.5 G, is similar but the CH-24 SCF–CI(S) value is +25 G. Application of the cusp constraint to the CH-24 basis has a large effect on the splitting reducing it to +5.86 G (CI(S)) and −1.2 G (CI(S+D)). This is an indication that even the near HF basis is still not complete enough for a stable value of a^C.

It should be noted that in all these STO basis sets there are only two carbon orbitals which are nonzero at r_C, namely $1s_c$ and $1s_c'$. This is likely insufficient to adequately describe both the inner- and valence-shell occupied and virtual SCFMO. The above calculations of ^{13}C hyperfine couplings thus point to the need for quite extended basis sets for the σ electrons.

In contrast with the case of proton splittings, comparison of INDO with nonempirical calculations of ^{13}C splittings indicates the possibility of serious shortcomings in the semiempirical method. The INDO theory neglects the inner shell which makes an essential contribution to the hyperfine splitting. The linear regression of a^C *vs.* $\gamma_{2s_c2s_c}$ yields $2s^2(r_C) = 2.042$, a value which differs considerably from the SCF result, 2.767. This deviation would be even larger if vibrational effects were taken into account. Also, the calculated spin-unrestricted value of $\gamma_{2s_c2s_c}$ for $CH_3\cdot$, 0.0542, differs considerably from the Slater and BMMO SCF–CI(S) values, 0.1637 and 0.1105, respectively.

V. Conclusions

In the Introduction a number of questions regarding the calculation of hyperfine splittings were posed. Some partial answers have been obtained from the variational calculations of $CH_3\cdot$ and $CH\cdot$. The main points are summarized. (1) Minimum basis set calculations using the hybrid basis yield fairly accurate values of the proton hyperfine splitting. (2) This supports the validity of an approximation made in developing the McConnell equation, namely the expansion of the half-filled π SCFMO in a minimum set of atomic orbitals. (3) Minimum basis sets of STO's are not adequate for the calculation of ^{13}C hyperfine splittings. (4) Comparison of the nonempirical calculations with INDO calculations supports the accuracy of the semiempirical method for proton splittings but not for ^{13}C splittings.

Acknowledgment. It is a pleasure to acknowledge my collaborators in this work, Professor E. R. Davidson, Dr. S. Y. Chang, and Mr. S. M. Poling. I also wish to thank Mr. W. J. Campion and Dr. A. Warshel for helpful discussions.

(30) A. L. H. Chung, *J. Chem. Phys.*, **46**, 3144 (1967).

Discussion

J. HARRIMAN. You indicated at one point that the spin density should improve as the quality of the wave function, *e.g.*, by an energy criterion, is improved. Could you clarify this? In Li atom, for example, as the energy is improved from one calculation to another the spin density at the nucleus changes significantly and irregularly. It is not until the energy has reached about 10^{-3} au of the true nonrelativistic value that the spin density improves monotonically with decreasing energy.

G. VINCOW. I agree that for small basis sets the spin density at the nucleus ($\gamma(\mathbf{r}_H)$) need not improve with an energy criterion. My reference was not to $\gamma(\mathbf{r}_H)$ but rather to the element $\gamma_{\lambda\lambda}$ of the spin density coefficient matrix as obtained from minimum basis calculations.

J. R. BOLTON. The nomenclature of "spin density" appears to be causing some confusion. I would propose that your γ factors be called "spin occupation coefficients" and reserve the term "spin density" for the difference between α and β electron density at a nucleus.

G. VINCOW. The designation "spin density" as applied to $\gamma_{ij}^{(0)}(\rho_{ij}^{\pi})$ is indeed a misnomer since it is in no sense a density. Your suggestion appears to be a reasonable one.

On Nuclear and Electron Spin Polarizations during Radical Reactions

by Hanns Fischer* and Manfred Lehnig

Physikalisch-chemisches Institut der Universität, Zürich, Switzerland *(Received December 22, 1970)*

Publication costs assisted by Kanton Zürich

Nuclear polarizations of products of radical reactions are explained by transitions between singlet and triplet states of radical pairs which follow the steps of pair formation by decompositions of precursor molecules or by diffusive radical encounters and by the spin selectivity of radical–radical reactions. The transition rates depend on radical g factors and hyperfine interactions. A kinetic formulation of the mechanism is given. From applications to high-field nuclear polarization patterns of products of independently and photolytically generated alkyl radicals g factors and hyperfine parameters of transient radicals may be estimated. For instance, $\cdot CHCl_2$: $g = 2.0080 \pm 0.0003$, $a_H = (-17.0 \pm 1.0)$ G. The magnetic field dependence of nuclear polarizations is discussed. An extension of the treatment to cover electron spin polarizations of free radicals is outlined.

1. Introduction

Since 1967[1,2] many authors have observed emission and enhanced absorption lines in nmr spectra taken of free-radical reaction products shortly after product formation. These effects reflect selective populations of the nuclear spin states caused by the chemical reactions. After an early interpretation[3,4] they are called chemically induced dynamic nuclear polarizations (CIDNP). The currently accepted theories of CIDNP involve transitions between the electronic singlet and triplet states of transient radical pairs occurring with nuclear spin dependent transition probabilities and formations of radical–radical reaction products selectively from singlet state pairs.[5–10] This explanation has first been offered by Closs[5] and by Kaptein and Oosterhoff.[6]

To summarize some of our work in this paper a kinetic formulation of the radical pair mechanism is outlined[7b] and applied to calculate the CIDNP patterns of the reaction products of some independently generated alkyl radicals obtained in a high magnetic field. For one of the products the magnetic field dependence of the nuclear polarizations is presented. Further it is shown that the mechanism responsible for CIDNP may also lead to electron-nuclear polarizations of transient free radicals and may give rise to emission and enhanced absorption lines in their esr spectra. Under conditions of short radical lifetimes such electron spin polarizations have been ob-

(1) J. Bargon, H. Fischer, and U. Johnsen, *Z. Naturforsch. A*, **22**, 1551 (1967).

(2) H. R. Ward and R. G. Lawler, *J. Amer. Chem. Soc.*, **89**, 5518 (1967).

(3) J. Bargon and H. Fischer, *Z. Naturforsch. A*, **22**, 1556 (1967).

(4) R. G. Lawler, *J. Amer. Chem. Soc.*, **89**, 5519 (1967).

(5) (a) G. L. Closs, *ibid.*, **91**, 4552 (1969); (b) G. L. Closs and A. D. Trifunac, *ibid.*, **92**, 2183 (1970).

(6) R. Kaptein and L. J. Oosterhoff, *Chem. Phys. Lett.*, **4**, 195, 214 (1969).

(7) (a) H. Fischer, *ibid.*, **4**, 611 (1970); (b) H. Fischer, *Z. Naturforsch. A*, **25**, 1957 (1970).

(8) H. R. Ward, *Accounts Chem. Res.*, in press; R. G. Lawler, *ibid.*, in press.

(9) S. H. Glarum, private communication.

(10) F. J. Adrian, *J. Chem. Phys.*, **53**, 3374 (1970).

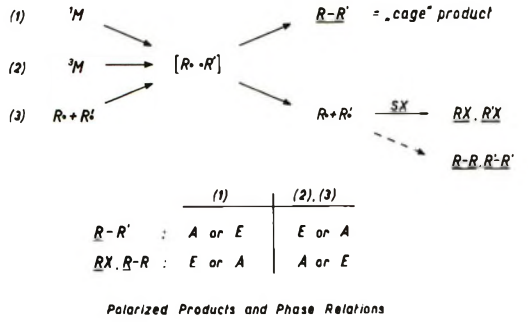

Figure 1. Reactions leading to CIDNP effects.

served.[11-15] The limited information available and the preliminary character of our calculations render our conclusions on the electron polarizations highly speculative, however.

2. Nuclear Polarizations

A. The Radical Pair Mechanism. Reactions exhibiting CIDNP are generalized in Figure 1. Decompositions or other reactions of precursor molecules M from singlet (1) or triplet (2) states or diffusive encounters of free radicals (3) lead to radical pairs, *i.e.*, two radicals in close proximity. These pairs may react to products, for instance combine to the products R–R′ which are properly called cage products for some of the reactions, or they may separate into two free radicals. The free radicals may undergo transfer reactions with suitable agents, or they may lead to further radical–radical reaction products after subsequent encounters. CIDNP is often observed for all the reaction products. Experimentally, important phase relations for the CIDNP patterns have been established for reactions carried out in high magnetic fields, *e.g.*, within the probes of nmr spectrometers. If an nmr transition of a nucleus, a proton say, shows enhanced absorption (A) or emission (E) for the pair reaction product, then the corresponding transition of this nucleus shows emission (E) or enhanced absorption (A) for the products of the radicals escaping the pair. The signs of the polarizations of a product are like for pair formations from reaction paths 2 and 3 and opposite for path 1. This is evidence that the polarizations are caused by interactions within the radical pairs.

For the radical pair mechanism leading to CIDNP various interactions in the radical pairs are considered.[5-10] The most important interactions are Coulomb, exchange, and magnetic dipole–dipole interactions between the unpaired electrons, the Zeeman interactions of the electron spins with the magnetic field, and the electron nuclear hyperfine interactions. For small interradical distances R Coulomb and exchange interactions dominate. Then the electronic states of the pairs are states of pure multiplicity S and T_σ where $\sigma = +, 0$ or $-$. For larger R these states are mixed by the other interactions, the states

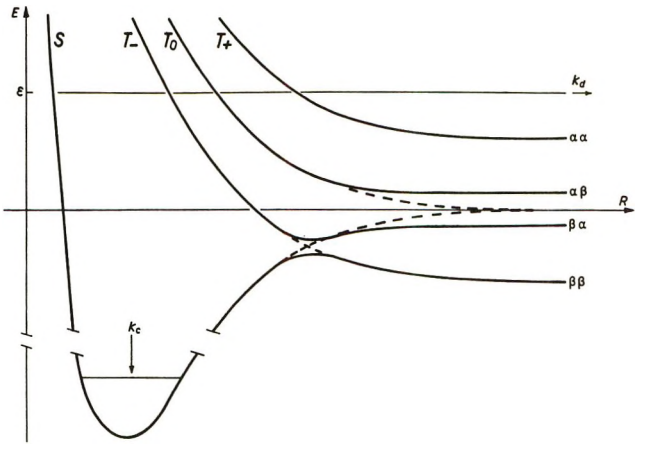

Figure 2. Schematic representation of the electronic energies of a radical pair in a high magnetic field for a hypothetical nuclear spin configuration.

T_σ are mixed by the electron dipole interactions, S and T_σ are mixed by the hyperfine interactions within the individual radicals, and in magnetic fields by the difference of the individual Zeeman interactions.[5-10,16] Since the hyperfine interactions involve the nuclear spins, the mixing between S and T_σ will be nuclear spin dependent. It will also occur essentially then when the pairs have distances R for which the electronic energies of the states of pure multiplicity cross or approach. In Figure 2 the energies of states S and T_σ (dotted lines) and of the mixed, adiabatic states (full lines) are sketched schematically for a pair with a hypothetical nuclear spin state in a high magnetic field. Mixing within the T_σ manifold is neglected. Obviously mixing of S and T_- will occur when the exchange energy J equals the Zeeman interaction ω_s; mixing of S and T_ζ occurs when J equals the hyperfine interactions a. As is also seen from Figure 2, mixing between S and T_0 will predominate for high fields whereas mixing of S with all states T_σ becomes probable for low fields.

Now, these nuclear spin dependent mixings of pure states provide the pathway for CIDNP when combined with the basic assumptions that the formation of the pair reaction products, *e.g.*, R–R′ in Figure 1, occurs only[5-10] or at least predominantly[8] from pairs in S states and that free-radical formation occurs from all states with equal probabilities. The various authors[5-10] used slightly different quantitative formula-

(11) R. W. Fessenden and R. H. Schuler, *J. Chem. Phys.*, **39**, 2147 (1963).

(12) B. Smaller, J. R. Remko, and E. C. Avery, *ibid.*, **48**, 5174 (1968).

(13) H. Paul and H. Fischer, *Z. Naturforsch. A*, **25**, 443 (1970).

(14) P. W. Atkins, I. C. Buchanan, R. C. Gurd, K. A. McLauchlan, and A. F. Simpson, *Chem. Commun.*, 513 (1970).

(15) R. Livingston and H. Zeldes, *J. Chem. Phys.*, **53**, 1406 (1970).

(16) J. E. Harriman, M. Twerdochlib, M. B. Milleur, and J. O. Hirshfelder, *Proc. Nat. Acad. Sci. U. S.*, **57**, 1558 (1967).

tions of this problem. We have assumed[7b] that a pair may undergo several transitions through the regions of mixing during its random walk diffusion through the solutions before finally reacting or escaping from the region of interaction. Thereby its eigenstates develop adiabatically with small but finite probabilities. In terms of pure states this leads to transitions between the states, a pair starting from an S state for small R will be found afterwards at small R in S with a probability deviating from one by a nuclear spin dependent quantity. It may be said to have undergone intersystem crossing with a rate constant $k_{ij\sigma}$. To include reaction and escape we introduce the rate constants k_c and k_d, denote the S states of different nuclear spin configurations by i and the T_σ states by $j\sigma$, and thus arrive at rate equations for the state populations of the pairs

$$\dot{N}_i = r_i - (k_c + k_d + \sum_{j\sigma} k_{ij\sigma})N_i + \sum_{j\sigma} k_{j\sigma i}N_{j\sigma} \quad (1)$$

$$\dot{N}_{j\sigma} = r_{j\sigma} - (k_d + \sum_i k_{j\sigma i})N_{j\sigma} + \sum_i k_{ij\sigma}N_i \quad (2)$$

r_i and $r_{j\sigma}$ are the production rates and may be adapted to the reaction pathways. For singlet precursors $r_i = r/n$, $r_{j\sigma} = 0$, for triplet precursors $r_i = 0$, $r_{j\sigma} = r/3n$, for diffusive encounters $r_i = r_{j\sigma} = r/4n$ have been chosen (Figure 1), r being the total pair production rate and n the total number of nuclear spin substates. From the pairs the products are formed in the individual nuclear spin states with rates

$$\dot{M}_i = k_c N_i \quad (3)$$

pairs of free radicals with rates

$$\dot{R}p_i = k_d(N_i + \sum_\sigma N_{i\sigma}) \quad (4)$$

For times corresponding to small thermal polarizations $\langle I_{ii'}\rangle_0$ of the product R–R′ the enhancement factor of a nmr transition of this product becomes

$$V_{ii'} = \frac{\dot{M}_i - \dot{M}_{i'}}{(\dot{M}_i + \dot{M}_{i'})}\langle I_{ii'}\rangle_0 \quad (5)$$

and enhancement factors of the products of the escaping radicals may be defined similarly.

For the application of (1) to (5) to calculate CIDNP patterns steady-state solutions are most convenient. In fact, these do correspond to the often used experimental conditions of stationary radical concentrations. In the following k_c and k_d are regarded adjustable parameters, $k_{ij\sigma}$ is calculated from

$$k_{ij\sigma} = K^{-1}|\Omega_{ij\sigma}|^2 \quad (6)$$

where $\Omega_{ij\sigma}$ is the matrix element of the spin Hamiltonian

$$\hbar^{-1}\mathcal{H} = (\omega_s S_z + \omega_s' S_z') + \frac{J}{2}(1 + 4S\cdot S') + \sum a_\lambda S I_\lambda + \sum a_\lambda' S' I_\lambda' \quad (7)$$

between pure states S and T_σ, and K is another fitting constant. In (7) primed symbols refer to radical R′· in R· ·R′, unprimed symbols to R··. $\omega_s = \hbar^{-1}g\beta H_0$. Using this Hamiltonian we neglect electron dipole interactions, anisotropic hyperfine interactions, g factor anisotropies, and other small nuclear interactions. Some of these neglections are justified by the reasonable predictions for CIDNP obtained, only.

As has been mentioned above, for large fields transitions between S and T_0 states predominate. They occur between states of equal nuclear configurations and we have

$$k_{it_0} = k_{it_1} = \frac{K^{-1}}{4}\{(g - g')\beta H_0\hbar^{-1} + \sum a_\lambda m_{I_\lambda} - \sum a_\lambda' m_{I_\lambda'}\}^2 \quad (8)$$

From (8) and (1), (2), (3), (4) the phase relations of CIDNP (Figure 1) are easily obtained. For low fields, transitions between all the states become of similar importance.

B. CIDNP of Products of Independently Generated Alkyl Radicals. The kinetic formulation of the pair mechanism outlined above is capable to explain quantitatively the CIDNP effect of products of reactions of some independently generated alkyl radicals.[17] CIDNP has been observed previously during such reactions[18] but has not yet found detailed explanation. We have observed the polarizations in high- and low-field experiments.

During the high field experiments solutions of benzoyl peroxide (BPO, 0.1 *m*) in binary mixtures of methyl iodide, methyl formate, methylene chloride, carbon tetrachloride, monochloroacetic acid, and acetone were photolyzed by the unfiltered radiation of an AH-6 1-kW high-pressure mercury lamp within a suitably modified probe[19] of a VARIAN HA-100 spectrometer. The reaction products are explained by the scheme

$$\mathrm{BPO} \longrightarrow 2C_6H_5CO_2 \longrightarrow 2C_6H_5\cdot + 2CO_2 \quad (9a)$$

$$C_6H_5\cdot + \mathrm{RX} \longrightarrow C_6H_5X + \mathrm{R}\cdot \quad (9b)$$

$$C_6H_5\cdot + \mathrm{R'X'} \longrightarrow C_6H_5X' + \mathrm{R}\cdot' \quad (9c)$$

$$\mathrm{R}\cdot + \mathrm{R}\cdot' \longrightarrow \mathrm{R\text{–}R'} \quad (9d)$$

$$\mathrm{R}\cdot + \mathrm{R}\cdot \longrightarrow \mathrm{R\text{–}R} \quad (9e)$$

$$\mathrm{R}\cdot' + \mathrm{R}\cdot' \longrightarrow \mathrm{R'\text{–}R'} \quad (9f)$$

$$\mathrm{R}\cdot + \mathrm{R'X'} \longrightarrow \mathrm{RX'} + \mathrm{R}\cdot' \quad (9g)$$

$$\mathrm{R}\cdot' + \mathrm{RX} \longrightarrow \mathrm{R'X} + \mathrm{R}\cdot \quad (9h)$$

CIDNP was observed for all products, but only the

(17) M. Lehnig and H. Fischer, *Z. Naturforsch. A*, **25**, 1963 (1970).
(18) G. L. Closs and A. D. Trifunac, *J. Amer. Chem. Soc.*, **92**, 2186 (1970).
(19) G. L. Closs and L. E. Closs, *ibid.*, **91**, 4549 (1969).

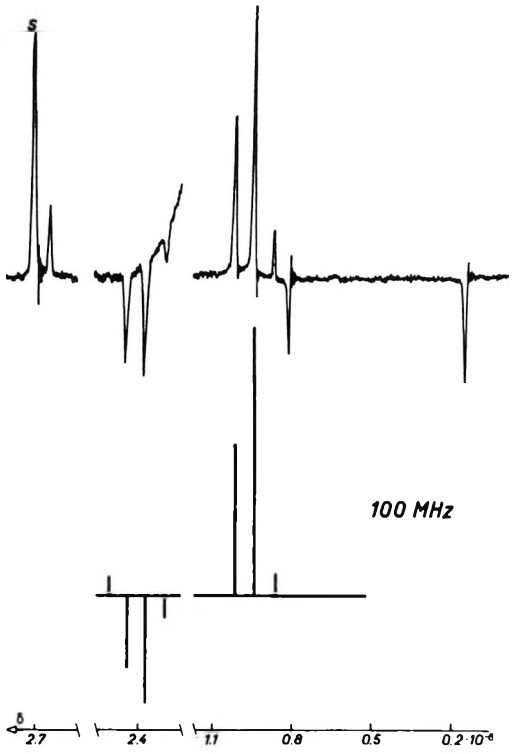

Figure 3. CIDNP during photolysis of BPO in a 1:100 mixture of CH_3I and CH_3COCH_3.

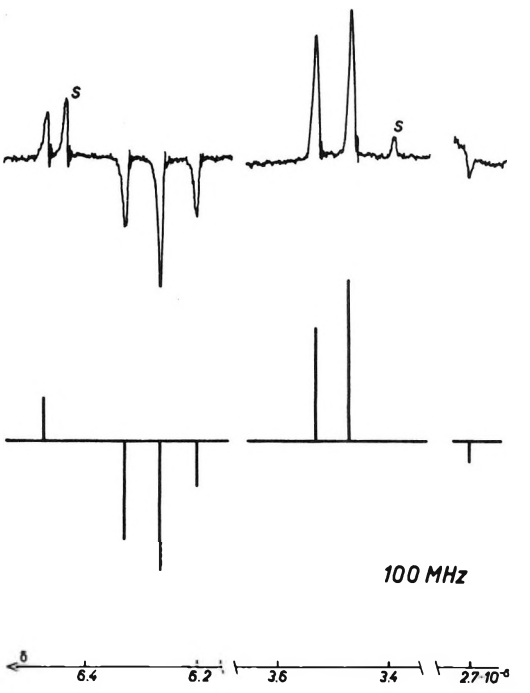

Figure 4. CIDNP during photolysis of BPO in a 1:2 mixture of CH_2Cl_2 and CH_3COCH_3.

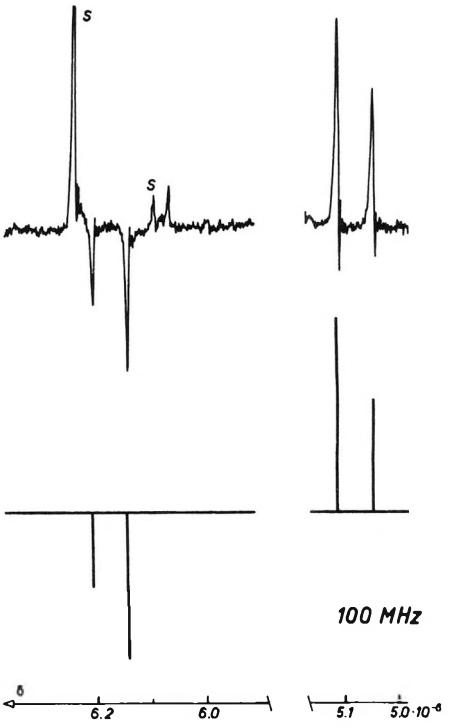

Figure 5. CIDNP during photolysis of BPO in a 3:1 mixture of CH_2Cl_2 and $CH_2ClCOOH$.

polarizations of the products of (9d) to (9h) are treated here. By use of other peroxides instead of BPO the independence of the polarizations of these reaction products of independently generated radicals on the modes of radical formation (9a) to (9c) was ascertained. Enhancement factors of the transitions were determined from

$$V_{\text{exptl}} = \frac{A^*}{A_0} \cdot \frac{t}{T_1} \qquad (10)$$

where A^* and A_0 are the transition amplitudes during and after irradiation, t is the total irradiation time, and T_1 is the longitudinal relaxation time of the transition. Since (10) is applicable only if $|A_0| \ll |A^*|$, this condition was carefully observed. Commercially available chemicals were used. Sample temperatures were (26 ± 4)°.

For three of the systems studied the CIDNP effects are summarized in Table I. Experimental spectra are displayed in the upper parts of Figures 3 to 5. Line assignments are given in Table I (δ units, standard TMS), peaks denoted by S and C^{13}-satellites of the solvents.

From section 2A the high-field CIDNP effects may be attributed to $S–T_0$ transitions in the pairs R· ·R′, R· ·R, and R,′ ·R′. It is easily derived from (8) that transitions in the symmetric pairs R· ·R and R·′ ·R′ can cause so-called multiplet type polarizations only[5−10] which are not observable in the nmr spectra of the symmetric products. Thus the observed effects are caused by transitions in the unsymmetric pairs R· ·R′. This immediately explains the phase relations between the polarizations of the various products (Table I, Figures 3 to 5). Since the polarizations of the radicals R· and R·′ which are built up in R· ·R′ decay during the lifetime of R· and R·′ by nuclear re-

Table I: CIDNP of Reaction Products during Photolysis of BPO in Mixed Solvents

R–R′			R–R, RX′, R′–R′, R′X		
	1. CH_3I–CH_3COCH_3, R· = ·CH_3, R·′ = ·CH_2COCH_3				
CH_3–CH_2COCH_3	δ = 1.03	A	CH_3–CH_3	δ = 0.82	E
	δ = 0.95	A	CH_4	δ = 0.16	E
	δ = 0.88	A			
CH_3–CH_2COCH_3	δ = 2.51	A	$(CH_2$–$COCH_3)_2$	δ = 2.63	A
	δ = 2.44	E			
	δ = 2.37	E			
	δ = 2.29	E			
	2. CH_2Cl_2–CH_3COCH_3, R· = ·$CHCl_2$, R·′ = ·CH_2COCH_3				
$CHCl_2$–CH_2COCH_3	δ = 6.32	E	$CHCl_2$–$CHCl_2$	δ = 6.47	A
	δ = 6.26	E			
	δ = 6.20	E			
$CHCl_2$–CH_2COCH_3	δ = 3.53	A	$(CH_2$–$COCH_3)_2$	δ = 2.68	E
	δ = 3.47	A			
	3. CH_2Cl_2–$CH_2ClCOOH$, R· = ·$CHCl_2$, R·′ = ·CHClCOOH				
$CHCl_2$–CHClCOOH	δ = 6.19	E	$CHCl_2$–$CHCl_2$	δ = 6.06	A
	δ = 6.13	E			
$CHCl_2$–CHClCOOH	δ = 5.11	A			
	δ = 5.04	A			

Table II: Enhancement Factors for Products R–R′

Group	T_1, sec	δ	V_{exptl}	V_{calcd}	$\frac{k_d}{k_d + k_c}$	K, sec^{-2}
CH_3–CH_2COCH_3	13.4	1.03	+429	+416	0.95	2.0×10^{17}
		0.95	+370	+393		
		0.88	+125	+63		
CH_3–CH_2COCH_3	14.1	2.51	+58	+307		
		2.44	−317	−287		
		2.37	−424	−450		
		2.29	−299	−250		
$CHCl_2$–CH_2COCH_3	25.0	6.32	−381	−645	0.93	2.0×10^{17}
		6.26	−351	−354		
		6.20	−305	−236		
$CHCl_2$–CH_2COCH_3	12.3	3.53	+481	+425		
		3.47	+573	+633		
$CHCl_2$–CHClCOOH	15.8	6.19	−320	−334	0.94	1.0×10^{17}
		6.13	−630	−670		
$CHCl_2$–CHClCOOH	17.4	5.11	+816	+798		
		5.04	+522	+465		

laxation, our result on the origin of polarization also explains why the CIDNP amplitudes of symmetric coupling and transfer products are generally much lower than those of R–R′ (Figures 3 to 5). Obviously nuclear relaxation in R· and R·′ also allows for only small polarizations of the radicals entering the pairs R··R′. Under neglect of these small polarizations the enhancement factors of R–R′ should then be given by eq 1 to 8.

For the pertinent calculations we used the high-field basis set of states $i = |S, m_1 \ldots m_\lambda, m_1' \ldots m_\lambda'\rangle$, $j_0 = |T_0, m_1 \ldots m_\lambda, m_1' \ldots m_\lambda'\rangle$ and the free-radical parameters: ·CH_3: $g = 2.00252$, $a_H = -22.83$ G;[11,20,21] ·CH_2COCH_3: $g = 2.00441$, $a_H(\alpha) = -19.75$ G;[20] ·CHClCOOH: $g = 2.00677$, $a_H(\alpha) = -20.2$ G;[22] and ·$CHCl_2$: $g = 2.0080$, $a_H = -17.0$ G. In Table II experimental and calculated enhancement factors are listed. Calculated line amplitudes are given in the lower parts of Figures 3 to 5. The fitting constants K and $k_d/k_d + k_c$ are also included in Table II. We think the agreement between experimental and theoretical CIDNP patterns found in other

(20) H. Zeldes and R. Livingston, *J. Chem. Phys.*, **45**, 1946 (1966).
(21) H. Fischer and H. Hefter, *Z. Naturforsch. A*, **23**, 1763 (1968).
(22) K. Moebius, K. Hoffmann, and M. Plato, *ibid.*, **23**, 1209 (1968).

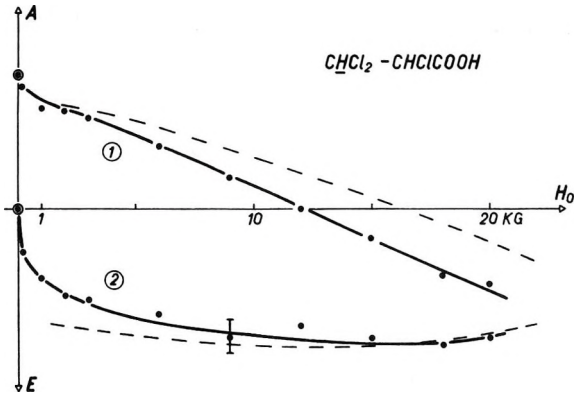

Figure 6. Magnetic field dependence of CIDNP of $CHCl_2$–CHClCOOH. $CHCl_2$ transitions: ①, δ = 6.19; ②, δ = 6.13.

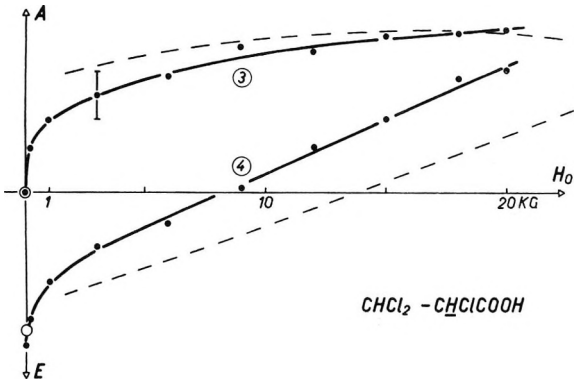

Figure 7. Magnetic field dependence of CIDNP of $CHCl_2$–CHClCOOH. CHClCOOH transitions: ③, δ = 5.11; ④, δ = 5.04.

cases is also[17] rather good. The calculated spectra should be considered as demonstrative rather than best fits, however, since similar agreement may be obtained with slightly modified parameters also. In particular the errors of the hitherto unknown parameters of $\cdot CHCl_2$ are estimated as ± 0.0003 for g and ± 1.0 G for a_H.

To test the validity of our treatment further, the magnetic field dependence of the nuclear polarization of $CHCl_2$–CHClCOOH was studied in some detail. So far the magnetic field dependence of polarizations has found only limited attention.[23-25] Solutions of BPO in methylene chloride–monochloroacetic acid mixtures were photolyzed for 5 sec in a separate magnet at various field strength. They were quickly (2–3 sec) transferred into the probe of the spectrometer. Then the individual transitions of the product were observed about 10 sec after the end of the irradiation. Relative amplitudes of the four nmr transitions are shown in Figures 6 and 7. The broken lines given in these figures represent theoretical line amplitudes calculated in the high-field approximation ($S-T_0$ transitions only) with the parameters given above. For $H_0 \geq 1$ kG they do reproduce the trends of the experimental field dependences. For lower fields the high field treatment breaks down, as expected. To include the low-field polarizations in our treatment we have performed calculations for $H_0 = 0$. The results are also given in Figures 6 and 7. In these calculations the parameters given above were applied again, and we assumed that the nmr levels of the product develop adiabatically during transfer of the sample. To set up the balance eq 1 and 2 the basis set of states $|S,s>$, $|S, t_\sigma>$, $|T_\sigma, s>$, and $|T_\sigma, t_\sigma>$ was used, lower case letters designating the zero-field nuclear spin functions. The matrix elements between these states were calculated from (7). The agreement for $H_0 = 0$ is rather fair, again. It should be mentioned that the high-field treatments of CIDNP by Closs[5b] and by Adrian[10] do allow similar fits of the field dependence in the high-field region.

3. Comments on Electron Spin Polarization

In our treatment of CIDNP we assumed (section 2A) that the spin eigenstates of a radical pair develop in part adiabatically during the diffusive displacements changing R in the regions where degeneracies or near degeneracies of the pure states S and T_σ occur. As is seen from Figure 2 this adiabatic behavior may lead to electron spin polarizations of the radicals escaping from the pairs. Their nuclear spin polarizations given by eq 4 do not influence the corresponding esr spectra grossly since esr transitions occur between magnetic substates with equal nuclear configurations. The electron spin polarizations, however, give rise to anomalous spectra as have been observed.[11-15] For the specific nuclear spin state considered in Figure 2 in particular, a pair prepared in an S state for small R may transform with increasing R into two free radicals with β-electron spins. Thus enhanced esr absorption would result. Pairs decomposing from equally populated T states would lead to esr emission, on the other hand. These types of esr polarizations would both arise from $S-T_-$ transitions. As has been pointed out earlier these transitions are rather improbable in high magnetic fields as employed in the esr experiments, and $S-T_0$ transitions are of higher importance. To estimate the potential influence of $S-T_0$ transitions we consider the energies of the adiabatic eigenstats of a pair $HR\cdot R'H'$ for large R, *i.e.*, small exchange interactions. They are easily calculated from (7) and displayed (solid lines) in Figures 8 and 9 for two sets of free-radical parameters as functions of the exchange integral. The analytical forms of the spin functions for $J = 0$ are also given, α and β referring to electron, + and − to

(23) M. Lehnig and H. Fischer, *Z. Naturforsch. A.*, 24, 1771 (1969).
(24) H. R. Ward, R. G. Lawler, H. Y. Loken, and R. A. Cooper, *J. Amer. Chem. Soc.*, 91, 4928 (1969).
(25) J. F. Garst, R. H. Cox, J. T. Barbas, R. D. Roberts, J. I. Morris, and R. C. Morrison, *J. Amer. Chem. Soc.*, 92, 5761 (1970).

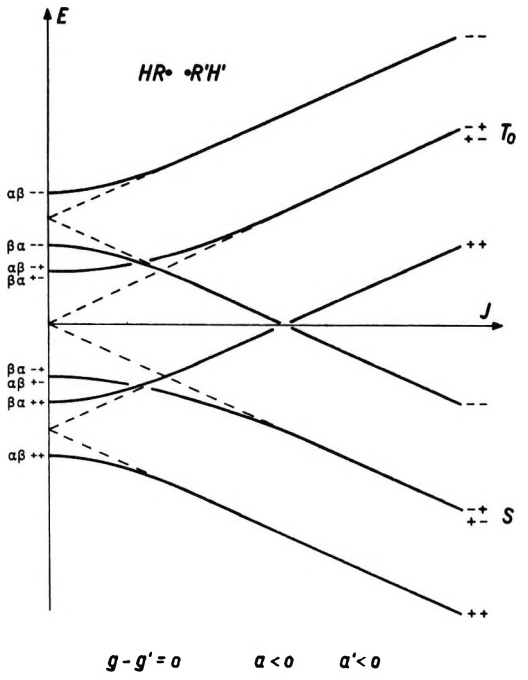

Figure 8. Adiabatic electronic energies of the spin states of HR· ·R'H', $\Delta g = 0$.

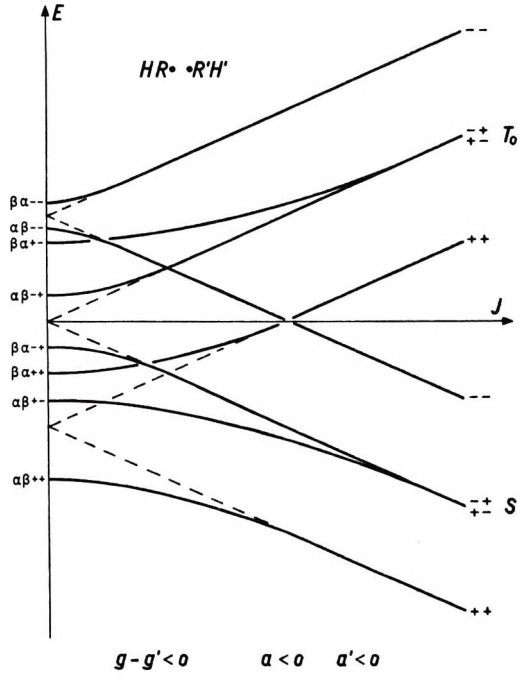

Figure 9. Adiabatic electronic energies of the spin states of HR· ·R'H', $\Delta g \neq 0$.

nuclear spins, the first letter designing the spin state of HR·, the latter that of ·R'H'. For the case of decompositions of T state pairs the excess populations of the electron nuclear spin states of the two free radicals follow immediately from Figures 8 and 9. They are given in Figure 10. The corresponding esr spectra will show emission for low-field and enhanced

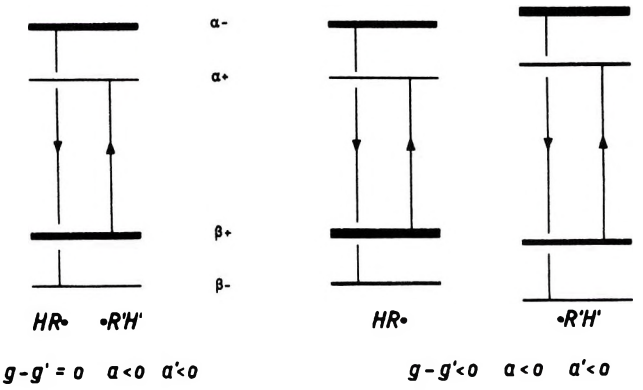

Figure 10. Excess level populations of the free radicals HR· and H'R'.

absorption for high field lines. For $g - g' \neq 0$ small net emission and enhanced absorption of the total spectra are also expected. Emission and enhanced absorption lines interchange if the decompositions occur from S states. In contrast to CIDNP patterns the patterns of electron polarization do not depend on the signs of the hyperfine coupling constants.

Preliminary quantitative calculations based on the ideas outlined here have been carried out under inclusion of the nuclear polarizations of the radicals. They are not reproduced here because of the following reasons. Firstly, the magnitudes of electron spin polarizations are expected to be small because of the smallness of the probabilities for adiabatic transitions. Enhancement factors of the order of one are calculated, yet higher values have been observed.[12,14,26] Secondly, in many cases the chemistry of the systems studied[11-15,27] is not easily reconciled with the idea that the origin of electron polarizations are interactions in radical pairs. Some of the data reported do in fact indicate[13,15,27] that the polarizations occur during radical abstraction or addition steps rather than during radical–radical reactions. Though one might formulate transition states for these reactions also involving more than one unpaired electron and allowing nuclear spin dependent transitions, for instance between doublet and quartet states, further discussion of the electron polarizations seems inconclusive until the formation modes of the polarized radicals and their subsequent reactions are more clearly established.[28]

Acknowledgment. The communication of results by Dr. S. H. Glarum and Dr. R. W. Fessenden prior to publication is gratefully appreciated.

(26) S. H. Glarum, private communication.

(27) K. Eiben and R. W. Fessenden, private communication.

(28) NOTE ADDED IN PROOF. While this paper was in press we found that the deviations of experimental from theoretical CIDNP patterns in Figures 3 to 7 are caused by intra- and intermolecular relaxations of the product protons. Also the parameters of $\cdot CHCl_2$ were measured by esr ($g = 2.00829 \pm 0.00010$, $|a_H| = 16.79 \pm 0.05$, $|a_{Cl}(35)| = 3.4 \pm 0.3$, $|a_{Cl}(37)| = 2.9 \pm 0.3$).

The Role of Lipid Spin Labels in Membrane Biophysics[1a]

by O. Hayes Griffith,*[1b] Louis J. Libertini,[1c] and G. Bruce Birrell[1d]

Institute of Molecular Biology and Department of Chemistry, University of Oregon, Eugene, Oregon 97403
(Received January 14, 1971)

Publication costs assisted by The National Cancer Institute of The National Institutes of Health

Current applications of lipid-soluble spin labels in studies of membrane model systems and biological membranes are discussed. The electron spin resonance spectra contain information regarding solvent polarity, orientation and motion of the spin labels, and proximity of two or more spin labels. New high-frequency esr experiments on di-*tert*-butyl nitroxide (DTBN) partitioned between the aqueous and membrane phases of a crude beef brain myelin preparation are described. In contrast to the 9.5-GHz result, full resolution is obtained at 35 GHz. The 35-GHz data allow measurements of coupling constants and g values when both phases are present. Also reported is the first single crystal study of nitroxide–nitroxide interactions. DTBN molecules occupy substitutional sites in single crystals of tetramethyl-1,3-cyclobutanedione grown in the presence of DTBN. At high concentrations of DTBN, weak five-line patterns are observed displaced about the normal three-line monomer spectrum. The weak lines arise from occasional neighboring pairs of interacting DTBN molecules. Using this system, relationships which may find use in dinitroxide-labeling experiments are explored.

1. Introduction

Spin labeling is becoming a popular method for studying membrane model systems and biological membranes. The technique consists of introducing a nitroxide free radical (spin label) into the system of interest and observing the free radical by electron spin resonance spectroscopy. Information available from the esr spectrum includes polarity of environment, orientation and motion of the spin label, and proximity of two or more spin labels. The purpose of this paper is to report the first spin-labeling study at 35 GHz and some potentially useful measurements of oriented nitroxide radical pairs. A few applications of spin labels are discussed to provide an overview of current trends. However, much work has necessarily been omitted. For a more complete list of applications, a number of recent review articles may be consulted.[2-4] In addition, one methods article has been written to help those interested in applying the spin-labeling technique.[5]

The success of the experiment depends to a large degree on the choice of spin label. Some useful spin labels are drawn in Figure 1.[6-14] Molecules I and II represent the general classes of nitroxide free radicals synthesized in the early 1960's by Rozantsev, Nieman, Rassat, and others.[2-5] Di-*tert*-butyl nitroxide (III) reported by Hoffmann[6] in 1961 is the simplest nitroxide of this general type whereas VI, VIII, and X are examples of more complex lipid nitroxides.

Spin labels of class IV were introduced sometime later by Keana, *et al.*,[7] as a general method of converting ketones into one type of nitroxide (which we will refer to as the doxyl moiety). This approach is attractive since ketone derivatives of naturally occurring membrane lipids are frequently obtainable. Spin labels V, VII, IX, and XI and many related structures have been prepared by the Keana method (and XIII is derived from XI). New lipid spin labels are constantly being reported. The steroid XII, for example, has recently been prepared and will find use in studies of orientation and motion.[8] Other classes of nitroxides are undoubtedly being synthesized, and the availability of suitable probes is becoming less of a problem. It remains to discuss some of the ways that esr spectra of

(1) (a) This work was supported by U. S. Public Health Service Grant CA 10337-03 from the National Cancer Institute; (b) Alfred P. Sloan Foundation Fellow; (c) National Science Foundation Predoctoral Fellow; (d) NIH Postdoctoral Fellow (Fellowship No. 5 FO3 CA42789-02 from the National Cancer Institute).

(2) H. M. McConnell and B. G. McFarland, *Quart. Rev. Biophys.*, **3**, 91 (1970).

(3) I. C. P. Smith in "Biological Applications of Electron Spin Resonance Spectroscopy," J. R. Bolton, D. Borg, and H. Swartz, Ed., Wiley-Interscience, Inc., New York, N. Y., 1971.

(4) P. C. Jost, A. S. Waggoner, and O. H. Griffith in "Structure and Function of Biological Membranes," L. I. Rothfield, Ed., Academic Press, New York, N. Y., 1971.

(5) P. C. Jost and O. H. Griffith in "Methods in Pharmacology," Vol. 2, C. Chignell, Ed., Appleton-Century-Crofts, New York, N. Y., 1971.

(6) A. K. Hoffmann and A. T. Henderson, *J. Amer. Chem. Soc.*, **83**, 4671 (1961).

(7) J. F. W. Keana, S. B. Keana, and D. Beetham, *ibid.*, **89**, 3055 (1967).

(8) J. F. W. Keana and R. J. Dinerstein, *ibid.*, **93**, 2808 (1971).

(9) P. C. Jost, L. J. Libertini, V. Hebert, and O. H. Griffith, *J. Mol. Biol.*, **59**, 77 (1971).

(10) W. L. Hubbell and H. M. McConnell, *Proc. Nat. Acad. Sci. U. S.*, **63**, 16 (1969).

(11) A. S. Waggoner, A. D. Keith, and O. H. Griffith, *J. Phys. Chem.*, **72**, 4219 (1968).

(12) R. Briere, H. Lemaire, and A. Rassat, *Bull. Soc. Chim. Fr.*, **32**, 3273 (1965).

(13) A. S. Waggoner, T. J. Kingzett, S. Rottschaefer, O. H. Griffith, and A. D. Keith, *Chem. Phys. Lipids*, **3**, 245 (1969).

(14) A. D. Keith, A. S. Waggoner, and O. H. Griffith, *Proc. Nat. Acad. Sci. U. S.*, **61**, 819 (1968).

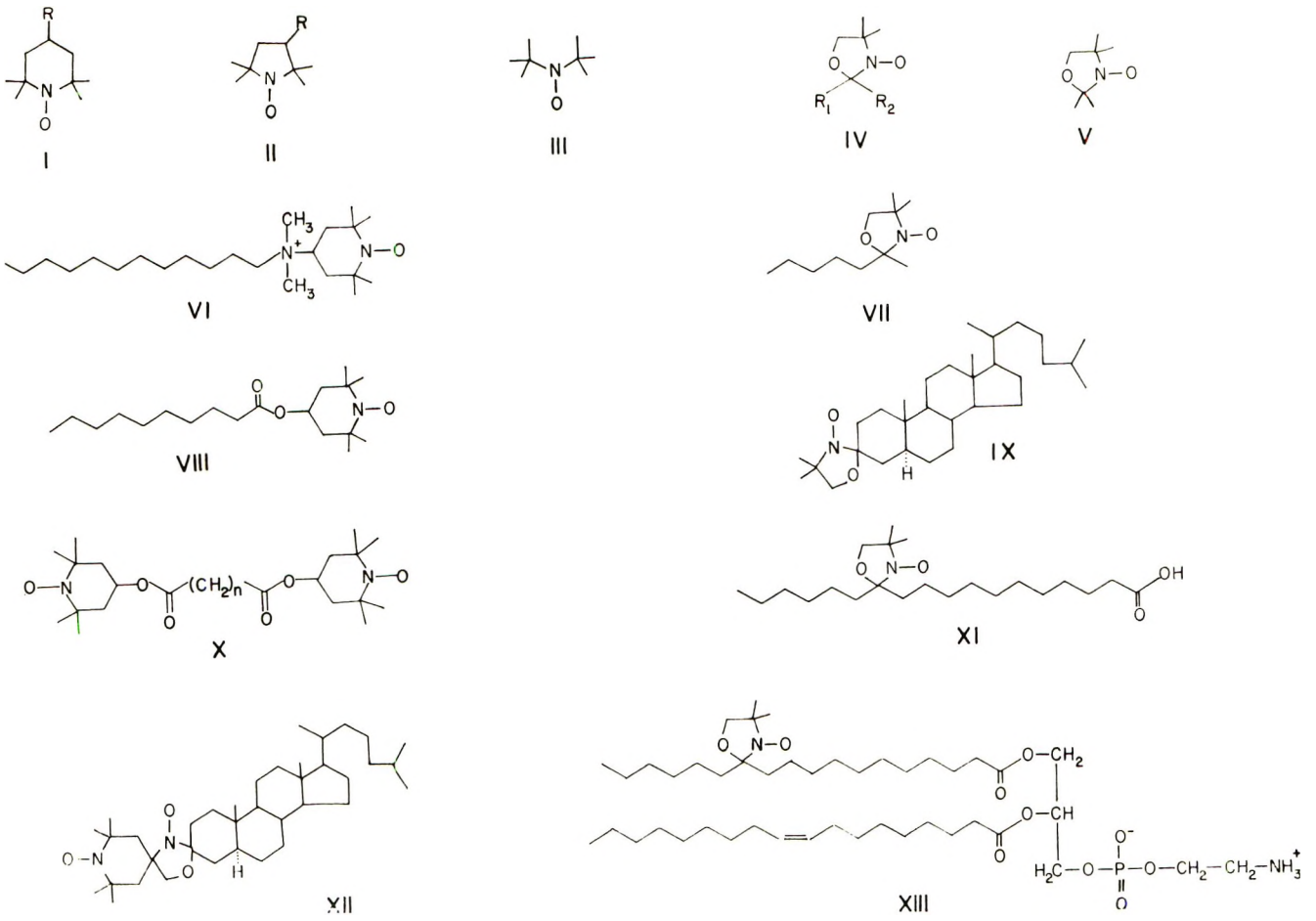

Figure 1. Examples of spin labels useful in studies of membrane models and biological membranes (references: III,[6] V,[9] VI,[10] VII,[7] VIII,[11] IX,[7] X,[12] XI,[9,13] XII,[8] XIII[14]).

these spin labels can provide useful information about membrane structure.

2. Solvent Effects at 9.5 and 35 GHz

One of the interesting aspects of spin labeling is that the esr spectra of all of the molecules of Figure 1 are very much the same providing the spin labels are rapidly tumbling in water or other nonviscous solvents. The resulting spectrum is displayed in various forms in Figure 2. This three-line spectrum is characterized by one coupling constant a_0 and one g value g_0, both of which are solvent dependent. In general, a_0 decreases and g_0 increases slightly as the solvent polarity is decreased. These changes can be an obstacle or an asset depending on the spin-labeling experiment. In line shape studies of moderately immobilized spin labels such as IX or XI in phospholipid vesicles, for example, the solvent dependence is troublesome because it is difficult to estimate the effects on the hyperfine and g_0 value tensor elements. However, when small rapidly tumbling nitroxides (*e.g.*, III or V) are used the solvent effects can produce useful results as shown in Figure 3.

To obtain the data of Figure 3, stock solutions containing 5×10^{-4} M di-*tert*-butyl nitroxide (III, DTBN) in water and degassed dodecane were prepared. The DTBN was synthesized by the method of Hoffmann and Henderson.[6] A third sample consisted of a small amount of DTBN in an aqueous dispersion of crude beef brain myelin. The three samples were drawn into separate 0.4 mm i.d. thin-walled capillary tubes and sealed with wax. (Note DTBN is soluble in wax and contact must be avoided.) Varian E-3 and V-4502 esr spectrometers were used to record the 9.5 and 35 GHz spectra, respectively. All spectra were recorded at room temperature.

Di-*tert*-butyl nitroxide has not been previously used as a probe of membrane structure. However, some time ago Kawamura, Matsunami, and Yonezawa reported a careful 9.5-GHz study of the solvent dependence of this nitroxide.[15] They found, for example, that in water $a_0 = 16.7$ G and $g_0 = 2.0056$ whereas in hexane $a_0 = 14.8$ G and $g_0 = 2.0061$. The decrease in the coupling constant, a_0, on going from water to hexane contracts the hyperfine pattern while the corresponding increase in g_0 shifts all three lines to lower magnetic

(15) T. S. Kawamura, S. Matsunami, and T. Yonezawa, *Bull. Chem. Soc. Jap.*, **40**, 1111 (1967).

Figure 2. The 9.5-GHz esr spectra of di-*tert*-butyl nitroxide (III) in water at room temperature. Bottom: typical first derivative spectrum; middle: absorption presentation of the same spectrum; top: first integral of the absorption spectrum. The weak satellite lines result from ^{13}C nuclei in natural abundance.

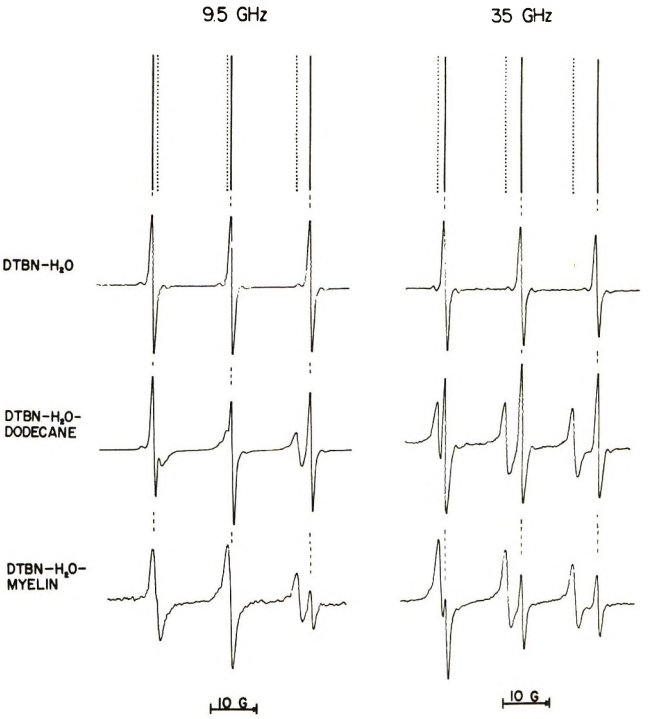

Figure 3. Solvent effects on 9.5- and 35-GHz esr spectra of di-*tert*-butyl nitroxide (DTBN) at room temperature. Top row: the relative line positions for DTBN in water (solid lines) and hexane (dotted lines). Second row: the esr spectra of a capillary filled with 5×10^{-4} *M* DTBN in water. Third row: the spectra recorded using two samples; a capillary containing 5×10^{-4} *M* DTBN in degassed dodecane (the relative peak heights are not significant since the capillaries were not inserted the same distance into the microwave cavity). Bottom row: the esr spectra of DTBN in a crude beef brain myelin preparation. Spectra are aligned using the aqueous DTBN esr signals as a reference.

fields. If DTBN is present in both environments, the spectra overlap but the high-field lines are well separated (see solid and dotted lines at the top left of Figure 3). Hubbell and McConnell have observed this effect previously with a similar small nitroxide (nitroxide I with R = H) in an interesting study of wet nerve fibers.[16]

In considering solvent effects we have found it convenient to use the aqueous spectrum as an internal reference. All spectra of Figure 3 are aligned with respect to DTBN–water esr lines. When DTBN is present in the dodecane and water, the high-field line of the normal three-line esr spectrum is, as expected, replaced by two lines. The relative intensities of the two lines can provide a measure of the amount of spin label in the hydrocarbon and aqueous environments. The same effect is observed when DTBN partitions between water and myelin as shown in the bottom 9.5-GHz spectrum of Figure 3. The essential point is that the resolution at 9.5 GHz is incomplete. *The a_0 and g_0 values are needed to characterize the hydrocarbon environment, but these important parameters cannot be directly measured if only the high-field lines are resolved.*

At 35 GHz, the esr spectrum of a rapidly tumbling nitroxide is very nearly the same as the 9.5-GHz spectrum. However, the sum of two spectra is quantitatively different because of the electron Zeeman term (see Figure 3). At a constant microwave frequency, $h\nu = g_1\beta H_1 = g_2\beta H_2$, where the subscripts 1 and 2 refer to the nitroxide in water and the second environment, respectively. Defining $\Delta g_{21} = g_2 - g_1$ and $\Delta H_{21} = H_2 - H_1$, it readily follows that $\Delta H_{21} = -(H_2/g_1)\Delta g_{21}$ or simply $\Delta H_{21} = -(H/2)\Delta g_{21}$. Using this simple expression and the shift in the center line position, ΔH_{21}, the unknown g_2 is obtained. The splitting between the center line and either outside line of the 35-GHz spectrum gives a_0 directly, and the position of the third line provides a convenient check. From the 35-GHz water–dodecane spectrum of Figure 3, DTBN in dodecane yields $a_0 = 14.8$ G and $g_0 = 2.0061$. For the crude myelin preparation, $a_0 = 14.6$ G and $g_0 = 2.0061$. *As judged by these parameters, the spin label diffused into myelin is in a remarkably hydrocarbonlike environment.* This is consistent with the view that DTBN is tumbling in a fluid lipid bilayer region of the myelin. Of course, the evidence is not conclusive since nonpolar protein environments undoubtedly exist (DTBN is very nearly spherical and could rotate rapidly

(16) W. L. Hubbell and H. M. McConnell, *Proc. Nat. Acad. Sci. U. S.*, **61**, 12 (1968).

in a fluid environment or in a much more rigid structure). It is interesting that, even at 35 GHz, only two environments are observed in the myelin–water sample. Additional information will come from similar high-frequency experiments on membrane proteins and lipoprotein aggregates.

3. Orientation and Motion

Anisotropy in Single Crystals. The majority of spin-labeling experiments rely on effects of orientation and molecular motion. The spin Hamiltonian which describes the esr spectrum of nitroxide free radicals is

$$\mathcal{H} = |\beta_e|\mathbf{H}\cdot\mathbf{g}\cdot\mathbf{S} + \mathbf{S}\cdot\mathbf{A}\cdot\mathbf{I} \qquad (1)$$

where β_e, **H**, **g**, **S**, **A** (also denoted by **T**), and **I** are the electron Bohr magneton, laboratory magnetic field, the g tensor, electron spin operator, electron-nuclear hyperfine tensor, and the nuclear spin operator, respectively. A detailed discussion of this Hamiltonian including approximate analytical solutions and comparisons with experimental data on di-*tert*-butyl nitroxide oriented in a host crystal has been published.[17] The nuclear Zeeman term is omitted since its effect is negligible in most spin-labeling work.[17]

The six important parameters of the **A** and **g** tensors, A_{xx}, A_{yy}, A_{zz} and g_{xx}, g_{yy}, g_{zz} are measured from nitroxides oriented in a diamagnetic matrix. These parameters are related to the isotropic a_0 and g_0 values through the familiar relations $a_0 = (1/3)(A_{xx} + A_{yy} + A_{zz})$ and $g_0 = (1/3)(g_{xx} + g_{yy} + g_{zz})$. Typical spectra recorded at the three principal orientations of 2-doxylpropane are shown in Figure 4, and all six parameters may be measured from these spectra. In Table I[18] complete sets of parameters for the three nitroxides studied thus far are listed. Some of the differences between III and V may be attributable to molecular motion of di-*tert*-butyl nitroxide in the crystal lattice. The only significant difference between V and IX is in A_{zz} and this could result, in part, from a solvent effect. The important A_{zz} parameter can also be estimated from rigid glass spectra (see Figure 4). The rigid glass spectrum results from a simple superposition of spectra of randomly oriented spin labels. It is most easily visualized by summing the three individual absorption spectra of Figure 3 along with all intermediate orientations (and then mentally differentiating the result to obtain the first derivative esr spectrum). The values of A_{zz} determined from rigid glass spectra of nitroxides III, V, and IX are 37.1, 35.1, and 35.0 G, respectively, when dissolved in a 1:4 mixture of methanol–chloroform at −196°. The significant difference between A_{zz} of III and V evidently reflects structural differences. The agreement between V and IX is encouraging since a number of current membrane studies involve a series of doxyl derivatives, and it is convenient to assume the parameters are the same (when the probes are in the same environment).

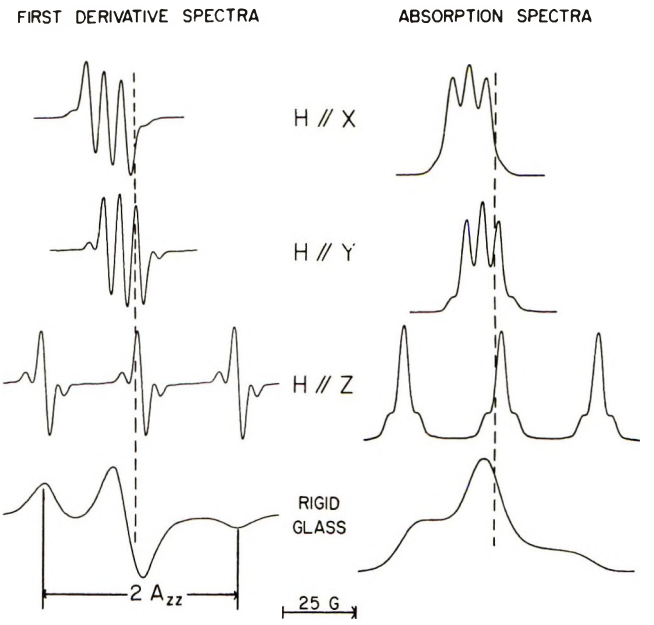

Figure 4. The 9.5-GHz esr spectra of representative spin labels in a rigid matrix. All esr spectra (except the bottom row) are of 2-doxylpropane (V) oriented in the crystal tetramethyl-1,3-cyclobutanedione. The host crystal orients the nitroxide molecules so that their x, y, and z molecular axes are aligned in well-defined directions relative to the crystalline axes. The molecular x axis is parallel to the N–O bond, the z axis is parallel to the nitrogen 2p orbital associated with the unpaired electron, and y is perpendicular to the x and z axes. The crystal was rotated until the laboratory magnetic field (H) was parallel to the x, y, and finally the z molecular axis. The rigid glass spectrum (bottom row) was obtained using a sample of randomly oriented 12-doxylstearic acid (XI) in egg lecithin at −196°. In each case the first derivative spectrum was recorded, digitilized, and then integrated to yield the corresponding absorption spectrum. The dashed vertical lines mark the position of a 2,2-diphenyl-1-picrylhydrazyl reference sample (g = 2.0036).

Once the principal values are known, the orientation dependence of A and g is accurately described by the equations

$$A(\theta) = [A_{xx}^2 \sin^2\theta + A_{zz}^2 \cos^2\theta]^{1/2} \qquad (2)$$

and

$$g(\theta,\varphi) = g_{xx}\sin^2\theta\cos^2\varphi + g_{yy}\sin^2\theta\sin^2\varphi + g_{zz}\cos^2\theta \qquad (3)$$

where θ and φ are the usual polar coordinates defining the direction of the external magnetic field with respect to the molecular axes of the nitroxide. A considerably less accurate but simpler equation for A is

$$A(\theta) = A_{xx}\sin^2\theta + A_{zz}\cos^2\theta \qquad (4)$$

Equations 2 and 4 assume axial symmetry (A_{xx} =

(17) L. J. Libertini and O. H. Griffith, *J. Chem. Phys.*, **53**, 1359 (1970).

(18) W. L. Hubbell and H. M. McConnell, *Proc. Nat. Acad. Sci. U. S.*, **64**, 20 (1969).

Table I: Principal Values of the Splitting and g Value Determined for the Indicated Nitroxides Oriented in Host Crystals[a]

	A_{xx}	A_{yy}	A_{zz}	g_{xx}	g_{yy}	g_{zz}
Di-*tert*-butyl nitroxide (III)[b]	7.6	6.0	31.8	2.0088	2.0062	2.0027
2-Doxylpropane (V)[c]	5.9	5.4	32.9	2.0088	2.0058	2.0022
3-Doxyl-5α-cholestane (IX)[d]	5.8	5.8	30.8	2.0089	2.0058	2.0021

[a] All splittings are in Gauss. [b] Host: tetramethyl-1,3-cyclobutanedione (TMCB); uncertainties: A, ±0.1 G; g, ±0.0001. Data of Libertini and Griffith.[17] [c] Host: TMCB; uncertainties: A, ±0.5 G; g, ±0.0005. Data of Jost, *et al.*[9] [d] Host: cholesteryl chloride; uncertainties; A, ±0.5 G; g, ±0.001. Data of Hubbell and McConnell.[18]

A_{yy}), but the more general expressions are available if needed.[17] Equation 4 is the simple first-order perturbation result, while eq 2 is obtained when the terms which make the greatest contribution to a second-order perturbation treatment (S_zI_x and S_zI_y) are taken into account exactly. Equation 4 is frequently preferred in membrane model and membrane studies. Integrations or summations over the angular variables are required to simulate molecular motion of spin labels. When integrating over all possible orientations, eq 4 averages to the correct value ($a_0 = 1/3(2A_{xx} + A_{zz})$), whereas eq 2 averages to a value larger than a_0.[19] The simple form of eq 4 is attractive when considering approximate models for anisotropic motion. The accuracy of eq 4 improves when H is near one of the molecular axes and eq 2 and 4 give the same result (*i.e.*, $A = A_{xx}$ or A_{zz}) along the molecular axes.

Anisotropy and Motion in Phospholipid Multilayers. Phospholipid bilayers have played a central role in theories of membrane structure for many years.[20] Recent studies involving differential scanning calorimetry[21] and X-ray diffraction[22,23] provide renewed support for the idea that biological membranes contain lipid-rich regions approximated by a phospholipid bilayer. It is clearly important to understand the orientation and motion in lipid bilayers and to assess the potential usefulness of esr in distinguishing between the bilayer model and other models of biological membranes. This is a troublesome matter when dealing with a single bilayer, for example of the Mueller and Rudin type,[24,25] because of esr sensitivity limitations. Fortunately, techniques for preparing stacks of bilayers by drying down phospholipid dispersions out of water and chloroform–methanol or by shear have recently been developed.[26-28] In our first spin-labeling study of phospholipid multilayers,[26] small quantities of 12-doxylstearic acid (XI) or 3-doxyl-5α-cholestane (IX) were introduced into aqueous dispersions of lecithin, and the mixtures were evaporated onto glass slides. The marked anisotropy observed from these preparations indicates a nonrandom structure of the lecithin film and demonstrates that these spin labels are not sufficiently large perturbations to cause gross local disorder. Similar lecithin preparations containing IX have been independently studied by Hsia, *et al.*, and their work is focused on orientation in the presence and absence of cholesterol and water.[28] More recently, Jost, *et al.*, examined the lecithin multilayers using 5-, 7-, 12-, and 16-doxylstearic acid spin labels.[9] Representative esr spectra are reproduced in Figure 5. The doxyl groups are rigidly bonded through a spirane structure to the flexible backbone of the stearic acid molecules. Molecular models indicate that the z axes (the direction of maximum splitting) are essentially parallel to the extended fatty acid chains. From Figure 5, the large splitting (solid line) always occurs when the magnetic field is normal to the glass slide. Thus, all four doxylstearic acids tend to align with their long axes perpendicular to the glass slide, reflecting alignment of the surrounding lecithin molecules as depicted in Figure 6. However, there is a pronounced systematic variation in maximum splitting, depending on the positional isomer used (see Figure 5). The splittings can be accounted for in terms of a simple model in which the molecular z axes execute a rapid random walk about the normal to the multilayer plane, pointing with equal probability in all directions within the cone defined by an angle γ. Expressions are easily derived using eq 4 which relate the splitting to the parameter γ. Computer simulations based on this model of restricted anisotropic motion assuming a Gaussian distribution of orientations are in good agreement with the experimental esr spectra. The main conclusions of this study

(19) Strictly speaking, neither eq 2 nor 4 should be used in this manner. Instead, the integration or averaging process should be carried out on the Hamiltonian itself. It is only a useful accident that averaging the first-order perturbation result is equivalent to averaging the corresponding approximate Hamiltonian.

(20) J. D. Robertson in "Principles of Biomolecular Organization," G. E. W. Wolstenholme and M. O'Connor, Ed., J. & A. Churchill Ltd., London, 1966.

(21) J. M. Steim, M. E. Tourtellotte, J. C. Reinert, R. N. McElhaney, and R. L. Rader, *Proc. Nat. Acad. Sci. U. S.*, **63**, 109 (1969).

(22) D. M. Engleman, *J. Mol. Biol.*, **47**, 115 (1970).

(23) D. M. Engleman, *ibid.*, **58**, 153 (1971).

(24) P. Mueller, D. O. Rudin, H. T. Tien, and W. C. Wescott, *Nature*, **194**, 979 (1962).

(25) T. E. Thompson and F. A. Henn in "Membranes of Mitochondria and Chloroplasts," E. Racker, Ed., Van Nostrand-Reinhold, New York, N. Y., 1970.

(26) L. J. Libertini, A. S. Waggoner, P. C. Jost, and O. H. Griffith, *Proc. Nat. Acad. Sci. U. S.*, **64**, 13 (1969).

(27) Y. K. Levine and M. H. F. Wilkins, *Nature*, **230**, 69 (1971).

(28) J. C. Hsia, H. Schneider, and I. C. P. Smith, *Biochim. Biophys. Acta*, **202**, 399 (1970).

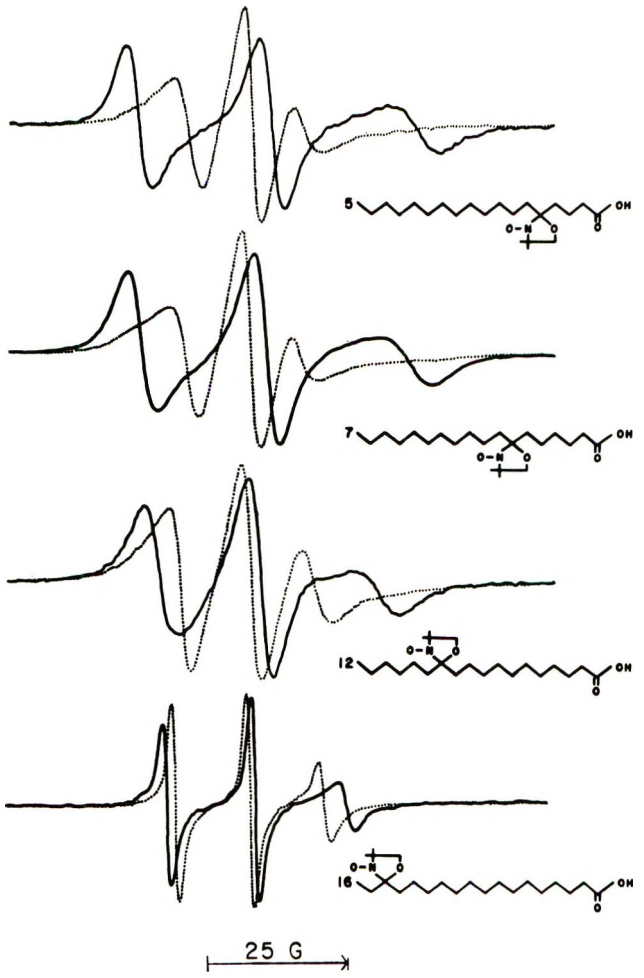

Figure 5. The 9.5-GHz room-temperature spectra of 5-, 7-, 12-, and 16-doxylstearic acids incorporated in oriented lecithin multilayers. The multilayers were in equilibrium with air maintained at 81% relative humidity. The spectra correspond to the external magnetic field parallel (solid line) and perpendicular (dotted line) to a normal to the surface of the phospholipid multilayer. This figure is reproduced from the work of Jost, *et al.*[9]

are that the probes are oriented and molecular motion increases as the label is moved further from the carboxyl end. In addition, lowering the relative humidity decreases the molecular motion of the labels in lecithin multilayers, the effect being most pronounced when the label is near the carboxyl group of the stearic acid probe. As might be expected, increasing the temperature increases the molecular motion. If the slides are exposed to osmium tetroxide vapors, however, the motion is reduced and orientation is eliminated.[29] Phospholipid multilayers will continue to be an important model system for studying the effects of stains used in electron microscopy, drugs, and other chemicals thought to affect membrane structure.

Other Membrane Model Systems and Biological Membranes. Phospholipid multilayers and liquid crystals yield information regarding orientation and motion of lipids. However, molecular motion is being studied in a number of other systems. The earliest example is micelles of sodium dodecyl sulfate. The known (monomer to micelle) phase transition was easily observed using spin labels such as VIII.[11,30] Spin labels are still highly mobile after solubilization by micelles. Micelles are of interest in transport, but vesicles of phospholipids have subsequently yielded spectra more like those of spin-labeled membranes. Consequently more recent efforts have usually been focused on phospholipid dispersions. Barratt, *et al.*,[31] observed the phase transition (chain-melting transition) in a dipalmitoyl lecithin–water system and observed a cholesterol effect using lipid-soluble spin labels. Waggoner, *et al.*,[13] noted cholesterol reduced the notion of 12-doxylstearic acid in egg lecithin vesicles. Hubbell and McConnell observed anisotropic motion of a series of doxyl steroids[10] (similar to IX) and studied a series of doxyl fatty acids (including XI) in phospholipid dispersions.[18] They noted that the structure is more rigid near the polar region than in the hydrophobic tail region of the lipid. These and other studies are discussed in recent review articles.[2-4]

Studies of biological membranes using lipid spin labels are still in a preliminary stage. Keith, *et al.*, have observed biosynthetic incorportation of 12-doxylstearic acid into phospholipids of *Neurospora* crassa, the common bread mold.[14] Esr spectra indicate the presence of molecular motion, although greatly reduced from rapid tumbling in solution or in micelles of sodium dodecyl sulfate. An interesting paper by Hubbell and McConnell reports orientation of doxyl steroids and fatty acids diffused into partially oriented nerve fibers and erythrocytes.[18] The direction of orientation is consistent with that expected from a bilayer structure. Other studies have been reported on membranes using lipid spin labels.[2-4] As the techniques for orienting the samples and analyzing the esr spectra become more quantitative, additional information regarding orientation and motion will be obtained.

One difficulty that has been encountered in spin-labeling studies of vesicles and membranes is the occurrence of composite spectra. These spectra result when the lipid spin label is in two or more environments. The rapidly tumbling spin label in the aqueous phase exhibits a sharp three-line spectrum which obscures the important vesicle spectrum. This effect is simulated by using two samples to obtain the top spectrum in Figure 7. Until recently this difficulty hampered work with fatty acid spin labels in certain pH ranges. However, we have recently found a solution to this problem using a small 8K digital computer. The composite spectrum is first recorded, digitilized, and

(29) P. C. Jost and O. H. Griffith, manuscript in preparation.

(30) A. S. Waggoner, O. H. Griffith, and C. R. Christensen, *Proc. Nat. Acad. Sci. U. S.*, **57**, 1198 (1967).

(31) M. D. Barratt, D. K. Green, and D. Chapman, *Chem. Phys. Lipids*, **3**, 140 (1969).

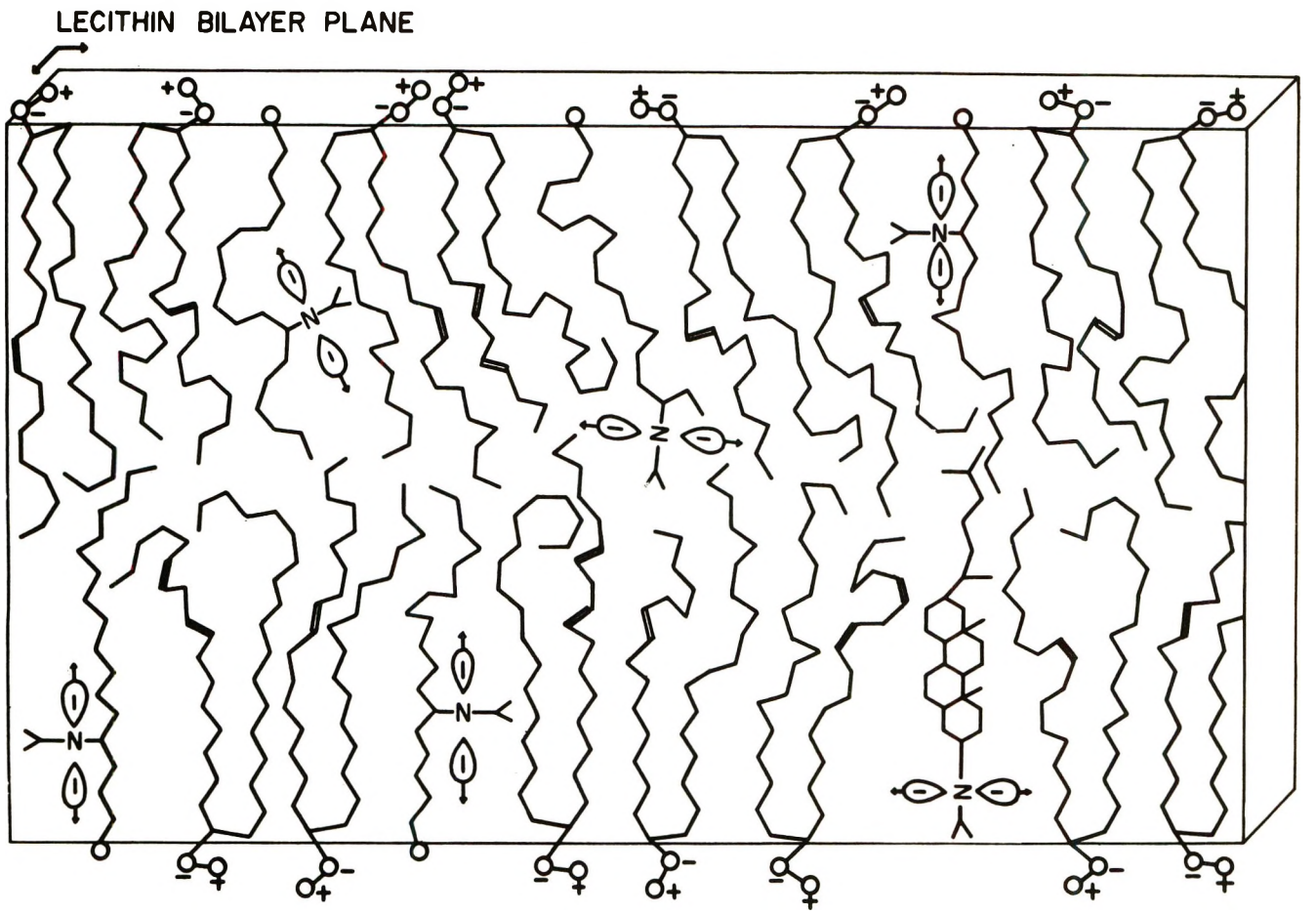

Figure 6. Schematic illustration of a lecithin bilayer region containing lipid spin labels. The doxylstearic acids tend to align with their z axes perpendicular to the plane of the phospholipid bilayer whereas the z axis of 3-doxyl-5α-cholestane is more nearly parallel to the bilayer plane. (An angle of tilt may be present in some cases. See footnote 13 of ref 26.)

placed in the computer memory. The sharp three-line spectrum of the free nitroxide is then recorded and placed in a second computer memory location. The spectrum of the free nitroxide is easily obtained by dissolving the spin label in water or other appropriate solvent. The concentration of label is not important. Using the computer it is possible to perform a "spectral titration" as illustrated in Figure 7. Small increments of the free spectrum are subtracted until eventually the free spectrum is entirely removed (as in the fourth spectrum from the top of Figure 7). If subtraction is carried beyond the "end point," a weak free spectrum of opposite phase is observed as shown in the bottom spectrum of Figure 7. Thus, the computer readily performs the titration of the composite spectrum and displays both components at the end point. Many applications of small computers in spin labeling are discussed elsewhere.[4]

4. Nitroxide–Nitroxide Interactions

Linking together two nitroxides can greatly increase the amount of information (and difficulties) in spin labeling. In an important early study, Falle, *et al.*, were able to show that X and other dinitroxides orient in liquid crystals of *p*-azoxyanisole.[32] Rassat and his colleagues have studied many other dinitroxides.[12] Ohnishi, *et al.*, recently examined micelles of sodium dodecyl sulfate using a dinitroxide which partitions between the micelle and aqueous phases.[33] Calvin, *et al.*, have explored the behavior of a lipid-soluble dinitroxide in an excitable nerve.[34] The use of dinitroxide spin labels is clearly growing. Most studies depend on changes in the exchange parameter, J, or the dipolar splitting D. Generally, situations are sought where the dinitroxides tumble rapidly, where the spin labels are partially oriented, or where it is permissible to freeze the sample to remove complications resulting from intermediate or slow molecular motion. Before membrane model and membrane studies can yield quantitative information many questions must be answered. We wish to report here partial answers to two of the more basic (and easier) questions based on a preliminary

(32) H. R. Falle, G. R. Luckhurst, H. Lemaire, Y. Marechal, A. Rassat, and P. Rey, *Mol. Phys.*, **11**, 49 (1966).

(33) S. Ohnishi, T. J. R. Cyr, and H. Fukushima, *Bull. Chem. Soc. Jap.*, **43**, 673 (1970).

(34) M. Calvin, H. H. Wang, G. Entine, D. Gill, P. Ferruti, M. A. Harpold, and M. P. Klein, *Proc. Nat. Acad. Sci. U. S.*, **63**, 1 (1969).

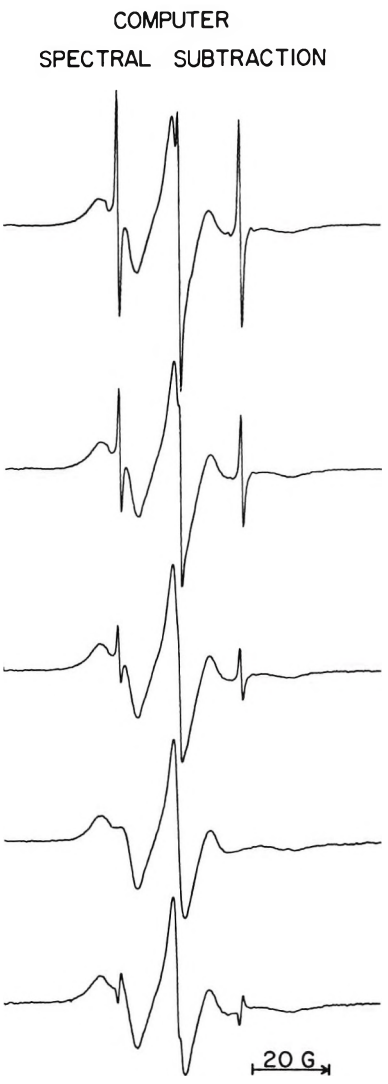

Figure 7. Spectral subtraction by computer. The top spectrum is a typical room temperature composite spectrum. To simulate this common situation, two capillary tubes were placed in the cavity. One contained an aqueous dispersion of 1.5×10^{-3} *M* 5-doxylstearic acid in 20 wt % lecithin and the second capillary contained 5×10^{-5} *M* ketone nitroxide (2,2,6,6-tetramethyl-4-piperidone-1-oxyl, molecule I with a ketone in place of R) in water. The ketone nitroxide was used since 5-doxylstearic acid is not sufficiently soluble in water. The remaining traces result from subtracting increasing amounts of the sharp three-line spectrum from the composite spectrum. Total subtraction occurs in the fourth spectrum. In the bottom spectrum, too much of the sharp three-line component has been subtracted (note the phase reversal in the sharp lines of this spectrum). This figure was reproduced from the paper by Jost, *et al.*[4]

study of nitroxide radical pairs trapped in a single crystal. (1) What quantitative relationships between the orientation and the observed dipolar splitting are useful? (2) Can the simple point dipole approximation be used to estimate distances between two nitroxides?

When crystals of tetramethyl-1,3-cyclobutanedione (TMCB) are grown in the presence of di-*tert*-butyl nitroxide (III), the nitroxide incorporates into substitutional sites in the crystal. This results in a collection or oriented nitroxides useful in anisotropy studies (*e.g.*, data of Table I). When sufficient nitroxide is included, we observe weak lines resulting from neighboring pairs of interacting nitroxides. One of the spectra obtained is reproduced in Figure 8. The two five-line patterns arising from nitroxide pairs are indicated by arrows. The three-line pattern in the center is the normal spectrum of an isolated nitroxide at this orientation.

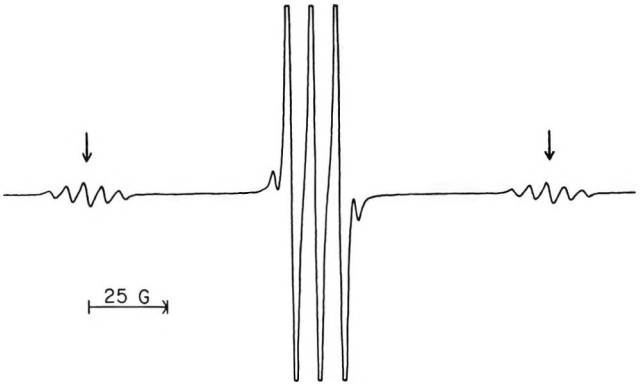

Figure 8. The 9.5-GHz room-temperature spectrum of di-*tert*-butyl nitroxide (III) oriented in a crystal of tetramethyl-1,3-cyclobutanedione. The magnetic field was in the crystalline ac plane, approximately 20 and 84° from the *a* and *c* axes, respectively. The concentration of di-*tert*-butyl nitroxide was sufficiently high in this crystal that interacting radical pairs can easily be seen (note arrows) symmetrically displaced about the normal three-line esr spectrum.

The electron–electron dipolar interaction is responsible for the large splitting, $d(\theta,\phi)$, between centers of the two five-line patterns visible in Figure 8. The dipolar Hamiltonian is usually written in the form

$$\mathcal{H}_d = D(S_z^2 - {}^1/_3\mathbf{S}^2) + E(S_x^2 - S_y^2) \qquad (5)$$

where D and E are in energy units (ergs, joules, etc.), and useful expressions for $d(\theta,\phi)$ have been derived in classical treatments of triplet states for large and small values of D and E.[35,36] In this preliminary study we have examined the spectral anisotropy in three nonorthogonal planes of the host crystal. The orientation dependence of $d(\theta,\phi)$ is adequately described by the first-order perturbation result[36]

$$d(\theta,\phi) = |D(3\cos^2\theta - 1) + 3E\cos 2\phi \sin^2\theta| \qquad (6)$$

where θ and ϕ are the usual polar coordinates. In our study the value of $|D/g\beta|$ is found to be 126 G. The value of $|E/g\beta|$ has been difficult to determine accurately, but is approximately 1 G. Deviations in experimental and calculated $d(\theta,\phi)$ appear to be statistical and are no greater than 2 G (~3%). It is interesting

(35) C. A. Hutchinson, Jr., and B. W. Mangum, *J. Chem. Phys.*, **34**, 908 (1961).

(36) D. B. Chesnut and W. D. Phillips, *ibid.*, **35**, 1002 (1961).

to note that except for orientations where the hyperfine splitting is small enough to result in extensive overlap of the lines, a five-line pattern is observed in the ratio 1:2:3:2:1. This is true even when the hyperfine splitting is maximum, indicating that $J \gg 30$ G for this radical pair.

The second question can be examined by considering the known X-ray crystallographic data for the host crystal.[37] Since the maximum value of $d(\theta,\phi)$ occurs near the crystal a axis, the number of possible nitroxide pairings can be reduced to three[38] with separations (calculated from the distances between carbonyl carbons for the host crystal structure) of 4.5, 6.55, and 8.45 Å. Given $|D/g\beta| = 126$ G and the point dipole approximation,[5] the distance is calculated to be 6.05 Å which is in moderate agreement with the value of 6.55 Å. Use of a distributed dipole calculation may give somewhat better agreement. In any case the point dipole approximation is capable of giving distance and conformational information in dinitroxide spin-labeling experiments.

Acknowledgment. We wish to thank Dr. Patricia Jost for the samples of myelin and for stimulating discussions.

Discussion

H. C. ROBERTS (Rochester, N. Y.). Are 35-GHz spectra of spin labels in mixed solvent systems sufficiently well resolved to permit use of computerized titration techniques to tell how much of the label is in each solvent system?

O. H. GRIFFITH. Yes, the resolution is ideal for this type of data treatment. After computer subtraction, each spectrum should be integrated twice to obtain the ratio of concentrations. We have not done this because our V-4502 35-GHz spectrometer has not yet been interfaced to the Varian 620/i 8K computer. However, we have carried out similar operations on other samples using an E-3 spectrometer interfaced to the 620/i. It is surprising how deceptive the peak heights can be. Where we have checked the results, the computer double integrations have proved to be quite reliable.

R. N. DIEBEL (Richland, Wash.). In your preparation of multilayers by dehydration of emulsions, how many layers would you estimate are present?

O. H. GRIFFITH. We have not determined the number of layers. There is considerable variation in the thickness depending on the method of preparation. All we can say at this point is that these are thick, clearly visible films of phospholipids. (I would not be surprised if many films were over 1000 layers thick).

D. S. LENIART (Palo Alto, Calif.). Recent work on tanone in the liquid phase (n-heptane at $\sim -60°$) fast tumbling region has shown that nonsecular processes ($I_{\pm}S_{\mp}$) are more important than pseudo-secular ($S_zI_{\pm}$) terms in determining the relaxation properties of the system. As you and others (Freed) have mentioned, pseudo-secular terms still remain important when experiments are carried out in the slow tumbling region. However, in this region the esr line shape is not very sensitive to changes in temperature, etc. It seems probable that saturation studies may serve as a more sensitive probe for examining molecular properties when τ_0 ranges from 10^{-7} to 10^{-9} sec by giving a more pronounced change in the observable line shape. Have you or others employed saturation techniques to complement the usual esr studies?

O. H. GRIFFITH. That is a good point. There is information available from saturation measurements not obtainable by conventional esr, particularly in the slow tumbling region. I am not aware of anyone using saturation measurements in membrane spin-labeling experiments, although people undoubtedly will make use of this approach. Dr. James Hyde, Dr. Jack Freed, and others are actively investigating saturation phenomena in free radicals.

D. B. CHESNUT (Duke University, Durham, N. C.). For the triplet paired ($S = 1$) nitroxide radical pair in the single crystal, has the singlet–triplet splitting been ascertained?

O. H. GRIFFITH. Unfortunately, no. The only information we were able to obtain was that J must be much greater than 30 G. It would be very useful to know the magnitude and distance dependence of J.

T. M. PIETRZAK (University of Alabama, Tuscaloosa). We have had recent success with simulating nitroxide esr spectra with a different model which includes pseudosecular terms in the solution of a static Hamiltonian and then simulating motional behavior with a discrete-jump model. We have been able to simulate different modes of anisotropic–rotationally averaged esr spectra as experimentally found in nematic liquid crystals for the nitroxide group approximately parallel and also perpendicular to the static magnetic field. This model can be interpreted in terms of ordering parameters (S_{11}, S_{22}, S_{33}) as is usual for restricted motion in nematic solvents.

(37) P. H. Friedlander and J. M. Robertson, *J. Chem. Soc.*, 3083 (1956).

(38) Other signals are observed at some orientations. They are weak compared to the lines discussed here but evidently correspond to pairs of radicals in different substitutional sites.

Electron Spin Resonance and Endor Studies of Radiation-Produced Radical Pairs

by Harold C. Box

Biophysics Department, Roswell Park Memorial Institute, Buffalo, New York 14203 *(Received January 4, 1971)*

Publication costs assisted by the Atomic Energy Commission

Esr and endor spectroscopy were used to study radical pair formation in several organic systems, namely (1) formation of pairs of phenyl radicals by elimination of two molecules of CO_2 from dibenzoyl peroxide in mixed crystals (solid solutions) subjected to ultraviolet irradiation at 4.2°K; (2) formation of pair of benzoyloxy radicals by dissociation of dibenzoyl peroxide in mixed crystals X-irradiated at 4.2°K; (3) formation of radical pairs by dehydrogenation of adjacent potassium hydrogen malonate molecules in single crystals X-irradiated at 4.2°K. Of the three processes for forming radical pairs, elimination, dissociation, and dehydrogenation, only the latter appears to have general significance as a radiation damage process. The mechanism involved in the dehydrogenation of adjacent molecules is discussed in some detail.

Introduction

When two free radicals are formed in close proximity, there is an exchange interaction between electrons which separates the spin states into singlet and triplet states. The triplet levels are lower in energy than the singlet level and can be examined by esr and endor spectroscopy. In this presentation we shall be concerned with radical pairs produced in several organic solid systems by either ultraviolet or ionizing radiation. Our principal objectives will be (1) to distinguish various radiation-induced chemical processes which generate radical pairs, and (2) to assess the significance of radical pair production as a radiation damage process.

Theoretical Considerations

The spin Hamiltonian for a radical pair takes the form

$$\mathcal{H} = \beta\mathbf{H}\cdot\mathbf{g}\cdot(\mathbf{S}_1 + \mathbf{S}_2) + J\mathbf{S}_1\cdot\mathbf{S}_2 + \mathbf{S}_1\cdot\mathbf{D}\cdot\mathbf{S}_2 \quad (1)$$

where $\mathbf{S}_1$ and $\mathbf{S}_2$ are the unpaired spins.[1] The $\mathbf{g}$ tensor defines the effective magnetic moment of the electrons and the $\mathbf{D}$ tensor, which is traceless, defines the dipole–dipole coupling between electrons. The exchange coupling is measured by J. Assuming the g value is isotropic and equal to the free spin value, g_{fs}, and ignoring the dipole–dipole coupling term, the eigenenergies of the Hamiltonian consisting of the Zeeman and exchange energies can be found. A first-order correction for the anisotropy in $\mathbf{g}$ and for the dipole–dipole coupling energy can then be added. The resultant energies for the triplet states, E_M, are given by

$$E_1 = \beta g_{HH}H + (J + D_{HH})/4 \quad (2a)$$

$$E_0 = J/4 - D_{HH}/2 \quad (2b)$$

$$E_{-1} = -\beta g_{HH}H + (J + D_{HH})/4 \quad (2c)$$

where

$$g_{HH} = g_{fs} + \sum_{ij}\alpha_{Hi}\alpha_{Hj}\Delta g_{ij} \quad (3)$$

$$D_{HH} = \sum_{ij}\alpha_{Hi}\alpha_{Hj}D_{ij} \quad (4)$$

The subscripts in (3) and (4) refer to orthogonal axes fixed with respect to the radical pair. The components of the tensors, D_{ij} and $g_{ij} = g_{fs}\delta_{ij} + \Delta g_{ij}$, are defined with respect to these axes as is the direction of the applied field by means of the direction cosines α_{Hi}. When the distance between the unpaired spins is large compared to atomic dimensions, the spins may be regarded as point dipoles and an explicit expression for the dipole–dipole coupling is given by

$$D_{HH} = \frac{g_{fs}^2\beta^2}{R^3}(1 - 3\cos^2\theta) \quad (5)$$

where $g_{fs} = 2.0023$, R is the distance between dipoles, and θ is the angle between the vector $\mathbf{R}$ and the field $\mathbf{H}$. Esr measurements allow us, through (3) and (4), to evaluate experimentally the tensors $\mathbf{g}$ and $\mathbf{D}$.

When there are also hyperfine couplings to be accounted for, another term

$$\mathcal{H}' = -\sum_n \beta_N g_n \mathbf{I}_n\cdot(\mathbf{H} - \mathbf{A}_n\cdot(\mathbf{S}_1 + \mathbf{S}_2)) \quad (6)$$

must be added (1) where $\mathbf{I}_n$ and g_n refer to a nuclear spin and its g value and $\mathbf{A}_n$ defines its hyperfine coupling. The energy levels of the entire spin system become

$$E_{M,m_1,\ldots} = E_M - \sum_n \beta_N g_n m_n h_M{}^n \quad (7)$$

where m_n is the magnetic quantum number of the nth nuclear spin. The quantity $h_M{}^n$ is the magnitude of the effective field at the nth nucleus. The effective field is given by

(1) J. Kurita, *J. Chem. Soc. Jap.*, **85**, 833 (1964).

$$\mathbf{h}_M{}^n = \mathbf{H} - M\sum_{ij}\mathbf{u}_i A_{nij}\alpha_{Hj}/g_n\beta_N \qquad (8)$$

where the $\mathbf{u}_i$ are unit vectors.

Experimental Section

Esr and endor spectroscopy at K band (24 GHz), as well as esr spectroscopy at V band (70 GHz), were used to examine radical pairs formed in single crystals irradiated at 4.2°K. Mixed crystals (solid solutions) consisting of dibenzoyl peroxide (approximately 3%) in dibenzoyl disulfide were grown by evaporation from toluene solution. The morphology of the crystals was like that of pure crystals of dibenzoyl disulfide which belong to the space group $P2_1/c$.[2] Single crystals of potassium hydrogen malonate[3] (space group $C2/m$ with four molecules per unit cell) and of hydroxyurea[4] (space group $P2_1/c$ with four molecules per unit cell) were grown by evaporation of aqueous solution. Single crystals of dimethylglyoxime[5] (space group $P\bar{1}$ with two molecules per unit cell) were grown from alcohol solution.

The sample cavity of the spectrometer[2] was immersed in a liquid helium bath contained in a dewar equipped with either a beryllium or a sapphire window. Irradiation of the peroxide–disulfide solid solution with radiation from a high-pressure Hg lamp produced radical pairs by eliminating CO_2 from the peroxide molecules. Irradiation by X-rays produced radical pairs by dissociation of the peroxide molecules. X-Irradiation of potassium hydrogen malonate, hydroxyurea, and dimethylglyoxime crystals produced radical pairs by dehydrogenation of adjacent molecules. However, radical pairs were obtained in dimethylglyoxime only after warming considerably above 4.2°K.

Results

Radical Pairs by Elimination. The esr absorption pattern obtained from a solid solution of dibenzoyl peroxide in deuterated dibenzoyl disulfide following ultraviolet irradiation at 4.2°K is shown in Figure 1. The absorption is due to pairs of phenyl radicals produced from the peroxide by elimination of CO_2

$$C_6H_5COOCC_6H_5 \xrightarrow{h\nu} 2C_6H_5 + 2CO_2 \qquad (9)$$

The doublet pattern arises from the allowed transitions ($E_0 \rightarrow E_1$ and $E_{-1} \rightarrow E_0$) between energy levels defined by eq 2. The doublet splitting was measured for various orientations of the crystal with respect to the applied field, and the components of the dipole–dipole coupling tensor were deduced using eq 2 and 4. The principal values and the direction cosines of the principal axes of the tensor are given in Table I. Using (5) the distance between spins, R, was calculated to be 6.5 Å. The direction cosines of the vector **R**, listed in Table I, were calculated from the crystal structure of

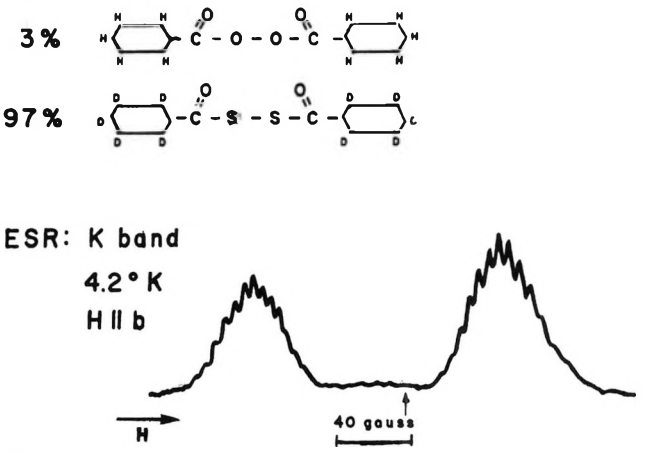

Figure 1. The esr spectrum from an irradiated single crystal of deuterated dibenzoyl disulfide with approximately 3% of the molecules substituted with dibenzoyl peroxide. The ultraviolet irradiation and measurements were carried out at 4.2°K. Arrow indicates resonance for DPPH.

dibenzoyl disulfide.[2] In this calculation **R** was taken as the vector between nuclei of the pair of phenyl carbon atoms linked by the O=CSSC=O group. These direction cosines are expected to define approximately the direction of a corresponding vector for the dibenzoyl peroxide guest molecules. This direction should coincide with the direction of maximum dipole–dipole coupling for the phenyl radical pair. Table I shows how well this expectation is fulfilled.

Table I: The Principal Values, in Gauss, of the Dipole–Dipole Coupling Tensor for the Pair of Phenyl Radicals Produced in Dibenzoyl Disulfide–Dibenzoyl Peroxide Crystals by Ultraviolet Irradiation[a]

	a'	b	c
−203	+0.86	+0.23	−0.43
+101	−0.12	+0.96	+0.26
+103	+0.47	−0.17	+0.86
R	+0.857	0.269	−0.438

[a] The direction cosines are given with respect to an orthogonal set of axes where $a' = b \times c$. There is a second radical pair related in orientation to this one by a twofold rotation about the b axis. The direction cosines of **R** were calculated from the crystal structure of dibenzoyl disulfide as described in the text.

The resolution of the hyperfine pattern associated with the phenyl radical pair is somewhat improved if the host molecules are deuterated. However, the reso-

(2) H. C. Box, H. G. Freund, K. T. Lilga, and E. E. Budzinski, *J. Phys. Chem.*, **74**, 40 (1970).

(3) G. Ferguson, J. G. Sime, J. C. Speakman, and R. Young, *Chem. Commun.*, 162 (1968); R. Parthasarathy, J. G. Sime, and J. C. Speakman, *Acta Crystallogr., Sect. B*, **25**, 1201 (1969).

(4) I. Larsen and B. Jerslev, *Acta Chem. Scand.*, **20**, 983 (1966).

(5) L. L. Merritt, Jr., and E. Lauterman, *Acta Crystallogr.*, **5**, 811 (1952).

Table II: Radical Pairs by Elimination

Parent molecule	Molecule eliminated	Radical produced	Separation of radicals, A	Experimental conditions	Reference
Diarylcarbonates	CO	RO R = tolyl or phenyl	5.9	Polycrystal, γ rays, 77°K	9
Azobisisobutyronitrile	N_2	$(CH_3)_2CCN$	5.6	Polycrystal, photolysis, 77°K	8
Dibenzoyl peroxide	$2CO_2$	C_6H_5	6.5	Single crystal, photolysis, 4.2°K	7
Dibenzoyl peroxide	$2CO_2$	C_6H_5	6.5	Crystal solid solution, photolysis, 4.2°K	This report

lution is still incomplete for most crystal orientations. The width of the absorption shown in Figure 1, measured between outermost hyperfine peaks, is 43 G. This is somewhat less than the overall hyperfine splitting reported by Kasai, *et al.*,[6] who found the sum of the hyperfine couplings was 48 G in phenyl radicals produced in a glass by the photolysis of phenyl iodide. Attempts to get a complete specification of the hyperfine tensors for the phenyl radical using the endor technique have been unsuccessful thus far. The width of the doublet lines in Figure 1 limits the accuracy of g value determinations. The change in resonant field with crystal orientation due to g value variation is small compared with line width.

The phenyl radicals generated by ultraviolet irradiation probably lie near the surface of the crystal. Prolonged irradiation or warming substantially above 4.2°K destroys the simple radical pair spectrum.

Pairs of phenyl radicals can also be produced by ultraviolet light in pure crystals of dibenzoyl peroxide irradiated at 4.2°K.[7] Apparently the first observation of radical pairs formed by elimination was by Lebedev[8] who observed the photolytic decomposition of azobisisobutyronitrile at 77°K with the release of a nitrogen molecule. Radical pairs have also been obtained from X-irradiated organic carbonates[9] wherein elimination of CO occurs. Table II is a compilation of pertinent facts concerning radical pairs produced by the process of elimination.

Radical Pairs by Dissociation. The peroxide molecules in the peroxide–disulfide mixed crystals of the preceding section can also be made to undergo simple dissociation. If the excitation energy is delivered *via* ionizing radiation, simple dissociation of the peroxide bond is achieved. Figure 2 shows the esr spectrum

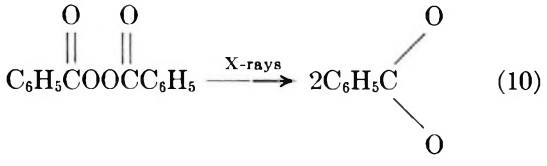

(10)

from a mixed crystal X-irradiated at 4.2°K. The spectrum contains the expected components, labeled β_0 and α_0 in Figure 2, due to oxidized and reduced disulfide molecules.[2] In addition there are the γ components which are attributed to pairs of dibenzoyloxy radicals. The size of the radical pair absorption indicates that excitation energy is efficiently transferred intermolecularly by the host molecules and deposited with the guest molecules which thereupon dissociate. The number of dissociated peroxide molecules is comparable with the number of oxidized and reduced disulfide molecules. Maximum separation of the γ lines (K band) indicates a distance between spins, as calculated using (5) of 3.6 Å. Presumably the disulfide matrix provides oversized spaces for the peroxide guest molecules so that upon dissociation of the peroxide bond the benzoyloxy radi-

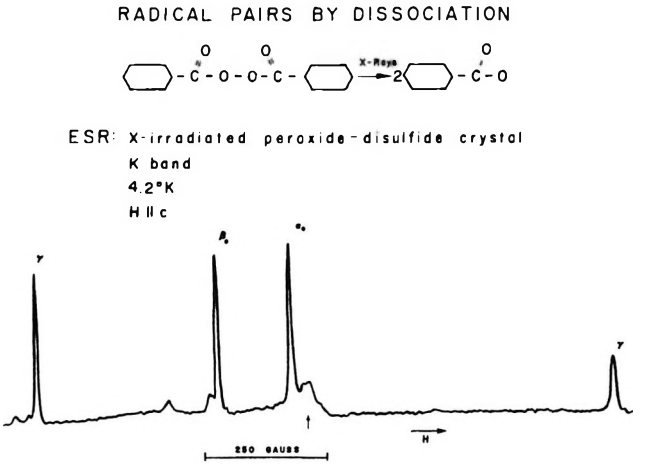

Figure 2. The esr spectrum from an X-irradiated single crystal of dibenzoyl disulfide with 3% of the molecules substituted with dibenzoyl peroxide. The irradiation and measurements were carried out at 4.2°K. Arrow indicates resonance for DPPH.

(6) P. H. Kasai, E. Hedaya, and E. B. Whipple, *J. Amer. Chem. Soc.*, **91**, 4364 (1969).

(7) H. C. Box, E. E. Budzinski, and H. G. Freund, *ibid.*, **92**, 5305 (1970).

(8) Y. S. Lebedev, *Dokl. Akad. Nauk SSSR*, **171**, 378 (1966).

(9) A. Davis, J. H. Golden, J. A. McRae, and M. C. R. Symons, *Chem. Commun.*, 398 (1967).

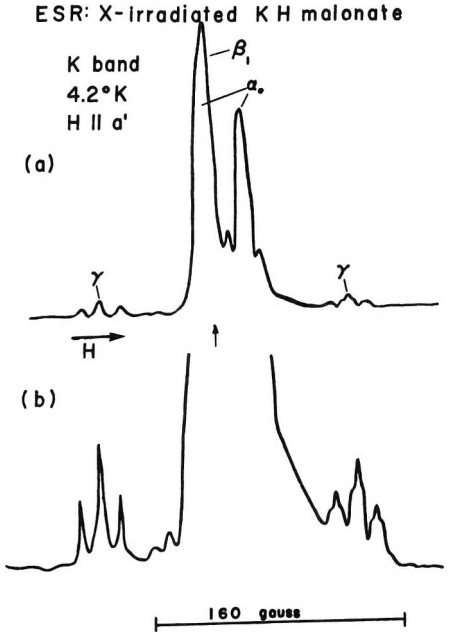

Figure 3. (a) The spectrum for an X-irradiated single crystal of potassium hydrogen malonate at 4.2°K. (b) The spectrum enlarged to show the γ lines associated with a radical pair. Arrow indicates resonance for DPPH.

cals can separate somewhat and thereby gain a measure of stability. Warming a few degrees above 4.2°K causes the radical pair absorption to disappear, undoubtedly because of recombination. Benzoyloxy radical pairs are not observed in single crystals of pure dibenzoyl peroxide crystals irradiated at 4.2°K.

The esr absorption indicates two sets of radical pairs related by a twofold axis. This is consistent with the $P2_1/c$ space group of dibenzoyl disulfide.[2] However, there is a perplexing feature of the absorption in that the intensities of the two sets of γ spectra (which can be distinguished for certain crystal orientations where the magnetic field is neither parallel or perpendicular to the twofold axis) are usually unequal. Also an interesting dependence of the esr absorption on magnetic field strength has been observed and is still being investigated.

At least one other example of radical pair production by dissociation exists in the literature. Gordy and Morehouse[10] produced pairs of methyl radicals and hydrogen atoms by γ irradiation of methane at 4.2°K.

Radical Pairs by Dehydrogenation of Adjacent Molecules. Figure 3 shows an esr spectrum obtained from a single crystal of potassium hydrogen malonate X-irradiated at 4.2°K. The β_1 and α_0 components of the spectrum are due to paramagnetic species produced by oxidation and reduction processes, respectively.[11] The smaller components labeled γ in Figure 3 are due to radical pairs produced by dehydrogenation of adjacent molecules. The radicals in each pair are formed with

$$2KOOCCH_2COOH \xrightarrow{\text{X-rays}} 2KOOCCHCOOH + H_2 \quad (11)$$

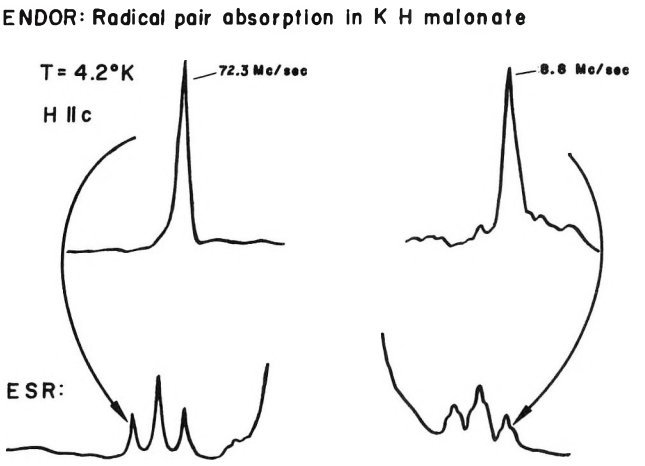

Figure 4. The endor lines obtained from the triplet state esr absorption in potassium hydrogen malonate.

the CH bond along the b axis of the crystal which is a twofold axis of rotation. The two radicals in each pair are related by a mirror plane perpendicular to the twofold axis.

The hyperfine structure associated with the γ absorption in Figure 3 is particularly interesting. One of the γ components has a nine-line hyperfine pattern; the other has a three-line pattern as is shown more clearly in Figure 3b. The entire hyperfine pattern arises from the two CH protons and can be accounted for quantitatively by calculating the transition probabilities associated with the allowed and "forbidden" transitions.[11]

Figure 4 shows the endor spectrum obtained from the γ components of the esr absorption. The endor frequencies are obtained from (7) for transitions between levels for which $\Delta m = 1$, $M = \pm 1$. From the

$$h\nu = \beta_N g_n h_M{}^n \quad (12)$$

definition of $h_M{}^n$ given in (8) it is clear that the higher endor frequency corresponds to transitions of the proton in the case where the component of effective magnetic field at the proton due to the unpaired electron augments the applied field; the lower frequency corresponds to the case where the two fields are opposed.

Table III: Principal Values in Gauss and Direction Cosines of the Principal Axes for the Hyperfine Coupling Found by Endor for the Radical Pair Produced in X-Irradiated Potassium Hydrogen Malonate

	a'	b	c
−4.5	−0.69	0	0.72
−10.0	0.72	0	0.69
−15.8	0	1	0

(10) W. Gordy and R. Morehouse, *Phys. Rev.*, **151**, 207 (1966).
(11) H. C. Box, E. E. Budzinski, and W. Potter, *J. Chem. Phys.*, **55**, 315 (1971).

Table IV: Radical Pairs by Dehydrogenation of Adjacent Molecules[a]

Parent molecule	Radical produced	Separation of radicals, Å	Reference
Dimethylglyoxime[b]	$HONC(CH_3)C(CH_3)NO$	5.6	1, 13
Glyoxime	HONCHCHNO	<4.8, <6.9	14
Methylglyoxime	$HONCHC(CH_3)NO$	<5.2, <7.9	14
p-Chlorobenzaldoxime	ClC_6H_4CHNO	6.1, 5.0[c]	15
Hydroquinone[d]	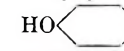	5.1	*h*
Oxalic acid	HOOCCOO	6.3, 9.9[e]	*i*
Hydroxyurea	NH_2CONHO	6.4[f]	19
Potassium hydrogen[g] malonate	KOOCCHCOOH	5.6	This report

[a] Except where indicated otherwise, all measurements were made on single crystals exposed to ionizing radiation at 77°K. [b] In partially deuterated dimethylglyoxime an additional radical pair is observed (ref 14). [c] Values quoted are for syn and anti forms, respectively. [d] Crystals were clathrates of hydroquinone and acetonitrile. [e] Values refer to radical pairs observed in dihydrate and anhydrous crystals, respectively. [f] A different separation is observed in crystals irradiated at 5°K. [g] Irradiation and measurement at 4.2°K. [h] M. Kashiwagi and Y. Kurita, *J. Phys. Soc. Jap.*, **21**, 558 (1966). [i] G. C. Moulton, M. P. Cernasky, and D. C. Straw, *J. Chem. Phys.*, **46**, 4292 (1967).

The endor spectra in Figure 4 are single lines because, as follows from the symmetry conditions mentioned above, the two protons in each pair are equivalent. Moreover, all radical pairs are equivalent. The hyperfine coupling tensor deduced from the endor measurements is described in Table III. As expected the principal values of the hyperfine coupling tensors are approximately half the values obtained for a proton in an isolated radical.[12] The principal values of the **g** tensor for the γ absorption are 2.0055, 2.0052, and 2.0022.[11]

The distance between radicals in each pair is 5.6 Å calculated from the observed dipole–dipole splitting using (5). This separation may be compared in Table IV with that found for other radical pairs generated by dehydrogenation of adjacent molecules.

It is of considerable interest to know the mechanism by which the radical pairs listed in Table IV are generated. The radical pairs produced in oxime crystals have been thoroughly studied by Kurita and coworkers.[1,13–15] Cook[16] has obtained the endor spectrum of the nitrogen resonance of the triplet state absorption in X-irradiated crystals of dimethylglyoxime. Symons[17] has proposed a mechanism for the formation of oxime radical pairs. Symons suggests that when a molecule is ionized, the ejected electron is captured by an adjacent molecule. The newly formed cation loses a proton forming the first radical of the required pair. Loss of hydride ion by the anion produces the second radical. The essential step in this sequence, and the most difficult to rationalize, is the primary step wherein the electron is trapped preferentially by a molecule adjacent to the cation. We have examined single crystals of dimethylglyoxime irradiated at 4.2°K (Figure 5a) and find no evidence of radical pair formation at this temperature. If the proposed scheme were true,

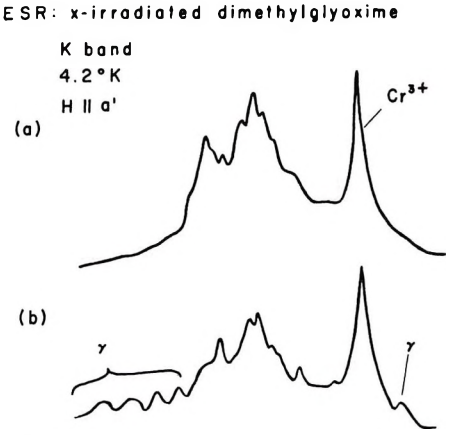

Figure 5. The esr absorption obtained from a single crystal of dimethylglyoxime: (a) X-irradiated and observed at 4.2°K; (b) observed at 4.2°K after warming to 77°K. Cr^{3+} peak is a reference absorption.[2] The γ peaks are attributed to radical pairs.

one should find pairs of radicals, either neutral radicals or radical ions, immediately following ionization. In fact, radical pairs are formed only after warming to 77°K (Figure 5b). This difficulty is avoided if one assumes that the ejected electron is captured by a molecule not necessarily adjacent to the cation.[18] The

(12) W. C. Lin and C. A. McDowell, *Mol. Phys.*, **4**, 343 (1961).

(13) Y. Kurita, *J. Chem. Phys.*, **41**, 3926 (1964).

(14) Y. Kurita and M. Kashiwagi, *ibid.*, **44**, 1727 (1966).

(15) H. Ohigashi and Y. Kurita, *Bull. Chem. Soc. Jap.*, **40**, 704 (1967).

(16) R. J. Cook in "Magnetic Resonance and Radio Frequency Spectroscopy," North-Holland Publishing Co., Amsterdam, 1969, pp 270–273.

(17) M. C. R. Symons in "Radiation Research 1966," North-Holland Publishing Co., Amsterdam, 1967, pp 131–147.

(18) Through Dr. Keiji Kuwata the author was made aware that this mechanism has been proposed previously by M. Iwasaki, T. Ichikawa, and T. Ohmori, *J. Chem. Phys.*, **50**, 1991 (1969).

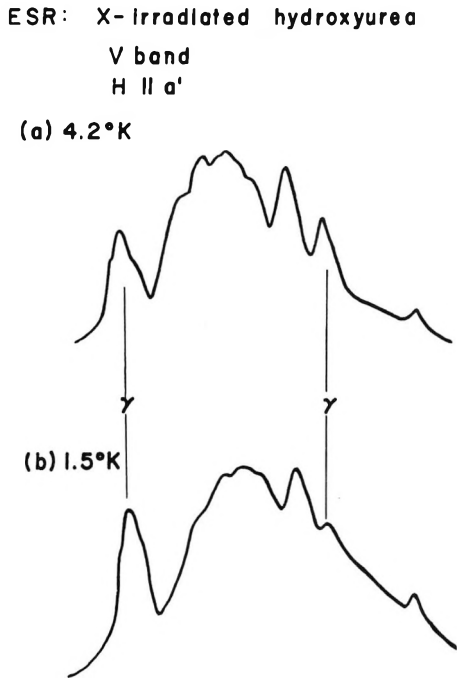

Figure 6. The esr spectra obtained at V band (70 GHz) from an X-irradiated single crystal of hydroxyurea. The spectra show the effect of temperature on the radical pair absorption (γ lines).

cation loses a proton to a neighboring molecule, producing the first radical of the radical pair. Upon warming electrons are able to migrate and combination of electrons with the protonated species occurs. Evolution of a hydrogen molecule produces a second radical in the vicinity of the first radical, thus creating a pair.

Another of the compounds in Table IV which we have examined at 4.2°K is hydroxyurea.[19] It is somewhat more difficult to sort out the radical pair absorption in hydroxyurea crystals irradiated at 4.2°K because of overlap with other absorption components. To clearly identify the radical pair contribution to the esr spectrum (Figure 6) use was made of the temperature dependence of the absorption which is characteristic of the triplet state. In Figures 1–3 the integrated absorptions of the two components of the radical pair absorption are not equal. This is a consequence of the fact that at 4.2°K the difference in population between the upper levels of the triplet state is slightly less than the difference between the lower levels. The fraction of the former compared to the latter is given approximately by

$$F = \frac{1 - \exp(-g_{fs}\beta H/kT)}{\exp(g_{fs}\beta H/kT) - 1} = \exp(-g_{fs}\beta H/kT) \quad (13)$$

where k is the Boltzmann constant and T is the absolute temperature. A useful technique is to lower the temperature of the sample below 4.2°K, by pumping a few minutes on the space above the helium. A radical pair absorption manifests itself by a noticeable change in F as the temperature is lowered. The temperature dependence is illustrated in Figure 6 for the radical pair produced in hydroxyurea[15] by X-irradiation at 4.2°K. The spectra were recorded on a V band (70 GHz) spectrometer and the components labeled γ are due to the radical pair. Clearly in hydroxyurea, as in potassium hydrogen malonate, radical pairs are created by ionizing radiation at liquid helium temperature. It is not clear whether a different mechanism is needed to explain radical pair formation in these compounds[20] or whether the neutralization step postulated in the case of the oximes can occur to a limited extent at low temperature in these compounds.

Summary

Our main interest is to discover how significant radical pair production is as a radiation damage mechanism. The experiments reported in this paper and the reports summarized in Tables II and IV, without exception, refer to radicals which remain paired only so long as the irradiated compounds are kept at low temperature. Clearly radical pair production is significant only insofar as it represents a primary stage of a radiation damage process. Radical pair production by the elimination process is limited to molecules having a special structure. Radicals generated in pairs by a process of dissociation often recombine on warming. Only the process which we have referred to as dehydrogenation of adjacent molecules may possibly be of general significance as a radiation damage process. Radicals formed by this process often have the capability, in effect, of diffusing apart at higher temperatures by virtue of intermolecular transfers of hydrogen. Thus discrete radicals can be produced which are stable at room temperature.

Acknowledgments. I wish to acknowledge my coworkers, Harold G. Freund, Edwin E. Budzinski, William Potter, and Kenneth T. Lilga. This work was supported by Contract AT(30-1)3558 with the Atomic Energy Commission and Public Health Grant EC-00009.

(19) K. Reiss and H. Shields, *J. Chem. Phys.*, **50**, 4368 (1969).

(20) M. Iwasaki and K. Toriyama, *ibid.*, **46**, 4693 (1967); M. Iwasak and B. Eda, *Chem. Phys. Lett.*, **2**, 210 (1968).

Electron Spin Resonance Spectra of Some σ-Type Aromatic Radicals[1]

by J. E. Bennett* and B. Mile

Shell Research Ltd., Thornton Research Centre, Chester CH1 3SH, England *(Received December 21, 1970)*

Publication costs assisted by Shell Research Limited

The phenyl, 2-pyridyl, and 2-pyrimidinyl radicals have been prepared by specific chemical reaction at low temperature (77°K) and trapped in a suitable inert matrix using a rotating cryostat. The hyperfine structure from naturally occurring carbon-13 atoms in the free valence position has been observed in the esr spectra of the three radicals or their deuterated analogs. The isotropic carbon-13 coupling constants are large (129–241 G) which shows that there is a considerable spin density (0.12–0.22) in the 2s orbital of the valence carbon atom. Thus, all three radicals are σ-type radicals in which the unpaired electron is localized mainly in an sp-hybrid orbital on one carbon atom and it is not delocalized in the π-orbital system of the aromatic ring. The spin density in the 2p orbital of the valence carbon atom is approximately the same (0.68) for each radical giving a total spin density on the valence carbon atom of 0.8–0.9. The spin distribution in the phenyl radical is in reasonable agreement with the values calculated by INDO theory.

Introduction

The electron spin resonance (esr) spectrum of a σ-type radical is of interest because detailed information about the hybridization of the orbital of the unpaired electron can often be obtained from an analysis of the spectrum. In this context the observation of the carbon-13 hyperfine structure from the valence carbon atom is of particular value. However, because of the low natural abundance of carbon-13 (≈1%) it is necessary either to use isotopically enriched compounds or to prepare the radicals in high concentration and purity. The former alternative is the more satisfactory but is often impractical because of high cost and non-availability of the isotopically enriched precursors for the more complex free radicals. The second method has been used successfully with a variety of radicals, but it is usually difficult to prepare σ radicals in high concentrations because of their reactivity compared to that of π radicals. With the exception of the benzoyl radical, all σ radicals that have been studied by esr spectroscopy have been trapped in an inert matrix at low temperature.

The formyl[2a] and vinyl[2b] radicals were among the first σ-type radicals to be studied by esr spectroscopy and the carbon-13 hyperfine structure in the spectrum of the formyl radical was observed by using isotopically enriched materials.[3] More recently, the carbon-13 spectra have been recorded for other acyl radicals, namely acetyl,[4] benzoyl,[5] and a substituted acetyl radical.[6] A large value of the isotropic hyperfine coupling was characteristic of the carbon-13 spectrum of each acyl radical, showing that the orbital of the unpaired electron possessed considerable 2s character.

The phenyl radical, which is the simplest σ-type aromatic radical, has been studied fairly extensively by esr spectroscopy.[7–10] It has been concluded from an analysis of the hyperfine coupling and g tensor that the phenyl radical is a σ-type radical with the unpaired electron in an sp-hybrid orbital. Recently[10] a tentative value for the isotropic carbon-13 coupling has been obtained which confirms the above conclusion about the structure of the phenyl radical.

The esr spectrum observed from γ-irradiated pyridine at 77°K has been attributed to the 2-pyridyl radical[11] which is also a σ-type radical with the unpaired electron in a hybrid orbital similar to that of the phenyl radical. The esr spectrum of the 2-pyridyl radical trapped in a matrix of argon at 4°K has been reported very recently[12] and confirms the above assignment.

In the present paper we report the observation of the carbon-13 spectra of the phenyl, 2-pyridyl, and 2-pyrimidinyl radicals at 77°K. The radicals were prepared by a specific chemical reaction and trapped in an inert matrix at 77°K using a rotating cryostat.

(1) Presented at the Second Esr Symposium of the Physical Chemistry Division of the American Chemical Society, University of Georgia, Athens, Ga., Dec 7–9, 1970.

(2) (a) F. J. Adrian, E. L. Cochran, and V. A. Bowers, *J. Chem. Phys.*, **36**, 1661 (1962); (b) E. L. Cochran, F. J. Adrian, and V. A. Bowers, *ibid.*, **40**, 213 (1964).

(3) E. L. Cochran, F. J. Adrian, and V. A. Bowers, *ibid.*, **44**, 4626 (1966).

(4) J. E. Bennett, B. Mile, and B. Ward, *Chem. Commun.*, 13 (1969).

(5) P. J. Krusic and T. A. Rettig, *J. Amer. Chem. Soc.*, **92**, 722 (1970).

(6) R. C. McCalley and A. L. Kwiram, *ibid.*, **92**, 1441 (1970).

(7) V. A. Tolkachev, I. I. Chkheidze, and N. Ya. Buben, *Zh. Strukt. Khim.*, **3**, 709 (1962).

(8) J. E. Bennett, B. Mile, and A. Thomas, *Proc. Roy. Soc., Ser. A*, **293**, 246 (1966).

(9) P. H. Kasai, E. Hedaya, and E. B. Whipple, *J. Amer. Chem. Soc.*, **91**, 4364 (1969); P. H. Kasai, P. A. Clark, and E. B. Whipple, *ibid.*, **92**, 2640 (1970).

(10) S. Nagai, S. Ohnishi, and I. Nitta, *J. Phys. Chem.*, **73**, 2438 (1969).

(11) H. J. Bower, J. A. McRae, and M. C. R. Symons, *J. Chem. Soc. A*, 2696 (1968).

(12) P. H. Kasai and D. McLeod, *J. Amer. Chem. Soc.*, **92**, 6085 (1970).

Experimental Section

The rotating cryostat technique for the preparation of free radicals by chemical reaction at low temperature has been described in detail previously.[8,13] In general, the free radicals were prepared by the specific reaction between sodium (or potassium) atoms and the parent halohydrocarbon at 77°K

$$RX + Na\cdot \longrightarrow R\cdot + NaX$$

Briefly the technique involved the deposition of alternate layers of the reactants and a suitable matrix on the outer surface of a drum which was filled with liquid nitrogen and rotated rapidly under high vacuum ($\approx 10^{-6}$ Torr). Gaseous beams of the reactants were directed onto the drum from jets located close to the surface. The rates of deposition were adjusted so that several monolayers of the inert matrix, but less than a monolayer of each reactant, were laid down every revolution. This procedure ensured that the free radicals were formed in isolated sites in the matrix and thus were unable to react with each other. The free radicals were covered up and trapped rigidly by a fresh layer of matrix which was deposited during the next revolution of the drum.

When sufficient material had been laid down (approximately 75,000 revolutions; 1 g of matrix; 10^{-2} to 10^{-1} g of halohydrocarbon; 10^{-3} g of sodium), the deposit was removed from the surface of the drum and transferred to a tube suitable for esr measurements. The complete transfer was carried out at 77°K and under high vacuum.

The phenyl radical was prepared from phenyl iodide and the 2-pyridyl and 2-pyrimidinyl radicals from the corresponding bromides. The fully deuterated phenyl-d_5 radical was prepared from phenyl-d_5 bromide. Because of the high reactivity of the phenyl radical only benzene, benzene-d_6, and deuterium oxide were used as matrices in the present experiments. Earlier studies[8] had shown that the phenyl radical reacted with other organic materials, even at 77°K. It was assumed that the 2-pyridyl and 2-pyrimidinyl radicals would also have a similar reactivity.

An interesting, alternative method of preparation of the phenyl radical was discovered during other studies involving unsuccessful experiments to prepare and trap the radical anion, N_2O^-, by the reaction between nitrous oxide and sodium in the rotating cryostat. N_2O^- was not stabilized but dissociated into molecular nitrogen and O^- which was trapped readily in water or deuterium oxide at 77°K. However, O^- reacted rapidly with trace hydrocarbons present, including benzene, by hydrogen abstraction to give the corresponding free radical. Thus, by using either benzene or benzene-d_6 as the matrix the corresponding phenyl radical could be prepared and trapped in high concentration. Well-defined carbon-13 hyperfine structure was observed in the spectrum of the phenyl-d_5 radical prepared in this manner and confirmed the results obtained for the phenyl radical prepared by the usual method.

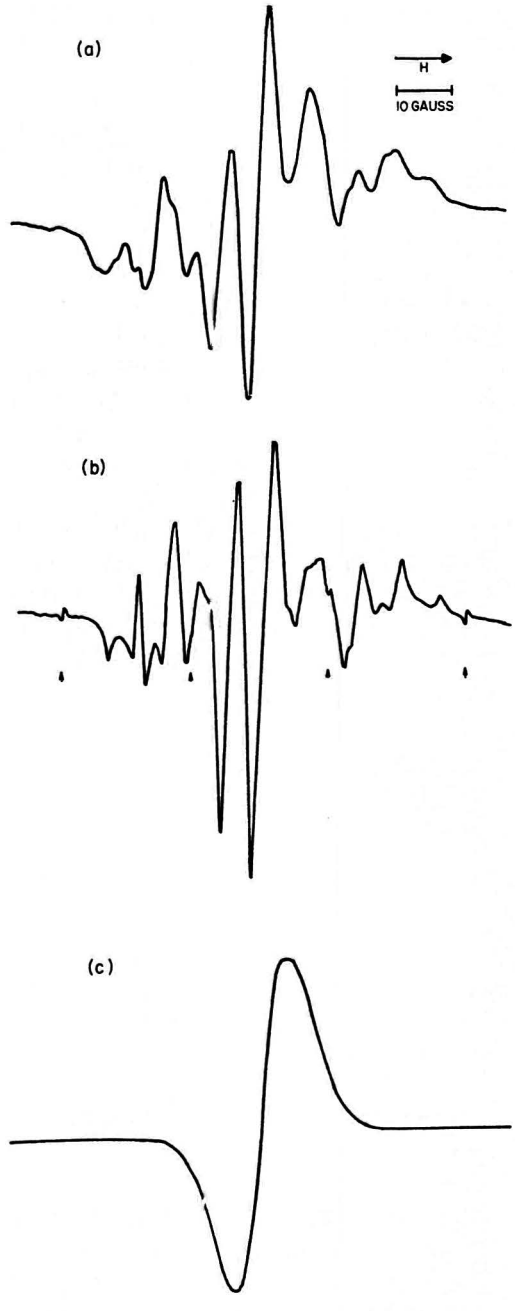

Figure 1. First-derivative esr spectrum of (a) $C_6H_5\cdot$ in C_6D_6 at 77°K; (b) $C_6H_4D\cdot$-$4d_1$ in xenon at 4°K (from ref 9); arrows indicate quartet due to methyl radical; (c) $C_6D_5\cdot$ in C_6D_6 at 77°K.

It was also found that the 2-pyridyl-d_4 radical could be prepared from pyridine-d_5 by this method involving nitrous oxide. The esr spectrum showed that O^- reacted very cleanly with pyridine-d_5 to give the 2-pyridyl-d_4 radical almost exclusively. Much better carbon-13 spectra were obtained from these samples

(13) J. E. Bennett and A. Thomas, *Proc. Roy. Soc., Ser. A*, **280**, 123 (1964).

than from the 2-pyridyl radical produced from 2-bromopyridine.

Results

Phenyl. The esr spectra of the phenyl and phenyl-d_5 radicals trapped in matrices of benzene-d_6 are shown in Figures 1a and c, respectively. For comparison the spectrum of the phenyl-d_1 radical (para-substituted) trapped in a matrix of xenon[9] at 4.2°K is shown in Figure 1b. The assignment of the proton hyperfine couplings has been discussed fully in earlier papers.[8,9] The corresponding deuterium hyperfine structure in the phenyl-d_5 radical was too small to be resolved, and thus the spectrum consisted of a single line. The spectrum of the phenyl-d_5 radical recorded under much higher sensitivity is shown in Figure 2. The assignment of the carbon-13 coupling constants is indicated in the figure, based on the assumption that the coupling tensor has approximately cylindrical symmetry. The values of the coupling constants and the corresponding values of the isotropic and anisotropic contributions are given in Table I.

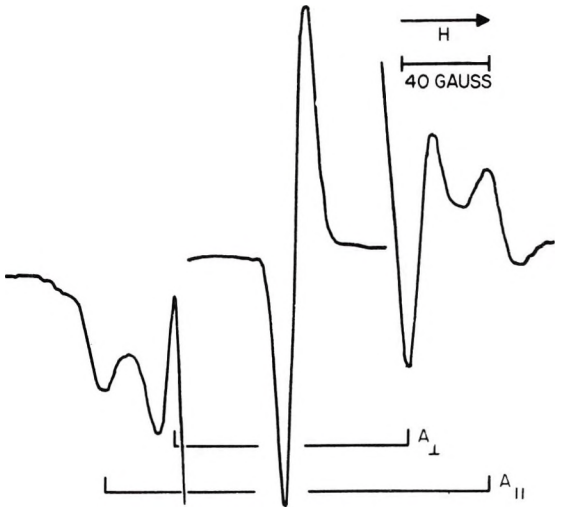

Figure 2. First-derivative esr spectrum of $C_6D_5\cdot$ in C_6D_6 at 77°K, showing carbon-13 hyperfine structure. Wings of spectrum at increased sensitivity (×1000).

Table I: Carbon-13 Hyperfine Coupling Tensors and Spin Densities

	Phenyl[a]	2-Pyridyl a	2-Pyridyl b	2-Pyrimidinyl[a]
$A_{\|\|}$, G	174	217	200	284
$A_{\perp}$, G	107	147	155	220
A_{iso}, G	129	171	170	241
B, G	22	23	15	21
ρ_{2s}	0.12	0.15	0.15	0.22
ρ_{2p}	0.69	0.72	0.45	0.65

[a] This work; values ±2 G. [b] Results from ref 11.

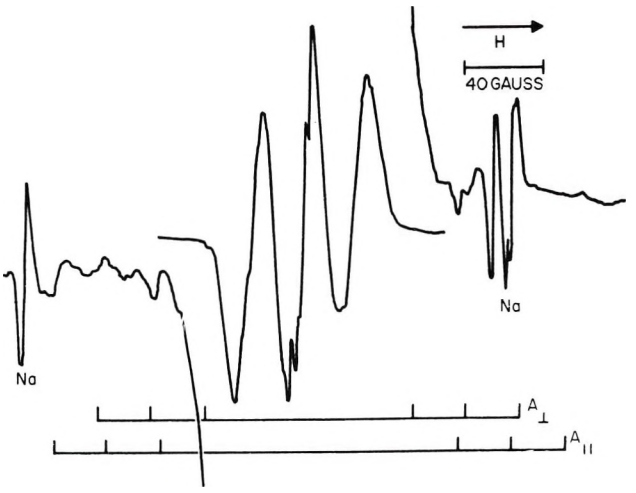

Figure 3. First-derivative esr spectrum of 2-pyridyl in C_6D_6 at 77°K, showing carbon-13 hyperfine structure. Wings of spectrum at increased sensitivity (×100).

2-Pyridyl. The spectra of the 2-pyridyl radical recorded at low and high instrumental sensitivity are shown in Figure 3. The major triplet structure is caused by hyperfine coupling to the nitrogen nucleus, and the shape of the outer lines shows that the coupling is slightly anisotropic. The central line, which was mainly unaffected by the anisotropy, exhibited a poorly resolved quartet structure at 77°K. At 120°K the resolution improved slightly, and the four lines became approximately equal in intensity. These lines are attributed to hyperfine couplings to two nonequivalent protons. The values of the nitrogen and proton hyperfine couplings are given in Table II. (The assignment of the major hyperfine splitting to interaction with the nitrogen atom and the minor splittings to proton interactions is confirmed by the spectrum of the 2-pyridyl-d_4 radical which is discussed below.)

At high sensitivity, lines which are attributed to interaction with carbon-13 nuclei can be observed in the wings of the spectrum of the 2-pyridyl radical (Figure 3). Unfortunately, there are also other lines which arise from sodium atoms trapped in four distinct sites in the matrix (benzene-d_6), and these obscure some of the carbon-13 lines. The behavior of the lines as the sample is warmed from 77 to 130°K allows the carbon-13 lines to be identified. It is not possible to evaluate completely the carbon-13 coupling tensors, but the positions of the observed lines are in fair agreement with those observed from the 2-pyridyl-d_4 radical formed by reaction of O^- with pyridine-d_5 (Figure 4).

The spectrum of the 2-pyridyl-d_4 radical is shown in Figure 4. The nitrogen hyperfine coupling is identical with that observed for the 2-pyridyl radical and confirms that the reaction between O^- and pyridine-d_5 yields the 2-pyridyl-d_4 radical almost exclusively. The absence of any further hyperfine structure shows that the additional hyperfine structure in the spectrum of

Table II: Nitrogen and Proton Hyperfine Coupling Constants

Hyperfine coupling, G	Phenyl	2-Pyridyl			2-Pyrimidinyl
		a	*b*	*c*	
A_N (iso)	...	31 ± 1	30	27	28.5 ± 1.5
B_N	...	4.5 ± 0.5	2.8	...	1.5 ± 1.5
A_H (ortho)	18.1 ± 1.0	8.0 ± 0.5	...	7.0	...
A_H (meta)	6.4 ± 0.5	4.0 ± 0.5	...	7.0	...

[a] This work. [b] Results from ref 11. [c] INDO calculations from ref 12.

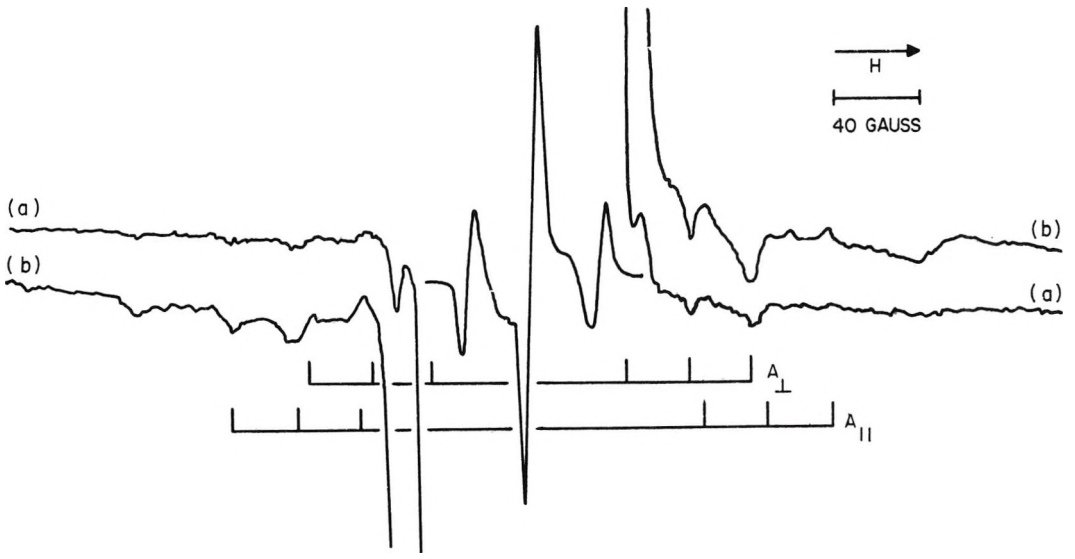

Figure 4. First-derivative esr spectrum of 2-pyridyl-d_4 in C_5ND_5 at 77°K, showing carbon-13 hyperfine structure. Wings of spectrum at increased sensitivity; (a) ×125 and (b) ×400.

the 2-pyridyl radical arises from interaction with the ring protons. Because of the anisotropy of the nitrogen hyperfine coupling, the outer lines are slightly asymmetric and broader than the central line. Thermal annealing experiments show that the sharp peak which is visible at high gain on the low-field side of the spectrum and the two shoulders on the central line are due to an impurity radical (or radicals). After warming the sample to 130°K and recooling to 77°K the intensities of the carbon-12 and carbon-13 spectra of the pyridyl radical had decreased considerably, whereas the intensities of the lines attributed to the impurity radicals had hardly decreased. The assignment of the carbon-13 hyperfine structure, which is visible at high gain, is shown under the spectrum (Figure 4). The absence of lines from trapped sodium atoms allows a complete assignment of the carbon-13 coupling constants to be made (Table I).

2-Pyrimidinyl. The esr spectrum (Figure 5) of the 2-pyrimidinyl radical trapped in a matrix of benzene-d_6 at 77°K consists basically of five equally spaced lines (intensity ratios approximately 1:2:3:2:1) which are caused by hyperfine coupling with two equivalent nitrogen nuclei. The analysis of the spectrum to obtain the isotropic and anisotropic hyperfine couplings (Table II) is complicated because the coupling tensors of the two nitrogen atoms will not have common in-plane axes. A partial simulation of the spectrum shows that the major inflexions on the individual lines can arise from the anisotropy of the nitrogen hyperfine coupling. Consequently, any proton hyperfine coupling must be small and unresolved.

At high sensitivity the carbon-13 hyperfine lines are observed in the wings of the spectrum (Figure 5). There should be five sets of lines on each side of the main spectrum corresponding to the five nitrogen hyperfine lines, but some of the innermost lines are obscured by the main lines. On the assumption that the carbon-13 hyperfine coupling has approximately axial symmetry, the assignment of the lines is as indicated in Figure 5. The principal values of the coupling tensor derived from this analysis are given in Table I.

Discussion

Phenyl Radical. In our earlier paper[8] we discussed the spectrum of the phenyl radical trapped in a variety of matrices. In water at 77°K the spectrum was reasonably symmetrical and values for the isotropic proton

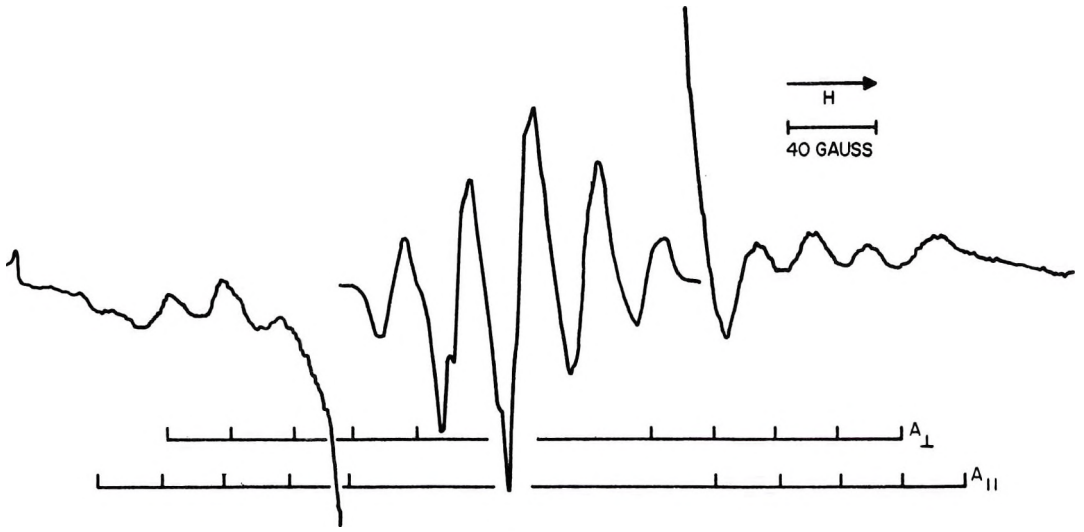

Figure 5. First-derivative esr spectrum of 2-pyrimidinyl in C_6D_6 at 77°K, showing carbon-13 hyperfine structure. Wings of spectrum at increased sensitivity (×200).

coupling constants were obtained. With benzene or benzene-d_6 as a matrix the spectrum was more asymmetric and showed indications of additional structure, which we attributed to the existence of two discrete trapping sites in which the coupling constants of the phenyl radical were different.

More recently Kasai, Hedaya, and Whipple[9] have obtained a better resolved spectrum of the phenyl radical in xenon at 4.2°K and have shown that the asymmetry is caused by anisotropic g and hyperfine tensors. Comparison of the two spectra (Figures 1a and b) shows that, apart from a slightly poorer resolution, our original spectrum in benzene-d_6 at 77°K is virtually identical with that observed in xenon at 4.2°K. The two sets of values of the hyperfine coupling constants, which we erroneously attributed to the effect of multiple sites, agree reasonably well with the more accurate values obtained by Kasai, *et al.* (Table III). The isotropic values of the coupling constants observed in a matrix of water at 77°K are also in reasonable accord with those obtained by Kasai, *et al.* (Table III).

Table III: Proton Hyperfine Coupling Constants for Phenyl Radical

	Matrix	Hyperfine coupling constant, G Ortho	Meta	Para	Reference
A (iso)	Xenon	17.4	5.9	1.9	9a
	C_6D_6	18.1	6.4	<3.0	8b
A_x	Xenon	21.9	6.6	2.0	9
	C_6D_6	21.2	6.6	...	8
A_y	Xenon	15.4	6.1	2.5	9
A_z	Xenon	14.9	5.0	1.2	9
A_y, A_z	C_6D_6	16.9	6.4	...	8

[a] All values ±0.1 G. [b] All values of ortho ±1.0 G; meta ±0.5 G.

The fact that the spectrum of the phenyl radical in water at 77°K is less anisotropic than that in benzene (or benzene-d_6) at 77°K indicates that the phenyl radical is less rigidly held in a matrix of water than of benzene (*i.e.*, the greater motional freedom tends to average out the anisotropic contributions to the g and hyperfine tensors). This difference arises presumably because the phenyl radical can be accommodated in the benzene without any appreciable distortion of the crystal structure, whereas this does not occur in water.

The observed carbon-13 hyperfine couplings can be treated in the usual manner to yield the isotropic and anisotropic terms of the hyperfine coupling tensor. In turn these values may be used to calculate the spin densities in the carbon 2s and 2p orbitals, respectively (Table I). (The theoretical values of the hyperfine couplings for fully occupied 2s and 2p orbitals are taken as 1110.7 and 32.4 G, respectively).[14]

The isotropic value (129 G) is smaller than that (140 G) reported recently for the phenyl radical trapped on silica gel,[10] but this latter value may be high because no account was taken of the anisotropic contribution. Our experimental value is also smaller than that (151 G) calculated[15] assuming sp^2 hybridization of the free valence orbital. If this is a genuine difference, then it may indicate that the 2s contribution to the hybrid orbital is less than that expected for sp^2 hybridization. The experimental spin densities support this conclusion, as they yield a hybridization ratio (p/s) of 5.9, whereas that expected for sp^2 hybridization is 2.0. As a result of this change in hybridization, the CĈC bond angle at the valence carbon atom is probably larger than 120°. (The experimental results

(14) D. H. Whiffen, *J. Chim. Phys.*, 61, 1589 (1964).

(15) J. A. Pople, D. L. Beveridge, and P. A. Dobosh, *J. Amer. Chem. Soc.*, 90, 4201 (1968).

give a value of 138°, but this should be treated with considerable caution.)

2-Pyridyl. The esr spectra from pyridine exposed to β or γ irradiation at 77°K have been studied in some detail previously.[11,12] Recently, Bower, McRae, and Symons[11] have reinterpreted the spectrum observed initially at 77°K in terms of the 2-pyridyl radical. The results of our experiments, in which the 2-pyridyl radical was prepared by a much more specific method, confirm their assignment. The nitrogen hyperfine coupling tensors observed in both experiments are in good agreement (Table II). A value of 27 G for the nitrogen hyperfine coupling has been observed recently by Kasai and McLeod[12] for the 2-pyridyl radical trapped in argon at 4°K. However, the line width is larger than that at 77°K and neither the anisotropy of the nitrogen hyperfine coupling nor the proton hyperfine couplings are clearly resolved. Their INDO calculations predict a value of 27 G for the isotropic nitrogen hyperfine coupling.

The proton hyperfine couplings cannot be assigned unambiguously, but by comparison with those of the phenyl radical it is resonable to assign the larger splitting (8.0 G) to the 3 proton (ortho position relative to the free valence carbon) and the smaller splitting (4.0 G) to the 4 proton (meta). These values are less than the corresponding ones observed for the phenyl radical. The reduction is probably caused by delocalization of the unpaired electron on to the nitrogen atom. If this assignment is correct then coupling to the other meta proton (6 position) across the nitrogen atom must be small and not resolved. The lack of proton hyperfine coupling in the 2-pyrimidinyl radical lends support to this conclusion. The recent INDO calculations[12] support the conclusion that the proton coupling across the nitrogen is negligible, but, on the other hand, predict that the hyperfine couplings to the 3 and 4 protons should be equal (7 G).

The carbon-13 isotropic coupling constant is in reasonable agreement with that obtained for the 2-pyridyl-d_4 in γ-irradiated pyridine-d_5.[11] However, our value for the anisotropic coupling is significantly larger than that observed in γ-irradiated pyridine-d_5. Consequently, although the calculated values of spin density in the 2s orbital are very similar, those in the 2p orbital of the valence carbon atom differ significantly (Table I).

2-Pyrimidinyl. The isotropic nitrogen hyperfine coupling is slightly less in the 2-pyrimidinyl radical than that in the 2-pyridyl radical (Table II). This reduction is reasonable if it is assumed that there is some delocalization of the unpaired electron onto the nitrogen atom. The anisotropic coupling is rather less than the corresponding coupling in 2-pyridyl, but in view of the error associated with the measurement of these values the difference is probably not significant. For both radicals the anisotropy is much smaller than that observed for nitrogen-centered radicals and is thus further evidence that their structures have been assigned correctly.

The assignment of the carbon-13 hyperfine couplings appears to be satisfactory. The isotropic and anisotropic couplings and the spin densities, which are calculated on the basis of this assignment, are given in Table I. A less likely assignment leads to values of the isotropic and anisotropic couplings of 193 and 27 G, respectively. The corresponding spin densities in the 2s and 2p orbitals are 0.17 and 0.83, respectively.

Spin Density Distribution. It is evident from the results (Table I) that the phenyl, 2-pyridyl, and 2-pyrimidinyl radicals are all σ-type radicals with the unpaired electron located mainly on the free valence carbon atom. The spin distribution is similar for all three radicals and the total spin density in the sp-hybrid orbital of the free valence carbon atom is about 0.85.

The spin densities in the 2p orbitals are virtually the same for all the radicals. Our value for the 2-pyridyl radical is more in line with those of the phenyl and 2-pyrimidinyl radicals than the value obtained by Bower, *et al.*[11] There is no apparent reason for this difference, though admittedly the anisotropic coupling (and consequently the spin density in the 2p orbital) cannot be measured very accurately from the spectrum of polycrystalline samples. Our values are in reasonable accord with that (0.70) calculated by Kasai, *et al.*,[9] using extended Hückel theory. However, it should be noted that their calculations give a very low value (0.05) for the 2s contribution.

The participation of the 2s orbital in the orbital of the unpaired electron increases through the series phenyl, 2-pyridyl, 2-pyrimidinyl (this is also true if the alternative interpretation of the spectrum of the 2-pyrimidinyl radical is accepted). It has been suggested[11] that in the 2-pyridyl radical overlap of the sp-hybrid orbital on the carbon atom with the lone-pair orbital on the nitrogen atoms leads to the formation of pseudo-π orbitals, one bonding and the other antibonding. The unpaired electron would be in the antibonding orbital, and thus would be located mainly on the less electronegative carbon atom, as found experimentally. The increase in the 2s-orbital contribution from the carbon in the 2-pyridyl radical suggests that the antibonding orbital has a higher 2s character than the original sp-hybrid orbital on the carbon atom in the phenyl radical. A similar set of pseudo-π orbitals can be envisaged for the 2-pyrimidinyl radical and are consistent with the further increase in the 2s-orbital contribution to the orbital of the unpaired electron.

Acknowledgment. We thank Mr. C. P. Rimmer and Mr. R. Summers for assistance with the experimental work.

Electron Spin Resonance Studies of Conformations and Hindered Internal Rotation in Transient Free Radicals[1]

by Paul J. Krusic, Paul Meakin,* and J. Peter Jesson

Central Research Department, E. I. du Pont de Nemours and Company, Wilmington, Delaware 19898
(Received March 26, 1971)

Publication costs assisted by E. I. du Pont de Nemours and Company

The temperature-dependent esr spectra of a series of alkyl and substituted alkyl radicals are discussed from the point of view of their internal dynamics and their equilibrium conformations. Two effects are considered in detail: the temperature dependence of β-proton hyperfine splittings and the temperature dependence of the line shapes. Quantum mechanical calculations are used to determine the heights of the barriers hindering rotation about C_α–C_β or C_α–O bonds by fitting the experimental $a_\beta^H(T)$ curves. These barriers are compared with the values obtained by a classical anisotropic averaging of the $\cos^2 \alpha$ dependence of the coupling constants for β protons. For simple alkyl radicals with low barriers and relatively large reduced moments of inertia the two methods yield identical results. For the hydroxymethyl radical, which exhibits a marked line width effect at low temperatures in addition to a temperature-dependent β-hydroxylic splitting, the rotational barrier is also studied by the analysis of the line shapes using the density matrix method. Quantitative treatment of both effects yields a barrier of about 4 kcal/mol restricting the rotation about the C–O bond in this radical. Alternating line width phenomena are also reported for several alkyl radicals and are used in conjunction with the magnitudes of a_β^H to establish the equilibrium conformations. Certain anomalies in the magnitudes of the β-proton couplings and the slopes of their temperature dependences compared with expectations based on a $\cos^2 \alpha$ angular dependence are interpreted in terms of distortions from tetrahedral geometry at the β carbon atom. It is concluded that the $\cos^2 \alpha$ law does not adequately represent the angular dependence of the β-proton isotropic hyperfine coupling constants in these radicals. INDO molecular orbital calculations are used in support of these conclusions.

Introduction

Although the unique applicability of electron spin resonance (esr) spectroscopy to the quantitative study of hindered internal rotation in free radicals is well recognized, most of the existing investigations in this area[2] have dealt with relatively stable free radicals. The two approaches to the problem, *viz.*, the study of the temperature dependence of the isotropic hyperfine coupling constants for β protons and the study of the line shapes as a function of temperature, require accurate spectral measurements over a wide temperature range which, until recently, could not be carried out easily for transient free radicals in solution.

A few such studies on reactive radicals nevertheless exist. The temperature dependence of β-proton coupling constants for a few simple alkyl radicals (*n*-propyl, isobutyl, 3-butenyl, and deuterated ethyl radicals), generated by electron radiolysis of liquid hydrocarbons, were interpreted in terms of the quantum theory of hindered rotation by Fessenden,[3a] who was able to extract values for the barriers restricting rotation about the C_α–C_β bond. In a more recent study, Golde, Möbius, and Kaminski[3b] applied the modified Bloch equations[4] to the analysis of the alternating line width effect observed in the radical $\dot{C}H_2COCH_3$ produced by hydrogen atom abstraction *via* photolytically generated OH radicals in a flow system.[5] By matching the calculated line shapes to the experimental ones over a wide temperature range, they obtained the activation energy for rotation of the $\dot{C}H_2$– fragment. While our work was nearing completion,[6] Hudson[7] independently reported the line width alternation observable in the spectrum of the hydroxymethyl radical at temperatures below $-50°$. His activation parameters for the rotation of the hydroxy group about the C–O bond in this important radical are, however, substantially different from those we report in this study.

The development of photolytic methods for the esr detection of reactive radicals in static, nonaqueous so-

(1) Contribution No. 1820.

(2) For reviews see (a) D. H. Geske, *Progr. Phys. Org. Chem.*, **4**, 125 (1967); (b) A. Hudson and G. R. Luckhurst, *Chem. Rev.*, **69**, 191 (1969); (c) P. D. Sullivan and J. R. Bolton, *Advan. Magn. Resonance*, **4**, 39 (1970).

(3) (a) R. W. Fessenden, *J. Chim. Phys.*, **61**, 1570 (1964); (b) G. Golde, K. Möbius, and W. Kaminski, *Z. Naturforsch. A*, **24**, 1214 (1969).

(4) H. S. Gutowsky and C. H. Holm, *J. Chem. Phys.*, **25**, 1228 (1956).

(5) R. Livingston and H. Zeldes, *ibid.*, **44**, 1245 (1966).

(6) (a) Aspects of this work were previously presented: Abstracts, 159th National Meeting of the American Chemical Society, Houston, Texas, Feb 1970, No. PHYS 089; (b) a small portion of this work also appeared in a review: *Chem. Soc. (London) Spec. Publ.*, **24**, 147 (1970).

(7) (a) A. Hudson, *J. Chem. Soc. A*, 2513 (1969); (b) A. Hudson and K. D. J. Root, *Tetrahedron*, **25**, 5311 (1969).

lutions[8] has opened the way to the ready examination of spectral changes over wide temperature ranges thus allowing the detailed study of a variety of intramolecular dynamic processes in such radicals. One of the major goals of this paper is to show that the temperature dependence of β-coupling constants and the line shape effects can be used complementarily on the same radical species to obtain by independent routes quantitative information on the potential which restricts rotation and to establish the equilibrium conformation in a variety of radical systems. A nearly ideal case for these purposes, which we shall therefore discuss in greater detail, is the hydroxymethyl radical $\dot{C}H_2OH$ where the two effects are operative simultaneously.

Experimental Section

The esr instrumentation, the source of uv radiation, the optical system, and the handling of the samples are described elsewhere.[9]

The temperature of the sample was monitored by a thermocouple placed just below the sensitive part of the cavity. Because of the intense radiation from the mercury arc, the temperature of the irradiated sample was several degrees higher than that monitored by the thermocouple despite the presence of a cooling cell through which was circulated a 0.1 M aqueous $NiCl_2 \cdot 6H_2O$ solution. Periodically this difference in temperature was measured by a second thermocouple. The latter was placed in a sample tube containing methyl alcohol and was carefully positioned to be in the center of the cavity. The temperature difference between the two thermocouples was applied as a correction to the temperatures measured by the monitoring thermocouple. This correction amounted to 10–20°. We consider that the temperatures reported here are within, at most, 5° of the true temperature in the irradiated region of the sample.

All compounds employed in this study were reagent grade commercial samples which were used without further purification.

Mathematical Section

Temperature Dependence of β-Proton Coupling Constants. The temperature dependence of β-proton hyperfine coupling constants has been the subject of several investigations.[3a,10] In this section we shall therefore only briefly review the theory to have a basis for the description of the computational methods employed in this work. We shall also give a classical approximation for the temperature dependence of a_β^H which we have found to be quite useful for relatively low barriers to rotation.[9]

The isotropic hyperfine coupling constant of a proton situated relative to a carbon radical center as in structure I is always strongly temperature dependent. It is assumed that as the temperature varies, the most important contribution to the change in the H_β coupling

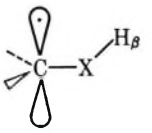

I

X = C, O

constant is due to a different average torsional angle about the $\dot{C}$–X internuclear axis. In general, we can write the dependence of a_β^H on the torsional angle α as a Fourier series of even terms

$$a_\beta^H(\alpha) = a_0 + a_2 \cos 2\alpha + a_4 \cos 4\alpha + \ldots \quad (1)$$

where α is measured from the direction of the half-occupied p_z orbital. If we assume that a_4, a_6, etc., are so small that they can be ignored, we have the conventional $\cos^2 \alpha$ form of the angular dependence of a_β^H (eq 3) which is consistent with the hyperconjugative mechanism for spin density transmission to the β proton. The less familiar but entirely equivalent

$$a_\beta^H(\alpha) = a_0 + a_2 \cos 2\alpha \quad (2)$$

$$= A + B \cos^2 \alpha \quad (3)$$

$$= A' \sin^2 \alpha + B' \cos^2 \alpha \quad (4)$$

form of eq 4 has recently been proposed by Sullivan[11] for the angular dependence of β-hydroxylic protons in aromatic radical cations.

In the radicals considered here the rotating group has C_2 symmetry and the barrier to internal rotation can similarly be represented by a cosine series of even terms which can be truncated to

$$V(\theta) = \frac{V_2}{2}(1 - \cos 2\theta) \quad (5)$$

where θ is measured from the minimum of the potential function.

The conventional model for calculating the temperature dependence of the β-coupling constant assumes that transitions between the torsional levels are rapid on the time scale of the esr experiment so that the observed splitting is the average of the quantum mechanical expectation values of a_β^H for all torsional states weighted by their populations. Assuming Boltzmann statistics

(8) (a) P. J. Krusic and J. K. Kochi, *J. Amer. Chem. Soc.*, **90**, 7155 (1968); (b) J. K. Kochi and P. J. Krusic, *ibid.*, **91**, 3940 (1969); (c) A. Hudson and H. A. Hussain, *Mol. Phys.*, **16**, 199 (1969).

(9) P. J. Krusic and J. Kochi, *J. Amer. Chem. Soc.*, **93**, 846 (1971).

(10) (a) C. Heller and H. M. McConnell, *J. Chem. Phys.*, **32**, 1535 (1960); (b) E. W. Stone and A. H. Maki, *ibid.*, **37**, 1326 (1962); (c) M. Kashiwagi and Y. Kurita, *ibid.*, **39**, 3165 (1963); (d) O. H. Griffith, *ibid.*, **41**, 1093 (1964); (e) C. Corvaja, *Trans. Faraday Soc.*, **63**, 26 (1967); (f) M. D. Sevilla and G. Vincow, *J. Phys. Chem.*, **72**, 3647 (1968); (g) G. Chapelet-Letourneux, H. Lemaire, R. Lenk, M. Marechal, and A. Rassat, *Bull. Soc. Chim. Fr.*, **10**, 3963 (1968); (h) P. B. Ayscough, M. C. Brice, and R. E. D. McClung, *Mol. Phys.*, **20**, 41 (1971).

(11) P. D. Sullivan, *J. Phys. Chem.*, **73**, 2790 (1969).

$$a_\beta^H(T) = \frac{\sum_i \langle a_\beta^H(\alpha)\rangle_i \exp(-E_i/kT)}{\sum_i \exp(-E_i/kT)} \quad (6)$$

where E_i are the torsional energies and the brackets $\langle\ \rangle$ denote a quantum mechanical expectation value. Since

$$\langle a_\beta^H(\alpha)\rangle_i = a_0 + a_2\langle\cos 2\alpha\rangle_i \quad (7)$$

the problem of calculating a_β^H at a given temperature from eq 6 requires the knowledge of the constants a_0 and a_2 (or equivalently A and B of eq 3), the expectation values of the operator cos 2α, the torsional energies E_i, and the phase specifying the relationship between the angles α and θ or, in other words, the equilibrium conformation of the radical. In Figure 1 the four equilibrium conformations are shown together with the corresponding phase angles which need be considered for simple alkyl radicals in solution.

In general, the reduced moment of inertia for the internal rotation will be a function of the torsional angle θ and may be expanded as a Fourier series in θ. However, in most cases the constant term in the Fourier series is by far the largest and the angle-dependent terms are smaller than the uncertainty in the reduced moment of inertia arising from the uncertainty in the structural parameters for the radical. In this case the expectation value for cos $n\alpha$ and the energies are calculated using the simple torsional Hamiltonian

$$\mathcal{H} = -\left(\frac{\hbar^2}{2I}\right)\frac{\partial^2}{\partial\theta^2} + V(\theta)$$

where $I = I_a I_b/(I_a + I_b)$ is the reduced moment of inertia relative to the moments of inertia I_a and I_b of the two rotating groups about the axis of internal rotation calculated at the equilibrium conformation. The Hamiltonian matrix is set up in a truncated $1/\sqrt{2\pi}\ e^{\pm im\theta}$ basis and is diagonalized to obtain the energies.

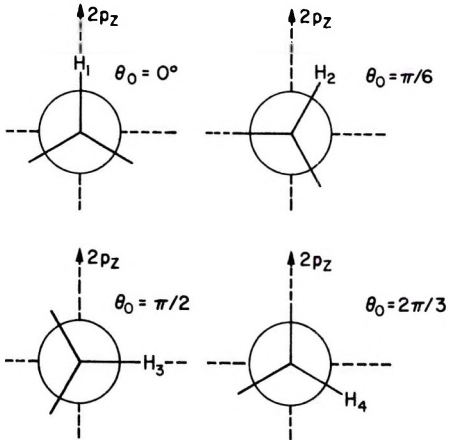

Figure 1. Equilibrium conformations for β protons in simple alkyl radicals in solution and corresponding phases for the angular dependence.

Sixty-one basis functions were used and give torsional energies which are, in fact, far more accurate than is required in view of the uncertainty in the reduced moments of inertia. The transformation matrix T which diagonalizes the Hamiltonian, and its inverse T^{-1}, are then used to transform the matrix of the operator cos $n\alpha$ calculated in the original basis to the new basis, *i.e.*, $T^{-1}[\cos n\alpha]T = [\cos n\alpha]'$. The expectation values of cos $n\alpha$ are then the diagonal elements of the matrix $[\cos n\alpha]'$.

This finite number of energies and expectation values of cos $n\alpha$ can then be used in eq 6 and 7 to obtain a_β^H at any temperature with appropriate values for the parameters a_0 and a_2 (or A and B of eq 3) and for the phase θ_0 (Figure 1) specifying the equilibrium conformation. The parameters a_0 and a_2 as well as V_2 can be varied to give best agreement, in a least-squares sense, between the calculated and the experimental coupling constants for as many temperatures as there are data points. In theory this would lead to the determination of the two parameters a_0 and a_2 in the angular dependence of a_β^H and the barrier to rotation. Unfortunately, the solutions one obtains allowing all parameters to vary are not meaningful. To obtain reliable convergence one must therefore choose a reasonable value for either a_0 or a_2 or both.

The motional averaging of the angular dependence of a_β^H (eq 3) can also be treated from a classical point of view.[9] In this approach we consider the classical limit to which eq 6 tends as the reduced moment of inertia for internal rotation increases. The separation between the torsional states ΔE_i diminishes, and in the limit all values of the potential function become allowed. The classical limit of eq 6 is then given by

$$a_\beta^H(T) = \frac{\int_{-\pi}^{\pi} a_\beta^H(\theta)\exp[-V(\theta)/kT]d\theta}{\int_{-\pi}^{\pi}\exp[-V(\theta)/kT]d\theta} \quad (8)$$

where $V(\theta)$ is the potential function of eq 5 and

$$a_\beta^H(\theta) = A + B\cos^2(\theta + \theta_0) \quad (9)$$

in which the phase distinguishing the equilibrium conformation (Figure 1) is shown explicitly. This classical formulation simply represents the anisotropic average of a_β^H using as statistical weight the Boltzmann probability that the radical may be found in a state with torsional energy $V(\theta)$ and, therefore, with an accompanying angle of twist θ.

The classical anisotropic averaging of a_β^H is, of course, much simpler to handle than the quantum mechanical approach. A computer program was written which can vary the parameters A and B and the barrier height V_2 to give a least-squares fit of eq 8 to a set of experimental coupling constants at various temperatures. Once again, the solutions are not meaningful if all three parameters of the problem are allowed

to vary. However, if reasonable values of A or B or both are available, as is often the case, the least-squares fit yields the barrier to rotation from the experimental $a_\beta^H(T)$ curve. In a later section the barriers obtained by the classical formulation will be compared with those obtained by the quantum mechanical averaging. It will be seen that for simple alkyl radicals with low barriers, where the rotating part is either a $-\dot{C}H_2$ or a $-\dot{C}R_2$ fragment, the two approaches yield virtually identical barriers to rotation.

In the limit of high temperature or very low barriers to rotation, eq 8 reduces to the isotropic average of $a_\beta^H(\alpha)$ given by

$$a_\beta^H = A + {}^1/_2B \tag{10}$$

Since methyl groups attached to a radical center approach this limit, eq 10 can be applied to $a_\beta^{CH_3}$ to determine the parameter B. The value of A is usually assumed to be negligible, although 1–3 G for this parameter in alkyl radicals is indicated by several experimental and theoretical considerations. Thus, if we can neglect A, the B parameter is simply given by

$$B = 2a_\beta^{CH_3} \tag{11}$$

Application of eq 11 to the ethyl radical ($a_\beta^{CH_3}$ = 26.9 G), to the isopropyl radical ($a_\beta^{CH_3}$ = 24.7 G), and to the *tert*-butyl radical ($a_\beta^{CH_3}$ = 22.7 G) gives suitable values for the B parameter to use for primary (B = 53.8 G), secondary (B = 49.4 G), and tertiary (B = 45.4 G) radicals, respectively.

For hydroxylic β protons, $\dot{C}$–O–H_β, whose coupling constant can also be represented by eq 3,[10e,h,12] the choice of the appropriate A and B parameters is more problematic although values for these parameters have been suggested by Whiffen.[13] Lacking more conclusive experimental information on this point we shall use parameters obtained from INDO molecular orbital calculations. The sense of the variation of a_β^{OH} with temperature and the isotope effect (*vide infra*) demand a substantial and *negative* value for A which can no longer be neglected.

Calculation of Line Shapes by the Density Matrix Method. Esr spectra exhibit selective broadening of certain lines when two or more isotropic hyperfine coupling constants are modulated by fluctuating fields at rates comparable to their difference expressed in frequency units. A number of reviews have appeared recently on line width effects in esr spectroscopy.[2] We shall be concerned here only with those cases where the modulation of the coupling constants is brought about by hindered internal rotation in the presence of twofold potential barriers. If the potential barrier is sufficiently high so that the radical spends most of the time near the potential minima, the phenomenon can be treated as an exchange between conformational isomers.

Several methods have been developed to calculate the effects of exchange processes on line shapes in magnetic resonance.[2,14] In this work the line shapes were calculated using the phenomenological density matrix equation of motion of Kaplan[15] and Alexander.[16] Since the details of these calculations are discussed elsewhere[17] we shall give here only a brief outline of the method.

For the case of mutual exchange (where the Hamiltonian is the same before and after the exchange process except that some nonequivalent spins have been permuted) the equation of motion for the density matrix can be written

$$\frac{d\rho}{dt} = 2\pi i[\rho,H] + \left(\frac{d\rho}{dt}\right)_{relax} + (P\rho P^\dagger - \rho)/\tau \tag{12}$$

where ρ is the mean spin density matrix, H is the mean spin Hamiltonian, including interactions with the microwave field, and τ is the average time between exchanges. P is the exchange matrix defined by

$$\psi'(t) = P\psi(t)$$

where $\psi(t)$ and $\psi'(t)$ are the spin wave functions before and after exchange, respectively. P transforms the density matrix ρ into ρ' after exchange, *i.e.*

$$\rho' = P\rho P^\dagger$$

The relaxation term in eq 12 is given by

$$\left(\frac{d\rho_{ij}}{dt}\right)_{relax} = -\frac{\rho_{ij}}{T_2}$$

for the off-diagonal density matrix elements. T_2 represents a relaxation time which determines the line widths in the absence of exchange.

Under the conditions of high temperature, slow passage, and weak microwave fields, eq 12 leads to an expression for the absorption intensity at angular frequency ω of the form

$$Im(-i\mathbf{M}^-\cdot\mathbf{A}(\omega)^{-1}\cdot\mathbf{M}^-) \tag{13}$$

where $\mathbf{M}^-$ is a vector containing the matrix elements of $M^- = \sum_i \gamma_i I_i^-$, I_i^- being the lowering operator for the ith spin. $\mathbf{A}(\omega)$ is a complex non-Hermitian matrix of the form

$$\mathbf{A}(\omega) = \mathbf{B} - i\omega\mathbf{E}$$

where $\mathbf{E}$ is the unit matrix.

(12) W. Derbyshire, *Mol. Phys.*, **5**, 225 (1962).

(13) D. H. Whiffen, *Colloq. Int. Cent. Nat. Rech. Sci.*, **164**, 169 (1966); "Structure Hyperfine Magnetique des Atomes et des Molecules," *Cent. Nat. Rech. Sci.*, 167 (1967).

(14) C. S. Johnson, *Advan. Magn. Resonance*, **1**, 33 (1965).

(15) J. I. Kaplan, *J. Chem. Phys.*, **28**, 278 (1958); **29**, 462 (1958).

(16) S. Alexander, *ibid.*, **37**, 967, 974 (1962); **38**, 1787 (1963); **40**, 2741 (1964).

(17) P. Meakin, E. L. Muetterties, F. N. Tebbe, and J. P. Jesson, *J. Amer. Chem. Soc.*, **93**, 4701 (1971).

The spectrum can be calculated from eq 13 either by inversion of $\mathbf{A}(\omega)$ at each frequency ω or by employing the much more efficient numerical techniques developed by Gordon and McGinnis,[18] Binsch,[19] and Schirmer, Noggle, and Gaines[20] which require the diagonalization of the complex non-Hermitian matrix **B** as the only matrix operation.

In those cases where the spectra are first order considerable simplifications are possible and the density matrix method reduces to the equations given by Sack.[21] The calculations reported here assume that the spectra are first order. They have, however, been compared with the results of complete density matrix calculations which indicate that no serious errors are introduced by this approximation in our case.

The analysis of the data consists in calculating spectra which match the experimental spectra at various temperatures by varying $1/\tau$ (the rate of the exchange process). In addition to this rate, the computer program requires the coupling constants of the exchanging protons (which can be obtained experimentally if the rate process can be slowed down to the slow exchange limit), the coupling constants of the nonexchanging protons and their multiplicities, and finally the relaxation time T_2 which can be obtained from the width of the lines not affected by the exchange.

According to the classical theory of rate processes, $1/\tau$ is related to the temperature through the Arrhenius expression

$$1/\tau = \nu_0 \exp(-E_0/RT) \qquad (14)$$

where ν_0 is the frequency factor and E_0 is the activation energy. The latter can therefore be extracted from a plot of log $1/\tau$ against $1/T$ using the τ values determined by the comparison of the theoretical and experimental spectra.

The accurate determination of exchange rates by the visual curve matching method requires spectra of high quality and line shapes unaffected by instrumental and adventitious disturbances. In practice this is difficult to achieve particularly with short-lived radicals. Some of the main difficulties encountered in the curve matching method should be mentioned. Spectra obtained by photolysis of stationary samples typically exhibit a gradual decrease in the peak-to-peak intensities during the time required to record the entire spectrum. For optimum signal-to-noise ratios some overmodulation is nearly always required which alters the true line shapes. Modulation effects are particularly insidious with alternating line widths since they influence differently the amplitudes of lines with different widths. In many cases, the presence of unresolved second-order effects, which were not taken into account by our calculations, may also distort the line shapes and reduce the intensities of certain lines. Finally, the presence of minor radical species with lines overlapping those of interest can also alter the true line shapes and intensities. In view of these difficulties, which can vary greatly from system to system, and those associated with the uncertainty in the temperature of the sample, it is difficult to assess the accuracy of the activation energies obtainable by this method. In the case of the hydroxymethyl radical (*vide infra*), we consider the activation energy to be reliable to within ±1.0 kcal/mol.

Results and Discussion

The Hydroxymethyl Radical. The hydroxymethyl radical can be generated in high yields by ultraviolet irradiation of stationary methanol–cyclopropane solutions containing di-*tert*-butyl peroxide. This technique for the generation of transient radicals in nonaqueous media has been employed previously with a variety of substrates[6b,8] and involves the abstraction of hydrogen atoms by *tert*-butoxy radicals produced in the primary photolytic act. The use of cyclopropane as diluent is, in fact, crucial in the present case for it allows the observation of the $\dot{C}H_2OH$ radical in a medium of low viscosity at temperatures where pure methanol would be very viscous or frozen and where the spectra would be consequently severely broadened by incomplete averaging of dipolar interactions. It also has the added advantage of reducing the strong dielectric loss typical of neat alcohols and thus allows the use of rather wide cylindrical sample tubes (4 mm i.d. Suprasil tubing). In the presence of a more reactive component the spectrum of the cyclopropyl radical is not seen with appreciable intensity although it can be detected with neat cyclopropane. Figure 2 shows the experimental and calculated (*vide infra*) spectra of the hydroxymethyl radical at several low temperatures. At −58° the familiar spectrum is recorded consisting of a triplet for the two equivalent α protons further split into doublets by the hydroxylic proton. At −90° the central lines of the triplets are broadened and therefore appear with reduced amplitudes. This selective broadening continues as the temperature is lowered until at −107° each broadened $M_I = 0$ line is partially resolved into two lines. With further decreases in the temperature the central lines become narrower, and at −125° the spectrum consists of three doublets, overlapping in the central region, with lines of nearly equal width. At this temperature the two α protons are therefore magnetically nonequivalent. The coupling constants measured at this temperature are given below. The assignment of the two α-proton coupling constants is based on a comparison with MO calculations.

(18) R. G. Gordon and R. P. McGinnis, *J. Chem. Phys.*, **49**, 2455 (1968).

(19) G. Binsch, *J. Amer. Chem. Soc.*, 91, 1304 (1969).

(20) R. E. Schirmer, J. H. Noggle, and D. F. Gaines, *ibid.*, 91, 6240 (1969).

(21) R. A. Sack, *Mol. Phys.*, 1, 163 (1958).

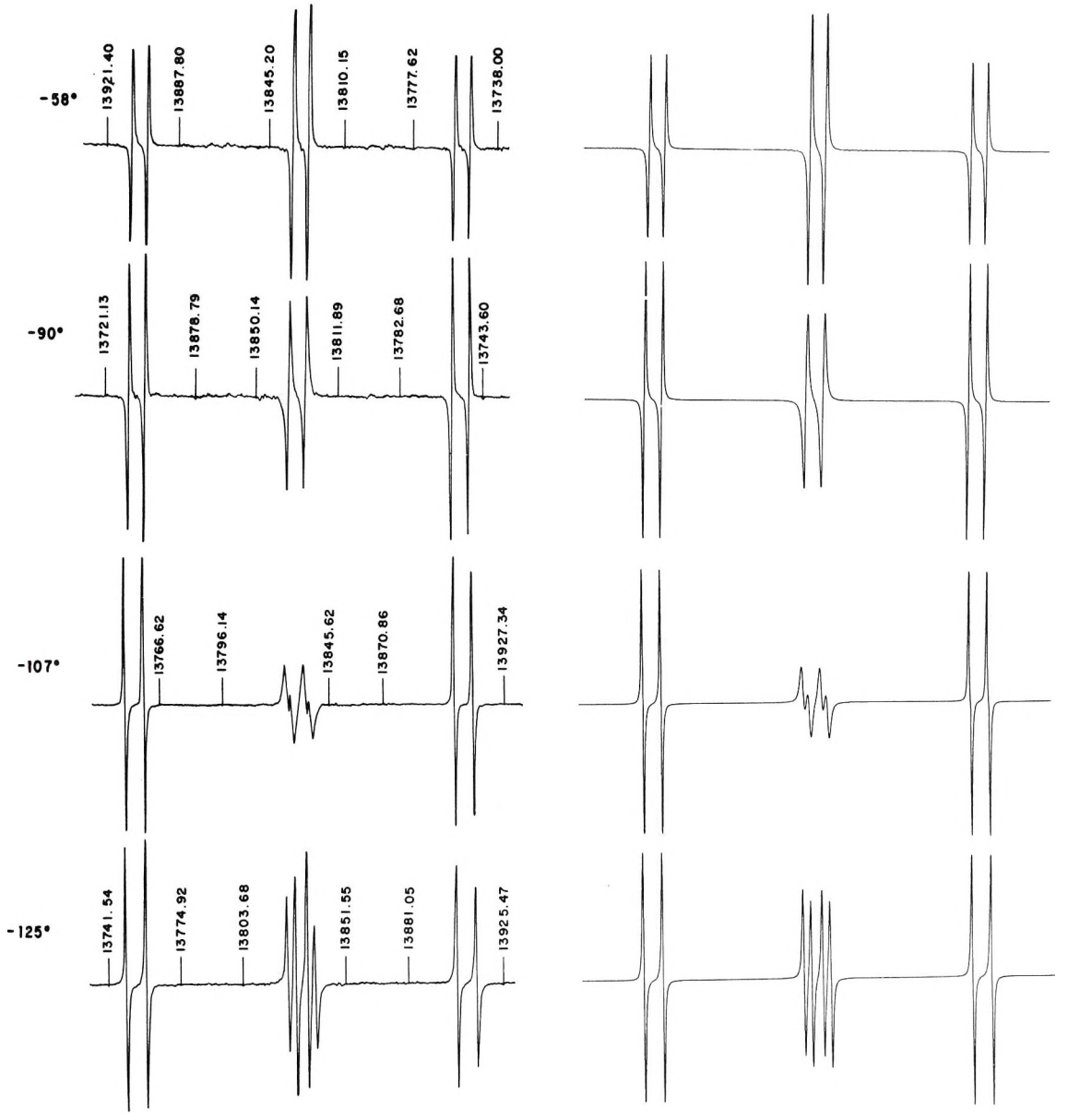

Figure 2. Experimental (left) and calculated (right) esr spectra of the hydroxymethyl radical at various temperatures. The proton nmr field markers are in kilohertz.

$$\begin{matrix}(17.65\text{ G})\ H_2 \\ (18.53\text{ G})\ H_1\end{matrix}\!\!>\dot{C}\!-\!O\!-\!H\ (2.16\text{ G}) \qquad T = -125°$$

Concomitant with these changes, but less apparent in Figure 2, is a steady variation with temperature of the magnitude of the hydroxylic proton hyperfine coupling constant which is shown in Figure 3. This variation was noted by Livingston and Zeldes,[5] but was not treated quantitatively. Although the esr experiment provides only the absolute magnitude of the coupling constants, a^{OH} is plotted in Figure 3 as a negative quantity since this is the only sign consistent with the theory (*vide infra*). The average α-coupling constant, $(a_\alpha^1 + a_\alpha^2)/2$, also shows a slight temperature dependence which is analogous to that observed with the methyl radical[22] and which can similarly be attributed to vibronic effects. Assuming a negative sign for this coupling constant, the temperature coefficient is $da/dt = +4.7$ mG/°C or about twice that found for methyl.

The photolytic method for generating reactive radicals in stationary solutions, requiring only small amounts of starting materials, lends itself readily to the examination of isotopically substituted species from enriched samples.[23] Thus, perdeuteriomethanol in cyclopropane reacts with photolytically generated *tert*-

(22) I. A. Zlochower, W. R. Miller, Jr., and G. K. Fraenkel, *J. Chem. Phys.*, **42**, 3339 (1965).

(23) (a) P. J. Krusic and T. A. Rettig, *J. Amer. Chem. Soc.*, **92**, 722 (1970); (b) P. Bakuzis, J. K. Kochi, and P. J. Krusic, *Tetrahedron*, to be published.

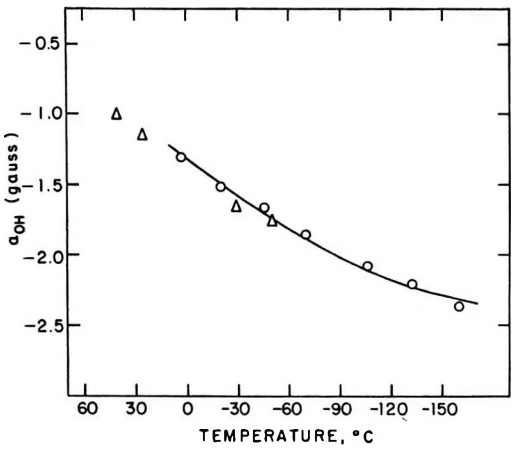

Figure 3. Experimental and calculated temperature dependence of the hydroxylic proton hyperfine coupling constant in hydroxymethyl. The experimental points denoted by triangles are taken from ref 5.

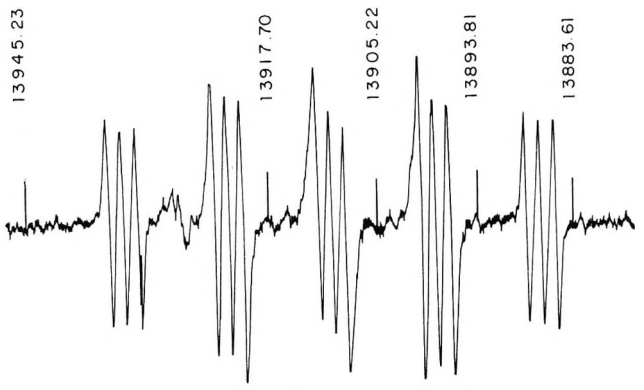

Figure 4. Esr spectrum of $\dot{C}D_2OD$ in cyclopropane solution at −119°. The peak-to-peak amplitudes for the quintet deviate from the expected 1:2:3:2:1 ratios due to incomplete averaging of the α deuterons. The proton nmr field markers are in kilohertz.

butoxy radicals and yields the radical $\dot{C}D_2OD$. In the spectrum of Figure 4, taken at −119°, the experimental peak-to-peak amplitudes of the quintet due to the two α deuterons depart considerably from the theoretical 1:2:3:2:1 ratios expected for two *equivalent* nuclei of spin $I = 1$ indicating that the inner triplets (1:1:1, due to the hydroxylic deuterium), particularly the central one, are selectively broadened. At lower temperatures it is again possible to bring out the magnetic nonequivalence of the α deuterons. However, this leads to a rather complex spectrum with overlapping lines and incomplete resolution because of the reduced deuterium splittings ($^1/_2[a_\alpha(D_1] + a_\alpha(D_2)] = 2.78$ G, $a^{OD} = 0.38$ G, $T = -119°$). These splittings can be compared with the proton splittings by multiplication with the proton–deuteron moment ratio, $\mu_H/\mu_D = 6.5144$. For the α deuterons we obtain 18.11 G which compares with $^1/_2[a_\alpha(H_1) + a_\alpha(H_2)] = 18.09$ G at −125° for the analogous protons. Because of the temperature dependence of the coupling constants and the uncertainty in the temperature measurements, this very small isotope effect may be somewhat in error. For a very accurate determination of the isotope effect for the α position the two radicals should be generated in the same sample by photolyzing mixtures of CH_3OH and CD_3OD. A much greater isotope effect is observed, however, for the hydroxylic position with the greater degree of motion for this nucleus. Thus, $0.38 \times \mu_H/\mu_D = 2.48$ G which should be compared with $|a^{OH}| = 2.16$ G. The sense of the isotope effect ($|a^{OD}| \times \mu_H/\mu_D > |a^{OH}|$) is in agreement with a *negative* a^{OH} which becomes more positive as the excursion of the hydroxylic proton from the equilibrium position increases with increasing temperature.

We have also examined the species $\dot{C}H_2{}^{17}OH$ and $^{13}\dot{C}H_2OH$ generated from isotopically enriched samples of methanol (11% ^{17}O and 55% ^{13}C, respectively) in cyclopropane solutions. In the first case, each line of the main species was accompanied by six weak satellite lines due to ^{17}O with $I = 5/2$. The oxygen-17 coupling constant was found to be 9.7 G at −90°. The spectrum obtained with the ^{13}C-enriched methanol at −79° is shown in Figure 5. At this temperature $a(^{13}C) = 45.33$ G. A single sample containing about 250 mg of ^{13}C-enriched methanol was sufficient to obtain spectra at seven different temperatures from −9 to −111°. Expectedly, the ^{13}C-coupling constant was found to vary substantially with temperature as shown in Figure 6. The sense of this dependence is in accordance with elementary theory. As the out-of-plane vibrations increase in amplitude with increasing temperature, the half-filled orbital containing the unpaired electron rapidly assumes more s character and the isotropic coupling increases. Unfortunately we did not have enough material to establish whether the apparent leveling off of the curve at higher temperatures (Figure 6) is a real effect. This leveling would not accommodate the value for $a(^{13}C)$ reported by Fischer[24] at room temperature. On the other hand, forcing all points, including Fischer's, to fit a straight line, as shown in Figure 6, produces a deviation (about 0.2 G) for the point at −9° which is outside of the experimental error in our measurement of coupling constants. Neglecting this problem and accepting a linear behavior for $a(^{13}C)$ with temperature, we obtain an approximate temperature coefficient of 22 mG/°C.

Determination of the Potential Barriers in $\dot{C}H_2OH$ and $\dot{C}H_2OCH_3$ by the Density Matrix Method. The line shape effect and the temperature dependence of the β-hydroxylic proton coupling constant are caused by hindered internal rotation of the OH group about the C–O bond. Generally, if the potential barrier is sufficiently high so that the radical spends most of the time in conformations near the potential minima, the line

(24) H. Fischer as quoted by R. W. Fessenden, *J. Phys. Chem.*, 71, 74 (1967).

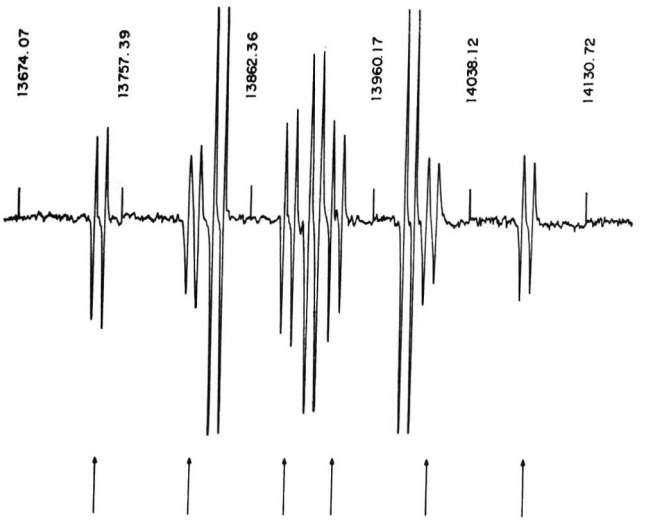

Figure 5. Esr spectrum obtained from methanol enriched in ^{13}C (T −79°). The arrows indicate the spectrum of $^{13}\dot{C}H_2OH$. At this temperature the M_I = 0 lines for the α protons are broadened and appear with reduced amplitudes. The proton nmr field markers are in kilohertz.

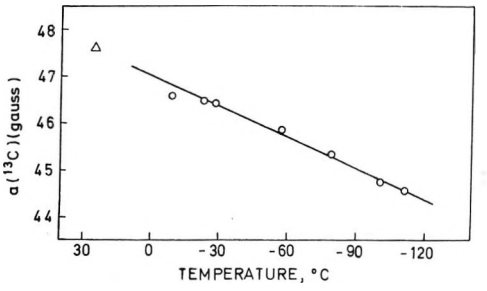

Figure 6. Experimental temperature dependence of $a(^{13}C)$ in hydroxymethyl. The point denoted by a triangle is taken from ref 24.

width effect can be treated as an exchange between conformational isomers. For the hydroxymethyl radical the small magnitude of a^{OH} and the presence of a line shape effect require an exchange between the two *planar* conformations II and III at rates comparable to the difference between the α hyperfine coupling constants expressed in frequency units (Δa_α = 0.88 G = 1.6×10^6 Hz).

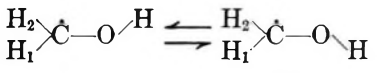

II III

This exchange can be treated by the density matrix method if the coupling constants of the exchanging protons are known. These can be measured from the spectrum at −125° (Figure 2). At higher temperatures (and higher rates of exchange) only the average value of these coupling constants, which is slightly temperature dependent, can be measured. We have calculated $a(H_1)$ and $a(H_2)$ at higher temperatures from the average values assuming that the difference $a(H_1)$ −

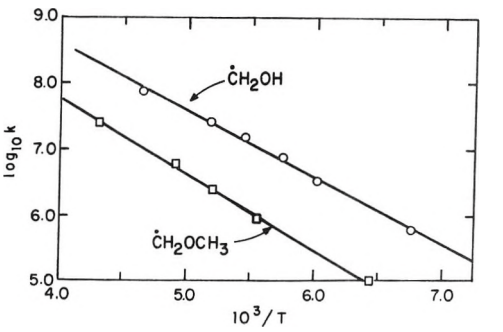

Figure 7. Arrhenius plots for the hydroxymethyl and the methoxymethyl radicals.

$a(H_2)$ is independent of the temperature. The remaining constants (a^{OH} and T_2) were taken directly from the spectra at each temperature. The experimental spectra could then be fitted (*cf.* Figure 2) by varying the rate of exchange $1/\tau$. In Figure 7 log $(1/\tau)$ is plotted against $1/T$. From the resulting linear relationship one obtains E_0 = 4.6 kcal/mol and a frequency factor $\nu_0 = 10^{12.6}$ sec^{-1}. The latter compares well with the value $10^{12.9}$ sec^{-1} obtained for the rotation of the $\dot{C}H_2$– fragment in $\dot{C}H_2COCH_3$ (*cf.* ref 3b) and with the value 2.7×10^{12} sec^{-1} predicted by transition state theory for rotation about a single bond.[25] Our E_0 and ν_0 for $\dot{C}H_2OH$ are, however, quite different from the values reported by Hudson[7a] (E_0 = 2.3 kcal/mol, $\nu_0 = 10^{9.9}$ sec^{-1}) which we consider to be in error.

It is interesting to note that the barrier of 9.4 kcal/mol[3b] in $\dot{C}H_2COCH_3$, which must also have a planar equilibrium conformation, is substantially higher than in $\dot{C}H_2OH$. One could invoke for the former a greater delocalization of the unpaired electron over the C=O π system and therefore a greater partial double bond character to the $\dot{C}$–CO bond. At first glance it is difficult to reconcile this interpretation with a larger value of $|a_\alpha|$ for $\dot{C}H_2COCH_3$ (19.7 G *cf.* ref 26) compared with $|a_\alpha|$ for $\dot{C}H_2OH$ (18.1 G) on the basis of a simple $a_\alpha = Q\rho^C$ relationship for the spin densities. This discrepancy may be only apparent, however, since the two α-coupling constants are not directly comparable. It is generally felt (*cf.* ref 24) that the anomalously low absolute values of the α-coupling constants in α-hydroxyalkyl radicals are due to a slight nonplanarity of the radical site (*vide infra*). The value of a_α in $\dot{C}H_2COCH_3$ should rather be compared with a_α in ethyl (22.3 G) which is also planar at the radical site. Using this comparison, a substantial delocalization of the unpaired electron over the C=O π system in $\dot{C}H_2COCH_3$ appears quite plausible. A valence bond form of the type $CH_2{=}\dot{O}H$, involving interaction with the filled p orbitals on oxygen, although presumably responsible for the barrier in $\dot{C}H_2OH$, must then be

(25) S. Glasstone, K. J. Laidler, and H. Eyring, "The Theory of Rate Processes," McGraw-Hill, New York, N. Y., 1946.

(26) H. Zeldes and R. Livingston, *J. Chem. Phys.*, 45, 1946 (1966).

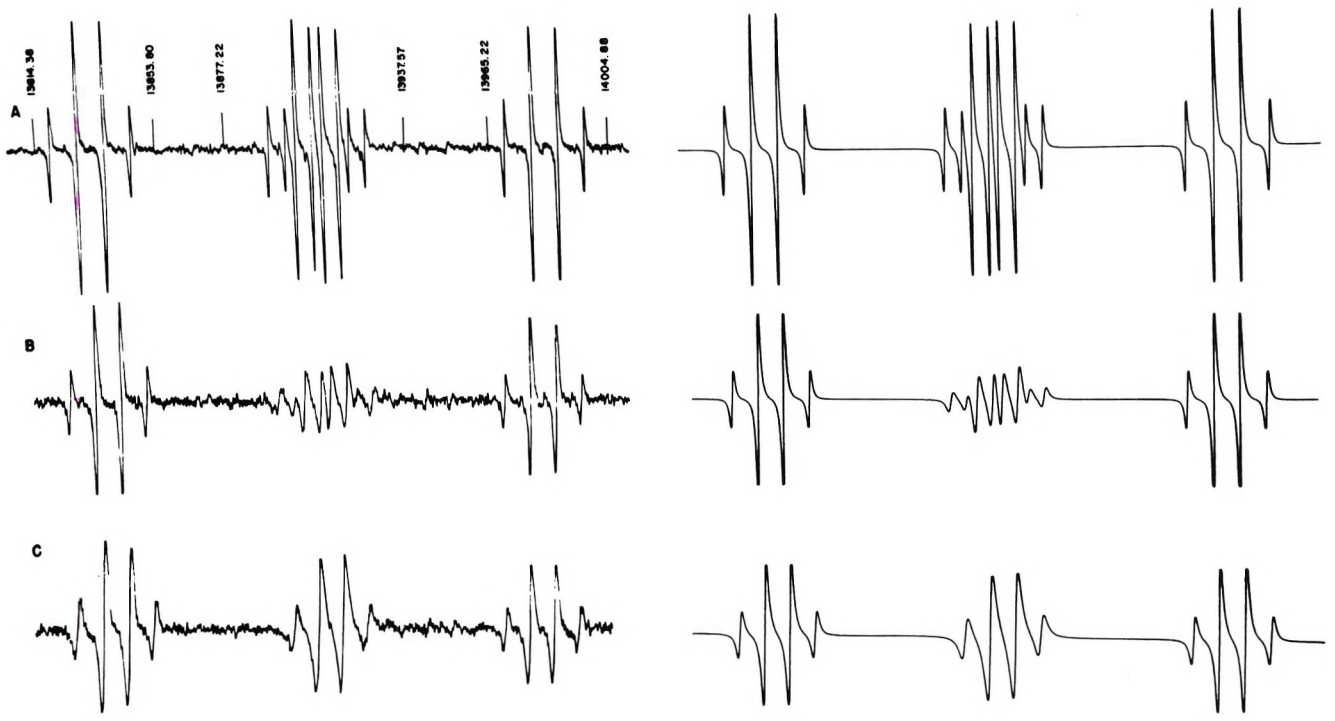

Figure 8. Experimental and calculated spectra for the methoxymethyl radical in ethane–cyclopropane solution at three temperatures (T, −117, −81, and −41° from top to bottom). The proton nmr field markers are in kilohertz.

less favorable than the valence bond form $CH_2{=}C(O)CH_3$ judging by the lower barrier in $\dot{C}H_2OH$.

We have also studied in detail the homologous radical $\dot{C}H_2OCH_3$ generated in dilute cyclopropane–ethane solution by the action of *tert*-butoxy radicals on dimethyl ether.[6,7b] The spectral features of this radical are similar to those of $\dot{C}H_2OH$ except that the hydroxylic proton doublets are now replaced by quartets for the three equivalent methoxy protons (Figure 8) which also show a slight temperature dependence. The coupling constants at −117° are given below.

$$\begin{matrix}(17.13\text{ G})\ H_2 \\ (18.43\text{ G})\ H_1\end{matrix}\!\!>\!\dot{C}\!-\!O\!-\!CH_3\ (2.09\text{ G}) \qquad T = -117°$$

The log $(1/\tau)$ values obtained by fitting the calculated line shapes to the experimental spectra are plotted against $1/T$ in Figure 7, and the resulting activation parameters are $E_0 = 5.3$ kcal/mol and $\nu_0 = 10^{12.5}$ sec^{-1}. The activation energy E_0 is closely related to but not identical with the barrier to internal rotation V_2.[27]

In cases such as ours where the barrier is small the difference between E_0 and V_2 may become quite important. A more direct measure of V_2 is provided by the temperature dependence of the β-coupling constant.

Determination of the Potential Barrier for $\dot{C}H_2OH$ from the Temperature Dependence of the β-Proton Coupling Constant. It was pointed out in the theoretical section that it is impossible to determine from the experimental temperature dependence of a_β^H alone the three parameters of the problem, *viz.* the constants A and B of eq 3 and the barrier height V_2. The nonlinear least-squares procedure to fit eq 6 to the experimental a_β^H (T) curve does not lead to meaningful convergence if all three parameters are allowed to vary. It is essential, therefore, to have some knowledge concerning the constants A and B. In the case of $\dot{C}H_2OH$ with a planar equilibrium conformation the radical spends most of the time near $\theta = 90°$ (measuring the torsional angle from the $2p_z$ axis), and the $B\cos^2\alpha$ term contributes only weakly to the observed value of a^{OH}. It was decided therefore to seek a reasonable value for B through molecular orbital calculations and to determine A and V_2 by the least-squares procedure.

INDO molecular orbital calculations have proved to be quite successful in predicting the isotropic proton hyperfine coupling constants in a large variety of organic radicals.[28,29] We have therefore used the INDO method to investigate the dependence of the coupling constants in $\dot{C}H_2OH$ on the angle of twist θ about the C–O bond as well as on the angle α (Figure 9) specifying the departure from planarity of the radical site. The remaining structural parameters were taken from the structure of the parent compound, *i.e.*, methanol.[30]

(27) M. Menzinger and R. Wolfgang, *Angew. Chem., Int. Ed. Engl.*, **8**, 438 (1969).

(28) (a) J. A. Pople, D. L. Beveridge, and P. A. Dobosh, *J. Amer. Chem. Soc.*, **90**, 4201 (1968); (b) D. L. Beveridge, P. A. Dobosh, and J. A. Pople, *J. Chem. Phys.*, **48**, 4802 (1968).

(29) We obtained a copy of this program from The Quantum Chemistry Program Exchange, Indiana University.

(30) "Tables of Interatomic Distances and Configurations in Molecules and Ions," *Chem. Soc. (London), Spec. Publ.*, **18**, m66s (1965).

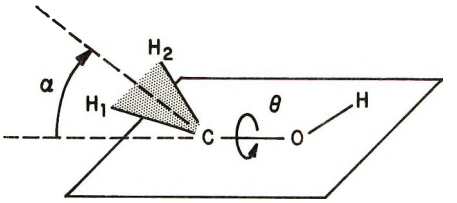

Figure 9. Angular parameters for the hydroxymethyl radical.

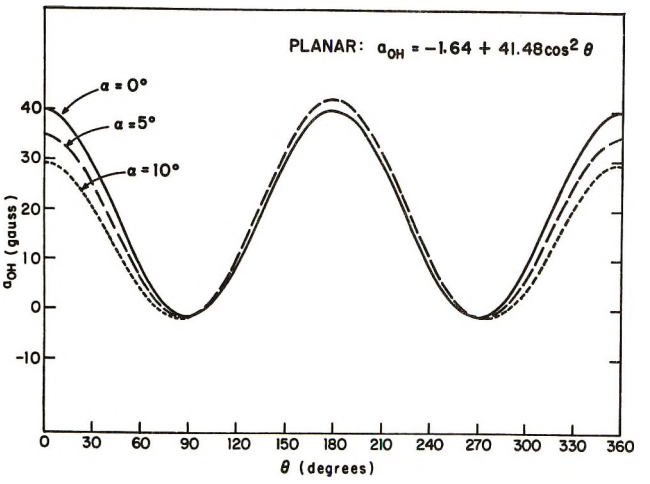

Figure 10. INDO hydroxylic proton coupling constant for the hydroxymethyl radical as a function of the torsional angle θ about the C–O bond and the angle α specifying the departure from planarity at the radical site.

These are as follows: l(CH) = 1.095 Å, l(CO) = 1.428 Å, l(OH) = 0.96 Å, and ∠COH = 109°. It was further assumed that the angle H_1CH_2 is equal to 120°. The results of these calculations are shown in Figures 10, 11, and 12 in which the angle θ = 0 corresponds to the bisected conformation with the hydroxylic proton eclipsed by the $2p_z$ orbital on carbon. The coupling constant for ^{17}O shows weaker dependences on the angles θ and α which are not shown graphically. For the planar radical (α = 0) the values for $a(^{17}O)$ vary between the limits of 11 G for the bisected conformation and 3.3 G for the planar conformation.

Inspection of the INDO results reveals a number of interesting points regarding the structure of the hydroxymethyl radical. It is seen that for a planar structure the α-proton coupling constants (Figure 11) would be quite normal (*ca.* −21 G) but that they decrease rapidly in absolute value and that they become increasingly dependent on θ as the radical center becomes more pyramidal. It is also seen that the two α protons are inequivalent in the planar conformation (θ = 90°). For the planar radical the calculated nonequivalence (Δa_α = 0.7 G) compares quite well with the experimental value of 0.88 G. It is thus evident that a very small departure from planarity ($\alpha < 5°$) is sufficient to decrease sensibly the magnitude of the α-coupling constants. It can also be seen that only a very small

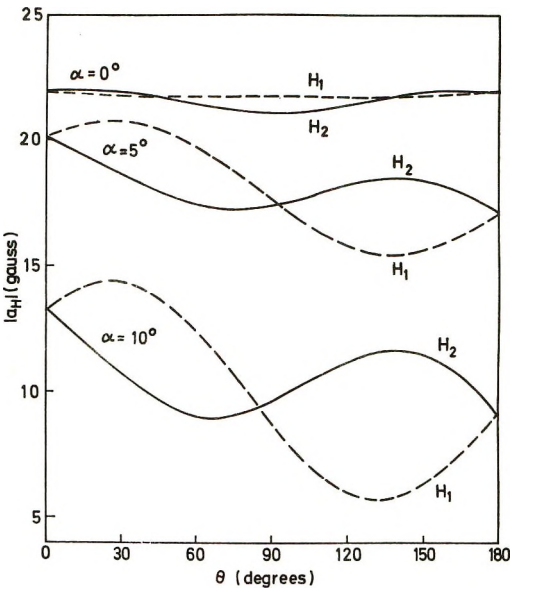

Figure 11. INDO coupling constants for the α protons in the hydroxymethyl radical as a function of the torsional angle θ about the C–O bond and the angle α specifying the departure from planarity at the radical site.

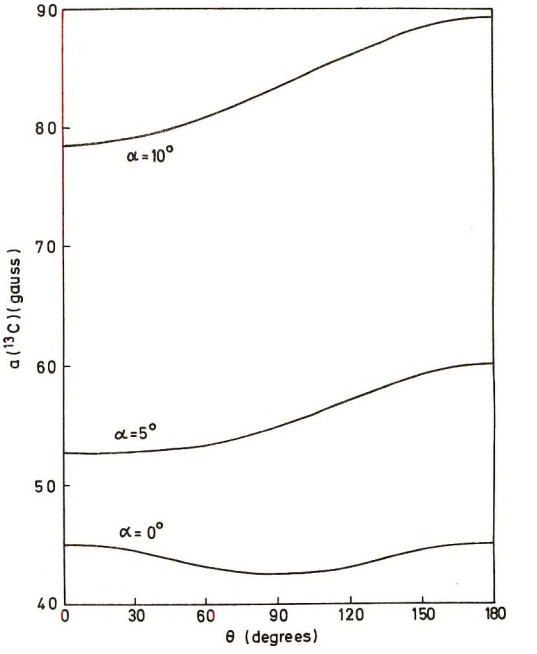

Figure 12. INDO coupling constant for ^{13}C in the hydroxymethyl radical as a function of the torsional angle θ about the C–O bond and the angle α specifying the departure from planarity at the radical site.

degree of nonplanarity is involved by consideration of the ^{13}C-coupling constant (Figure 12) which soon becomes much larger than is experimentally observed [$a(^{13}C)$ ~44.5 G at −110°]. We have, therefore, chosen to regard $\dot{C}H_2OH$ as essentially planar in its equilibrium conformation.

Of more direct interest is the angular dependence of a^{OH} (Figure 10). For the planar structure the cal-

culated angular dependence is represented quite well by $a^{OH} = -1.64 + 41.48 \cos^2 \alpha$. The predicted value of A is thus negative, as expected from the temperature dependence of a^{OH} and from the isotope effect, but not sufficiently negative to account for the experimental values of a^{OH} at the lowest temperature (*cf.* Figure 3). This negative contribution to a^{OH} is a measure of the spin density induced on the hydroxylic proton by the spin density on the oxygen atom through spin polarization of the O–H σ bond. The constant B, on the other hand, is a measure of the direct spin density transmission to the hydroxylic proton by hyperconjugation and is expected to be more reliably predicted by INDO calculations. We have, therefore, taken $B = 41.48$ for the determination of the barrier with A to be determined by the least-squares procedure.

It is now possible to carry out the quantum mechanical calculations described in the theoretical section and to fit in a least-squares sense eq 6 to the experimental points of $a^{OH}(T)$ (Figure 3) varying V_2 and A. From the assumed structure used for the INDO calculations we have for the reduced moment of inertia $I_r = 0.55$ amu Å^2. The rapidly converging least-squares fit yields $A = -5.3$ G and $V_2 = 4.0$ kcal/mol. The latter is thus in good agreement with $E_0 = 4.6$ kcal/mol obtained by the density matrix treatment of the line width effect. The calculated temperature dependence of a^{OH} for these values of A and V_2 (and I_r) is also shown in Figure 3.

We have repeated the calculations for various values of the reduced moment of inertia I_r to establish the extent to which the calculated barrier depends on the assumed structure. The results of these calculations are shown in Figures 13 and 14. It is seen that the barrier is not very sensitive to changes in the reduced moment of inertia in the neighborhood of the chosen value. Also shown in Figures 13 and 14 are the least-squares values of the two parameters obtained by the classical approximation (eq 8, with $\theta_0 = \pi/2$) which correctly represent the extrapolation of the quantum mechanical results to very large values for the reduced moment of inertia. At such values for I_r the inadequacy of the truncated basis set for the solution of the Hamiltonian shows up in the curves in Figures 13 and 14.

For the hydroxymethyl radical with a relatively large barrier and a small reduced moment of inertia the classical approach is clearly not a good approximation leading to a larger barrier (6.9 kcal/mol) than the quantum mechanical calculations. It will be seen in the next section, however, that for alkyl radicals with lower barriers and with rotating parts of larger moments of inertia (–$\dot{C}H_2$ or –$\dot{C}R_2$ fragments) the classical approximation gives barriers which are identical with those calculated by the quantum mechanical method.

Equilibrium Conformations and Rotational Barriers in Alkyl Radicals. Fessenden[3a] has studied in detail

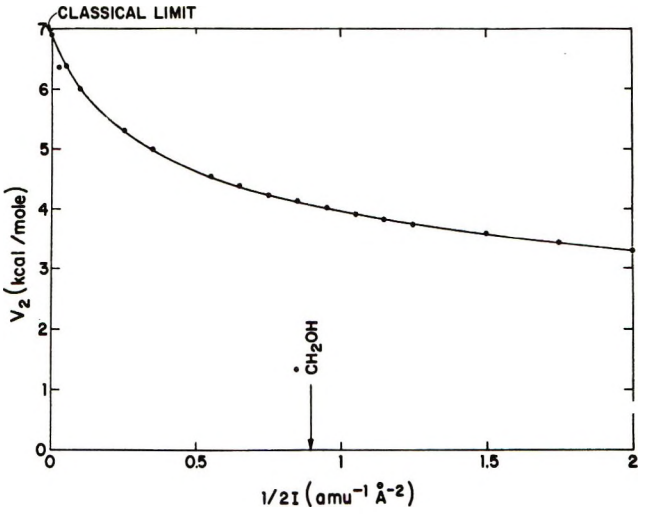

Figure 13. Rotational barriers for $\dot{C}H_2OH$ obtained by least-squares fitting of the quantum mechanical theory to the experimental temperature dependence of a_β^{OH} as a function of the reduced moment of inertia. The analogous fitting using the classical theory correctly represents the extrapolation to very large values for the moment of inertia. For large values of I the truncated basis set (see text) is inadequate as shown by the departure of the last point from a smooth curve.

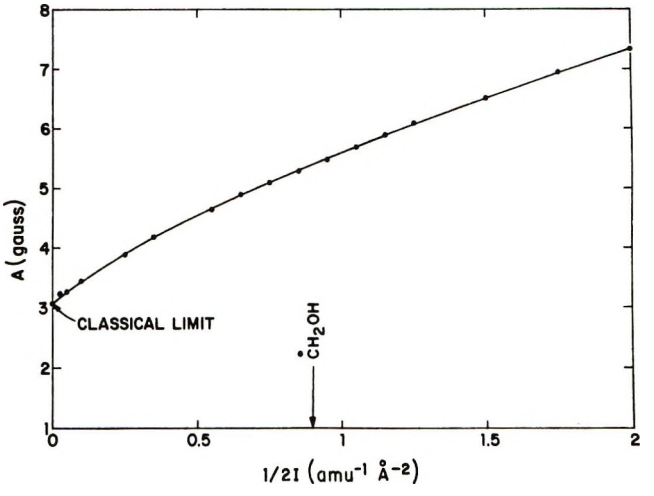

Figure 14. Behavior of the parameter A for $\dot{C}H_2OH$ obtained by least-squares fitting of the quantum mechanical theory to the experimental temperature dependence of a_β^{OH} as a function of the reduced moment of inertia.

the temperature dependence of the β-proton hyperfine coupling constants in the isobutyl radical $\dot{C}H_2$-$CH(CH_3)_2$, and *n*-propyl radical, $\dot{C}H_2CH_2CH_3$ (Figure 15). From the relative magnitudes of the β-coupling constants he inferred the equilibrium conformations IV and V for these radicals. The most favorable

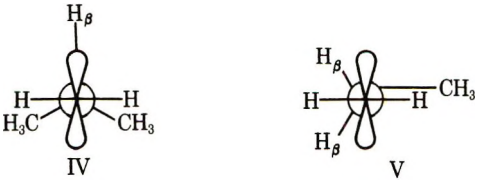

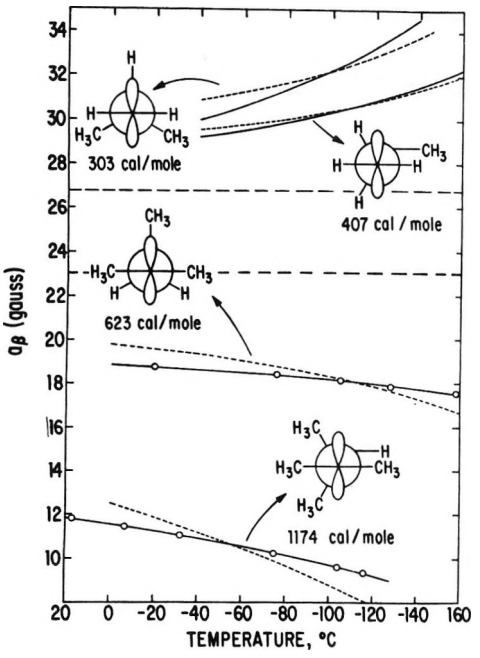

Figure 15. Experimental and calculated temperature dependences of β-coupling constants for isobutyl, *n*-propyl, *tert*-amyl, and dimethylisopropylcarbinyl radicals (the experimental curves for isobutyl and *n*-propyl are taken from ref 3a). The two horizontal lines indicate the temperature independent values of $a_\beta^{CH_3}$ for ethyl (upper) and *tert*-butyl (lower). The former represents the high-temperature limit of a_β for the two primary radicals while the latter is the same limit for the two tertiary radicals.

orientation of the β proton relative to the half-filled p orbital in IV ($\theta_0 = 0$, cf Figure 1) leads to the largest a_β whereas in V($\theta_0 = \pi/6$) the β coupling is somewhat reduced. We have also studied these radicals by the stationary photolytic technique[8b,9] and have in addition observed line shape effects for the *n*-propyl radical affecting the $M_I = 0$ lines for the α protons (Figure 16). The isobutyl radical, on the other hand, does not exhibit any selective broadening of the spectral lines. The line shape effect confirms the equilibrium conformation for *n*-propyl proposed by Fessenden since it is due to the mechanism pictured below which exchanges the α protons between magnetically nonequivalent sites.

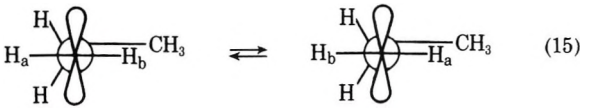

We have studied two other alkyl radicals, generated from the corresponding parent hydrocarbons by reaction with *tert*-butoxy radicals, which show β splittings of markedly different magnitude from those in IV and V. The temperature dependence of a_β^{H} for the *tert*-amyl radical, $(CH_3)_2\dot{C}CH_2CH_3$, and the dimethylisopropylcarbinyl radical, $(CH_3)_2\dot{C}CH(CH_3)_2$, are also shown in Figure 15. From the greatly reduced magnitudes of a_β in these radicals we infer the equilibrium conformations VI and VII ($\theta_0 = 2\pi/3$ and $\theta_0 = \pi/2$), respectively. The absence of any selective line broadening in VI is also consistent with a symmetric equilibrium

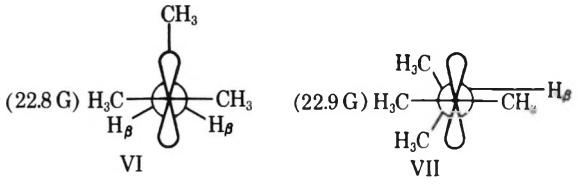

conformation. The values of the coupling constants for the β-methyl protons in these radicals (shown above) are temperature independent and are quite similar to $a_\beta^{CH_3}$ in *tert*-butyl (22.7 G). This value would represent the high temperature limit for a_β in the tertiary radicals much as $a_\beta^{CH_3}$ for ethyl (26.8 G) would represent the high temperature limit for the primary radicals (*cf.* Figure 15).

We have treated the temperature dependences of a_β in these radicals by the quantum mechanical and classical methods varying the barrier height V_2. The parameters A and B were chosen as follows. INDO calculations as a function of the torsional angle θ about the C_α–C_β bond on "standard" structures for these alkyl radicals predict a value for A about +1.5 G for the primary and +1.0 G for the tertiary radicals. A "standard" structure involves tetrahedral and trigonal angles, l(CC) = l(ĊC) = 1.54 Å, and l(CH) = l(ĊH) = 1.09 Å. These structures reproduce quite well the α- and β-proton coupling constants in these radicals. For the two primary radicals B was calculated from eq 10 with A = 1.5 G and $a_\beta^{CH_3}$ = 26.8 G for the ethyl radical giving B = 50.6 G. For the two tertiary radicals A = 1.0 G and the observed $a_\beta^{CH_3}$ for the two radicals (*cf.* structures VI and VII) were used giving B = 43.6 G for *tert*-amyl and B = 43.8 G for dimethylisopropylcarbinyl. The classical and quantum mechanical methods give in these cases virtually identical barriers. Those obtained by the classical method are shown in Figure 15 together with the temperature dependences calculated from eq 8. For comparison, Fessenden obtained 295 cal/mol for isobutyl and 412 cal/mol for *n*-propyl.

Unfortunately, a quantitative analysis of the line broadening effect in *n*-propyl cannot be carried out since we were unable to study the radical at sufficiently low temperatures to observe the inequivalence of the exchanging β protons. This situation generally obtains in simple alkyl radicals where the rotational barriers are low and the slow exchange limit would be reached at temperatures below the freezing point of the solutions employed in the experiments. We have attempted, however, to estimate the quantities responsible for the line width effect of Figure 16.

INDO calculations of the "standard" structure for *n*-propyl in its equilibrium conformation (structure V) predict for the magnetic inequivalence of the α protons

Figure 16. Esr spectrum of *n*-propyl radical from the photolysis of *n*-butyryl peroxide in cyclopropane solution at −140° showing second-order splittings (*cf.* third multiplets from each end of the spectrum) and the broadening of the lines corresponding to M_I = 0 for the α protons. The calculated first-order spectrum corresponds to an exchange rate for the α protons of 25 MHz. The proton nmr field markers are in kilohertz.

Δa_α = 1.1 G. Using this value for the difference of the α couplings and the experimentally determined average value (21.86 G at −140°) we obtain the values of $a_\alpha{}^a$ and $a_\alpha{}^b$ to use in the density matrix program. Figure 16 shows the calculated first-order spectrum with $1/\tau$ = 25 × 10^6 sec^{-1}, which best matches the experimental one. Using eq 14 we can calculate the corresponding activation energy assuming a frequency factor of $10^{12.5}$ sec^{-1}. Discouragingly, the resulting value of 3.1 kcal/mol for E_0 is nearly a factor of 10 larger than the value for the barrier obtained from the temperature dependence of the coupling constant. Although this value for E_0, considering the assumptions involved, may be substantially in error (the line shape calculations neglect second-order effects clearly visible in Figure 16), the presence of a line width effect in *n*-propyl requires a larger barrier to rotation than 400 cal/mol.

Another problem associated with the alkyl radicals is that the calculated curves for $a_\beta{}^H(T)$, based on a $\cos^2$ α angular dependence, give a rather poor fit to the experimental points especially as regards the slopes of the temperature dependences (*cf.* Figure 15). Much steeper curves for $a_\beta{}^H(T)$ than could be accounted for by the theory were also noticed for ethyl radicals with –SR groups substituted in the β position. These have an equilibrium conformation in which the sulfur atom is eclipsed by the p orbital of the radical center (θ_0 = $2\pi/3$).[9] In addition the radicals exhibit β couplings of anomalously low magnitudes. We interpreted these anomalies in terms of the distorted equilibrium structure pictured in Figure 17 in which the β hydrogens are displaced away from their tetrahedral positions toward the nodal plane while the sulfur atom is placed closer to the p orbital of the radical center. Such a distortion, which arises by tilting the axis of the tetrahedral β carbon away from the C_α–C_β bond direction as in Figure 17, is the first step toward a bridged structure which has, in fact, been postulated for such radicals on chemical evidence.[31] We believe that the failure of the theory to reproduce the temperature dependence of $a_\beta{}^H$ for simple alkyl radicals may also be ascribed to departures from tetrahedral geometries and hence to the inadequacy of a simple $\cos^2$ α angular dependence for the β protons.

The very large values of a_β for isobutyl and the magnitude of its temperature dependence (Figure 15) suggest a distortion entirely analogous to that proposed for the β-alkylmercaptoethyl radicals with the β proton replacing the sulfur atom and the two β-methyl groups replacing the β protons of the thiyl radical. Supporting evidence for this distortion comes also from INDO calculations on a "standard" structure (*vide supra*) for isobutyl in its equilibrium conformation as a function of the angle of tilt α pictured in Figure 17. The INDO energies depend strongly on α and indeed reach a minimum for α = +6°.

Although we have not carried out such INDO cal-

(31) P. S. Skell, *Chem. Soc. Spec. Publ.*, **19**, 131 (1965).

culations on the remaining radicals of Figure 15, we propose similar distortions for these radicals to account for the slopes of their $a_\beta(T)$ curves. In *n*-propyl the tilt would occur in the nodal plane and in such a sense as to bring the β protons somewhat closer to the p orbital thus increasing the distance between the eclipsed α protons and the γ-methyl group. In dimethylisopropylcarbinyl a similar tilt increases the distance between the eclipsed α-methyl group and the unique β proton and should produce a less steep curve for $a_\beta^H(T)$ than that expected for a tetrahedral structure. For *tert*-amyl the choice is less clear. We favor a tilt in the same plane as for isobutyl but with a negative α (*cf.* Figure 17). This distortion which places the γ-methyl group farther from the p orbital is qualitatively supported by the small magnitude of the γ-proton splittings which do not lead to resolvable structure. For rough comparison, the γ splitting in *n*-propyl amounts to 0.3 G.

In nontetrahedral alkyl radicals the angular dependence of a_β^H is no longer adequately represented by a simple $\cos^2\alpha$ law and therefore by the two-term Fourier expansion of eq 2. Instead one ought to consider a three-term expansion with $a_4 \neq 0$. We are planning to carry out the quantum mechanical and classical calculations of $a_\beta^H(T)$ varying this parameter in a least-squares sense. For the present, it is difficult to assess the effect of the new parameter on the calculated barriers. The limits of reliability for the barriers calculated on the basis of a simple $\cos^2\alpha$ law remain rather uncertain. For *n*-propyl, at least, the calculated barrier of 0.4 kcal/mol is too low to account for the line width phenomenon discussed above.

The Cyclopropylcarbinyl Radical. In previous esr studies,[32] we have discussed the metastable cyclopropylcarbinyl radical and its ready rearrangement into the allylcarbinyl radical at temperatures higher than $-120°$. From the small magnitude of its β-proton

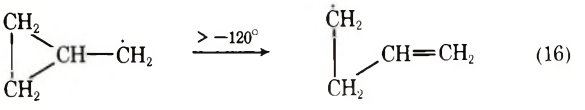

(16)

coupling constant (2.55 G at $-140°$) we have inferred a bisected equilibrium conformation which places the single tertiary hydrogen in the nodal plane of the half-filled p orbital ($\theta_0 = \pi/2$). The preference of the cyclopropyl group for the bisected conformation has been demonstrated also in other radicals.[33] In this section we wish to elaborate on the structure and the dynamics of this interesting radical in the light of the arguments developed in this paper.

The cyclopropylcarbinyl radical can be generated below $-120°$ either by hydrogen atom abstraction from methylcyclopropane with *tert*-butoxy radicals or by photolysis of cyclopropane solutions of *tert*-butyl peroxycyclopropylacetate. The esr spectrum at $-135°$

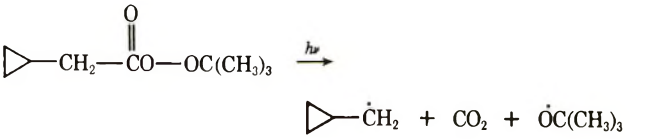

is shown in Figure 18. It is seen that the central group of lines corresponding to $M_I = 0$ for the two α protons have a broader line width than the wing lines indicating that the α protons are exchanging between two nonequivalent sites at a sufficiently slow rate to produce a line shape effect. Judging by similar observations on

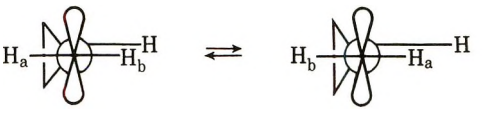

(17)

n-propyl (and allylcarbinyl, *cf.* ref 32), we consider that the activation energy for this exchange (eq 17) cannot be larger than about 2–3 kcal/mol. Barriers of this magnitude were also reported for several cyclopropyl-substituted radical ions.[33] It is important to note that even at $-150°$ the two α protons, although partially averaged, are still far from the slow exchange limit which ought to have been reached at these temperatures if the barrier were higher (compare $\dot{C}H_2OH$). Unfortunately, problems associated with solubility in the solutions employed in the experiment prevented the examination of the spectrum at lower temperatures and hence the direct measurement of the magnetic inequivalence of the α protons.

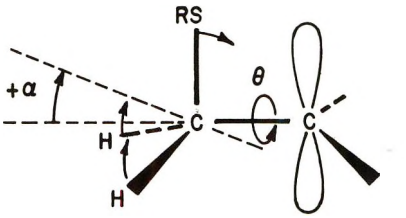

Figure 17. Distorted model for β-substituted alkyl radicals.

Having established a relatively low barrier for cyclopropylcarbinyl and the equilibrium conformation $\theta_0 = \pi/2$, it must be concluded that the β-proton coupling constant of 2.55 G is anomalously small. This anomaly is strikingly evident if the α-dimethyl-substituted cyclopropylcarbinyl radical[32b] (VIII) is coupared with the open-ring homolog dimethylisopropylcarbinyl (IX) which has the same equilibrium conforma-

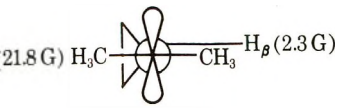

VIII, $T = -150°$

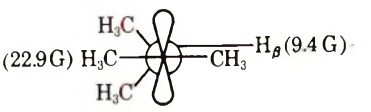

IX, $T = -120°$

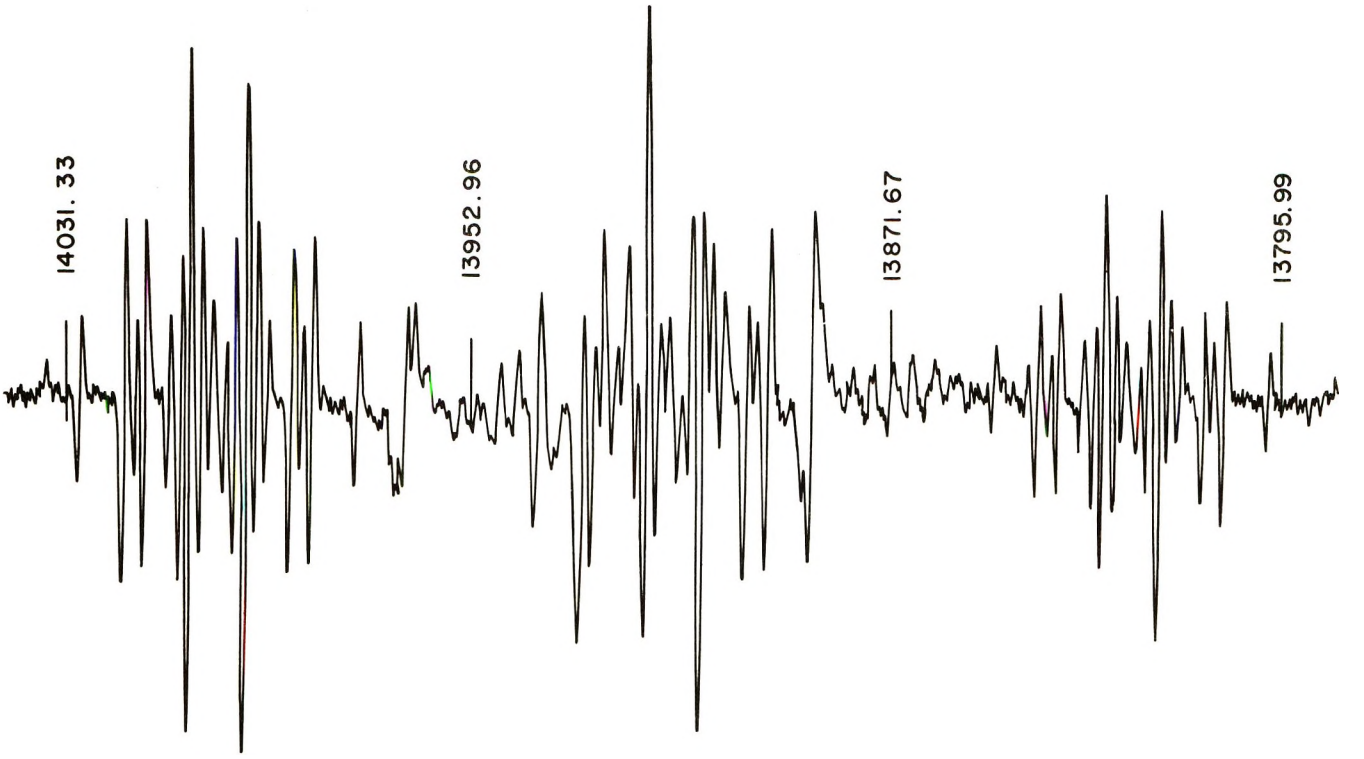

Figure 18. Esr spectrum of cyclopropylcarbinyl radical obtained by photolysis of *t*-butyl peroxycyclopropyl acetate in cyclopropane solution at −135°. The central lines of the spectrum are broadened by incomplete averaging of the α protons. Several extraneous lines are also visible probably belonging to the isomeric allylcarbinyl radical. The proton nmr field markers are in kilohertz.

tion and for which we have determined a barrier of 1.1 kcal/mol, presumably only slightly lower than the barrier for the small-ring radical. It should be pointed out that the coupling to the β-methyl protons in VIII (21.8 G) is only slightly lower than the corresponding coupling in IX (22.9 G). This observation has important implications. It is generally accepted that the β-methyl splitting is a good measure of the π-spin density on the α carbon, *i.e.*, $a_\beta^{CH_3} = Q^{CH_3}\rho^C$ with $Q^{CH_3} = 29.3$ G[34] Comparison on this basis of the $a_\beta^{CH_3}$ values for VIII and IX implies that the presence of the cyclopropyl ring produces a reduction of the spin density on the α carbon of somewhat less than 5%. Secondly, the similar $a_\beta^{CH_3}$ values imply that the B parameters for the two radicals are also comparable unless the A parameters differ substantially (*cf.* eq 10). INDO calculations on cyclopropylcarbinyl based on the structural parameters for methylcyclopropane[35] (with a trigonal α carbon and $l(\text{CH}) = 1.09$ Å) predict a value for A of about 1 G which is quite similar to the corresponding values for acyclic alkyl radicals. Using this value for A and the experimental $a_\beta^{CH_3}$ of 21.8 G we have $B = 41.6$ G which compares with $B = 43.8$ G used for the calculations of the temperature dependence of a_β for IX. Using these values of A and B for α-dimethylcyclopropylcarbinyl we can carry out the classical calculation of $a_\beta(T)$ (eq 8 and 9 with $\theta_0 = \pi/2$) for various values of the barrier to rotation. We conclude that barriers higher than 3 kcal/mol would be needed to reduce the B-coupling constant to the observed value of 2.3 G at −150°. Since barriers of this magnitude are not consistent with the weak line width phenomenon in cyclopropylcarbinyl, we again suspect that a distortion affecting the structure at the β carbon must accompany radical formation in the cyclopropylcarbinyl system. One likely distortion is analogous to that postulated for dimethylisopropylcarbinyl (IX)

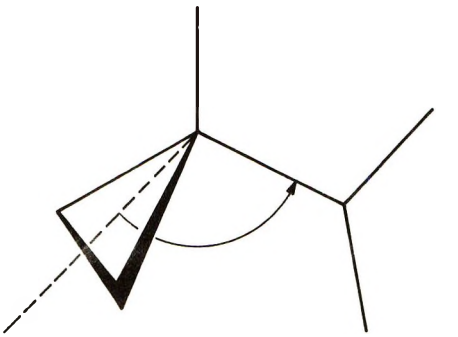

Figure 19. Postulated distortion for the cyclopropylcarbinyl radical.

(32) (a) J. K. Kochi, P. J. Krusic, and D. R. Eaton, *J. Amer. Chem. Soc.*, 91, 1877 (1969); (b) 91, 1879 (1969).

(33) N. L. Bauld, J. D. McDermed, C. E. Hudson, Y. S. Rim, J. Zoeller, Jr., R. D. Gordon, and J. S. Hyde, *ibid.*, 91, 6666 (1969).

(34) (a) R. W. Fessenden and R. H. Schuler, *J. Chem. Phys.*, 39, 2147 (1963); (b) H. Fischer, *Z. Naturforsch. A*, 20, 428 (1965).

(35) R. G. Ford and R. A. Beaudet, *J. Chem. Phys.*, 48, 4671 (1968).

and would close the angle between the bisector of the cyclopropyl ring and the C_α–C_β direction (124° in methylcyclopropane[35]) while increasing the distance between the eclipsed α and β protons (Figure 19). Our INDO calculations also indicate that such a distortion would tend to increase the magnitudes of the γ splittings leading to better agreement with the experimental values which are unusually large for cyclopropylcarbinyl (a_{γ_1} = 2.98 G (triplet) and a_{γ_2} = 2.01 G (triplet)).[32]

We conclude with a few remarks on the analogous carbonium ions. Recently there has been considerable interest in applying molecular orbital calculations to predict the equilibrium conformations and the rotational barriers in simple alkyl cations[36] which, in contrast with alkyl radicals, are not yet accessible experimentally. It is of interest to compare the results of some of these calculations with the experimental results for alkyl radicals. It is seen in Table I that the predicted equilibrium conformations for *n*-propyl- and isobutylcarbonium ions are quite different from those of the corresponding radicals and that the barriers involved are substantially larger. Only for the cyclopropylcarbinyl structure are the equilibrium conformations equivalent for the radical and the cation. Here too the corresponding barriers are quite different. Interestingly, our INDO calculations as a function of the torsional angle on "standard" structures wrongly predict for the *n*-propyl and isobutyl radicals equilibrium conformations similar to those predicted for the corresponding cations by *ab initio* calculations.[36] Considering the incomplete structural parameterization and the small energy differences involved we do not attach particular importance to this discrepancy. Only for the dimethylisopropylcarbinyl and the cyclopropylcarbinyl radicals are the conformations of minimum energy those required by the esr results. Finally, examination of Table I suggests that the equilibrium conformations in alkyl radicals are determined by a delicate balance between steric repulsions and the optimization of C–H hyperconjugation effects. There is little evidence that C–C hyperconjugation plays a significant role in determining the geometry in contrast to the conclusions reached for alkyl cations.[36] However, with alkyl radicals substituted in the β position with heteroatoms such as S, Si, Ge, and Sn[9] the "C–X hyperconjugation" geometry with the heteroatom eclipsed by the p orbital on the radical center generally prevails indicating a measure of d-orbital participation in the electronic structure of these radicals.

Table I: Equilibrium Conformations and Rotational Barriers for Some Alkyl Radicals and Cations[a]

Radical	Equilibrium conformation[b]	Rotational barrier[b]	Cation	Equilibrium conformation[c]	Calculated barrier[c]
n-Propyl	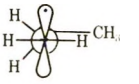	0.4	*n*-Propyl	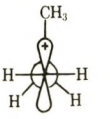	2.5
Isobutyl	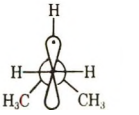	0.3	Isobutyl	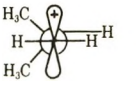	2.7
Dimethylisopropylcarbinyl	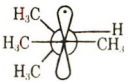	1.2			
Cyclopropylcarbinyl	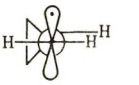	<3[d]	Cyclopropylcarbinyl	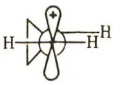	17.5
tert-Amyl	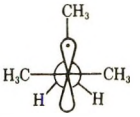	0.6			

[a] Energies in kcal/mol. [b] Present work. [c] *Cf.* ref **36**. [d] Estimated (see text).

Acknowledgments. We wish to thank Professor J. K. Kochi (Indiana) and Dr. R. J. Kempf (Du Pont) for useful comments and discussions. We are also grateful to Mr. M. Cushing for excellent technical assistance. One of the authors (P. J. K.) would like to thank Professor D. Hadzi (Ljubljana) for the hospitality extended to him during the latter stages of this work under a program of exchanges sponsored by the National Academy of Sciences and the Council of Yugoslav Academies.

(36) (a) L. Radom, J. A. Pople, V. Buss, and P. v. R. Schleyer, *J. Amer. Chem. Soc.*, **92**, 6380 (1970); (b) **92**, 6987 (1970).

Kinetic Electron Spin Resonance Studies on the Photolysis of Some Carbonyl, Nitroso, and Nitro Compounds

by P. B. Ayscough,* R. C. Sealy, and D. E. Woods

School of Chemistry, University of Leeds, Leeds 2, England *(Received January 25, 1971)*

Publication costs assisted by the Division of Physical Chemistry of the American Chemical Society

Radicals of the type $R\dot{C}(OH)R'$ are observed during the photolysis of ketones, keto acids, keto esters, etc., in organic solvents from which hydrogen atoms may be abstracted. Using esr spectroscopy and a computer for averaging transients we have shown that the average lifetimes for $CH_3\dot{C}(OH)COCH_3$ radicals derived from biacetyl correlate closely with calculated rates for diffusion-controlled combination reactions. Some relative rates of reaction of triplet biacetyl with organic solvents in which these radicals are generated have also been measured in a similar manner. Esr studies of the photolysis of nitrosobenzene, using photosensitizers and quenchers, show that dissociation to phenyl radicals and nitric oxide occurs without participation of the triplet state. The phenyl radicals then add to nitrosobenzene to give diphenyl nitroxide radicals or abstract from the solvent to give secondary radicals R which in turn add to nitrosobenzene to give radicals of the type $C_6H_5N(\dot{O})R$. Relative proportions of the two types of radicals correlate with the rates of hydrogen abstraction from the solvent. Further studies of the photolysis of nitrobenzene in isopropyl alcohol suggest that the complexity of the mechanism results in part from (1) the intermediate formation of nitrosobenzene which competes for the primary radicals $C_6H_5N(\dot{O})OH$ or $C_6H_5N(\dot{O})OR$, and (2) the involvement of $C_6H_5N(\dot{O})H$ radicals in an equilibrium with an unstable diamagnetic intermediate.

Introduction

Electron spin resonance spectroscopy has been widely used to identify paramagnetic intermediates in photochemical reactions when the steady-state concentration of radicals during illumination exceeds 10^{-6} or 10^{-7} M. Kinetic measurements have been relatively uncommon because the sensitivity of the conventional esr spectrometer depends on the integration of a signal over a period of time which is generally greatly in excess of the average lifetime of the radicals. In such cases it may be possible to overcome the difficulty by means of a suitable computer for averaging transients (C.A.T.) in which signal-to-noise enhancement is achieved by repeated sampling of the esr signal over very short periods of time (down to a few microseconds) and adding only the coherent components. Thus the lifetime of a reactive free radical in solution may be measured by applying repeated flashes of light to generate the radicals and following their decay during the intervening dark periods.

In conventional photochemical studies the intermittency is provided most simply by means of a rotating disk with suitable cut-out sections placed so as to interrupt the light beam before it reaches the sample. A similar system may be applied to the study of solutions in an esr cavity, and the C.A.T. may be triggered so as to examine either the buildup of radicals during the illumination period or the decay during the subsequent dark period. From the latter the kinetic order of the termination reaction, and its rate constant k_t may be determined. A number of studies of this kind have been reported.[1-5]

To obtain information about the rate of formation of radicals in photochemical systems it is necessary to study either the buildup process or the steady-state concentration when the rate of formation equals the rate of disappearance. Such studies can yield useful data only if the reaction mechanism is sufficiently well known that kinetic rate equations can be devised to describe the time dependence of the instantaneous radical concentration upon light intensity, reactant concentrations, temperature, etc. Conversely, a study of the effect of these variables on the radical concentrations may provide valuable tests of proposed reaction mechanisms.[5-8]

In an earlier communication we described some detailed studies of this kind on the photoreduction of biacetyl and pyruvic acid in a number of organic solvents.[5] Here we wish to report some further results concerning

(1) B. M. Monroe and S. A. Weiner, *J. Amer. Chem. Soc.*, **91**, 450 (1969).

(2) S. A. Weiner and G. S. Hammond, *ibid.*, **91**, 986 (1969).

(3) S. A. Weiner, E. J. Hamilton, Jr., and B. M. Monroe, *ibid.*, **91**, 6350 (1969).

(4) T. Fujisawa, B. M. Monroe, and G. S. Hammond, *ibid.*, **92**, 542 (1970).

(5) P. B. Ayscough and M. C. Brice, *J. Chem. Soc. B*, 491 (1971).

(6) D. H. Cho and G. Tollin, *Photochem. Photobiol.*, **8**, 317 (1968).

(7) D. C. Mukherjee, D. H. Cho, and G. Tollin, *ibid.*, **9**, 273 (1969).

(8) G. A. Russell and E. G. Janzen, *J. Amer. Chem. Soc.*, **89**, 300 (1967).

these systems and some related observations on the photoreduction of aromatic nitro and nitroso compounds.

Experimental Section

The esr spectrometer (Decca X3), Biomac 1000 computer, and optical system have been described earlier.[5] The 1-kW high-pressure mercury lamp used emits radiation mainly with $\lambda > 300$ nm. The procedures for estimating radical concentrations, based on numerical double integration of the esr first-derivative signal, have also been used in earlier studies.[5]

Research grade or Analar grade solvents were used where possible (benzene, toluene, cyclohexane, cyclohexene, pentane, isopropyl alcohol). Cumene, diphenylmethane, hexane, and heptane were of commercial grades (British Drug Houses Ltd.), redistilled at atmospheric pressure.

Biacetyl (Koch-Light Laboratories Ltd.) and nitrobenzene (Fisons Ltd., Analar grade) were used without further purification. Nitrosobenzene (Hopkin and Williams Ltd.) was recrystallized three times from ethanol, mp 66–68°.

Solutions containing biacetyl or nitrosobenzene were carefully degassed by freeze–pump–thaw cycles to pressures $< 5 \times 10^{-5}$ mm. Nitrobenzene solutions were degassed by purging with oxygen-free nitrogen.

Results and Discussion

1. Ketones and Keto Acids. The carbonyl group in these compounds absorbs in the ultraviolet with λ_{max} ~350–400 nm and extinction coefficient given by log ϵ (l. mol^{-1} cm^{-1}) = 1–2, corresponding to an n-π^* transition. There is ample evidence that the reactive state of carbonyl compounds in solution is the lowest triplet state, formed in very high yield because of very efficient intersystem crossing from the excited singlet state following absorption.[9-13] Radicals of the type >Ċ–OH are formed in the presence of suitable solvents from which H can be abstracted, and these have been observed by esr spectroscopy in many systems.

For biacetyl (B) in organic solvents (RH) the simplified reaction scheme reported earlier[5] is shown in Scheme I

Scheme I

$$B \underset{k_3}{\overset{I_a}{\rightleftharpoons}} B^s \xrightarrow{k_2} B^t \qquad (1\text{–}4)$$

$$B^t \xrightarrow{k_4}$$

$$B^t + Q \xrightarrow{k_5} B + Q^* \qquad (5)$$

$$B^t + C{=}C \xrightarrow{k_6} \text{molecular products} \qquad (6)$$

$$B^t + RH \xrightarrow{k_7} BH\cdot + R\cdot \qquad (7)$$

$$2BH\cdot \xrightarrow{k_8} (BH)_2 \qquad (8)$$

$$BH\cdot + R\cdot \xrightarrow{k_9} BHR \qquad (9)$$

$$2R\cdot \xrightarrow{k_{10}} \text{molecular products} \qquad (10)$$

where B^s = singlet excited biacetyl, B^t = triplet excited biacetyl, BH· = $CH_3\dot{C}(OH)COCH_3$, R· = radical derived from solvent by H abstraction, Q = triplet state quencher. For this system the rate constant for the termination reaction of BH· radicals is given by

$$k_t = 2k_8 + k_9(k_8/k_{10})^{1/2} \qquad (11)$$

though in most solvents $k_{10} \gg k_8$, so $k_t \approx 2k_8$.

The rate constant k_t is readily measured since the time of half-reaction $t_{1/2} \approx 10$ msec when [BH·] $\approx 10^{-6}$ M, *i.e.*, $k_t \approx 10^8$–10^9 M^{-1} sec^{-1} for many diketones, keto acids, and esters in isopropyl alcohol.[4,5] In other solvents k_t shows quite wide variations (see Table I), which may be related to the viscosity of the solvent in the manner predicted by the Debye relation for the encounter rate for diffusion-controlled reactions.[14]

Table I: Comparison of Theoretical Diffusion-Controlled and Experimental Rate Constants for the Bimolecular Termination Reactions of $CH_3\dot{C}(OH)COCH_3$ Radicals at 25°

Solvent	Viscosity, $10^3\eta$, P	Rate constant for termination— $10^{-9}k_t$(diff), l. mol^{-1} sec^{-1}	$10^{-9}k_t$(exptl), l. mol^{-1} sec^{-1}
Isopropyl alcohol	23.7	2.7	0.30 ± 0.06
Ethanol	11.9	5.5	2.1 ± 0.4
Cyclohexene	6.6	9.9	3.0 ± 0.6
Benzene	6.5	10.0	3.1 ± 0.6

Our observed values of k_t are about an order of magnitude lower than the predicted values, though Smaller has suggested[15] that in radical–radical encounters only one-quarter lead to the formation of product *via* a singlet transition state. Tabulated values of k_{diff} should therefore be divided by 4. The precise interpretation of k_t will also differ from solvent to solvent, and there may be a small activation energy for the recombination reaction. Preliminary measurements suggest that the apparent activation energy for the termination reaction is about 4 kcal mol^{-1} for $CH_3\dot{C}(OH)COCH_3$ and $CH_3\dot{C}$-(OH)COOH radicals in isopropyl alcohol. This is to be compared with value 5 kcal mol^{-1} derived from the

(9) H. L. J. Backstrom and K. Sandros, *Acta Chem. Scand.*, 12, 823 (1958).
(10) H. L. J. Backstrom and K. Sandros, *ibid.*, 14, 48 (1960).
(11) H. Ishikawa and W. A. Noyes, *J. Amer. Chem. Soc.*, 84, 1502 (1962).
(12) F. C. Henriques and W. A. Noyes, *ibid.*, 62, 1038 (1940).
(13) N. J. Turro and R. Engel, *ibid.*, 91, 7113 (1969).
(14) W. A. Noyes, *Progr. React. Kinet.*, 1, 129 (1961).
(15) B. Smaller, *J. Chem. Phys.*, 48, 5174 (1968).

temperature coefficient of viscosity of isopropyl alcohol. To enable a more detailed comparison to be made between theoretical and experimental rates we are measuring k_t in other solvents and over a wider range of temperatures.

As was shown earlier,[5] the steady-state concentration of [BH·] radicals during photolysis is given by

$$[BH\cdot]^2 = \frac{I_a k_7[RH]}{k_t(k_4 + k_7[RH])} \qquad (12)$$

if $k_2 \gg k_3$ and $k_4 \gg k_5[Q] + k_6[C{=}C]$. These conditions are applicable to the solutions we have examined. Thus plots of $1/[BH\cdot]^2k_t$ against $1/[RH]$ should be linear with the ratio of slope to intercept equal to k_4/k_7. Thus measurements of the steady-state concentrations [BH·] in mixed solvents, one of which is unreactive, *e.g.*, benzene, combined with measurement of k_t for each solution, will yield relative values of k_7, the rate of abstraction of H from the solvent.

Figure 1 shows the results for biacetyl in three solvents, using benzene as diluent. The graphs are linear within experimental error and yield, for k_t at 25° for cyclohexene, isopropyl alcohol, ethanol, the relative values 21:1.8:1. These preliminary figures are in qualitative agreement with the behavior of alkyl or alkoxy radicals and suggest that in these systems the triplet state molecules are behaving much like simple monoradicals.[16] They also confirm the earlier assumption[9,10] that H abstraction is the cause of quenching of triplet biacetyl in these solvents.

It must be noted that the implied assumption of this derivation is that k_4 is independent of solvent. This is difficult to prove experimentally though our evidence suggests that the assumption is valid in the solvents we have used so far. A possible way of circumventing this problem is to add known amounts of a well-characterized triplet state quencher such as anthracene, so that $k_5[Q] > k_4$ and small variations in k_4 will not be significant. Furthermore this will enable us to derive more reliable values of k_7 when $k_7[RH] \gg k_4$, as in the case of cyclohexene.

2. Nitroso Compounds. Despite the widespread use of nitroso compounds as radical scavengers[17-20] and in spin-labeling experiments[21-23] and in the preparation of nitroxides by photolysis,[24-26] little is known of the detailed photochemistry. In particular, the role of the triplet state has not been established.

Apart from the intrinsic interest in these compounds, the possible involvement of nitroso compounds as intermediates in the photoreduction of aromatic nitro compounds provided an incentive to examine the photolysis of nitrosobenzene in a number of organic solvents.

Absorption in the ultraviolet region (λ_{max} ~280 nm) probably involves $n_0 \rightarrow \pi^*$ transitions associated with the aromatic ring. Population of a nearby triplet state would not be unreasonable by analogy with

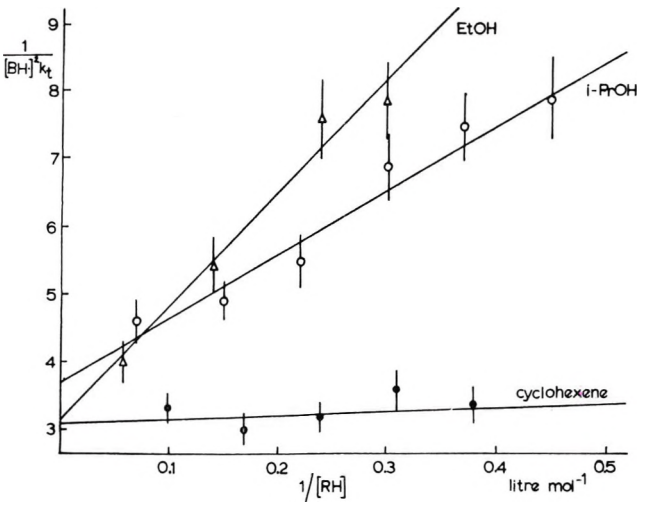

Figure 1. Reactions of triplet-state biacetyl with organic solvents; plots of $1/[BH\cdot]^2k_t$ against $1/[RH]$: for RH = ethanol, △; isopropyl alcohol, ○; and cyclohexene, ●, at 25°.

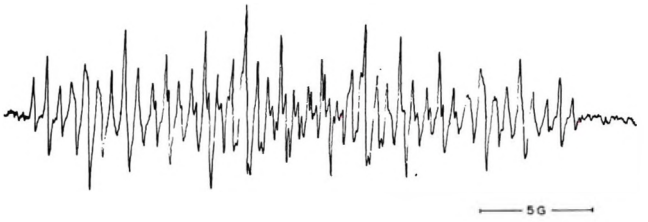

Figure 2. Esr spectrum of $C_6H_5N(\dot{O})H$ radicals from the photolysis of nitrosobenzene or nitrobenzene in isopropyl alcohol.

carbonyl compounds, given a reasonable intersystem crossing efficiency. Triplet nitrosobenzene might then be expected to abstract H from a solvent such as isopropyl alcohol to yield the radical $C_6H_5\dot{N}OH$ or C_6H_5-$NH\dot{O}$.

Figure 2 shows the spectrum observed during the photolysis of 0.01 *M* nitrosobenzene in deoxygenated isopropyl alcohol at 25°. The radical is stable for many hours, and analysis of the spectrum gives the

(16) C. Walling and M. J. Gibian, *J. Amer. Chem. Soc.*, **87**, 3361 (1965).

(17) A. Hoffman, A. Feldman, E. Gelblum, and W. Hodgson, *ibid.*, **88**, 639 (1964).

(18) C. Lagercrantz and S. Forschult, *Acta Chem. Scand.*, **23**, 708 (1969).

(19) C. Lagercrantz and S. Forschult, *ibid.*, **23**, 811 (1969).

(20) I. H. Leaver and G. C. Ramsay, *Aust. J. Chem.*, **22**, 1899 (1969).

(21) H. M. McConnell and C. L. Hamilton, *Proc. Nat. Acad. Sci. U. S.*, **60**, 776 (1968).

(22) H. M. McConnell, S. Ogawa, and A. Horwitz, *Nature*, **220**, 787 (1968).

(23) G. P. Rabold, *J. Polym. Sci., Part A1*, **7**, 1203 (1969).

(24) A. Mackor, Th. Wajer, Th. de Boer, and J. van Voorst, *Tetrahedron Lett.*, 2115 (1966).

(25) E. T. Strom and A. L. Bluhm, *Chem. Commun.*, 115 (1966).

(26) P. B. Ayscough, F. P. Sargent, and R. Wilson, *J. Chem. Soc. B*, 900 (1966).

Table II: Nuclear Hyperfine Couplings (Gauss) for Nitroxide Radicals Observed after Uv Irradiation of Nitrosobenzene in Organic Solvents at 25°

	Radicals observed						
	$(C_6H_5)_2N\dot{O}$			$C_6H_5N(\dot{O})R$			
Solvent	a^N	$a_{o,p}^H$	a_m^H	a^N	$a_{o,p}^H$	a_m^H	a_R^H
Benzene	9.6	1.8	0.8	...[a]	...	...	...
Toluene	9.7	1.8	0.82	10.4	2.8	0.93	6.4 (2)
Cyclohexane	9.3	1.8	0.8	10.3			
Cyclohexene	...	...	...	10.45			
Cumene	...	...	...	11.8	2.5	0.91	
Diphenylmethane	...	...	...	10.6	2.6	0.91	3.6 (1)
Pentane	9.4			10.6			
Hexane	9.4			10.7			
Heptane	9.4			10.6			
Methanol	...	...	...	10.3			
Isopropyl alcohol	...	...	...	9.1	3.1	1.05	12.1[b] (1)
n-Butyl alcohol	...	...	...	*c*			
Isobutyl alcohol	...	...	...	*c*			
Tetrahydrofuran	9.66	1.83	0.82	10.6			
Tetrahydropyran	9.3			10.7			

[a] ... indicates radical absent or in negligible concentration; blank entry indicates that hyperfine couplings were not measured. [b] R = H in this solvent. [c] Very complex spectra, probably mixture of $C_6H_5N(\dot{O})H$ and $C_6H_5N(\dot{O})R$.

hyperfine couplings $a^N = 9.1$, $a_{NH}^H = 12.1$, $a_{o,p}^H = 3.1$, $a_m^H = 1.05$ G, *cf.* literature values[27] 9.13, 12.12, 3.07, and 1.0 G, respectively. While this observation appears to indicate hydrogen abstraction from the solvent by triplet nitrosobenzene, it is in conflict with our earlier observation that the main radical product of photolysis of nitrosobenzene in tetrahydrofuran is diphenyl nitroxide.[26]

To clarify this situation we have now examined the esr spectra of uv-irradiated nitrosobenzene in a wide variety of organic solvents. The results are summarized in Table II, and it is clear that they do not in general correspond to the expected behavior of triplet-state molecules, taking carbonyl compounds as typical. For example, in benzene diphenyl nitroxide is formed with great facility (triplet carbonyl compounds react very slowly). Also, in cyclohexene, the radical formed very rapidly and in high yield is neither diphenyl nitroxide nor monophenyl nitroxide $C_6H_5N(\dot{O})H$. In all cases the radicals are stable for periods of hours.

A more likely mechanism involves the dissociation of photoexcited nitrosobenzene into phenyl radicals and nitric oxide from either the excited singlet or triplet state (k_{17}). Phenyl radicals then abstract H from the solvent (k_{20}) and the solvent radicals so produced combine (k_{21}) or add to nitrosobenzene (k_{22}).

$$C_6H_5NO \underset{k_{15}}{\overset{I_a}{\rightleftharpoons}} C_6H_5NO^s \xrightarrow{k_{14}} C_6H_5NO^t \quad (13\text{–}16)$$

$$\uparrow \qquad\qquad \downarrow k_{16}$$

$$C_6H_5NO^s \text{ (or } C_6H_5NO^t) \underset{k_{-17}}{\overset{k_{17}}{\rightleftharpoons}} C_6H_5\cdot + NO \quad (17)$$

$$C_6H_5\cdot + C_6H_5\cdot \xrightarrow{k_{18}} (C_6H_5)_2 \quad (18)$$

$$C_6H_5\cdot + C_6H_5NO \xrightarrow{k_{19}} (C_6H_5)_2N\dot{O} \quad (19)$$

$$C_6H_5\cdot + RH \xrightarrow{k_{20}} C_6H_6 + R\cdot \quad (20)$$

$$R\cdot + R\cdot \xrightarrow{k_{21}} R_2 \text{ etc.} \quad (21)$$

$$R\cdot + C_6H_5NO \xrightarrow{k_{22}} C_6H_5N(\dot{O})R \quad (22)$$

This mechanism predicts that we should observe a mixture of radicals $(C_6H_5)_2N\dot{O}$ + $C_6H_5N(\dot{O})R$ from all solvents except benzene, with the mixed nitroxide predominating in cases where the solvent hydrogen atoms are abstracted most readily. Our results, summarized in Table II, provide a very satisfactory support for the mechanism outlined above.

For example, in cumene and diphenylmethane, the predominant radicals are $C_6H_5(\dot{O})C(CH_3)_2C_6H_5$ and $C_6H_5N(\dot{O})CH(C_6H_5)_2$, respectively (see Figure 3), while in toluene and cyclohexane we obtain a mixture of $(C_6H_5)_2NO$ and the mixed radicals $C_6H_5N(\dot{O})R$ (see Figures 4 and 5). In aliphatic hydrocarbons diphenyl nitroxide predominates, but the mixed radicals $C_6H_5N(\dot{O})R$ cannot be identified positively since abstraction of H can take place at various positions in the hydrocarbon, and it is likely the several different solvent radicals R are involved in each hydrocarbon.

Relative yields of the two nitroxide radicals can of course be changed by varying the concentration of nitrosobenzene since the addition reaction 19 and abstraction reaction 20 are in competition. This is exemplified by Figure 5 for toluene solutions of different concentrations. Furthermore, the ratio $(C_6H_5)_2N\dot{O}$/

(27) Th. A. J. Wajer, A. Mackor, and Th. J. de Boer, *Tetrahedron*, 23, 4021 (1967).

Figure 3. Esr spectrum of $C_6H_5(\dot{O})C(CH_3)_2C_6H_5$ radicals from the photolysis of nitrosobenzene in cumene.

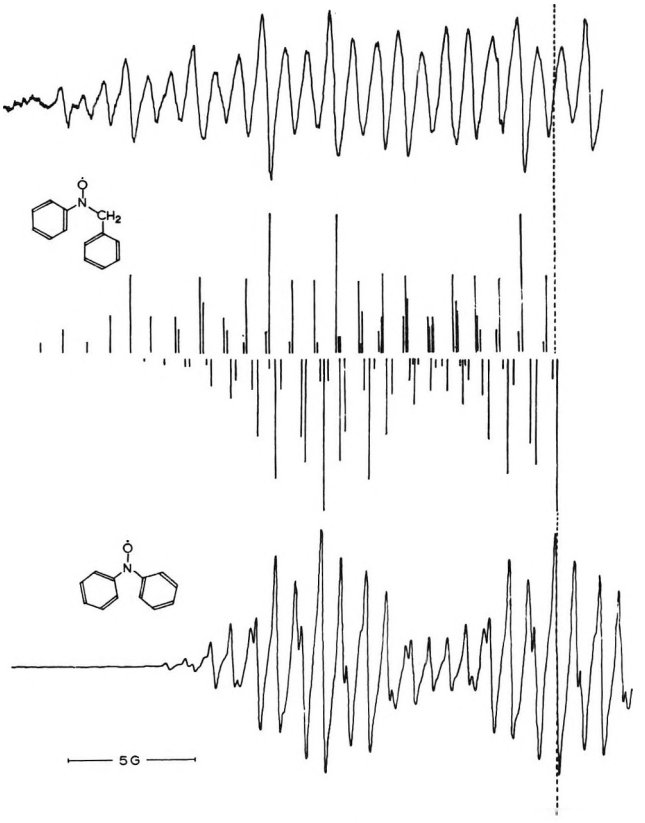

Figure 4. Esr spectra of $(C_6H_5)_2N\dot{O}$ and $C_6H_5N(\dot{O})CH_2C_6H_5$ radicals from the photolysis of nitrosobenzene in benzene and toluene, respectively.

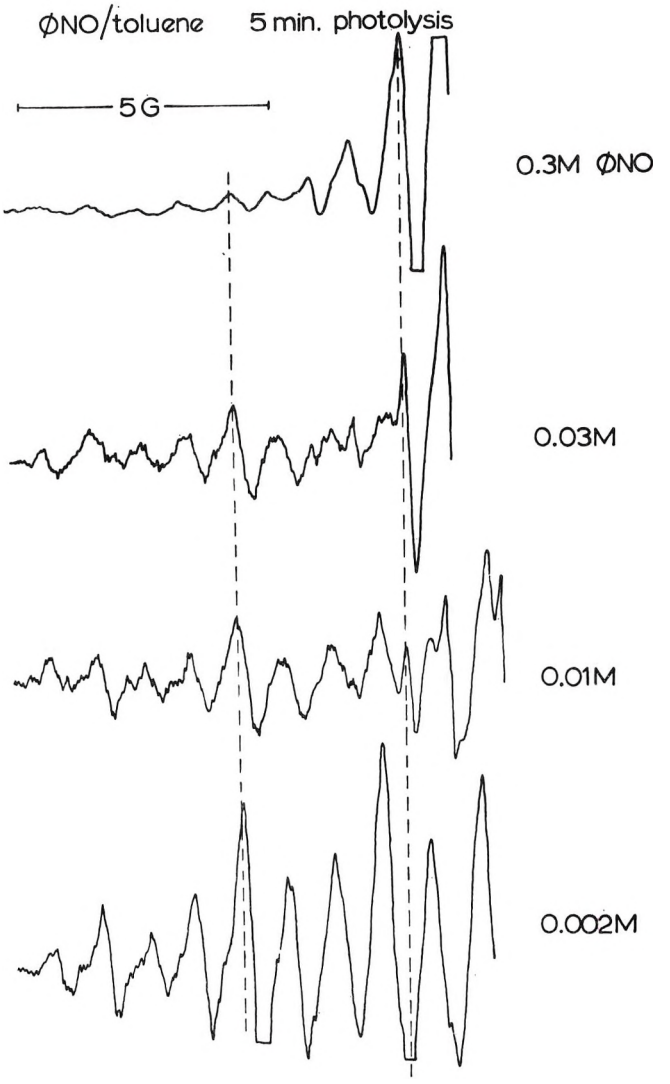

Figure 5. Part of esr spectra of mixtures of $C_6H_2N(\dot{O})CH_2C_6H_5$ and $(C_6H_5)_2N\dot{O}$ radicals formed during the photolysis of solutions of nitrosobenzene in toluene of different concentrations.

$C_6H_5N(\dot{O})R$ decreases during the course of the photolysis because nitrosobenzene is being consumed and the ratio $[C_6H_5NO]/[RH]$ is decreasing.

These observations are in complete agreement with the mechanism outlined earlier. If the combination reactions of phenyl and solvent radicals may be neglected in comparison with the abstraction and addition reactions, *i.e.*, if $k_{18}[C_6H_5\cdot] \ll k_{19}[C_6H_5NO]$ or $k_{20}[RH]$, and $k_{21}[R\cdot] \ll k_{22}[C_6H_5NO]$, it may be shown that

$$\frac{d[(C_6H_5)_2NO]/dt}{d[C_6H_5N(\dot{O})R]/dt} = \frac{k_{19}[C_6H_5\cdot]}{k_{22}[R\cdot]} = \frac{k_{19}[C_6H_5NO]}{k_{20}[RH]} \quad (23)$$

We have verified this relationship quantitatively only for the nitrosobenzene–toluene system in which the spectra of the two radicals can be separated relatively easily and the rates of formation of the two radicals can be measured in the early stages of the photolysis. On prolonged photolysis the ratio $[(C_6H_5)_2N\dot{O}]/[C_6H_5N(\dot{O})R]$ increases because some of the mixed nitroxide is lost, presumably by slow decomposition. In other hydrocarbons resolution of the two overlapping spectra is more difficult, and quantitative measurements have not been made. It seems that nitrosobenzene is a useful source of phenyl radicals and provides its own internal monitor, *i.e.*, the addition reaction giving diphenyl nitroxide. Thus we can use esr measurements on nitrosobenzene photolysis to measure rates of reactions of phenyl radicals, and presumably other nitroso compounds will behave in an analogous manner. Work on these systems is continuing.

The formation of $C_6H_5N(\dot{O})H$ in isopropyl alcohol remains anomalous since other alcohols appear to give

mixed nitroxides in which R is the alcohol radical, $\cdot CH_2OH$, etc. However, it seems likely that intramolecular proton transfer may take place followed by elimination of acetone. This reaction has important

$$C_6H_5N(\dot{O})C(CH_3)_2OH \longrightarrow C_6H_5N(\dot{O})H + (CH_3)_2CO \quad (24)$$

consequences in relation to the photoreduction of aromatic nitro compounds, to be considered in the following section.

These observations leave open the question whether dissociation of photoexcited nitrosobenzene takes place from the singlet or triplet state. To throw light on this problem we examined the photolysis of nitrosobenzene in cyclohexane in the presence of a number of molecules which are known to be excited to the triplet state readily by irradiation with ultraviolet light (see Table III). Although the energy of triplet nitrosobenzene is not known with certainty, it is probably in the region 50–60 kcal so that some of the added absorbers should act as photosensitizers and others as quenchers of the triplet state.

Table III: Effects of Triplet Sensitizers and Quenchers on the Photolysis of Nitrosobenzene in Cyclohexane at 25°

Additive[a]	λ_{max},[b] nm	log ϵ,[c] M^{-1} cm^{-1}	ΔE^t,[d] kcal	
Benzophenone	340	2.2	69	Large increase in initial rate of formation of radicals, then equally rapid decay to zero concentration
Xanthone	336	3.5	74	
Carbazole	337	3.5	70	No change in rate of formation of radicals, when corrected for light absorbed by additive
Chrysene	320	4.18	57	
Anthracene	355/375	3.9	42	

[a] Concentration adjusted so that additive absorbs 80–90% of incident radiation. [b] λ_{max} = wavelength of maximum absorption (>300 nm). [c] ϵ = molar decadic extinction coefficient. [d] ΔE^t = difference between energy of triplet state and ground state.

The results are summarized in the table. The effect of the two carbonyl compounds is ascribed to direct reaction of the carbonyl triplet with the solvent, while the other three absorbers appear to leave the rate of formation of nitroxide radicals unchanged when account is taken of the reduction in total light intensity available to the nitrosobenzene as a result of absorption by the additives. Thus our evidence suggests that triplet nitrosobenzene is not involved directly in the formation of phenyl radicals, which are therefore presumed to arise from dissociation of an excited singlet state.

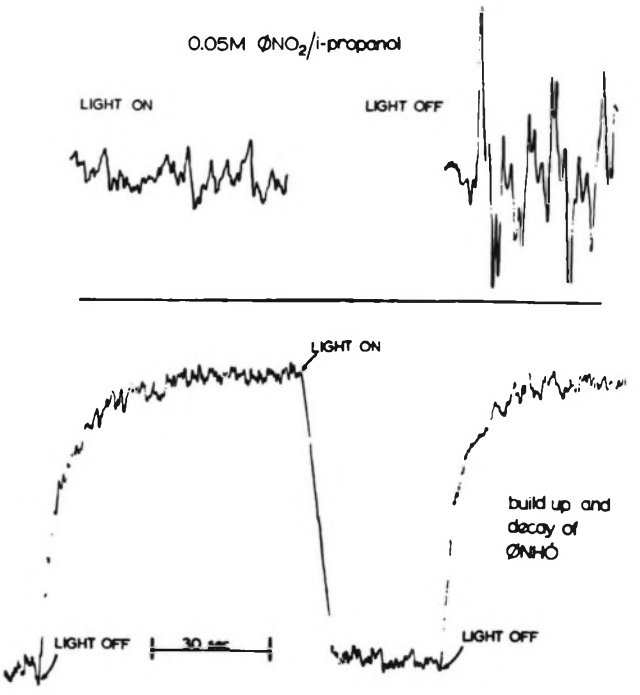

Figure 6. Photolysis of nitrobenzene in isopropyl alcohol: esr spectra observed during intermittent illumination showing the buildup and decay of $C_6H_5N(\dot{O})H$ radicals.

3. Nitro Compounds. The photoreduction of aromatic nitro compounds is much more complex than that of carbonyl or nitroso compounds because of the numerous oxidation states involved. The products are numerous and varied, depending very markedly on solvent, pH, and temperature. We have restricted our attention to neutral solutions with particular emphasis on the role of the primary monoradicals $C_6H_5N(\dot{O})OH$ and $C_6H_5N(\dot{O})OR$, where R = radical formed by abstraction of H from solvent, and the possible participation of nitrosobenzene as a reactive intermediate.

It is widely believed that photoreduction of nitrobenzene proceeds *via* the lowest triplet state when radiation of wavelengths > 290 nm is used.[28] The overall quantum yield for the loss of nitrobenzene during uv photolysis in 2-propanol is about 10^{-2}, and this low efficiency is thought to result from a low probability for intersystem crossing singlet → triplet.[29] All mechanisms so far postulated show triplet nitrobenzene abstracting from solvent to give the radical $C_6H_5N(\dot{O})OH$, though this has never been identified by means of esr spectroscopy. (The rather stable radicals observed by esr spectroscopy during the photolysis of nitrobenzene in tetrahydrofuran and other ethers, previously identified as $C_6H_5N(\dot{O})OH$,[30] have been shown to be adduct radicals with the structure $C_6H_5N(\dot{O})OR$.[31,32]) In

(28) P. de Mayo, *Advan. Org. Chem.*, **2**, 367 (1960).
(29) R. Hurley and A. C. Testa, *J. Amer. Chem. Soc.*, **88**, 4330 (1966).
(30) R. Ward, *J. Chem. Phys.*, **38**, 2388 (1963).
(31) D. J. Cowley and L. H. Sutcliffe, *Chem. Commun.*, 201 (1968).

isopropyl alcohol, with a labile hydrogen atom, we therefore might expect to observe radicals of these types. In the mechanism proposed by Hurley and Testa[29] for the photolysis in isopropyl alcohol, the reactive intermediates involved are $C_6H_5NO_2{}^t$, $C_6H_5N(\dot{O})OH$, $(CH_3)_2\dot{C}OH$, $C_6H_5N(OH)$ biradical, and $C_6H_5\dot{N}OH$. When we examined this system we found, instead, a very large signal from the stable radical $C_6H_5N(\dot{O})H$, identical with that observed during the photolysis of nitrosobenzene in the same solvent (Figure 2). Moreover, the size of this signal *increases* greatly over a period of several seconds when illumination ceases and reverts to the original size within milliseconds when illumination is restored (Figure 6). This fully reversible behavior has been observed independently in other solvents by Chachaty and Forchioni[33] and by Cowley and Sutcliffe.[34] In both cases the interpretation involves an equilibrium between $C_6H_5N(\dot{O})H$ or $C_6H_5N(\dot{O})R$ and a diamagnetic intermediate, the nature of which is a matter for speculation. We will return to this point later.

The presence of a large excess of a rather stable radical (with concentration changes on a time scale of seconds or longer) does not necessarily preclude the observation of transient spectra on a scale of milliseconds, when a C.A.T. is employed. On the basis of our observations on biacetyl, etc., we expect to be able to see species with $t_{1/2} \sim 1$ msec at concentrations of 10^{-6} M or more, *i.e.*, with $k_t \sim 10^9$ M^{-1} sec^{-1}. An estimate of k_t for $C_6H_5N(\dot{O})OH$ radicals in aqueous acid solutions, based on pulse radiolysis measurements,[35] is 6×10^8 M^{-1} sec^{-1} and recombination in isopropyl alcohol should be slower. However, we have not so far found any evidence for the existence of a transient species with $t_{1/2} \geq 1$ msec at the concentrations we are able to detect.

This negative evidence does not of course preclude the participation of $C_6H_5NO_2{}^t$ and $C_6H_5N(\dot{O})OH$ in the photoreduction; in fact the evidence that the analogous species exist during the photolysis of 2,3,5,6-tetrachloro- and 2,3,6-trichloronitrobenzene[36] and in glassy matrices containing nitrobenzene at 77°K[37] seems convincing. k_t for the $-N(\dot{O})OH$ type radicals in the chlorinated nitrobenzenes is estimated to be $\gtrsim 10^6$ M^{-1} sec^{-1} and a steady-state concentration of about 5×10^{-6} M was found.[36] This very low concentration, and our failure to observe the $C_6H_5N(\dot{O})OH$ radicals in isopropyl alcohol, is probably attributable to the very inefficient conversion of singlet to triplet state,[38,39] rather than to a particularly rapid reaction of the $-N(\dot{O})OH$ radicals. The use of light sources giving more radiation in the effective part of the ultraviolet region may make direct measurements on these radicals possible.

We have also examined briefly the effect of adding small amounts of nitrosobenzene to nitrobenzene undergoing photolysis in isopropyl alcohol. The important conclusions are as follows. (1) The addition of as little as 2% nitrosobenzene greatly increases the concentration of $C_6H_5N(\dot{O})H$ during photolysis and afterward. (2) The addition of more nitrosobenzene reduces the magnitude of the reversible intermittancy effect until with 20% nitrosobenzene the effect disappears entirely. These effects probably result from the ability of nitrosobenzene to scavenge radicals produced in the primary reaction of triplet nitrobenzene (*i.e.*, $C_6H_5N(\dot{O})OH$ and $(CH_3)_2\dot{C}OH$) as well as those produced by the reversible dissociation of the diamagnetic intermediate invoked to explain the reversible intermittency effect, *i.e.*, by the reactions

$$C_6H_5NO + (CH_3)_2\dot{C}OH \longrightarrow C_6H_5N(\dot{O})C(CH_3)_2OH \longrightarrow C_6H_5N(\dot{O})H + (CH_3)_2CO \quad (25)$$

$$C_6H_5NO + C_6H_5N(\dot{O})OH \longrightarrow C_6H_5N(\dot{O})H + C_6H_5NO_2 \quad (26)$$

(Some direct photolysis of nitrosobenzene must also occur but this reaction alone cannot explain these observations.)

Thus it seems that any mechanism for the photoreduction of nitrobenzene in isopropyl alcohol must contain the steps shown in Scheme II, where [D] = diamagnetic intermediate, presumably a hydrogen-bonded dimer which can dissociate before or after H transfer.

This mechanism, which remains tentative while investigations of individual steps continue, leads to the correct stoichiometry[29] and provides a qualitative interpretation of the effect of nitrosobenzene and of the reversible intermittency effect. The bracketed pairs of reactions are alternatives since each leads to the correct reaction products (C_6H_5NO, $C_6H_5N(\dot{O})H$, and C_6H_5NHOH, respectively) in isopropyl alcohol. For other solvents, such as ethers in which adduct radicals $C_6H_5N(\dot{O})OR$ are involved, and other alcohols in which $C_6H_5N(\dot{O})R$ replaces $C_6H_5N(\dot{O})H$, the mechanism is undoubtedly more complex.

Conclusions

Of the three functional groups examined, the photochemistry of the carbonyl group, exemplified by bi-

(32) E. G. Janzen and J. K. Gerlock, *J. Amer. Chem. Soc.*, **90**, 1652 (1968).

(33) C. Chachaty and A. Forchioni, *Tetrahedron Lett.*, **307**, 1079 (1968).

(34) D. J. Cowley and L. H. Sutcliffe, *J. Chem. Soc. B*, 569 (1970).

(35) K. D. Asmus, A. Wigger, and A. Henglein, *Ber. Bunsenges. Phys. Chem.*, **70**, 862 (1966).

(36) D. J. Cowley and L. H. Sutcliffe, *Trans. Faraday Soc.*, **65**, 2286 (1969).

(37) J. K. Brown and W. G. Williams, *Chem. Commun.*, 495 (1966).

(38) W. Trotter and A. C. Testa, *J. Amer. Chem. Soc.*, **90**, 7044 (1968).

(39) R. Hurley and A. C. Testa, *ibid.*, **90**, 1949 (1968).

Scheme II

$$C_6H_5NO_2 \underset{}{\overset{I_a}{\rightleftharpoons}} C_6H_5NO_2^s \longrightarrow C_6H_5NO_2^t \qquad (27\text{–}30)$$

$$C_6H_5NO_2^t + (CH_3)_2CHOH \longrightarrow C_6H_5N(\dot{O})OH + (CH_3)_2\dot{C}OH \qquad (31)$$

$$C_6H_5N(\dot{O})OH + (CH_3)_2\dot{C}OH \longrightarrow C_6H_5N(OH)_2 + (CH_3)_2CO \qquad (32)$$

$$C_6H_5N(\dot{O})OH + C_6H_5(\dot{O})OH \longrightarrow C_6H_5N(OH)_2 + C_6H_5NO_2 \qquad (33)$$

$$C_6H_5NO + (CH_3)_2\dot{C}OH \longrightarrow C_6H_5N(\dot{O})C(CH_3)_2OH \,[\longrightarrow C_6H_5N(\dot{O})H + (CH_3)_2CO] \qquad (25)$$

$$C_6H_5NO + C_6H_5N(\dot{O})\,OH \longrightarrow C_6H_5N(\dot{O})H + C_6H_5NO_2 \qquad (26)$$

$$C_6H_5N(\dot{O})\,H + (CH_3)_2\dot{C}OH \rightleftharpoons [D] \longrightarrow C_6H_5NHOH + (CH_3)_2CO \qquad (34)$$

$$C_6H_5N(\dot{O})H + C_6H_5N(\dot{O})\,OH \rightleftharpoons [D] \longrightarrow C_6H_5NHOH + C_6H_5NO_2 \qquad (35)$$

acetyl is best understood. Kinetic analysis using esr spectroscopy can apparently yield reliable values for rate constants of individual radical combination reactions and may permit the direct measurement of rates of reaction of triplet-state molecules. In nitroso compounds the triplet state is not involved, and the significance of our results so far lies in the possibility of using these species as sources of aryl and other radicals for kinetic studies, using yields of nitroxide radicals as a measure of the rate of reaction with solvent or other reactant species. In contrast, much more work is needed on the photolysis of nitro compounds before the mechanism is understood. Participation of triplet nitrobenzene is still not established unequivocally, and the complications arising from equilibria involving diamagnetic intermediates mean that kinetic studies using intermittent illumination are unusually difficult to interpret.

Acknowledgment. We thank the Science Research Council and the University of Leeds for financial assistance in the form of equipment and research studentships.

Discussion

H. LEVANON. What is the rise and decay time of the chopped light in conjunction with the response time of the spectrometer?

P. B. AYSCOUGH. The response time of the spectrometer is about 2×10^{-4} sec. The rise and decay time of the chopped light is determined by the size of the cutout in the rotating disk, the diameter of the light beam at the point it is cut, and the rate of rotation of the disk. Thus the ratio of rise or decay time to the period of illumination is constant (about 0.05) so, for our maximum rate of rotation, the rise and decay times are also about 2×10^{-4} sec.

E. THOMAS STROM. In the photolysis of nitrosobenzene in a solvent such as cyclohexane, your mechanism predicts the formation of benzene by abstraction of a hydrogen atom by phenyl radicals. Have you actually attempted to isolate benzene as a product?

P. B. AYSCOUGH. We have not yet carried out any product analyses on these systems, but benzene should be a product in all cases when phenyl radicals from nitrosobenzene abstract hydrogen from the solvent.

Nuclear Magnetic Resonance Studies of Phenoxy Radicals: Hyperfine Coupling Constants and Spin Densities of a Series of Partially Fluorinated Radicals

by Siddick Icli and Robert W. Kreilick*[1]

Department of Chemistry, University of Rochester, Rochester, New York 14627 *(Received February 12, 1971)*

Publication costs borne completely by The Journal of Physical Chemistry

We have taken proton and fluorine nmr spectra of a series of partially fluorinated phenoxy radicals. The spectra of two unfluorinated parent radicals were also taken. Hyperfine coupling constants were determined from the shifts of the lines while fluorine spin densities were estimated through an analysis of the line widths. The fluorine spin densities were found to be a constant fraction of the carbon spin densities, and we were unable to determine individual fluorine spin polarization parameters from our experimental data. The fluorine spin densities are found to be about 7.5% of the carbon spin densities.

I. Introduction

The hyperfine coupling constants of fluorine atoms in fluoro-substituted aromatic radicals depend on both the spin density at the adjacent carbon atom and the spin density at the fluorine. The coupling constants are related to the spin densities by spin polarization parameters (Q's) for the 1s and 2s electrons. Three types of equations have been proposed to relate coupling constants (A_F) to spin densities. These are[2-6]

$$A_F = Q_{CC}\rho_C \tag{1}$$

$$A_F = Q_{CC}\rho_C + Q_{FF}\rho_F \tag{2}$$

$$A_F = Q_{CC}\rho_C + [Q_{CF} + Q_{FC}]\rho_{CF} + Q_{FF}\rho_F \tag{3}$$

To evaluate the spin polarization parameters one must be able to determine the sign and magnitude of the fluorine coupling constant, the carbon spin density (ρ_C), and the fluorine spin density (ρ_F). In the case of eq 3 one must also know the sign and magnitude of the carbon–fluorine bond spin density (ρ_{CF}). The magnitude of the fluorine coupling and the sign and magnitude of the carbon spin density can normally be obtained from electron spin resonance spectra. Fluorine spin densities are usually not obtained by esr studies, and as a consequence most of the papers in which Q values have been reported rely on calculated values of fluorine spin densities.

Nuclear magnetic resonance spectroscopy can be used to determine the sign and magnitude of electron-nuclei hyperfine coupling constants in some instances. If a given radical is dissolved in a liquid radical solvent and spin exchange between solute and solvent rapidly averages the electron spin energy levels, one observes a single shifted nmr line from each group of equivalent nuclei.[7] The equation relating the shift of a given line (ΔH) to the hyperfine coupling constant (A) is

$$\Delta H = -A\left(\frac{\gamma_e}{\gamma_N}\right)\left(\frac{g\beta H}{4kT}\right) \tag{4}$$

The width of the nmr lines can be used to estimate the spin density at the fluorine atom in fluorinated radicals.[5] The width of the nmr lines is dominated by the electron-nuclei dipole–dipole interaction and the Fermi contact interaction.[8] In the case of fluorine one must consider dipolar terms from the spin at carbon and from the spin at fluorine. The equations for the line widths of signals from protons and from fluorine are given by[5,8]

$$\left(\frac{1}{T_2}\right)_H = {}^4/_3 S(S+1)\left(\frac{g^2\beta^2 g_N{}^2\beta_N{}^2}{\hbar^2}\right) \times \left(\frac{\rho_C{}^2}{r_{CH}{}^6}\right)t_e + {}^2/_3 S(S+1)\frac{A_H{}^2}{\hbar^2}t_e \tag{5}$$

$$\left(\frac{1}{T_2}\right)_F = {}^4/_3 S(S+1)\left(\frac{g^2\beta^2 g_N{}^2\beta_N{}^2}{\hbar^2}\right) \times \left(\frac{\rho_C{}^2}{r_{CF}{}^6} + \frac{\rho_F{}^2}{r_F{}^6}\right)t_e + {}^2/_3 S(S+1)\frac{A_F{}^2}{\hbar^2}t_e \tag{6}$$

(1) Alfred P. Sloan Foundation Fellow.

(2) (a) P. H. Fischer and J. P. Colpa, *Z. Naturforsch. A*, **24**, 1980 (1969); (b) S. V. Kulkarni and C. Trapp, *J. Amer. Chem. Soc.*, **92**, 4801, 4809 (1970).

(3) A. Hudson and J. W. Lewis, *Mol. Phys.*, **19**, 241 (1970).

(4) J. Sinclair and D. Kivelson, *J. Amer. Chem. Soc.*, **90**, 5074 (1968).

(5) W. Espersen and R. W. Kreilick, *Mol. Phys.*, **16**, 577 (1969).

(6) A. Hinchliffe and J. Murrell, *ibid.*, **14**, 147 (1968).

(7) W. Espersen and R. W. Kreilick, *J. Phys. Chem.*, **73**, 3370 (1969); R. W. Kreilick, *J. Amer. Chem. Soc.*, **90**, 2711, 5991 (1968).

(8) I. Solomon, *Phys. Rev.*, **99**, 559 (1955); N. Bloembergen, *J. Chem. Phys.*, **27**, 572 (1957); G. W. Canters and E. DeBoer, *Mol. Phys.*, **13**, 395 (1967); D. Stehlik and K. H. Hausser, *Z. Naturforsch. A*, **22**, 914 (1967).

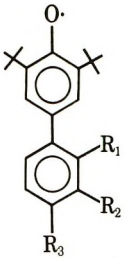

Compound	R_1	R_2	R_3
I	H	H	H
II	H	F	H
III	H	H	F
IV	H	CH_3	F
V	CH_3	H	F
VI	CH_3	H	H

Figure 1. Compounds investigated.

In these expressions t_e is the correlation time for spin exchange, r_{CH} is the separation between the electron in the carbon 2p orbit and the proton, r_{CF} is the separation between the electron in the carbon 2p orbit and the fluorine, and r_F is the separation between the electron in the fluorine 2p orbit and the fluorine.

In an earlier paper we reported the nmr and esr spectra of three fluorinated phenoxy radicals.[5] We have extended this work to a series of four new fluorinated phenoxy radicals along with two unfluorinated parent radicals. The compounds which have been studied are shown in Figure 1.

II. Experimental Section

The phenolic precursors of radicals I–VI were prepared by the technique of Ershov.[9] The overall yields, melting points, and analytical data for these compounds are listed in Table I. The radicals were made by oxidizing an ethereal solution of the parent phenols with aqueous alkaline K_3FeCN_6. After the ether layer was dried and evaporated, the radicals were dissolved in the liquid radical di-*tert*-butyl nitroxide (DBNO) for the nmr experiments.[7]

Table I: Analytical Data, Melting Points, and Yields of the Phenols[a]

	Analytical					
	Theoretical		Found		Mp,	Yield,
Phenol	%C	%H	%C	%H	°C	%
II	79.96	8.33	80.04	8.58	99	55
III	79.96	8.33	79.98	8.48	107	73
IV	80.22	8.65	80.14	8.76	105	41
V	80.22	8.65	79.85	8.60	78	27

[a] Compounds I and VI have previously been reported; ref 9 and 10.

The nmr spectra were taken on a JEOLCO 4H-100 100-MHz nmr spectrometer. A Princeton Applied Research Model HR-8 lock-in amplifier was used with the high-resolution spectrometer for the broad line studies. A Digital Equipment PDP-12 digital computer was used for the various calculations. Programs were written in FOCAL.

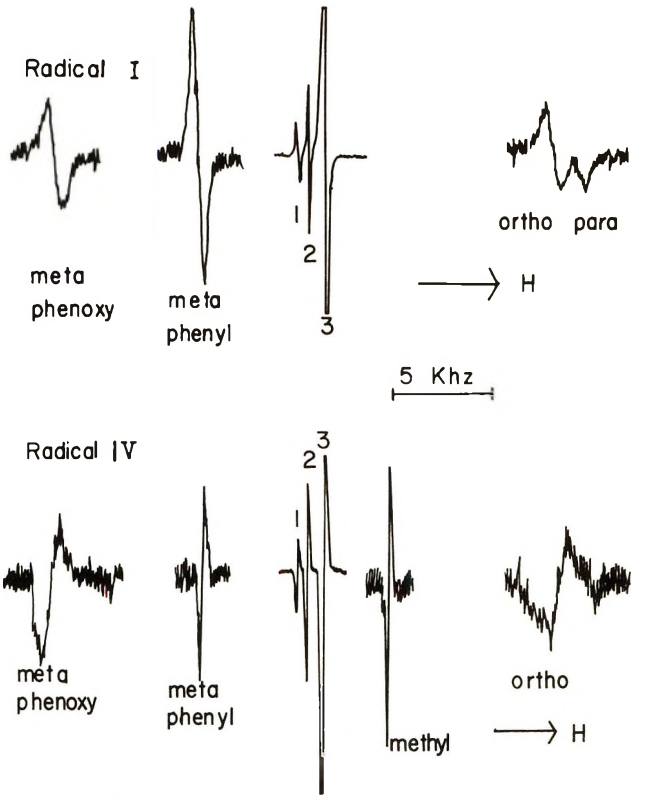

Figure 2. Nmr spectra of radicals I and IV: 1, diamagnetic aromatic peak; 2, diamagnetic *tert*-butyl peak; 3, DBNO peak.

III. Results and Discussion

The proton nmr spectra of the radicals showed peaks from each group of equivalent protons. Typical spectra are shown in Figure 2. Shifts and coupling constants are listed in Table II. The coupling constants from compound I are similar to those determined in an earlier esr study.[10] The signs of the coupling constants from the ortho and para protons of the phenyl ring are negative while the signs of the coupling from the meta protons of the phenyl and phenoxy rings are positive. The fluorine couplings had opposite signs from the corresponding proton couplings in each case.

The magnitudes of the fluorine spin densities were estimated from an analysis of the proton and fluorine line widths. A plot of the fluorine and proton line widths *vs.* the square of the coupling constants is shown in Figure 3. The plot also includes points from the three radicals reported in our earlier paper.[11] The experiments were carried out in a liquid radical solvent in which the correlation time for spin exchange is short

(9) V. V. Ershov, G. N. Bogdanov, and A. A. Volodkin, *Izv. Akad. Nauk*, 1, 157 (1963); G. N. Bogdanov and V. V. Ershov, *ibid.*, 6, 1084 (1963).

(10) A. Rieker and K. Scheffler, *Ann. Chem.*, 689, 78 (1965).

(11) We re-examined the spectra of these radicals and with better instrumentation found the fluorine line widths to be slightly smaller than the values previously reported.

Table II: Shifts and Coupling Constant for the Radicals

Radical	Phenoxy ring meta ΔH[a]	Phenoxy ring meta A[b]	Phenyl ring Ortho ΔH	Phenyl ring Ortho A	Phenyl ring Meta ΔH	Phenyl ring Meta A	Phenyl ring Para ΔH	Phenyl ring Para A	Methyl group ΔH	Methyl group A	Fluorine ΔH	Fluorine A
I	−126.6	+1.69	+131.0	−1.75	−51.4	+0.68	+143.6	−1.92				
II	−128.8	+1.72	+131.5	−1.75	−49.1	+0.66	+143.2	−1.91			+106.2	−1.42
III	−130.2	+1.74	+135.8	−1.81	−49.3	+0.66					−333.5	+4.51
IV	−127	+1.69	+134.9	−1.80	−47.2	+0.63			+43.8	−0.58	−312.3	+4.22
V	−133.2	+1.78	+79.8	−1.06	−47.9	+0.64			−64.2	+0.86	−194	+2.62
VI	−129	+1.74	+81.8	−1.11	−48	+0.63	+81.8	−1.11	−59.5	+0.81		

[a] The shifts are in ppm from the corresponding diamagnetic peaks. Positive signs indicate a shift to high field. [b] The coupling constants are in gauss.

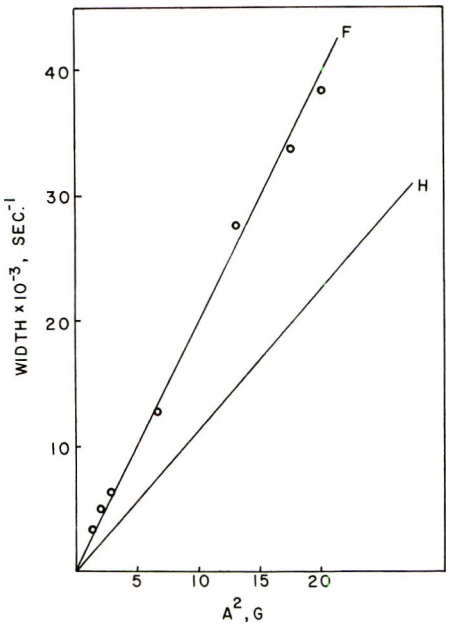

Figure 3. Proton and fluorine line widths *vs.* coupling constants squared. Data from our earlier study are included.

Table III: Carbon and Fluorine Spin Densities

Radical	Position	$\rho_C \times 10^2$	$\rho_F \times 10^2$	$\rho_F/\rho_C \times 10^2$
II	Meta	−2.45	−1.7	7.0
III	Para	+7.11	+5.28	7.4
IV	Para	+7.11	+4.94	7.0
V	Para	+4.1	+3.05	7.10
A[a]	Ortho	+3.64	+2.23	6.1
B	Meta	−1.77	−1.68	9.5
C	Para	+5.31	+4.61	8.6

[a] Compounds A, B, and C are the radicals studied in our previous paper; ref 5.

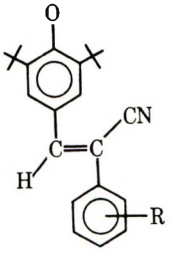

Compound	R
A	*o*-Fluoro
B	*m*-Fluoro
C	*p*-Fluoro

compared to the rotational correlation time. In this case t_e is the appropriate correlation time for both the dipolar and scalar interactions. One may determine the value of t_e from eq 5 if one estimates r_{CH}. We assumed r_{CH} to be the carbon–hydrogen bond length and find t_e to be 3.6×10^{-12} sec.

To determine ρ_F from eq 6 one must estimate r_{CF} and r_F. We used the carbon–fluorine bond length as an estimation of r_{CF} and calculated the value of $1/r_F^3$ from the 2p radical distribution function.[12] Slater screening constants were used to determine the effective nuclear charge. This calculation gives a value of 0.294 Å for r_F. We were unable to determine the sign of ρ_F as the dipolar term contains ρ_F^2. We assumed that ρ_F had the same sign as the spin density at the adjacent carbon in each case. Table III lists the fluorine spin densities obtained by this technique as well as the spin densities at the adjacent carbon atoms.

We assumed that the substitution of fluorine for hydrogen did not disturb the overall spin distribution and calculated carbon spin densities from the appropriate proton coupling constants. A Q_{CH} value of −27 G was used. This assumption appears to be justified as the proton couplings did not change very much upon introduction of a fluorine. The spin densities in the phenyl rings of the two compounds with *o*-methyl groups (radicals V and VI) were smaller than those from the other radicals. The phenyl ring in these compounds is probably twisted with respect to the phenoxy ring because of an interaction between the bulky methyl groups and the phenoxy ring.

In our earlier paper we estimated the Q values of eq 2 by plotting A_F/ρ_C *vs.* ρ_F/ρ_C. For this technique to be valid the spin density at fluorine cannot be a constant fraction of the spin density at the adjacent carbon. In cases in which $\rho_F = C\rho_C$ eq 2 can be written as

$$A_F = [Q_{CC} + CQ_{FF}]\rho_C \qquad (7)$$

(12) I. Waller, *Z. Phys.*, **38**, 635 (1926).

where C = constant. When this is the case, one cannot determine individual values for Q_{CC} and Q_{FF}. The sum of the terms in eq 7 gives an effective Q relating fluorine couplings to carbon spin densities.

Figure 4 shows a plot of the spin density at fluorine *vs.* the spin density at the adjacent carbon. This plot indicates that the spin density at fluorine is about 7.5% of the spin density at the adjacent carbon for this series of radicals. This result is similar to the result obtained through a study of the anisotropic coupling of the fluoroacetamide radical.[13] In this case the fluorine spin density was found to be about 14% of the carbon spin density.

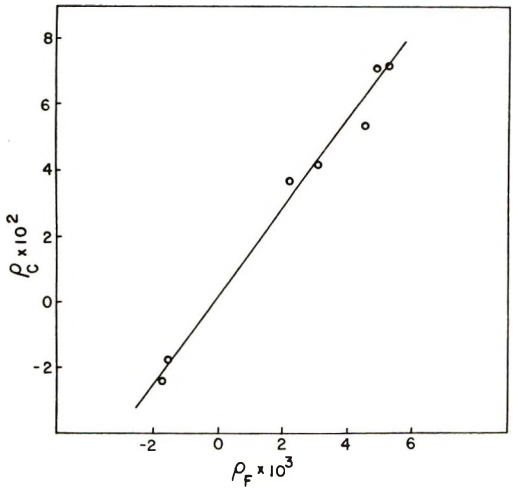

Figure 4. Carbon spin density *vs.* fluorine spin density. Data from our earlier study are included.

A plot of the carbon spin densities *vs.* fluorine coupling constants is given in Figure 5. The points from the radicals reported in this paper fall very close to the line while the points for the *o*- and *p*-fluoro radicals of our previous study fall slightly off the line. The slope of this line gives a value of +62 G for $Q_{CC} + CQ_{FF}$. In our earlier paper we attempted to estimate values of Q_{CC} and Q_{FF} from a limited set of experimental data. Our current work indicates that the ratio of ρ_F/ρ_C is nearly constant for this set of phenoxy radicals. One cannot determine individual values for polarization parameters when this is the case.

We carried out calculations of fluorine coupling constants using our spin densities along with the polarization parameter determined by Kulkarni and Trapp[2b] and by Fischer and Colpa.[2a] Table IV contains experimental fluorine coupling constants along with the coupling constants calculated with this technique. The results obtained with Kulkarni and Trapp's polarization parameters are completely different from the experimental results while Fischer and Colpa's values gave good results in most instances. The agreement with Fischer and Colpa's results can be explained by introducing their Q values into eq 7 along with our

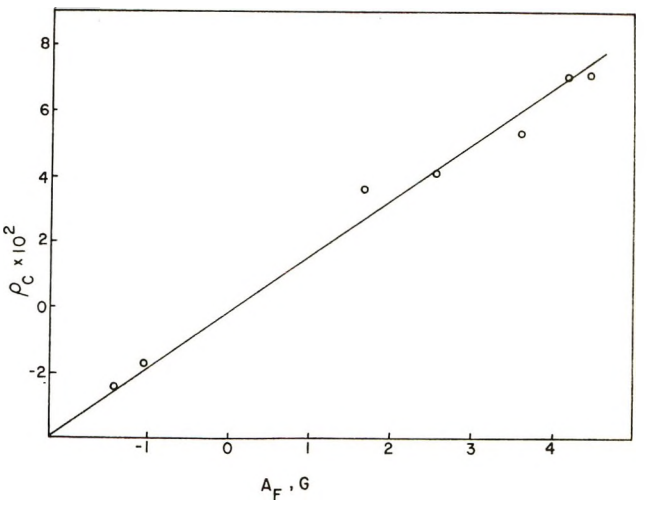

Figure 5. Carbon spin density *vs.* fluorine coupling constants. Data from our earlier study are included.

Table IV: Calculated and Experimental Fluorine Coupling Constants

Radical	Position	Experimental A_F	Kulkarni and Trapp[a] A_F	Fischer and Colpa[b] A_F
II	Meta	−1.42	+0.31	−1.43
III	Para	+4.45	−0.53	+4.18
IV	Para	+4.17	−0.88	+4.13
V	Para	+2.59	−0.47	+2.51
A[c]	Ortho	+1.66	−0.77	+2.07
B	Meta	−1.11	−0.24	−1.09
C	Para	+3.6	+0.30	+3.23

[a] Calculated with Q_{CC} = −85 G, Q_{FF} = 1043 G; ref 2b. [b] Calculated with Q_{CC} = 48.1 G, Q_{FF} = 146 G; ref 2a. [c] Radicals from previous paper; see Table III.

value for C. This calculation leads to a value of 59.1 G for $Q_{CC} + CQ_{FF}$.

Acknowledgment. This work was supported in part by National Science Foundation Grant No. GP-9339.

Discussion

ROGER V. LLOYD. Why is the ratio of A_F/A_H nearly constant in your radicals whereas in the simple fluorophenoxy radicals it differs for *o*-fluoro and *p*-fluoro?

R. W. KREILICK. Only one *o*-fluoro compound was included in our study. The ratio of A_F/A_H was different for this radical from any of the meta- or para-substituted radicals.

JAMES R. BOLTON. Trapp, *et al.*, have recently shown that A_F/A_H varies considerably in a series of fluoro-substituted triphenylmethyl radicals. Do you feel you can determine the Q's for this series?

R. W. KREILICK. We should be able to determine the fluorine couplings and spin densities for the fluoro-triphenylmethyl radicals if they are soluble in DBNO and are not dimerized.

(13) R. J. Cook, J. R. Rowlands, and D. H. Whiffen, *Mol. Phys.*, 7, 31 (1968).

Spin Trapping of Some Short-Lived Radicals by the Nitroxide Method

by Carl Lagercrantz

Department of Medical Physics, University of Göteborg, S-400 33 Göteborg 33, Sweden *(Received December 21, 1970)*

Publication costs assisted by the Division of Physical Chemistry of the American Chemical Society

The scavenger properties of *tert*-alkylnitroso compounds have been used for the trapping of short-lived free radicals as stable nitroxide radicals. As well as the main triplet splitting caused by the nitrogen nucleus of the nitroxide group, the esr spectra showed secondary splittings which originated from magnetic nuclei of the part of the nitroxide derived from the trapped radical. From these splittings it was in many cases possible to determine the structure of the trapped radical. A number of reactions and radicals have been studied with the nitroxide method, and this paper is mainly a résumé of the results obtained in our laboratories.

Introduction

A great number of stable mononitroxide radicals, RR'NO·, have been synthesized, and their esr spectra have been investigated. The subject has been reviewed up to the year 1968 by Forrester, *et al.*,[1] and by Rozantsev.[2]

A variety of free radicals readily add to *tert*-nitrosoalkanes and aromatic nitroso compounds to give nitroxides. Thus a series of nitroxides was prepared by decomposition of aliphatic azo compounds in the presence of *tert*-nitrosobutane.[3] Irradiation of solutions of aromatic nitroso compounds with ultraviolet light gives rise to diaryl nitroxides detectable by esr spectroscopy.[4,5] By the use of the esr technique de Boer and coworkers[6,7] have extensively studied the radicals produced in solutions of a variety of aliphatic as well as aromatic nitroso compounds. They found that the formation of nitroxide radicals was a general reaction during photolysis of *C*-nitroso compounds at room temperature. Alkyl and aryl radicals, formed by dissociation of the nitroso compounds, are very probably intermediates in these photoreactions (eq 1). The radicals add to an undissociated molecule of the nitroso compound in a subsequent reaction to give the nitroxide radical (eq 2).

$$\mathrm{RNO} \xrightarrow{h\nu} \mathrm{R}\cdot + \mathrm{NO}\cdot \qquad (1)$$

$$\mathrm{R}\cdot + \mathrm{RNO} \longrightarrow \underset{\mathbf{1}}{\mathrm{R_2NO}\cdot} \qquad (2)$$

Esr studies have revealed the formation of both dialkyl and alkylalkoxy nitroxides during photolysis of various alkyl nitrites with ultraviolet light in alkane and in alkylbenzene solvents.[8] The mechanism of these reactions most likely also involves the formation of intermediate nitrosoalkanes.

The Nitroxide Method

In connection with our studies of the nitroxides formed in reactions of tetranitromethane with 2-monosubstituted 1,3-dicarbonyl compounds,[9] it became evident that the scavenger properties of nitroso compounds leading to the formation of stable nitroxides could be utilized for the identification of short-lived radicals otherwise not detectable by esr spectroscopy (see eq 3).

$$\underset{\mathbf{2}}{\mathrm{R'NO}} + \mathrm{R}\cdot \longrightarrow \underset{\mathbf{3}}{\mathrm{R'\text{-}N(O\cdot)\text{-}R}} \qquad (3)$$

This method has been applied to the trapping of short-lived, free radicals produced in a variety of reactions, and this paper is mainly a résumé of the results obtained in our laboratories. In these experiments *tert*-nitrosoalkanes, such as 2-methyl-2-nitrosobutanone-3 or *tert*-nitrosobutane, were used as the nitroso scavenger, R'NO (**2**). Along with the main triplet splitting caused by the ^{14}N nucleus of the nitroxide group, the esr spectra showed secondary splittings which originated almost exclusively from magnetic nuclei in the part of the nitroxide radical derived from the trapped radical R·. From these splittings it was in many cases possible to determine the structure of the trapped radicals. The magnitude of the main ^{14}N splittings was also of value for the identification of the trapped radical. Thus the a_N value of the unsymmetrical nitroxide formed by trapping of aryl and alkyl radicals was in

(1) A. R. Forrester, J. M. Hay, and R. H. Thomson, "Organic Chemistry of Stable Free Radicals," Academic Press, New York, N. Y., 1968.

(2) E. G. Rozantsev, "Free Nitroxyl Radicals," translated from Russian by B. J. Hazzard, Plenum Press, New York, N. Y., 1970.

(3) A. K. Hoffmann, French Patent 1,357,477 (1964); *Chem. Abstr.*, **61**, 8191 (1964). U. S. Patent 3,253,015 (1966); *Chem. Abstr.*, **65**, 15225 (1966).

(4) K. Maruyama, R. Tanikaga, and R. Goto, *Bull. Chem. Soc. Jap.*, **37**, 1893 (1964).

(5) H. Mauser and H. Heitzer, *Z. Naturforsch. B*, **20**, 200 (1965).

(6) A. Mackor, Th. A. J. W. Wajer, Th. J. de Boer, and J. D. W. van Voorst, *Tetrahedron Lett.*, **19**, 2115 (1966).

(7) Th. A. J. W. Wajer, A. Mackor, Th. J. de Boer, and J. D. W. van Voorst, *Tetrahedron*, **23**, 4021 (1967).

(8) A. Mackor, Th. A. J. W. Wajer, Th. J. de Boer, and J. D. W. van Voorst, *Tetrahedron Lett.*, **5**, 385 (1967).

(9) C. Lagercrantz and K. Torssell, *Acta Chem. Scand.*, **22**, 1935 (1968).

the range between 11 and 16 G, whereas trapped alkoxy radicals, RO·, gave rise to nitroxides with a_N between 27 and 29 G.[8] Trapping of acyl radicals, R$\dot{C}$=O, gave nitroxides with a_N values between 6 and 8 G.[10]

Minor structural changes within the part of the nitroxide derived from the trapped radical R· induced small but significant changes of the a_N values.[11,12] These changes amounted to a few gauss at the most, but since solvent effects were of the same order of magnitude, it is necessary to make comparative measurements in the same solvent.

Aliphatic nitroxide radicals with an increasing number of keto groups on the carbon atoms in the position α to the nitrogen atom of the nitroxide group exhibited decreasing a_N values: no CO, 15.8 ± 0.5; 1 CO, 14.9 ± 0.5; 2 CO, 14.1 ± 0.5; 3 CO, 13.4 ± 0.5; 4 CO, 12.9 ± 0.5 G (methylene chloride). Other electron-attracting groups had the same lowering effect, *e.g.*, phenyl, hydroxy, and alkoxy groups.

The α-alkylmethylene and α-acylmethylene protons give rise to characteristic triplet splittings of *ca.* 10.5 and 8 G, respectively. The doublet splitting from a methine proton is smaller, between 1.5 and 6 G. The splittings from β-hydrogen atoms are small, $\leq$0.7 G, and could in many cases not be resolved.

However, it must be emphasized that the a_H values just given imply free rotation of the hydrogen atoms of the CH_2 and =CH groups. The presence of steric hindrance might lock the protons in a particular position, a situation which can introduce a highly selective coupling to only one of two protons of an α-methylene group, giving an a_H value about 20 G. This situation has been found to prevail in alicyclic nitroxides such as pyrrolidineoxyl and morpholineoxyl radicals,[13] but has been observed also in the case of nitroxides formed by trapping short-lived radicals such as that derived from *N*,*N*-dimethylformamide.[14]

The Nitroso Scavenger

The selection of the nitroso scavenger, R′NO (**2**), is of crucial importance. The unsymmetrical nitroxides RR′NO· formed upon trapping of various radicals R· must be stable enough to allow their esr spectra to be recorded. The group R′ of the nitroso scavenger should not make any contributions to the secondary splittings of the nitroxide; otherwise this interferes with the interpretation of the splittings derived from the trapped radical. Both aromatic and *tert*-alkyl nitroso compounds give rise to relatively stable nitroxide radicals, but the use of aromatic nitroso scavengers will introduce very disturbing overlap, originating from aromatic protons. Aromatic nitroso compounds are therefore ruled out, leaving us with *tert*-nitrosoalkanes as scavengers which were actually found to give no contribution at all, or only a very small one, to the secondary hfs. However, it must be emphasized that an increase in the resolution (<0.1 G) will sooner or later introduce disturbing overlap from magnetic nuceli in the part of the nitroxide derived from the scavenger.[15] Rather few nitroxides have been observed so far in which such splittings have been resolved.

To react with short-lived radicals the nitroso scavenger has to be present as a monomer, a requirement fulfilled by most aromatic nitroso compounds. On the other hand, many aliphatic nitroso compounds are present as inactive dimers, which have to be split into the monomeric state either thermally or by uv irradiation before any radical trapping can take place. However, the situation is rather favorable with *tert*-nitrosoalkanes, and especially in the case of *tert*-nitrosobutane. The equilibrium is sufficiently toward the monomeric state in these compounds to allow trapping of radicals at room temperature. Most of our trapping experiments were performed with *tert*-nitrosobutane as the scavenger. 2-Methyl-2-nitrosobutanone-3 was also used for some systems. This substance is sometimes a more efficient scavenger, but has the disadvantage of being partially degraded upon irradiation by uv light, with the formation of $CH_3\dot{C}$=O radicals which are trapped to give nitroxide radicals with an a_N value of about 7 G.

Irradiation of the reaction mixture in order to transfer the scavenger into the monomeric state, or in order to generate radicals photochemically, also produces the symmetrical nitroxide R′$_2$NO·, according to eq 1. In most cases the concentration of the symmetrical nitroxide was rather small, but in some cases its presence gave rise to overlapping peaks which interfered with the interpretation of the spectra of the unsymmetrical nitroxides. Thus, the symmetrical nitroxide will often dominate the spectrum when no radicals, or only very few radicals, have been trapped in the reaction studied. In the case of a very high concentration of the symmetrical nitroxide, the situation is further complicated by the presence of ^{13}C doublets, which might obscure the spectrum of small amounts of unsymmetrical nitroxides or be erroneously interpreted as a spectrum originating from such radicals.

The Trapping Reaction

The success of trapping short-lived radicals as nitroxides will depend on a number of factors. As mentioned earlier, the inherent stability of the nitroxides is a prerequisite. However, reactive reagents present in the system under study may compete with the nitroso scavenger for the short-lived radicals, or react with the

(10) A. Mackor, Th. A. J. W. Wajer, and Th. J. de Boer, *Tetrahedron*, **24**, 1623 (1968).

(11) S. Forshult, C. Lagercrantz, and K. Torssell, *Acta Chem. Scand.*, **23**, 522 (1969).

(12) K. Torssell, *Tetrahedron*, **26**, 2759 (1970).

(13) G. Chapelet-Letourneux, H. Lemaire, and A. Rassat, *Bull. Soc. Chim. Fr.*, 3283 (1965).

(14) C. Lagercrantz, unpublished observation.

(15) A sterically hindered rotation of the *tert*-butyl group might also introduce a detectable coupling to the protons of this group.

nitroxide radicals already formed, thereby decreasing their concentration. The stability of the nitroso scavenger in the presence of reactive reagents must also be taken into account. There is a general impression that small and very short-lived radicals, with a highly localized unpaired electron, such as methyl radicals, are more easily trapped than large and more stable species with the spin density distributed over the molecule.

The trapping reaction leading to observable nitroxides seems in many cases to be capricious, and in practice a negative result cannot be taken as definite proof for the absence of free radicals.

Experimental Conditions

Although the optimum conditions for trapping short-lived radicals by the nitroxide method have been found to vary depending on the system investigated, some general comments may be made concerning the experimental procedure.

The choice of the solvent is of utmost importance. Many solvents participate in the radical reactions to be studied, with the result that most of the trapped radicals may be derived from solvent molecules. Thus, it is not advisable to use methanol, ethanol, acetone, acetic acid, *N*,*N*-dimethylformamide, or dimethyl sulfoxide as solvents in reactions involving radical generation, for example by hydroxyl radicals. On the other hand, no radicals seem to be trapped from solvent benzene, at least at room temperature. Notwithstanding, benzene is not a convenient solvent, as the yield of trapped radicals was found to be very low in a variety of reactions performed in this solvent.

Water was found to be a suitable solvent for the study of radical reactions involving polar parent compounds (*cf.* sections III, VII, IX, and X). Methylene chloride was found well suited for a variety of reactions involving parent compounds of low polarity (*cf.* sections IV, V, VIII, and IX). The relatively low solidification point, −97°, makes this solvent useful for low temperature studies (*cf.* sections I, II, and V).

When the parent substance is liquid at room temperature, it will sometimes be profitable to study the radical reaction without the addition of solvent (*cf.* section IX).

It is essential that the concentration of the nitroso scavenger is kept rather low. In most of our experiments the concentration was 0.01 *M*, *i.e.*, about 0.5 mg in a reaction mixture of 0.5 ml. The scavenger was dissolved in the solvent or in the solution of the parent compound in the solvent immediately before use. It is sometimes beneficial to gently warm the solution of the scavenger before the addition of the parent compounds and other reagents to increase the concentration of the active monomeric state of the scavenger. The suitable amount of the parent compounds seems to vary widely. Generally, it is convenient to start with a certain excess, and later on reduce the amount of the parent compound to an optimum of spectral resolution as soon as radicals have been actually trapped. The amounts of other reagents present, such as hydrogen peroxide, lead tetraacetate, or ceric ions may be crucial. Insufficient amounts will produce too low a concentration of the radicals to be trapped. On the other hand, too high a concentration might destroy the radicals to be trapped, the nitroso scavenger, or the nitroxide formed.

The irradiation experiments were performed *in situ* by the use of a high-pressure mercury lamp, equipped with a variety of filters. It is essential that the light source is equipped with a movable shutter and an adjustable diaphragm, so that the duration of the irradiation and the intensity of the light can be easily varied. It seems probable that the failure to trap radicals in photochemical reactions has sometimes been associated with an excessive irradiation of the sample. In some experiments we found that the optimum time for irradiation was only a few seconds.

Scope and Limitations

The main advantage of the nitroxide method compared with flow systems for demonstrating the presence of short-lived radicals by esr spectroscopy is the small amount of material required. A few milligrams of the parent substance is often a sufficient quantity, whereas several grams is necessary in the flow methods. The nitroxide method is simple to handle and can be used in a variety of reaction systems for detecting intermediate radicals at various temperatures, including room temperature.

The limitations are connected with the inherent fact that the radical R· is transformed into a radical species with a spin distribution different from that of the original radical. The nitroxide radicals have a large spin density on the atoms of the nitroxide group, leaving relatively little density on the part derived from the trapped radical. The hyperfine splittings originating from this part are therefore generally narrow compared with those of the original untrapped radical. The contribution to the hfs from magnetic nuclei situated farther away than in the position β to the nitrogen atom of the nitroxide group are not resolved in nitroxides formed by the trapping of alkyl radicals.

The disadvantage of narrow splittings from the part derived from the trapped radical may be still more pronounced when more than one single radical species has been trapped. In such a case, the interpretation of the individual spectra of the nitroxides can be seriously hampered by overlap. In this connection, it should be pointed out that a quantitative estimation of the different radical species in a mixture can only be made approximately, since all species are not trapped with the same efficiency, and the resulting nitroxides are not equally stable.

Spin Trapping with Nitrone Scavengers

An alternative diamagnetic radical scavenger is the

nitrone **4**, phenyl *N-tert*-butyl nitrone, reacting with radicals according to eq 4. This scavenger has been

$$\mathrm{R\cdot} + \mathrm{C_6H_5CH{=}\overset{\displaystyle O^-}{\overset{|}{N}}{}^{+}\text{–}Bu^t} \longrightarrow \mathrm{C_6H_5CH\overset{\displaystyle R\ O\cdot}{\overset{|\ \ |}{N}}Bu^t} \quad (4)$$

4 **5**

employed in a number of reactions by Janzen, *et al.*[16–19] The nitrone **4** seems to have a greater thermal and photochemical stability than *tert*-nitrosobutane, but it has the very considerable disadvantage that the spectrum of the derived nitroxide **5** normally exhibits only a proton doublet and a nitrogen triplet. The identity of the trapped radical may be inferred only from precise measurements of a_N and a_H. Furthermore, the changes in these splitting constants as a function of R· are comparable in magnitude with variations brought about by changes in solvent.

The nitrone scavenger has been used in the solid state for trapping gas phase radicals produced in a stream of an indifferent carrier gas. These elegant experiments are apparently impossible to perform with the use of *tert*-nitrosoalkanes, since these scavengers are present as inactive dimers in the solid state.[19]

Reactions and Radicals Studied with the Nitroxide Method

I. Oxidative Decarboxylation of Carboxylic Acids with Lead Tetraacetate.[11] This reaction is known to proceed *via* radicals (eq 5). In accordance with expecta-

$$\mathrm{RCOOH} \xrightarrow[h\nu]{\mathrm{Pb(OAc)_4}} \mathrm{R\cdot} + \mathrm{CO_2} \quad (5)$$

tion, unsymmetrical nitroxide radicals were formed on irradiation by uv light of a solution of lead tetraacetate, the carboxylic acid, and the nitroso scavenger in methylene chloride. The spectra obtained at −40° indicate the trapping of alkyl radicals. It is worth noting that the nitroso scavenger is able to react at the low temperature involved. Both the nitroso scavenger and the oxidative reaction are probably activated by irradiation. Analogous results were obtained with thallic carboxylates at −50°.[12]

The esr spectra obtained at room temperature were completely different and indicated the trapping of radicals of the type R″ĊHCOOH. These radicals were formed by hydrogen abstraction from the acids, probably by the radicals produced in the decarboxylation reaction.

II. Oxidation of Aliphatic Hydroxyl Compounds by Lead Tetraacetate.[11] This reaction gives a variety of products, formed *via* several postulated secondary radicals

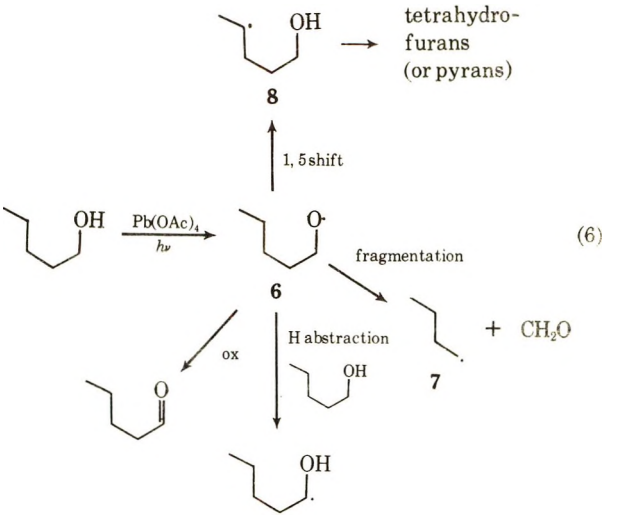

and the presence of more than one radical species is indicated by the overlapping spectra recorded from several alcohols. Some of the reactions are favored for certain alcohols. Thus, the oxidation of methanol at −70° in methylene chloride gave rise to methoxy radicals **6**, which were trapped by the nitroso scavenger. The nitroxide formed exhibited the large nitrogen splitting constant characteristic for alkoxy nitroxides (see Figure 1), *i.e.*, $(CH_3)_2(COCH_3)CN(O\cdot)OR$.

The oxidation of 2-phenyl-ethanol-1 gave rise to nitroxides with a secondary triplet (1:2:1), indicating the presence of the radical $C_6H_5\dot{C}H_2$ (**7**) from the fragmentation path $C_6H_5\text{–}CH_2\text{–}CH_2\text{–}O\cdot$.

At room temperature, aliphatic primary alcohols with a carbon chain of more than four atoms were found to give rise to secondary doublets, very probably as the result of the abstraction of a hydrogen atom from a methylene group *via* a 1,5-shift, **8**. This interpretation was supported by the result obtained with hexanol-1,1-d_2. The esr spectrum observed in this case also exhibited the doublet splitting found with a sample of nondeuterated hexanol, indicating that the hydrogen atoms on carbon atom 1 are not involved.

III. Radicals Generated by the Abstraction of a Hydrogen Atom with Photolytically Produced OH Radicals.[11,12] A number of different radical species can be generated by the abstraction of a hydrogen atom from substances such as aliphatic hydroxy and carbonyl compounds with photolytically produced OH radicals. The radicals derived from such substances could be trapped as nitroxides in many cases. In these experiments, the nitroxides were formed by irradiation with uv light of a solution containing the parent material, the nitroso scavenger, and H_2O_2. The esr spectra indicated that

(16) E. G. Janzen and B. J. Blackburn, *J. Amer. Chem. Soc.*, 90, 5909 (1968).
(17) E. G. Janzen and B. J. Blackburn, *ibid.*, 91, 4481 (1969).
(18) E. G. Janzen and J. L. Gerlock, *ibid.*, 91, 3109 (1969).
(19) E. G. Janzen and J. L. Gerlock, *Nature*, 222, 867 (1969).

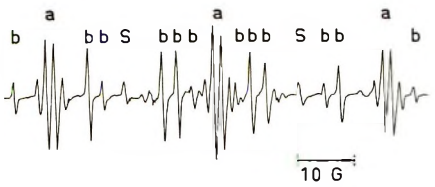

Figure 1. Esr spectrum of the nitroxide radicals formed by trapping of the radicals produced in the reaction between methanol and lead tetraacetate in methylene chloride at −70°. Scavenger, 2-methyl-2-nitrosobutanone-3; a, quartets (1:3:3:1) from trapped $CH_3O\cdot$ radicals derived from methanol, a_N = 29.4, a_H = 1.4 G; b, lines originating from trapped $CH_3\cdot$ radicals derived from lead tetraacetate, a_N = 15.5, a_H = 12.9 G; S, symmetrical nitroxide radicals derived from the scavenger.

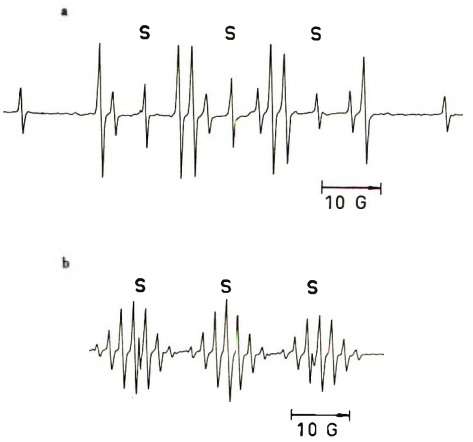

Figure 2. Esr spectrum of the nitroxide radicals formed by trapping of methyl radicals produced in the photochemical reaction between H_2O_2 and dimethyl sulfoxide at room temperature. Solvent, H_2O; scavenger, 2-methyl-2-nitrosobutanone-3; S, lines from the symmetrical nitroxide radicals derived from the scavenger; a, $CH_3\cdot$ radicals from $(CH_3)_2SO$; b, $CD_3\cdot$ radicals from $(CD_3)_2SO$, a_N = 15.9; a_H = 13.5; a_D = 2.1 G.

the trapped radicals generally had been produced by the abstraction of a hydrogen atom in the position α to the functional group. Thus, RĊHOH radicals were trapped from alcohols, RĊHCOOH radicals from carboxylic acids, and radicals of the type R'COĊHR'' from ketones.

The photolytically induced reaction between cyclic ketones, such as cyclohexanone and H_2O_2, gave rise to radicals formed by a ring-opening reaction. The mechanism was shown to involve an adduct between the ketone and H_2O_2.[12]

IV. Radicals Generated by the Action of Photosensitizers.[12] Benzophenone, excited to its triplet state, has been shown to abstract hydrogen atoms from a variety of alcohols, amines, phenols, sulfides, thiols, ethers, hydrocarbons, and amides, with the formation of radicals which were trapped by the nitroxide method.[20] The same technique was applied to a series of phenyl alkyl ketones with an increasing length of the alkyl chain.[12] The ketones reacted both as substrate and as sensitizers in these reactions. Methyl phenyl ketone and ethyl phenyl ketone gave rise to radicals formed by an intermolecular abstraction of hydrogen atoms from the alkyl chain, whereas the propyl and butyl derivatives gave rise to radicals *via* a six-membered transition state.

V. Radicals Formed by Photochemical Fission of Aryl Iodides[12] *and of Some Organometallic Compounds.*[11] The photochemical fission of a variety of aryl iodides was shown to produce aryl radicals in good yields at −60° which could be trapped as nitroxides.[12]

Irradiation of organometallic compounds by uv light produced radicals, the formation of which was demonstrated by the nitroxide method.[11] Alkyl radicals were easily trapped at room temperature from substances such as tetraethyllead. By carrying out the reaction at −70°, it was also possible to trap aryl radicals derived from parent substances such as tetraphenyllead.

VI. Radical Substitution.[12] Radical addition to the carbonyl group is a rarely encountered process, and in accordance with this no phenyl radicals could be trapped when benzophenone reacted with methyl radicals.

However, radical substitution was demonstrated in some other cases. Thus, *tert*-BuO· radicals formed by the spontaneous decomposition of *tert*-butyl peroxalate were found to attack tetraethyllead on the lead atom with the formation of the substituted compound *tert*-$BuOPbEt_3$. The leaving ethyl radicals were trapped and identified by the nitroxide method. Similar results were obtained in the reaction between *tert*-BuO· radicals and trialkylboranes.

VII. Radicals Formed in the Photochemical Reaction between Hydrogen Peroxide and Sulfoxides and Sulfones.[21]

Radicals of the general structure R· are formed from sulfoxides, R_2SO, by a cleavage of carbon–sulfur bonds in their photochemical reaction with hydrogen peroxide. These radicals were trapped by the nitroxide method. Methyl, ethyl, propyl, isopropyl, butyl, isobutyl, *sec*-butyl, pentyl, hexyl, and benzyl radicals were formed from the corresponding symmetrical sulfoxides and trapped by nitroso scavengers. Analogously, the unsymmetrical sulfoxides, R^1SOR^2, gave rise to two different radical species, $R^1\cdot$ and $R^2\cdot$, as seen from the superposition spectra obtained with methylethyl sulfoxide, methylpropyl sulfoxide, and methionine sulfoxide. No radicals could be detected in the reaction with diallyl sulfoxide, diphenyl sulfoxide, and bis(*p*-chlorophenyl) sulfoxide. Methylphenyl sulfoxide gave rise only to the trapping of methyl radicals. The spectra obtained from the nitroxides formed in reaction with DMSO and DMSO-d_6 are shown in Figures 2a and b.

The photochemical reaction between H_2O_2 and some sulfones was also studied by the nitroxide method. In general, the sulfones behaved very differently compared

(20) I. H. Leaver and G. C. Ramsay, *Tetrahedron*, **25**, 5669 (1969).
(21) C. Lagercrantz and S. Forshult, *Acta Chem. Scand.*, **23**, 811 (1969).

with the corresponding sulfoxides. No radicals could be trapped in the reaction with $(CH_3)_2SO_2$, $(C_2H_5)_2SO_2$, and $CH_3SO_2CH_2CH(NH_2)COOH$. $(n\text{-}C_3H_7)_2SO_2$ and $(n\text{-}C_4H_9)_2SO_2$ gave rise to a secondary doublet of about 2 G, further split into a narrow triplet, evidently caused by the trapping of radicals formed by abstraction of one of the hydrogen atoms from a methylene group.

In addition to the alkyl radicals, a further radical species was trapped in the reaction with the sulfoxides $(n\text{-}C_4H_9)_2SO$, $(n\text{-}C_5H_{11})_2SO$, and $(n\text{-}C_6H_{13})_2SO$. This radical species gave rise to a secondary doublet with a splitting constant almost identical with that obtained with the aliphatic sulfones. It is very probable that these species are derived from the corresponding sulfones, formed during the reaction by oxidation of the sulfoxides. With an increasing length of the alkyl chain of the sulfoxides, radicals might also be formed by abstraction of a hydrogen atom, in analogy with the radical formation observed in the case of the sulfones.

The abstraction of hydrogen atoms from the alkyl chain of sulfones and sulfoxides is obviously performed by photochemically generated OH radicals derived from H_2O_2. Norman, *et al.*,[22,23] have previously recorded methyl radicals in a flow system of DMSO, H_2O_2, and Ti^{3+} ions, after rapid mixing of the reagents. They suggested a mechanism involving an attack by OH radicals on the sulfur atom. In view of the results obtained here with a number of other sulfoxides this mechanism might be generalized

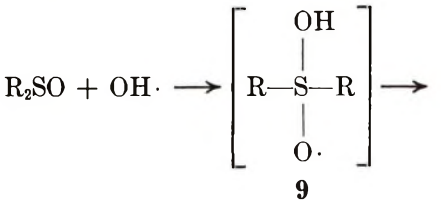

9

$$R\cdot + RSO_2H \quad (7)$$

This reaction is evidently not possible in the case of sulfones, where the sulfur atom is already bonded to four atoms, a situation which prevents the formation of the radical complex **9**, in agreement with the experimental results. However, it is clear from further studies of the mechanism that radical addition leading to the complex **9** is an oversimplification (see below).

Synthetic Application and Mechanistic Studies of the Radical Reactions of Sulfoxides.[24,25] The signal-to-noise ratio was very high for the spectra of the nitroxides obtained in the photochemical reactions between sulfoxides and hydrogen peroxide, indicating a high yield of alkyl radicals. The production of radicals was indeed high enough to warrant an investigation of possible synthetic applications. Torssell and coworkers found that various substrates in fact could be alkylated in reasonable yields under mild conditions. A brief résumé of their results seems to be justified because these syntheses were initiated by results obtained with the nitroxide method. The sulfoxides served both as solvent and reagent. Hydrogen peroxide was added to the mixtures, and the reaction was initiated either with uv light or in most cases by the addition of Fenton's reagent. A number of aromatic and heteroaromatic substances were alkylated. Reactive substances such as 1,3,5-trinitrobenzene or quinones, were readly alkylated at room temperature, but other substrates, *e.g.*, pyridine, thiophene, naphthalene, etc., needed a reaction temperature of 68–70° before reasonable yields of alkylated products were obtained. The free alkyl radicals were not considered to be the alkylating reagent. An adduct between the sulfoxide and hydrogen peroxide was postulated, which was subsequently fragmented into a hydroxyl radical and the radical complex **9** of eq 7. The radical complex was believed to be the actual alkylating reagent.

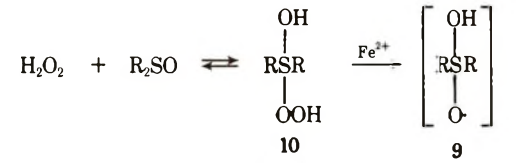

10 **9** (8)

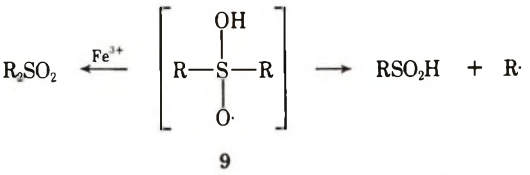

9 (9)

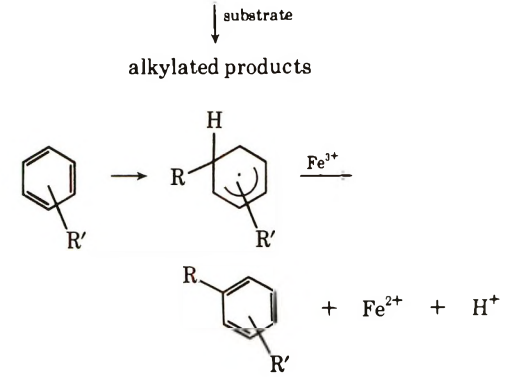

(10)

The formation of the radical complex **9** by fragmentation of the adduct **10** seems to be a more probable reaction path than its formation by a radical addition according to eq 7 on the following grounds. There was no sign of alkyl radicals and formation of sulfinic esters when the hydroxyl radicals were replaced by *tert*-butoxy radicals generated by several methods. Methylated products were formed, but it was proved by labeling (DMSO-d_6) and by the use of the nitroxide method that

(22) W. T. Dixon, R. O. C. Norman, and A. L. Buley, *J. Chem. Soc.*, 3625 (1964).

(23) R. O. C. Norman and B. C. Gilbert, *Advan. Phys. Org. Chem.*, **5**, 57 (1967).

(24) B.-M. Bertilsson, B. Gustafsson, I. Kühn, and K. Torssell, *Acta Chem. Scand.*, **24**, 3590 (1970).

(25 U. Rudqvist and K. Torssell, *ibid.*, in press.

the methyl radicals originated from *tert*-butoxy radicals *via*

$$\textit{tert}\text{-BuO}\cdot \longrightarrow (CH_3)_2CO + CH_3\cdot \qquad (11)$$

It was also shown by mass spectrometry that no methyl scrambling had occurred in solvents composed of a mixture of DMSO and DMSO-d_6 (1:1); *i.e.*, reaction 12 does not seem to occur.

$$CH_3\cdot + (CD_3)_2SO \not\longrightarrow$$

$$CH_3SO(CD_3)_2\cdot \longrightarrow CH_3S(=O)CD_3 + CD_3\cdot \qquad (12)$$

Thus, mechanistic studies of the radical reactions of sulfoxides have raised some doubt about the possibility of addition of hydroxyl radicals to sulfoxides. However, one radical species has been found which seems to add to sulfoxides, namely nitrogen dioxide.[26] Nitroxide radicals were formed after bubbling NO_2 through DMSO and irradiating the reaction mixture with uv light. By the use of deuterium substitution, the spectrum obtained in this reaction was analyzed and found to involve the following coupling constants: a_N = 12.2, a_H = 11.0 (quartet), a_H = 0.94 G (quartet). These findings implied that a nitroxide radical **14** was formed, which contains two nonequivalent methyl groups. The following reaction path was suggested.

$$NO_2\cdot + (CH_3)_2SO \longrightarrow (CH_3)_2S(O\cdot)NO_2 \longrightarrow$$

11

$$CH_3\cdot + CH_3S(=O)NO_2 \qquad (13)$$

12

$$CH_3S(=O)NO_2 \longrightarrow CH_3S(=O)NO \qquad (14)$$

12 **13**

$$CH_3S(=O)NO + CH_3\cdot \longrightarrow CH_3S(=O)(NO)CH_3 \qquad (15)$$

13 **14**

Thus, the intermediate radical **11** is analogous to the radical complex of eq 7 and 8, *i.e.*, **9**.

A direct intramolecular rearrangement of **11** into the observed radical **14** in the absence of free methyl radicals was very probably ruled out as the spectrum of radicals prepared from a mixture of DMSO and DMSO-d_6 (1:1) exhibited a number of new lines, in addition to the superposition of the spectra obtained with DMSO and DMSO-d_6. These extra lines were considered to originate from radical species with the structures $CD_3SO_2N(O\cdot)CH_3$ and $CH_3SO_2N(O\cdot)CD_3$, the formation of which indicates a scrambling of methyl groups consistent with the suggested reaction path.

VIII. Reactions of N-Bromosuccinimide and Other N-Halogen Imides.[27] It is generally accepted that bromination by *N*-bromosuccinimide (NBS) proceeds *via* free radicals, which are induced in a homolytic cleavage through the action of light or radical intiators.[28-30]

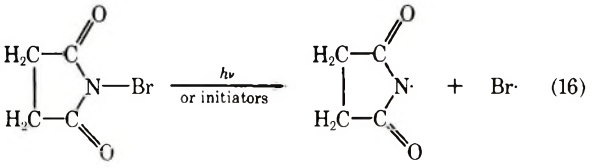

(16)

15

The propagation is thought to involve the abstraction of a hydrogen atom from the substrate HR, by either the succinimidyl radical **15** or Br·, to form the radical R·.

The following results were obtained when the trapping technique was applied to some reactions of NBS, *N*-chlorosuccinimide, *N*-bromotetramethylsuccinimide, and *N*-bromophthalimide.

i. Radicals Derived from the Imides. Irradiation with uv light of a solution of NBS or NClS and the nitroso scavenger (*tert*-nitrosobutane) in CCl_4, $CHCl_3$, or CH_2Cl_2 produced nitroxide radicals which exhibited a 3 × 3 line spectrum. Evidently, this spectrum is caused by the coupling of the unpaired electron with two nonequivalent ^{14}N nuclei (a_{N1} = 16.4, a_{N2} = 1.81 G) and is consistent with the trapping of the succinimidyl radical **15**, produced as in eq 16, with the formation of the nitroxide radical

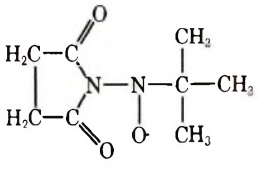

16

Spectra with almost identical splitting constants were obtained with *N*-bromotetramethylsuccinimide and

(26) C. Lagercrantz, *Acta Chem. Scand.*, 23, 3259 (1969).

(27) C. Lagercrantz and S. Forshult, *ibid.*, 23, 708 (1969).

(28) C. Walling, "Free Radicals in Solution," Wiley, New York, N. Y., 1957.

(29) L. Horner and E. H. Winkelmann in "Newer Methods of Preparative Organic Chemistry," Vol. III, W. Foerst, Ed., Academic Press, New York, N. Y., 1964.

(30) W. A. Pryor, "Free Radicals," McGraw-Hill, New York, N. Y., 1966.

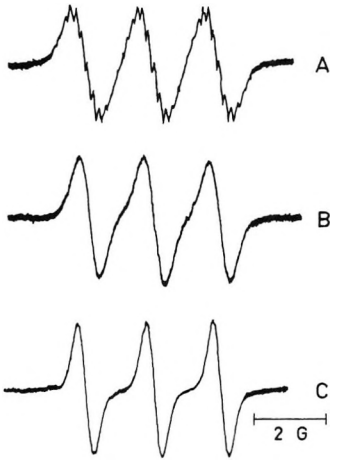

Figure 3. The center group of the three main components of the esr spectrum of the nitroxide radicals formed by trapping: A, succinimidyl radicals; B, tetramethylsuccinimidyl radicals; C, phthalimidyl radicals.

N-bromophthalimide by the trapping of tetramethylsuccinimidyl and phthalimidyl radicals, respectively.

Each of the nine lines in the spectrum obtained from the trapping of succinimidyl radicals was further incompletely split into a number of narrow lines, of which at least eight are seen (Figure 3). No such tertiary splittings could be resolved in the nitroxide spectra obtained after the trapping of tetramethylsuccinimidyl and phthalimidyl radicals, even after a very thorough degassing of the reaction mixtures. At first, these findings seemed to indicate that the narrow splittings originated from the four hydrogen atoms of the succinimidyl part of the nitroxides. However, preliminary extended Hückel calculations on the spin densities in radical **16** indicate that the actual splittings originate from the hydrogen atoms of the tertiary butyl group, and not from the hydrogen atoms of the succinimidyl group.[31] Further experiments, including deuterium substitution, are necessary before a final decision on the origin of the tertiary splittings may be made and an explanation given for the absence of such splittings in the nitroxide spectra obtained on trapping tetramethylsuccinimidyl and phthalimidyl radicals.

ii. Radicals Produced in the Reaction between N-Halogenimides and Olefinic Substances. By the use of the nitroxide method, radicals were trapped which had been formed in the reaction between the *N*-halogenimides and a variety of olefinic substances, such as 2-propen-1-ol, 2-buten-1-ol, 2-propenenitrile, 6-methyl-5-hepten-2-one, 3-methyl-2-cyclopenten-2-ol-1-one, cyclopentene, cyclohexene, and *d*-limonene. With an excess of the olefinic compounds, the nitroxide radicals formed in the presence of these substances were found to dominate over the species **16** derived from the trappings of the succinimidyl radicals.

The secondary splittings of these nitroxides were in many cases very complicated and exhibited a large number of narrow lines. Evidently, the trapped radicals were derived from the olefinic substances, but it was not possible to establish their structure, and it could not be decided whether the species had been formed by the abstraction of a hydrogen atom or by the addition of a halogen atom.

In view of the possible selective survival of certain nitroxides species, and the different ability of the *C*-nitroso scavengers to trap different species of short-lived radicals, it should be emphasized that the nitroxides actually observed do not necessarily represent the intermediate radicals of the main path of the reaction between *N*-halogenimides and the olefinic substances concerned.

It must also be emphasized that even if the nitroxide method has demonstrated the presence of a variety of free radicals in the reactions of *N*-bromosuccinimide, these observations did not help to identify the hydrogen abstracting species invoved. Perkins, *et al.*,[32] arrived at similar concusions from a study in which succinimidyl radicals were trapped, both by the use of nitroso compounds and by a nitrone scavenger.

IX. Phosphorus-Centered Radical Species.[33] Intermediate free radicals with the radical center located on a phosphorus atom are considered to be formed in many reactions of organophosphorus compounds, for example in the addition of primary and secondary phosphines to olefins.[34,35] The radical species considered to be present in the latter reactions, *i.e.*, phosphinyl radicals, $R^1R^2\dot{P}$, have not been demonstrated so far by the technique of esr spectroscopy. On the other hand, the esr spectra of phosphoranyl radicals such as $R^1R^2R^3\dot{P}OR$ and $R^1R^2\dot{P}(OR)_2$, formed by the addition of *tert*-butoxy radicals to phosphines, have been recorded at about $-80°$.[36,37]

Some phosphorus-centered radicals have been trapped by the nitroxide method. Figure 4 shows the esr spectrum of the nitroxides formed in a water solution of sodium phosphite, Na_2HPO_3, containing the scavenger *tert*-nitrosobutane. The spectrum consisted of six lines of equal intensity and appeared immediately after the sample had been irradiated with uv light for a few seconds. The yield of the radicals was increased when a few drops of H_2O_2 was added to the reaction mixture prior to the irradiation.

The spectrum is consistent with the interaction with

(31) S. Wold, personal communication.

(32) G. R. Chalfont, M. J. Perkins, and A. Horsfield, *J. Chem. Soc. B*, 395, 401 (1970).

(33) H. Karlsson and C. Lagercrantz, *Acta Chem. Scand.*, 24, 3411 (1970).

(34) C. Walling and M. S. Pearson, *Topics Phosphorus Chem.*, 3, 1 (1966).

(35) R. F. Hudson, "Structure and Mechanism in Organo-Phosphorus Chemistry," Academic Press, New York, N. Y., 1965.

(36) J. K. Kochi and P. J. Krusic, *J. Amer. Chem. Soc.*, 91, 3844 (1969).

(37) P. J. Krusic, personal communication.

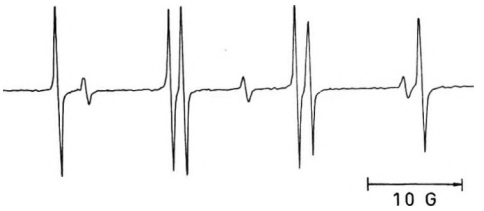

Figure 4. Esr spectrum of the nitroxide radical $O_3PN(O\cdot)C(CH_3)_3^{2-}$ formed by trapping the radical ion, $\cdot PO_3^{2-}$, produced by uv irradiation of a water solution of Na_2HPO_3 at room temperature. Scavenger, *tert*-nitrosobutane; a_N = 13.4, a_P = 12.0 G.

one ^{14}N and one ^{31}P nucleus, and the production of a nitroxide by the trapping of the radical ion, $\cdot PO_3^{2-}$, formed by the abstraction of the hydrogen atom bonded to the phosphorus atom of the parent ion, HPO_3^{2-}. In the presence of hydrogen peroxide, the abstraction of the hydrogen atom seems to be brought about by photochemically generated OH radicals, but in the absence of H_2O_2 it is not clear whether the abstraction is caused by a photochemical scission of the H–P bond, or by NO· or *tert*-butyl radicals derived from the scavenger.

Similar six-line spectra, but with somewhat different hyperfine splittings, were obtained with a number of phosphorus compounds, such as sodium hypophosphite and dialkyl phosphites, by the abstraction of a hydrogen atom bonded to the phosphorus atom. The radicals trapped from phenylphosphine gave rise to a 12-line spectrum with all lines of equal intensity, indicating the trapping of $C_6H_5\dot{P}H$ radicals after the abstraction of one of the two hydrogen atoms bonded to the phosphorus atom of the parent compound.

A six-line spectrum was obtained with tetramethylbisphosphine disulfide, $(CH_3)_2P(S)P(S)(CH_3)_2$, after uv irradiation of the reaction mixture. Evidently, the phosphorus-centered radical species trapped in this case was formed by a homolytic cleavage of the P–P bond.

Free untrapped phosphorus-centered radicals exhibit ^{31}P splittings of about 600 G.[36-38] These large splittings are caused by a 3s state contribution to the hybridized orbital containing the unpaired electron. The ^{31}P splittings of the nitroxides of this series are much smaller and were found to be between 6.5 and 13.2 G. It is evident that the large reduction of the ^{31}P splittings obtained on trapping phosphorus-centered radicals as nitroxides involves a drastic change of the interaction of the unpaired electron with the phosphorus nucleus. However, it is not known at present whether this change involves a very low spin density on the phosphorus atom in the nitroxides or depends on a hybridization with a reduced contribution from the 3s state after the trappings of the radicals as nitroxides.

X. Radicals Formed by γ Irradiation of Solid State Samples.[39,40] Numerous studies have been carried out using esr spectroscopy on the free radicals produced by high-energy irradiation of organic and inorganic substances in the solid state. It is well known that these radicals disappear on dissolution of the irradiated sample, in a series of more or less complicated reactions.

A number of such radical species has been trapped as nitroxides on dissolution of the irradiated samples.[39] The substances were irradiated at room temperature in the polycrystalline state by γ rays from a ^{60}Co source and were given about 5 Mrads each. The samples were then dissolved in an aqueous solution of the nitroso scavenger, and the esr spectra were recorded at room temperature.

In this way, γ-induced radicals were trapped from sodium acetate, glycine, DL-α-alanine, β-alanine, dipotassium malonate, succinic acid, and L-glutaminic acid hydrochloride. No radicals were obtained with nonirradiated samples. Thus, the spectra obtained with glycine and DL-α-alanine indicated that $\cdot CH_2COO(H)$ radicals had been trapped in the case of glycine, and $CH_3\dot{C}HCOO(H)$ radicals from DL-α-alanine.

Nitroxide radicals were formed on dissolution of γ-irradiated solid state samples of sodium phosphite, Na_2HPO_3, in a water solution containing *tert*-nitrosobutane.[40] A six-line spectrum was observed, which was identical with that obtained by uv irradiation *in situ* of a water solution of Na_2HPO_3 and the scavenger, indicating the trapping of the radical ion $\cdot PO_3^{2-}$. This radical has previously been investigated in the solid state by Horsfield, *et al.*[38] The radical was formed in γ-irradiated single crystals of $Na_2HPO_3\cdot 5H_2O$ after ejection of the hydrogen atom bonded to the phosphorus atom.

The results indicate that the radicals trapped on dissolution have a structure very similar to that of the corresponding species present in the γ-irradiated solid samples. We therefore conclude that apart from a possible difference in added protons, the trapped radicals are the primary species of the solid samples. Obviously, the reaction leading to nitroxide radicals, eq 3, competes effectively with other reactions in which the radicals take part and then disappear on dissolution of the crystalline matrix.

Conclusions

The nitroxide method has been shown to be of great value for the detection and identification of intermediate radicals present in a large number of reactions. Many of the radicals studied by the nitroxide method have been observed in the free untrapped state by the use of flow methods or by radical generation and detection at low temperature. However, aside from their detection in solid state samples, some radical species have so far been exclusively detected by the use of the

(38) A. Horsfield, J. R. Morton, and D. H. Whiffen, *Mol. Phys.*, **4**, 475 (1961).

(39) C. Lagercrantz and S. Forshult, *Nature*, **218**, 1247 (1968).

(40) G. Adevik and C. Lagercrantz, *Acta Chem. Scand.*, **24**, 2253 (1970).

nitroxide method, for example, the radicals derived from *N*-bromosuccinimide and the phosphinyl radicals.

Acknowledgment. This work was supported by grants from Wilhelm och Martina Lundgrens Vetenskapsfond and The Swedish Natural Science Research Council.

Discussion

R. W. FESSENDEN. With regard to radical trapping in radiolytic experiments, I would like to point out that we have been using an extension of this technique in *in situ* radiolysis of aqueous solutions. P. Neta and D. Behar have used the compounds $^{-}O_2CCH{=}CHCO_2^{-}$ and $CH_2{=}NO_2^{-}$ to trap various radiolytically produced radicals which are not otherwise observable. The resulting radicals, though not stable for long periods, are considerably longer lived than those which react by diffusion-controlled reaction. As examples, I mention the results of the reaction of CN and N_3 (as obtained from CN^{-} and N_3^{-} and OH) with $CH_2{=}NO_2^{-}$. In the case of CN, two substituted nitromethane anion radicals are formed, one of which shows an extra nitrogen splitting and with N_3 a radical is formed which shows a splitting by all three nitrogens from the N_3 group.

Electron Spin Resonance Studies of Adsorbed Alkene Molecules on Synthetic Zeolites: Cation Radicals of Tetramethylethylene and Cyclopentene[1]

by P. L. Corio

Department of Chemistry, University of Kentucky, Lexington, Kentucky 40506

and S. Shih*

Mobil Research and Development Corporation, Princeton, New Jersey 08540 *(Received December 29, 1970)*

Publication costs assisted by the Mobil Research and Development Corporation

Electron spin resonance spectra have been measured for the radical species derived from tetramethylethylene and cyclopentene. The experiments were performed by the adsorption of olefin molecules on the zeolite (synthetic mordenite), and spectra were obtained in the temperature range 77 to 300°K. Tetramethylethylene showed a well-resolved 13-line spectrum with 17.5-G splitting, which was attributed to the cation radical of tetramethylethylene. The esr spectrum of cyclopentene consisted of a quintet of 37.0-G splitting and a triplet of 14.5-G splitting and can be reasonably assigned to the cyclopentene cation radical. The observed line shape of cyclopentene cation radicals indicates that the species is rotating rapidly about its fivefold axis on the zeolite surface with an activation energy $E_a = 1.4 \pm 0.2$ kcal/mol.

Introduction

The nature of the reactive intermediates on activated zeolites has been studied by electron spin resonance (esr) techniques for some years.[2-4] Turkevich, *et al.*,[2a] demonstrated the formation of the cation radical of triphenylamine on the surface of synthetic Y-type zeolites due to direct interaction with the solid. Rooney and Pink[2b] observed the esr spectra of anthracene and perylene cations on silica–alumina; however, they failed to observe spectra for cation radicals of benzene of methyl-substituted benzenes. Hirschler, *et al.*,[3] were the first to report that benzene, methyl-substituted benzenes, and alkene molecules adsorbed on rare earth and calcium exchanged Y zeolites, and cerium-exchanged X zeolites showed esr signals. Due to poor resolutions and large line widths, some of their observations could be interpreted due to isomerization and other reaction mechanisms of the adsorbed species.

Recently, we have obtained esr spectra for cation radicals of benzene and its methyl-substituted derivatives.[4] Theories have been developed for the proton hyperfine anisotropic splittings of π-electron radicals;[5] these quantities are important for the interpretation of

(1) Presented at the Second Symposium on Electron Spin Resonance Spectroscopy, University of Georgia, Athens, Ga., Dec 7 and 8, 1970.

(2) (a) D. N. Stamires and J. Turkevich, *J. Amer. Chem. Soc.*, **86**, 749 (1964); (b) J. J. Rooney and R. J. Pink, *Trans. Faraday Soc.*, **58**, 1632 (1963).

(3) A. E. Hirschler, W. C. Neikam, D. S. Barmby, and R. L. James, *J. Catal.*, **4**, 628 (1965).

(4) P. C. Corio and S. Shih, *ibid.*, **18**, 126 (1970).

(5) (a) H. M. McConnell and J. Strathdee, *Mol. Phys.*, **2**, 129 (1958); (b) W. Derbyshire, *ibid.*, **5**, 225 (1962).

esr spectra of radical species adsorbed on amorphous solid.[6] In this paper, we apply these theories and report the first evidence for the existence of alkene cation radicals on the zeolitic surface of hydrogen mordenite.

It is generally accepted that the porous nature of solid zeolites plays a significant role in the separation of different kinds of molecules, which suggests that once the molecules or reactive intermediates diffuse into the zeolite crystals they will encounter considerable restriction to their translational motion. The high electrostatic field on the surface of catalytic materials[7] raises the question of whether the internal rotation of the molecules may be hindered, or whether a preferred direction of rotation may exist for the adsorbed species. These questions could be answered by temperature dependence studies of the radical species. To examine these effects, an alkene with four methyl groups and a cycloalkene with two α protons were studied.

Experimental Section

The synthetic zeolite, H-Zeolon, obtained from the Norton Co., was used in this study. The crystal structure consists of a three-dimensional network of AlO_4 and SiO_4 tetrahedra. The zeolite contains straight elliptical channels with major and minor axes of 7.0 and 5.8 Å. These main channels are connected by smaller side channels with a diameter of 3.9 Å.

The olefinic compounds were obtained from Matheson Coleman and Bell and were used without further purification. The preparation of the esr sample has been given in a previous paper.[4]

Esr spectra were obtained with a Varian 4502 X-band spectrometer with 100-kHz field modulation; g values and hyperfine splittings were measured relative to Fremy's salt. Low-temperature measurements were achieved with commercial temperature accessories.

Results and Discussion

The esr spectrum of tetramethylethylene adsorbed on H-Zeolon at room temperature is shown in Figure 1. It consists of a simple set of 13 equally spaced lines, derived from the interaction of the unpaired electron with 12 equivalent protons. Investigation of the temperature dependence reveals little change in the general features of the spectrum over the range 77–300°K. This observation indicates the existence of four methyl groups in the radical species and a very small internal rotation barrier for them. Thus, a model involving classical random rotation is applicable to this radical species.[8] Since this zeolite can oxidize the durene molecule to its cation radical under the same experimental conditions, the observed species was attributed to the cation radical of tetramethylethylene. The effects of anisotropic hyperfine interactions of β protons are mostly averaged out by the internal rotation of the methyl groups. The intensity ratios are not expected to be a binomial distribution because of the line width effects and frequency shifts.[9]

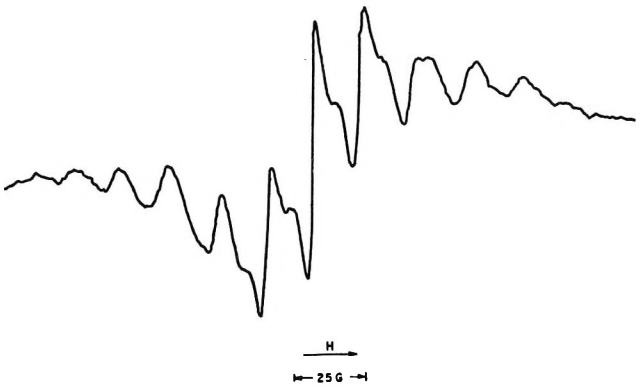

Figure 1. Esr spectrum of tetramethylethylene cation radical generated on molecular sieve at 25°.

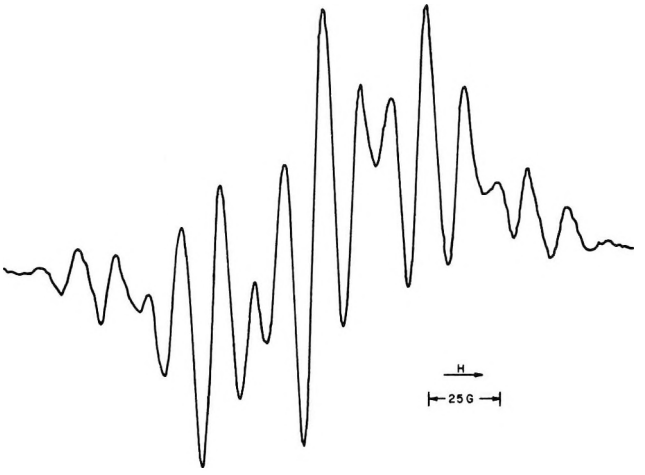

Figure 2. Esr spectrum of cyclopentene cation radical generated on molecular sieve at −125°.

The esr spectrum of cyclopentene adsorbed on amorphous H-Zeolon at −125° is shown in Figure 2. It can be accounted for by one set of four equivalent protons and another set of two equivalent protons. The apparent simplicity of the spectrum may suggest the complete random tumbling of the radical species on the zeolite. We feel such interpretation would probably be incorrect for the following reasons. (a) The existence of large electrostatic fields at the surface of catalytic materials such as silica gels and aluminosilicates was shown in recent years.[10] (b) Similar spectra but with larger line width have been observed at −180°,

(6) (a) R. Lefebvre, *J. Chem. Phys.*, **33**, 1826 (1960); (b) H. Sternlicht, *ibid.*, **33**, 1128 (1960); (c) R. Lefebvre and J. Maruani, *ibid.*, **42**, 1480 (1965).

(7) (a) J. A. Rabo, C. L. Angell, P. H. Kasai, and V. Schomaker, *Discuss. Faraday Soc.*, **41**, 328 (1966); (b) E. Dempsey, Conference on Molecular Sieves, London, 1968, p 293.

(8) J. H. Freed and G. K. Fraenkel, *J. Chem. Phys.*, **41**, 3623 (1964).

(9) (a) G. K. Fraenkel, *J. Phys. Chem.*, **71**, 139 (1967); (b) D. Kivelson, *J. Chem. Phys.*, **33**, 1094 (1960).

(10) (a) C. L. Gardner, E. J. Casey, and C. W. M. Grant, *J. Phys. Chem.*, **74**, 3273 (1970); (b) P. Monod, J. A. Cowen, and W. N. Hardy, *J. Phys. Chem. Solids*, **27**, 727 (1968).

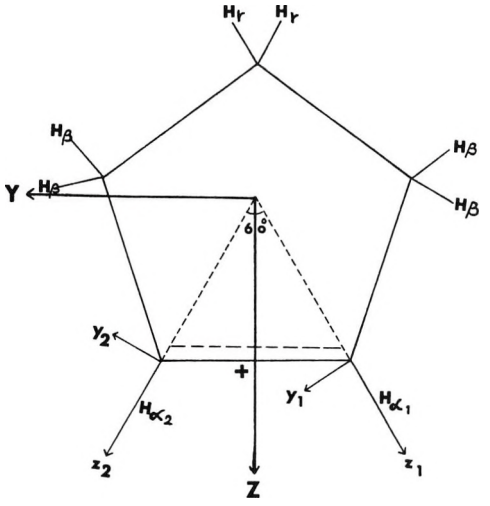

Figure 3. Principal inertia axes of cyclopentene cation radical (Y, Z), and the principal axes of hyperfine tensor for two α protons (y_1, z_1).

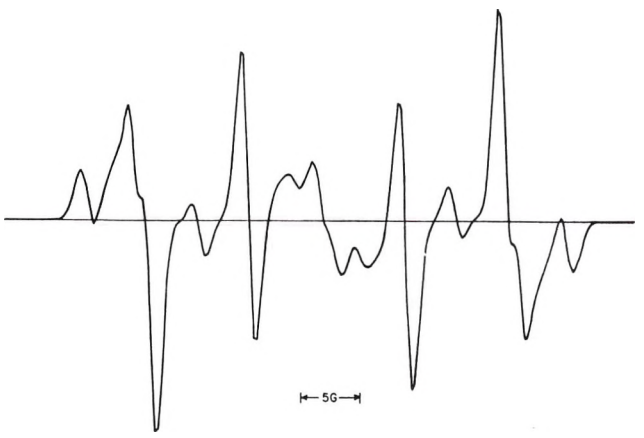

Figure 4. Calculated esr first-derivative spectrum at X band for two vicinal α protons adsorbed rigidly on zeolite solid, Gaussian line width 0.5 G.

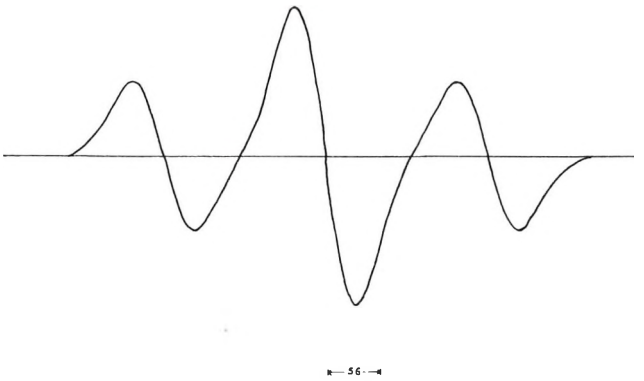

Figure 5. Calculated esr first-derivative spectrum at X band for two vicinal α protons rotating on catalytic zeolite surface, Gaussian line width 1.0 G.

which is far below the freezing point of cyclopentene ($-135°$); thus, random motions of cyclopentene molecule seem unlikely.[11] (c) The analysis, based on the theory of α-proton hyperfine anisotropy, which follows, shows the observed spectra can only be explained in terms of rotation about the fivefold axis of the radical species.

Neglecting four β protons in the cyclopentene cation radical and assuming two α protons with 60° separation as shown in Figure 3,[12] the theory of McConnell and Strathdee is used to calculate the principal values of the hyperfine tensor for the α proton. We obtain the values $|Axx| = 14.5$ G, $|Ayy| = 21.7$ G, $|Azz| = 7.2$ G where the x axis is parallel to the π-bonding orbital, the y axis is in the molecular plane, and the z axis is along the C–H bond (Figure 3). The effect of g anisotropy was neglected because of its deviations from the free-electron value of less than 0.3% in our system.

In our study of the line shape due to two α protons, we have used a computer program[6c] and have taken the proton Zeeman term ($g_\Theta\beta_\Theta H \cdot I_\Theta$) and all other transitions into account, the computer simulated spectrum for a radical species with two vicinal α protons adsorbed rigidly on amorphous solid at X-band is shown in Figure 4. It is very different from the observed spectra; thus, most of the radical species must reorientate very rapidly on the zeolite surface. Rotations about two principal axes of inertia in the molecular plane (y and z axes) were studied; one simulated spectrum gives an inner splitting of 12.7 G and an outer hump with 18.7 G, while the other one shows similar line shape with 10.9 and 16.6 G. Both simulated spectra do not agree with the observed hyperfine splittings and line shape. Only the model involving rotation about the axis perpendicular to the five-member ring gives a spectrum which is similar to the observed ones, at low temperature range (-196 to $-50°$). Such motions will not only cancel out dipolar contributions of the two vicinal α protons of the radical species, but also give the right intensity ratios (Figure 5).

The activation energy for this rotational motion on zeolite surface of hydrogen mordenite can be approximately estimated from the equation[13]

$$t_c = t_0 e^{E_a/kT}$$

where t_c is the rotational correlation time of cyclopentene cation radicals. A value of $E_a = 1.40 \pm 0.2$ kcal/mol was obtained from the temperature dependence measurements of line shape. The order of magnitude supports the idea that the adsorbed radical species is almost freely rotating on this particular zeolite surface. Also, it should be indicated at this point that the esr spectra changed at higher temperature and

(11) I. J. Lawrenson and F. A. Rushworth, *Proc. Phys. Soc. (London)*, **72**, 791 (1958).

(12) J. Laane and R. C. Lord, *J. Chem. Phys.*, **47**, 4941 (1967); G. W. Rathjens, Jr., *ibid.*, **36**, 2401 (1962); M. I. Davis and T. W. Muecke, *J. Phys. Chem.*, **74**, 1104 (1970).

(13) (a) A. Abragam, "The Principle of Nuclear Magnetism," Oxford, 1961, p 455; (b) H. C. Torrey, *Phys. Rev.*, **96**, 690 (1954).

revealed the presence of neutral allylic radicals (C_5H_7). A detailed analysis will be reported elsewhere.

Experimental results on these two cation radicals are listed in Table I. Taking the steric requirement of the five-member ring[12] and the MO Hückel theory into consideration, the unpaired electron in both species is in the bonding π orbital between two olefinic carbon atoms. Thus, the formal π spin (ρ_C) and charge densities at each of these carbon atoms would be 0.5. The observed a_α^H (14.5 G) in the cyclopentene cation radical is very close to the calculated value based on McConnell's relationship $\alpha^H = Q_{CH}\rho_C$ using the value 29.9 G for Q_{CH} obtained for the cyclopentadienyl radical.[14] This suggests that the charge effect on the proton hyperfine splittings[15] may not be important in this case. However, the observed a_β^H (17.5 G) for the noncyclic cation radical is much smaller than the predicted value (22 G) based on the $Q_{CH_3}^H$ for the planar durene cation ($Q_{CH_3}^H = 44$ G); presumably, other conformation effects such as internal rotation about the central C–C bond and the nonplanarity of the open-chain alkene cation radicals are responsible for the difference.[16]

Acknowledgment. The skillful technical assistance of Mr. O. M. Epifanio and the use of a computer program from Dr. J. Maruani are deeply appreciated. Helpful comments from Dr. E. Demspey and Dr. D. H. Olson are also acknowledged.

Table I: Observed Proton Hyperfine Splittings of Two Alkene Cation Radicals

Alkene	a_α^H, G[a]	a_β^H, G[a]	g value	Temp, °C
Tetramethylethylene	...	17.5	2.0028 ± 0.0003	25
Cyclopentene	14.5	37.0	2.0029 ± 0.0003	−125

[a] Estimated error is 0.4 G.

Discussion

T. Pietrzak (University of Alabama). What are the cations which balance the charge on the alumina tetrahedra in the zeolite structure? Is the major percentage NH_4^+ ions in this particular mordenite?

S. Shih. The ammonium ions balance the charge on the alumina tetrahedra in the synthetic mordenite.

(14) (a) V. Roggen and W. Gordy, *Phys. Rev.*, **105**, 50 (1957); (b) S. I. Ohnishi and I. Nitta, *J. Chem. Phys.*, **39**, 2848 (1963).

(15) J. A. Bolton, *ibid.*, **43**, 309 (1965).

(16) A. J. Merer and R. S. Mulliken, *Chem. Rev.*, **69**, 639 (1969).

An Electron Spin Resonance Study of the IO_2F^- Radical in γ-Irradiated Single Crystals of Potassium Oxyfluoroiodate[1]

by S. Subramanian and Max T. Rogers*

Department of Chemistry, Michigan State University, East Lansing, Michigan 48823 *(Received December 29, 1970)*

Publication costs borne completely by The Journal of Physical Chemistry

Single crystals of KIO_2F_2 γ-irradiated at room temperature, or irradiated at 77°K and allowed to warm above 140°K, give esr spectra characteristic of the 27-electron radical anion IO_2F^-. The g, $A(^{19}F)$, and $A(^{127}I)$ tensors have been evaluated, and the ^{127}I quadrupole interaction parameters Q' and Q'' have been estimated, from the spectra. The unpaired electron is predominantly delocalized over the iodine and oxygen atoms and interacts only weakly with the fluorine atom. The possible structure of the radical ion is discussed.

Introduction

Esr studies of paramagnetic oxy ions of nonmetals, usually produced by γ irradiation of salts of the appropriate diamagnetic ion, have been studied extensively.[2-17] Information concerning their electronic structures and geometry has been largely deduced from the g values and the hyperfine splittings by nuclei of the central atoms,[18,19] since ligand splittings can only be seen by enrichment with ^{17}O and this has only rarely been done.[20] Study of the isoelectronic fluoroxy ions has the advantage that ligand hyperfine splittings may be observed, as in the tetrahedral series[21] PO_4^{2-}, PO_3F^-, and PO_2F_2, each with 31 valence electrons. Also, substitution of oxygen by fluorine may lead to stable species in which the central atom apparently uses more than four orbitals; thus, the esr spectra of the 33-valence electron radical PF_4 indicate that d orbitals are used in bonding and that the structure is approximately trigonal pyramidal.[18,22]

In the present article we report the discovery of the radical anion IO_2F^- in γ-irradiated single crystals of KIO_2F_2. This ion is of unusual interest because it is one of the first paramagnetic oxy ions of iodine which has been observed and one of the first tetratomic radicals reported with more than 26 valence electrons. Although reports of esr investigations of several oxy ions of chlorine[3,4] and bromine[23] have appeared, few iodine-containing oxy ions appear to have been studied. The only well-established species showing iodine hyperfine interaction are the V_k centers[24,25] I_2^- and IF^-. The maximum number of valence electrons which can be accommodated in species of the type $XO_yF_{3-y}^{n-}$ and $XO_yF_{4-y}^{n-}$ without the use of d orbitals is 26 and 32, respectively. Species with less than these numbers would be expected to have approximately tetrahedral arrangements as observed for ClO_3 (25 electrons),[26] PO_3F^- (31 electrons),[21] and IO_4^- (32 electrons).[27] However, species where these numbers are exceeded have different structures such as ClF_3 (28 electrons) with a distorted T shape[28,29] and $IO_2F_2^-$ (34 electrons) with a distorted trigonal pyramidal arrangement,[30]

(1) This work was supported through a contract with the Atomic Energy Commission and this is AEC Document No. COO-1385-34.

(2) T. Cole, *J. Chem. Phys.*, **35**, 1169 (1961); *Proc. Nat. Acad. Sci. U. S.*, **46**, 506 (1960).

(3) P. R. Edwards, R. S. Eachus, S. Subramanian, and M. C. R. Symons, *J. Chem. Soc. A*, 1705 (1968); R. S. Eachus and M. C. R. Symons, *ibid.*, 2438 (1968).

(4) J. R. Byberg and S. J. K. Jensen, *J. Chem. Phys.*, **52**, 5902 (1970), and earlier papers of the series; J. R. Morton, *ibid.*, **45**, 1800 (1966).

(5) C. K. Jen, S. N. Foner, E. L. Cochran, and V. A. Bowers, *Phys. Rev.*, **112**, 1169 (1958).

(6) H. Zeldes and R. Livingston, *J. Chem. Phys.*, **35**, 563 (1961).

(7) J. R. Morton, *Mol. Phys.*, **5**, 217 (1962).

(8) R. A. Serway and S. A. Marshall, *J. Chem. Phys.*, **45**, 4098 (1966).

(9) E. Hughes and W. G. Moulton, *ibid.*, **39**, 1359 (1963).

(10) P. R. Edwards, S. Subramanian, and M. C. R. Symons, *Chem. Commun.*, 799 (1968).

(11) S. Subramanian, M. C. R. Symons, and H. W. Wardale, *J. Chem. Soc. A*, 1239 (1970).

(12) F. Jeffers, P. F. Wigen, and T. A. Cowen, *Bull. Amer. Phys. Soc.*, **8**, 343 (1963).

(13) M. Hampton, F. G. Herring, W. C. Lin, and C. A. McDowell, *Mol. Phys.*, **10**, 565 (1966).

(14) R. J. Cook, J. R. Rowlands, and D. H. Whiffen, *ibid.*, **8**, 195 (1964).

(15) M. C. R. Symons in "Radiation Chemistry," Vol. 2, American Chemical Society, Washington, D. C., 1968.

(16) A. Horsfield, J. R. Morton, and D. H. Whiffen, *Mol. Phys.*, **4**, 475 (1961).

(17) W. C. Lin and C. A. McDowell, *ibid.*, **7**, 223 (1964).

(18) P. W. Atkins and M. C. R. Symons, "The Structure of Inorganic Radicals," Elsevier, Amsterdam, 1967.

(19) C. A. Coulson, "Volume Commemoratif Victor Henri. Contributions à l'Etude de la Structure Moleculaire," Desoer, Liége, 1948, p 15.

(20) S. Schlick, B. L. Silver, and Z. Luz, *J. Chem. Phys.*, **49**, 4263 (1968).

(21) A. Begum, S. Subramanian, and M. C. R. Symons, *J. Chem. Soc. A*, 1323 (1970).

(22) J. R. Morton, *Can. J. Phys.*, **41**, 706 (1963); R. W. Fessenden and R. H. Schuler, *J. Chem. Phys.*, **45**, 1845 (1966); P. W. Atkins and M. C. R. Symons, *J. Chem. Soc.*, 4363 (1964); W. Nelson, G. Jackel, and W. Gordy, *J. Chem. Phys.*, **52**, 4572 (1970).

unshared pairs on the central atom being sterically active in each case. The radical IO_2F^- might therefore be expected to have a molecular orbital scheme similar to ClF_3 and an unusual structure, and this proves to be the case.

Spectra of a second species, believed to be $IO_2F_2^{2-}$ or IO_2F_2, are obtained in crystals of KIO_2F_2 irradiated and observed at 77°K, but analysis of these very complex spectra is not yet complete and a description of that species must be deferred.

Experimental Section

KIO_2F_2 crystals were prepared by dissolving analytically pure KIO_3 in excess of 48% hydrofluoric acid in a Teflon container and allowing the solution to evaporate slowly.[30] The crystals of KIO_2F_2 obtained were washed with HF and were purified further by recrystallization from HF. Transparent rectangular single crystals obtained by the above process were examined under a polarizing microscope to eliminate twinned crystals. The crystals were invariably single and showed all the morphological characteristics listed by Groth.[31]

Selected crystals of KIO_2F_2 were irradiated with γ rays from a ^{60}Co source producing an effective dose of 20×10^6 rads/hr. Irradiations at 300°K were performed by placing the samples in screw-capped vials in the γ source; for irradiation at 77°K sealed samples were immersed under liquid nitrogen in a Dewar vessel designed to fit inside the radiation compartment of the γ source. Samples were usually irradiated for a period of 3 to 4 hr.

Esr measurements were carried out using a Varian V-4502 X-band spectrometer with 100-kHz field modulation and a Varian V-4503 Q-band spectrometer. Magnetic field calibration and klystron frequency measurements were achieved by methods previously described.[32] Measurements at 77°K were done by immersing the crystal in a Dewar filled with liquid nitrogen the quartz tip of which fitted inside the Varian V-4531 multipurpose cavity.

Single crystals were mounted in selected orientations (±3°) by thin copper springs attached to one end of a quartz rod which fitted inside the Dewar; a large protractor calibrated in degrees permitted measurement of orientation in the magnetic field. Rotations were performed about the a, b, and c crystallographic axes of KIO_2F_2 with spectra recorded every 10° or, near certain orientations, every 5°.

A detailed X-ray crystallographic study of KIO_2F_2 showed[30] that the crystals are orthorhombic, four molecules per unit cell, with space group $C_{2v}^5(Pca)$. The unit cell dimensions are: $a_0 = 8.38$, $b_0 = 5.97$, and $c_0 = 8.41$ Å. We follow the notation of Rogers and Helmholz for the axes (which differs from that of Groth); the structure of the $IO_2F_2^-$ ion is shown in Figure 1.

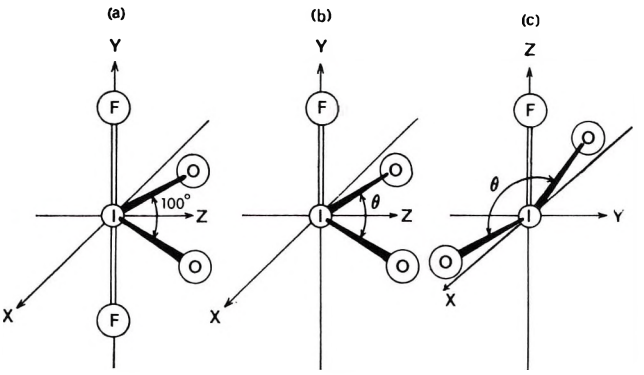

Figure 1. (a) Molecular structure of $IO_2F_2^-$. (b) Possible pyramidal arrangement of IO_2F^-. (c) Possible planar-T arrangement of IO_2F^-.

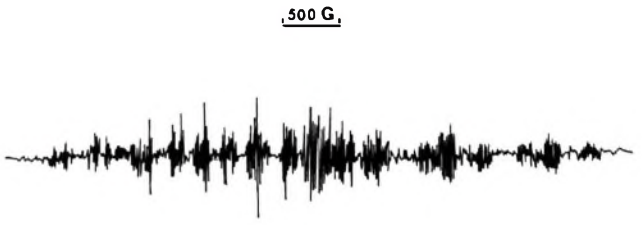

Figure 2. Second-derivative esr spectrum of γ-irradiated KIO_2F_2 at 77°K; the magnetic field is parallel to the b axis of the crystal.

Results

Single crystals of KIO_2F_2 γ-irradiated and observed at 77°K without warmup showed esr spectra spread over a range of about 4500 G (Figure 2); these are attributed to the species $IO_2F_2^{2-}$ (or IO_2F_2). When the crystals were warmed above 140°K, the lines from this primary radical were replaced by a new set spread over about 2500 G belonging to a secondary radical species which was stable even at room temperature. The esr spectrum of the 300°K radical with $H_0 \| b$ shown in Figure 3A, consists of a sextet of lines of equal intensity with hyperfine spacing 520 G, from hyperfine interaction with one iodine nucleus, split into doublets with spacing 40 G from hyperfine interaction with one fluorine nucleus. An extra feature marked "X" in the

(23) A. Begum, S. Subramanian, and M. C. R. Symons, *J. Chem. Soc. A*, 918 (1970).

(24) E. Boseman and D. Schoemaker, *J. Chem. Phys.*, **37**, 671 (1962).

(25) D. Schoemaker, *Phys. Rev.*, **149**, 693 (1966).

(26) P. W. Atkins, J. A. Brivati, N. Keen, M. C. R. Symons, and P. A. Trevalion, *J. Chem. Soc.*, 4785 (1962); P. F. Patrick and F. P. Sargent, *Can. J. Chem.*, **46**, 1818 (1968).

(27) E. A. Hazelwood, *Z. Kristallogr., Kristallogeometrie, Kristallphys., Kristallchem.*, **98**, 439 (1938).

(28) R. D. Burbank and F. N. Bensey, *J. Chem. Phys.*, **21**, 602 (1953).

(29) D. F. Smith, *ibid.*, **21**, 609 (1953).

(30) L. Helmholz and M. T. Rogers, *J. Amer. Chem. Soc.*, **62**, 1537 (1940).

(31) P. Groth, "Chemische Kristallographie," Teil II, Verlag W. Engelmann, Leipzig, 1908.

(32) H. A. Kuska and M. T. Rogers, *J. Chem. Phys.*, **40**, 910 (1964).

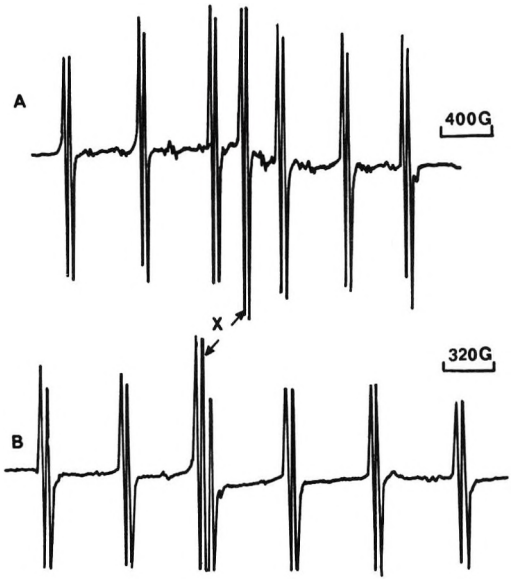

Figure 3. (A) First-derivative X-band spectrum of KIO_2F_2 γ-irradiated at 77°K and observed at room temperature; the magnetic field is parallel to the b axis of the crystal. (B) The same but at Q band.

middle of the spectrum does not belong to the main radical since it is shifted relative to the main sextet at Q band (Figure 3B).

Interpretation of the Spectra

It can be seen in the X-band spectrum of Figure 3A that the experimental hyperfine spacings are increasing toward low field while in the Q-band spectrum, Figure 3B, they are irregular and more nearly equal. This behavior is the result of two effects. The second-order field effect arises when the magnitude of the hyperfine field is sufficiently large relative to the applied field as is the case here; the low-field lines at X band appear at magnetic fields only four times the iodine hyperfine coupling. This effect has an m_I^2 dependence so produces a progressive increase or decrease in spacing in going from low to high applied field[33] and is relatively most important at X band. The second effect arises from the appreciable magnitude of the iodine quadrupole interaction terms in the Hamiltonian operator (eq 4). Off-diagonal elements of the simpler Hamiltonian are now introduced and the hyperfine spacings have an m_I (and m_I^3) dependence leading to a progressive increase or decrease in going from the center to the outer lines. Also, mixing of the nuclear m_I levels results, the selection rule $\Delta m_I = 0$ (for $\Delta M_s = \pm 1$) breaks down, and "forbidden" transitions with $\Delta m_I = \pm 1, \pm 2$ appear.[34,35] These are seen as the weak extra lines of Figure 3A when $H||b$ and as the stronger extra lines of Figure 4 ($H||a$ or $H||c$) where they become comparable to the normal transitions. The situation may be pictured physically as follows. The effective magnetic field (from the unpaired electron and the external field) and the electric field at the

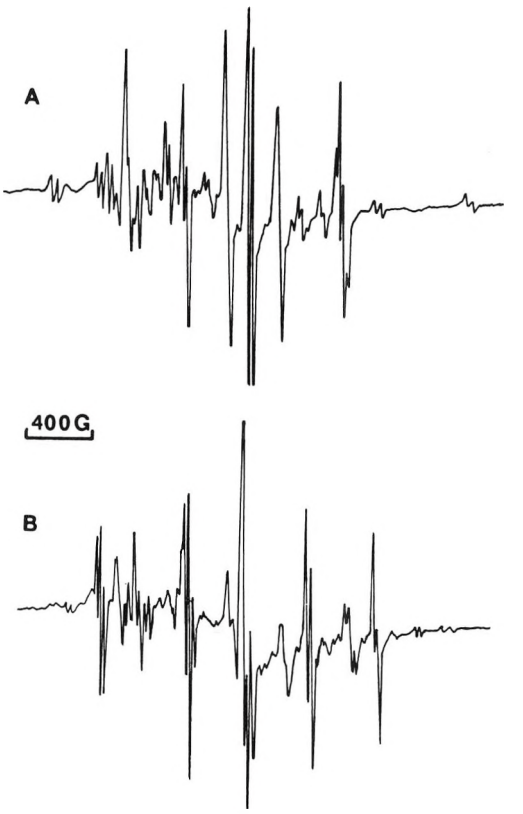

Figure 4. (A) First-derivative X-band spectrum of γ-irradiated KIO_2F_2 at room temperature with the magnetic field parallel to the a axis of the crystal. (B) The same but with the magnetic field parallel to the c axis of the crystal. The "forbidden" lines are of moderate intensity.

iodine nucleus each try to quantize it along their respective, but differently oriented, axes. The quantization then depends on the relative strengths of the magnetic and electric fields at the nucleus and the first-order assumption that it is always quantized along H_0 is no longer true. Extensive use of Q-band spectra has been made since H_0 is then four times larger, and the spectra are more nearly first order; also, the separations between the centers of the multiplets from magnetically distinct sites are larger.

For an arbitrary orientation of the magnetic field with respect to the crystal axes there are four sets of lines corresponding to the four magnetically distinct sites of the space group Pca. However, for $H||b$ or $H||c$ there is only one distinct site, while for $H||a$ two distinct sites are observed. The angular variation of the six lines of the main multiplet is shown in Figures 5A and B for rotation of the magnetic field in the ac and bc planes, respectively. The doublet spacing varies little with orientation, remaining in the range

(33) A. Abragam and M. H. L. Pryce, *Proc. Roy. Soc., Ser. A*, 199, 135 (1951); J. E. Nafe and E. B. Nelson, *Phys. Rev.*, 73, 718 (1948).

(34) B. Bleaney, "Hyperfine Interactions," A. J. Freeman and R. B. Frankel, Ed., Academic Press, New York, N. Y., 1967.

(35) W. Low, *Solid State Phys., Suppl.*, 2 (1961).

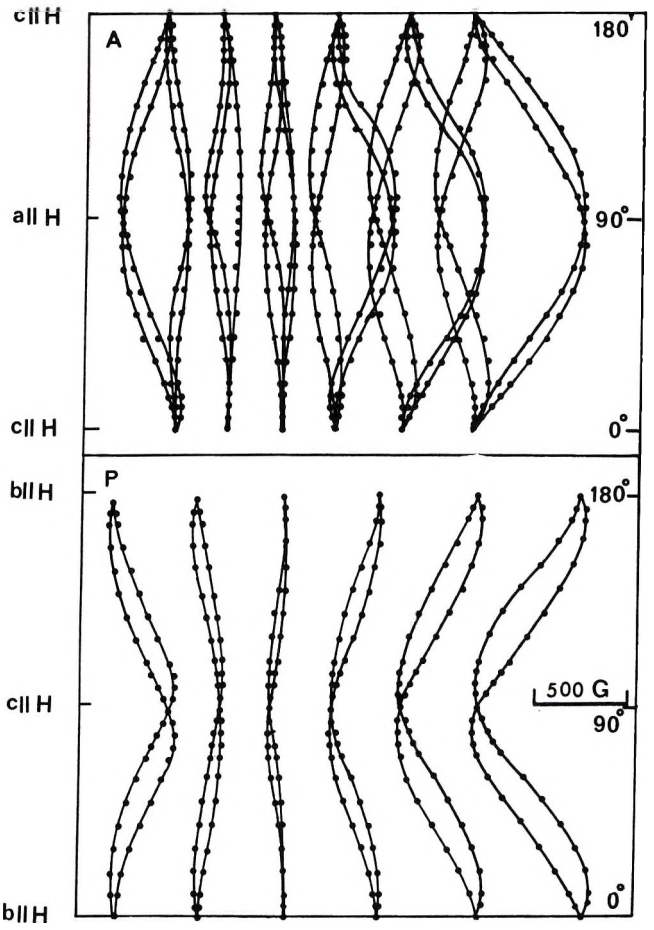

Figure 5. Variation of the resonance magnetic field with orientation for the six main lines from ^{127}I interaction in the spectrum of IO_2F^- for (A) the field in the *ac* plane, and (B) the magnetic field in the *bc* plane. The maximum experimental errors are indicated by the diameters of the plotted points.

39–41 G, and is not shown in Figure 5 to simplify the plots, which are based on the positions of the centers of the doublets. The principal values of the g tensor and the ^{127}I hyperfine interaction tensor, along with their direction cosines relative to the crystallographic axes, were evaluated by the method of Schonland[36] and are listed in Table I; it is seen that they are nearly coincident. The Breit–Rabi method[37] has been used to correct for the second-order field effect, and the values of Table I are average values for A, and corrected g values obtained by use of the equation[38]

$$H_0 = H(m_I) + Am_I + \frac{A^2}{2H(m_I)}[I(I+1) - m_I^2] + \ldots \quad (1)$$

where $g = H_0\beta/h\nu$, $H(m_I)$ is the resonance field corresponding to the nuclear quantum number m_I, ν is the klystron frequency (MHz), I is the nuclear spin of ^{127}I, and A is the average hyperfine splitting. The average multiplet spacings lead to A values correct to second order since the second-order field effect and the quadrupole effect both tend to average to zero.

Table I: Magnetic Parameters for the IO_2F^- Radical in KIO_2F_2

Tensor components[a]	Direction cosines[b] a	b	c
g Tensor			
$g_{xx} = 2.0989 \pm 0.0008$	0.971	0.233	0.055
$g_{yy} = 2.0164 \pm 0.0008$	−0.121	0.280	0.952
$g_{zz} = 1.9432 \pm 0.0005$	−0.206	0.931	−0.301
$A(^{127}I)$ Tensor			
$A_{xx} = 759 \pm 2$	0.984	0.180	0.101
$A_{yy} = 917 \pm 2$	−0.079	0.276	0.983
$A_{zz} = 1433 \pm 2$	−0.154	0.977	−0.180

$A(^{19}F)$ Tensor

$A_{xx} = A_{yy} = 107.8 \pm 0.1$ MHz; $A_{zz} = 117.6 \pm 0.1$; $a(F) = 111.1 \pm 0.1$; $2B(F) = 6.5 \pm 0.1$

Estimated Spin Densities

Iodine: $\rho_{5s} = 0.04$; $\rho_{5p} = 0.28$ (deviation from axial symmetry of the tensor included)

Fluorine: $\rho_{2s} = 0.002$ and $\rho_{2p} = 0.002$

Oxygen: ρ_{2s} and $\rho_{2p} \leq 0.58$ (both oxygens, by difference)

[a] All hyperfine interactions are in MHz. [b] Relative to the *a*,*b*,*c* crystallographic axes of KIO_2F_2; probable error is ±0.005.

An attempt has been made to evaluate, for ^{127}I in the radical, the quadrupolar parameters Q' and Q'' where

$$Q' = Q_{zz} - \tfrac{1}{2}(Q_{xx} + Q_{yy}) \quad (2)$$

and

$$Q'' = \tfrac{1}{2}(Q_{xx} - Q_{yy}) \quad (3)$$

Although the "forbidden" transitions are most sensitive to these parameters,[39] the weak lines could not be followed through the necessary complete rotations so an approximate method has been employed to extract Q' and Q'' from the positions of the normal transitions. Excluding the nearly isotropic hyperfine coupling to ^{19}F and assuming that the ^{127}I nuclear gyromagnetic ratio is isotropic, the Hamiltonian for the system can be written[40] as

$$\mathcal{H} = \beta(g_{xx}H_xS_x + g_{yy}H_yS_y + g_{zz}H_zS_z) + A_{xx}I_xS_x + A_{yy}I_yS_y + A_{zz}I_zS_z + Q'[I_z^2 - \tfrac{1}{3}I(I \pm 1)] + Q''(I_x^2 - I_y^2) - g_n\beta_n(H_xI_x + H_yI_y + H_zI_z) \quad (4)$$

where the terms have their usual significance. If the magnetic field H makes polar angle θ and azimuthal

(36) D. S. Schonland, *Proc. Phys. Soc. (London)*, **73**, 788 (1959).

(37) G. Breit and I. Rabi, *Phys. Rev.*, **38**, 2082 (1931).

(38) H. A. Kuska and M. T. Rogers in "Radical Ions," E. T. Kaiser and L. Kevan, Ed., Interscience, New York, N. Y., 1968.

(39) H. So, Ph.D. Thesis, University of Illinois, Urbana, Ill., 1970.

(40) A. Abragam and B. Bleaney, "Electron Paramagnetic Resonance of Transition Ions," Oxford University Press, New York, N. Y., 1970.

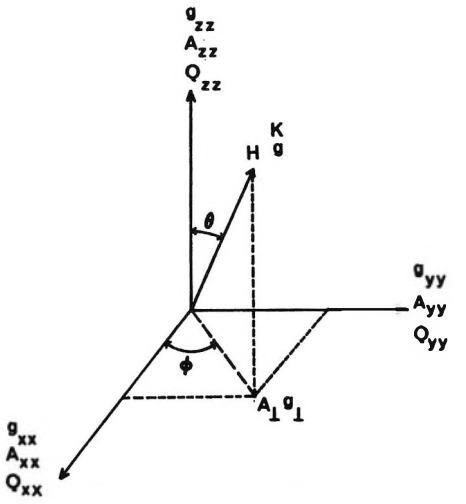

Figure 6. The coordinate system used in obtaining the angular variation of the esr spectrum of IO_2F^-. The axes of the g, A, and Q tensors are assumed to be coincident.

angle ϕ with the right-handed coordinate system of the principal axes of the g tensor, which are coincident with those of the hyperfine interaction tensor (see Figure 6), we may write

$$g_\perp^2 = g_{xx}^2 \cos^2\phi + g_{yy}^2 \sin^2\phi$$
$$g^2 = g_{zz}^2 \cos^2\theta + g_\perp^2 \sin^2\theta \qquad (5)$$
$$A_\perp^2 g_\perp^2 = A_{xx}^2 g_{xx}^2 \cos^2\phi + A_{yy}^2 g_{yy}^2 \sin^2\phi$$
$$K^2 g^2 = A_{zz}^2 g_{zz}^2 \cos^2\theta + A_\perp^2 g_\perp^2 \sin^2\theta$$

Here $g_\perp$ is the resultant of g_{xx} and g_{yy}, while $A_\perp$ is the resultant of A_{xx} and A_{yy}, in a direction making an angle ϕ with the x axis in the xy plane; g and K are the resultants of $g_\perp$ and g_{zz}, and of $A_\perp$ and A_{zz}, respectively, in the direction of the magnetic field. We have assumed that the axes of the g and A tensors, as well as that of the quadrupolar tensor, are coincident. The parameters of Table I were combined with eq 5 to give values of g, K, $A_\perp$, and $g_\perp$ which, with the Hamiltonian operator of eq 4, permitted the angular variation of the spectra to be computed by the second-order perturbation method of Tseng and Kikuchi.[41] The values so obtained were compared with the experimental angular variation curves corrected for second-order field effects by eq 1. These corrected experimental plots would agree with the calculated plots, setting $Q' = Q'' = 0$ in eq 4, if there were no iodine quadrupole interaction. In fact, they do not and values of Q', Q'' were introduced and adjusted until the difference between the corrected experimental line positions and the calculated ones for the normal ($\Delta m_I = 0$) transitions for ^{127}I reached a minimum. The values so obtained are listed in Table II and a typical plot of the corrected experimental line positions (circles) and the calculated positions obtained in this way with the parameters of Table II (solid lines) is shown in Figure 7. The

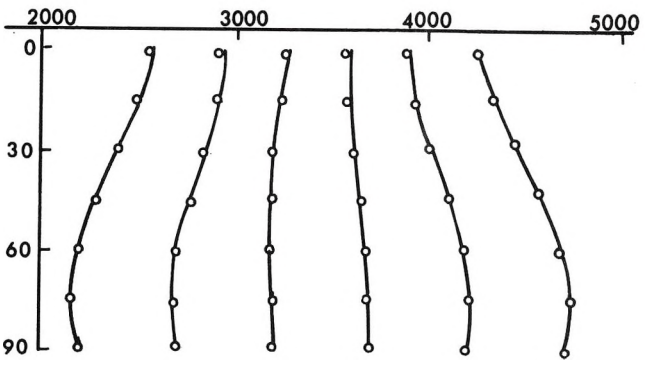

Figure 7. Experimental line positions corrected by eq 1 (solid lines) and calculated (circles) field positions for the six ^{124}I hyperfine lines in the spectrum of IO_2F^-. The magnetic field is in the bc plane and for $\theta = 0°$ is parallel to the c axis of the crystal. Values represented by the circles were calculated using the parameters of Tables I and II.

probable errors in Q', Q'' are rather large ($\pm 10\%$). From the values of Q', Q'' an iodine quadrupole coupling constant $e^2qQ = 1095$ MHz is obtained along with an asymmetry parameter $\eta = 0.11$.

Table II: Quadrupolar Parameters for IO_2F^- and for Some Related Species

Molecule	e^2Qq, MHz	η	Reference
IO_2F^- in KIO_2F_2	1095.5	0.110	This work
$Q' = 123 \pm 10$ MHz			
$Q'' = 4 \pm 0.4$ MHz			
HIO_3	1126.9	0.45	45
IO_3^- in $Ca(IO_3)_2$	1025.36	0	46
I_3^- in NH_4I_3 (central I)	1725	0.151	46

Discussion

From the hyperfine structure of the spectra it is apparent that the odd electron interacts with one iodine nucleus and one fluorine nucleus plus an undetermined number of oxygen nuclei ($I = 0$ for ^{16}O). Since the 77°K radical is $IO_2F_2^{2-}$ (or IO_2F_2), and the secondary radical has lost a fluorine atom, the room temperature radical studied here could be IO_2F^- formed by the process

$$IO_2F_2^{2-} \longrightarrow IO_2F^- + F^- \quad (T > 140°K)$$

The possibility IOF^- appears less likely since maximum stability should be achieved with the maximum number of I–O bonds; IF^- may be excluded since $A_{||}(F)$ has been observed for that species[25] and is $\sim$630 G (with $A_\perp \simeq 0$).

The experimental hyperfine splitting tensor for ^{127}I may be broken down in the usual manner[42] into iso-

(41) D. L. Tseng and C. Kikuchi, Technical Report, "Niobium Hyperfine Structure in Crystal Calcium Tungstate," University of Michigan, Ann Arbor, Mich., 1968.

tropic and dipolar terms, and the spin density in the iodine valence shell orbitals may be estimated from these components. Since the signs of the principal components of the tensor are not determined experimentally, there are eight possible choices. We assume that the isotropic term will be positive, that the dipolar term will be approximately axial and so approximately of the form $(2B, -B, -B)$, and that the p/s ratio will be within the range usually found. The only choice of signs which is compatible with these assumptions is that with all components positive. This permits a physically meaningful decomposition of the tensor into a large positive isotropic interaction (+1037 MHz) and a moderate dipolar term with principal components (−278, −119, +397). In view of the appreciable deviation of the dipolar tensor from axial symmetry it is, in turn, expressed as the sum of an axially symmetrical tensor and one representing the deviations from axial symmetry. Thus, the experimental tensor will be interpreted in terms of the following expression

$$\begin{vmatrix} 759 & & \\ & 918 & \\ & & 1434 \end{vmatrix} = \begin{vmatrix} 1037 & & \\ & 1037 & \\ & & 1037 \end{vmatrix} + \begin{vmatrix} -225 & & \\ & -225 & \\ & & +450 \end{vmatrix} + \begin{vmatrix} -53 & & \\ & +106 & \\ & & -53 \end{vmatrix}$$

Using the Hartree–Fock values[43] for the isotropic and anisotropic iodine 5s and 5p hyperfine interactions, $a_{5s}(^{127}\mathrm{I})$ = 26,000 MHz and $2B_0(^{127}\mathrm{I})$ = 1624 MHz, the unpaired spin densities in the iodine 5s and 5p orbitals may then be estimated to be 0.04 and 0.28, respectively, from $A(^{127}\mathrm{I})$ = 1037 and $2B(^{127}\mathrm{I})$ = 450.

The fluorine hyperfine interaction is nearly isotropic, $a(^{19}\mathrm{F})$ = 111.1 MHz and $2B(^{19}\mathrm{F})$ = 6.5 MHz. The calculated values[43] for an electron in pure 2s or 2p orbitals on ^{19}F are 47,910 MHz and 3030 MHz, respectively; hence the "experimental" spin densities are $\rho_{2s}(^{19}\mathrm{F})$ = 0.002 and $\rho_{2p}(^{19}\mathrm{F})$ = 0.002.

The total spin density on iodine and fluorine is then about 0.32, neglecting any spin density in the iodine 5d orbitals; this leads to a spin density of about 0.34 on each oxygen atom by difference. The deviation from axial symmetry (eq 6) indicates that there is additional spin density either in the σ bonding orbitals or in the d orbitals of iodine.

Structure of the Radical. No reliable theoretical calculations of spin density distribution in iodine compounds have been reported. It is, however, possible to carry out CNDO calculations on isoelectronic compounds of chlorine and these should serve as a guide in interpreting the present results. The structure of the undamaged $IO_2F_2^-$ anion in KIO_2F_2 is shown in Figure 1a. Removal of a fluorine would leave a radical IO_2F^- with the structure of Figure 1b, which would then distort to the stable configuration. CNDO calculations for the isoelectronic species ClO_2F^- were carried out for the arrangement of Figure 1b with the O–Cl–O angle varied from 90 to 180°, and for the planar-T arrangement[28,29] of Figure 1c with θ = 170 or 180°. The results are shown in Table III.

Table III: Unpaired Spin-Density Distribution in ClO_2F^- Calculated Using the CNDO Method

Orbital	Cl	O	F	Total energy (Hartrees)
	Structure of Figure 1 (b), θ = 90°			
s	0.0025	−0.002	0.0058	
p_x	−0.0019	0.0052	0.0001	−80.6361
p_y	0.5233	0.0374	0.1416	
p_z	0.0479	0.0019	0.0103	
d (Total)	0.0820			
	Structure of Figure 1 (b), θ = 140°			
s	0.0018	0.0005	0.0031	
p_x	−0.0020	0.0500	0.0000	
p_y	0.4241	0.0487	0.0765	−80.6865
p_z	0.1218	0.0146	0.0052	
d (Total)	0.1438			
	Structure of Figure 1 (b) θ = 160°			
s	0.0106	−0.0010	0.0002	
p_x	0.0052	0.1080	0.0001	−80.6769
p_y	0.0976	0.0250	0.0062	
p_z	0.2596	0.1630	0.0031	
d (Total)	0.0380			
	Structure of Figure 1 (b), θ = 170°			
s	0.0055	−0.0005	0.0003	
p_x	0.0027	0.0486	0.0000	−80.6749
p_y	0.0205	0.0087	0.0008	
p_z	0.2877	0.2967	0.0024	
d (Total)	−0.0221			
	Coplanar T-shape, θ = 170°			
s	0.0000	0.0000	0.0000	
p_x	0.0000	0.0000	0.0000	−80.6644
p_y	0.2933	0.3781	0.0007	
p_z	0.0000	0.0000	0.0000	
d (Total)	−0.0503			

The pyramidal structure of Figure 1b leads to too large spin densities on fluorine and on the central atom (Table III). The planar-T structure of Figure 1c with θ = 170 or 180° would predict zero isotropic interaction for both fluorine and the central atom and would lead to an axially symmetrical hyperfine interaction tensor for the central atom since the odd electron is placed largely in a p orbital perpendicular to the plane. The experimental data show that there is a small s orbital density on both ^{19}F and ^{127}I, a small anisotropy of the ^{19}F hyperfine splitting tensor, and a deviation of the ^{127}I hyper-

(42) M. T. Rogers and D. H. Whiffen, *J. Chem. Phys.*, **40**, 2662 (1964).

(43) C. M. Hurd and P. Coodin, *J. Phys. Chem. Solids*, **28**, 523 (1967); P. B. Ayscough, "Electron Spin Resonance in Chemistry," Methuen, London, 1967.

fine splitting tensor from axial symmetry. These qualitative features are best reproduced by moving the central atom of the planar-T-type arrangement out of the plane by a small amount giving a rather flat, irregular pyramid; the structure of Figure 1b with θ = 160 or 170° is of this type and may be considered as a slightly distorted ClF_3 or BrF_3 arrangement. Since small s densities are known not to be reliably reproduced by the CNDO method,[44] it is perhaps not surprising that the calculated values of ρ_s in Table III are about an order of magnitude lower than the "experimental" values.

Deviation of the $A(^{127}I)$ tensor from axial symmetry could arise from some odd-electron density in the 5d orbitals of iodine. A value of $\langle r^{-3}_{5d}$ for iodine does not appear to have been computed but one would expect it to be rather large and $2B_0$, the anisotropic dipolar interaction for one 5d electron, correspondingly small. It is, therefore, more probable that these deviations arise from asymmetry of the 5p distribution. If the values of Table III for ρ_{5p_x}, ρ_{5p_y}, ρ_{5p_z} for the nearly planar-T configuration with θ = 170° are used, along with $2B_0$ (^{124}I,5p) = 1624 MHz, the anisotropic dipolar tensor calculated has principal values (449, −246, −203), while for θ = 160° they are (337, −281, −56); the "experimental" values (assuming that all components of the observed tensor are positive) are (397, −278, −119).

Iodine Quadrupole Coupling Constant. The large quadrupole coupling constant observed for IO_2F^-, $e^2qQ(^{127}I)$ = 1096 MHz, and the asymmetry parameter, η = 0.11, are consistent with the nearly planar-T shape and the absence of axial symmetry. There are few values suitable for comparison with the above result but several experimental values of iodine quadrupole coupling constants in solids are listed in Table II. Since the extra electron will alter the field gradient at iodine, no detailed interpretation of the coupling constant has been attempted.

While the esr results do not serve to establish the extent to which iodine d orbitals are involved in bonding in IO_2F^-, it may be noted that the quadrupole coupling constants for I_3^-, ICl_2^-, ICl_4^-, and similar species, may be accounted for without use of the d orbitals.[46] The geometries and energies of such molecules appear to be given rather well by calculations using only s and p orbitals of iodine.[47] However, it is probable that a satisfactory account of the hyperfine interactions will require inclusion of d orbital contributions since this is found to improve molecular properties such as dipole moments.[48]

(44) J. A. Pople and D. L. Beveridge, "Approximate Molecular Orbital Theory," McGraw-Hill, New York, N. Y., 1970.

(45) R. Livingston and H. Zeldes, *J. Chem. Phys.*, **26**, 351 (1957).

(46) E. A. C. Lucken, "Nuclear Quadrupole Coupling Constants," Academic Press, New York, N. Y., 1969.

(47) B. M. Deb and C. A. Coulson, *J. Chem. Soc. A.*, 958 (1971).

(48) D. P. Santry and G. A. Segal, *J. Chem. Phys.*, **47**, 158 (1967).

Electron Paramagnetic Resonance Spectra of Pyrrolidino and Pyrrolino Free Radicals. The Structure of Dialkylamino Radicals[1]

by David W. Pratt,* John J. Dillon,

Department of Chemistry, University of Pittsburgh, Pittsburgh, Pennsylvania 15213

Roger V. Lloyd, and David E. Wood

Department of Chemistry and Mellon Institute, Carnegie-Mellon University, Pittsburgh, Pennsylvania 15213 *(Received December 7, 1970)*

Publication costs assisted by the Merck Foundation

The nitrogen-centered free radicals pyrrolidino and pyrrolino have been prepared by X irradiation of the corresponding amines in an adamantane matrix at 77°K. At temperatures near 200°K, the radicals undergo rapid reorientation in the matrix and exhibit isotropic epr spectra. Comparison of the ^{14}N hyperfine splittings and g values of these radicals with those found for several open-chain dialkylamino radicals indicates that all of these species appear to have similar electronic structures and RNR bond angles of less than 120°. This view is supported by steric considerations in the case of the cyclic radicals and by INDO calculations on the dimethylamino radical which show that the eclipsed form with a CNC bond angle of 117° is the most stable conformation. These calculations also indicate that $(CH_3)_2N\cdot$ is a π radical with very little σ character and predict hyperfine splittings in good agreement with the experimental values.

I. Introduction

The NH_2 radical has seven valence electrons and therefore, according to Walsh's rules,[2] the ground electronic state should be characterized by an HNH angle of less than 180°. This prediction has been verified by careful analysis of the so-called α bands of ammonia, which showed that the ground $^2B_1$ state of NH_2 in the gas phase has a bond angle of 103.4°.[3] Extensive optical[4] and epr[5] spectral studies of the amino radical in solid matrices have also been reported, but interpretation of these results is complicated by the influence of the environment on radical motion and structure. For example, the isotropic ^{14}N hyperfine splitting (hfs) constant of NH_2 appears to vary from 10.4 to 31 G in different matrices.[5] Symons has suggested that these variations might be attributed to effects of the local environment on the HNH bond angle,[6] but no additional information supporting this view has been published.

Similar difficulties have been encountered in interpretation of epr spectra of higher homologs of the amino radical. Alkylamino radicals of the general formula $R\dot{N}R'$ may be produced by high-energy irradiation of precursor amines at low temperatures, but the resulting complex powder spectra have not yielded a great deal of structural information.[7-9] On the other hand, if the radicals can be produced in an environment which allows them them to tumble freely, then detailed structural information can only be obtained by comparison of the resulting isotropic epr parameters with careful theoretical calculations.

It was of interest in the present study to explore further the possible relationships between these parameters and the CNC bond angles in several members of the dialkylamino radical family. In particular, use of the recently described adamantane matrix technique[10] has enabled us to prepare and characterize the

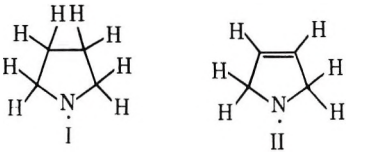

I II

pyrrolidino (I) and pyrrolino (II) free radicals in an environment which allows them to undergo rapid reorientation. While this work was in progress, Danen and Kensler[11] obtained the epr spectra of dimethyl-,

(1) Taken in part from the M.S. Thesis of J. J. Dillon, III, University of Pittsburgh, 1970.

(2) A. D. Walsh, *J. Chem. Soc.*, 2260 (1953).

(3) G. Herzberg and D. A. Ramsay, *J. Chem. Phys.*, **20**, 347 (1952); K. Dressler and D. A. Ramsay, *Phil. Trans. Roy. Soc.*, **251A**, 553 (1959).

(4) See G. W. Robinson, *Advan. Chem. Ser.*, **No. 36**, 10 (1962), and references contained therein.

(5) See D. R. Smith and W. A. Seddon, *Can. J. Chem.*, **48**, 1938 (1970), and references contained therein.

(6) M. C. R. Symons, *Advan. Chem. Ser.*, **No. 82**, 1 (1968).

(7) G. V. Pukhal'skaya, A. G. Kotov, and S. Ya. Pshezhetskii, *Dokl. Akad. Nauk SSSR*, **171**, 1380 (1966).

(8) S. G. Hadley and D. H. Volman, *J. Amer. Chem. Soc.*, **89**, 1053 (1967).

(9) D. Cordischi and R. DiBlasi, *Can. J. Chem.*, **47**, 2601 (1969).

(10) D. E. Wood and R. V. Lloyd, *J. Chem. Phys.*, **52**, 3840 (1970); **53**, 3932 (1970).

(11) W. C. Danen and T. T. Kensler, *J. Amer. Chem. Soc.*, **92**, 5235 (1970).

diethyl-, and diisopropylamino radicals in solution by *in situ* photolysis of the corresponding tetrazines. Since the cyclic radicals I and II would be expected to have CNC bond angles of less than 120° from steric considerations alone, a comparison of our results with those obtained for the open-chain dialkylamino radicals and with INDO calculations[12] on the prototype dimethylamino radical would be expected to shed considerable light on the geometry and electronic structure of this class of free radicals.

II. Experimental Section

Details of the adamantane matrix technique have been described previously.[10] Samples were X-irradiated for 15 min at 77°K by immersion in a foam dewar containing liquid nitrogen, and epr spectra were recorded on a Varian V-4502 spectrometer equipped with a V-4547 variable temperature accessory and rectangular TE_{012} cavity. Temperatures were measured with a calibrated copper–constantan thermocouple. Both pyrrolidine and pyrroline were obtained from Aldrich Chemical Co. and were used as received. Samples prepared on a vacuum line with degassed and trap-to-trap distilled pyrrolidine gave the same results as those prepared in air. *N*-Hydroxypyrrolidine was prepared by the peroxide oxidation of pyrrolidine.

III. Results and Discussion

Figure 1 shows the epr spectrum obtained at 247°K following X irradiation of pyrrolidine in adamantane at 77°K. The spectrum consists of a 1:4:6:4:1 quintet of 1:1:1 triplets which would be expected for four equivalent β protons and a single ^{14}N. The spectrum from pyrroline is identical except for the larger β-proton hfs. Both spectra were fit by computer simulation, and the resulting epr parameters are shown in Table I. Also shown in this table are the results for NH_2 in solid ammonia,[5] for the open-chain radicals obtained by Danen and Kensler,[11] and for di-*tert*-butylamino radical.[13] It is seen that all species listed in this table have nearly identical ^{14}N hfs and g values (where measured). The ^{14}N hfs are also similar to those reported for the corresponding nitroxide radicals; however, g values and β-proton hfs for the nitroxides are quite different. For example, the nitroxide radical corresponding to radical I, which was prepared from *N*-hydroxypyrrolidine, has $a_N = 13.5$ G, $a_H^\beta = 17.6$ G, and $g = 2.0060$ in an adamantane matrix at 215°K.

The hfs of the cyclic dialkylamino radicals are independent of temperature up to 270°K. Above this temperature, the epr spectrum of each radical decreases rapidly and irreversibly in intensity to reveal a new spectrum with a lower g value. The slight distortion of the spectrum shown in Figure 1 is caused by the presence of this as yet unidentified free radical, which could also be obtained exclusively by X irradiation of pyrrolidine in adamantane at room temperature. Whereas

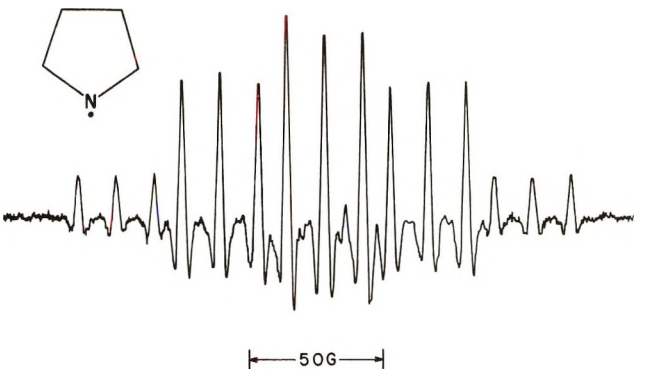

Figure 1. Second-derivative epr spectrum of pyrrolidino radical in adamantane at 247°K.

Table I: Isotropic Epr Parameters of NR_2 Radicals

Radical	a_N, G	a_H, G	g values[a]
NH_2 in ammonia[b]	15.2	25.4	2.0046
$(CH_3)_2N\cdot$[c]	14.8	27.4	...
$(CH_3CH_2)_2N\cdot$[c]	14.3	36.9 (4)	...
$[(CH_3)_2CH]_2N\cdot$[c]	14.3	14.3 (2)	...
$[(CH_3)_3C]_2N\cdot$[d]	14.2	...	2.0045
Pyrrolidino (I)[e]	14.4	39.1 (4)	2.0046
Pyrrolino (II)[f]	14.4	44.7 (4)	2.0046

[a] Compared to DPPH = 2.0036. [b] Reference 5. [c] Reference 11. [d] Reference 13. [e] This work, T = 228°K. [f] This work, T = 241°K.

the spectrum of the latter radical was easily power-saturated, as is usually observed for carbon-centered radicals, the cyclic dialkylamino radical spectra could not be saturated with the full output of a 100-mW klystron.

The similarities of the g values and ^{14}N hfs in these radicals to those found for the open-chain dialkylamino radicals suggest *either* that the CNC angles are not very different for the two groups of radicals *or* that the values of both g and a_N are not very sensitive to the bond angle. That the g value should be sensitive to the bond angle is expected on theoretical grounds because the magnitude of the deviation from the free spin value depends on the hybridization of both the lone-pair and unpaired electron orbitals.[14] This expectation has received recent experimental confirmation from the distribution of g values observed for Si–N–Si color centers in sodium silicate glasses[15] which are known to exhibit a distribution of SiOSi bond

(12) J. A. Pople, D. L. Beveridge, and P. A. Dobosh, *J. Amer. Chem. Soc.*, **90**, 4201 (1968).

(13) Obtained in neat di-*tert*-butylamine at 203°K; D. E. Wood, unpublished results.

(14) P. W. Atkins and M. C. R. Symons, "The Structure of Inorganic Radicals," Elsevier, Amsterdam, 1967.

(15) J. H. Mackey, J. W. Boss, and M. Kopp, *Phys. Chem. Glasses*, **11**, 205 (1970).

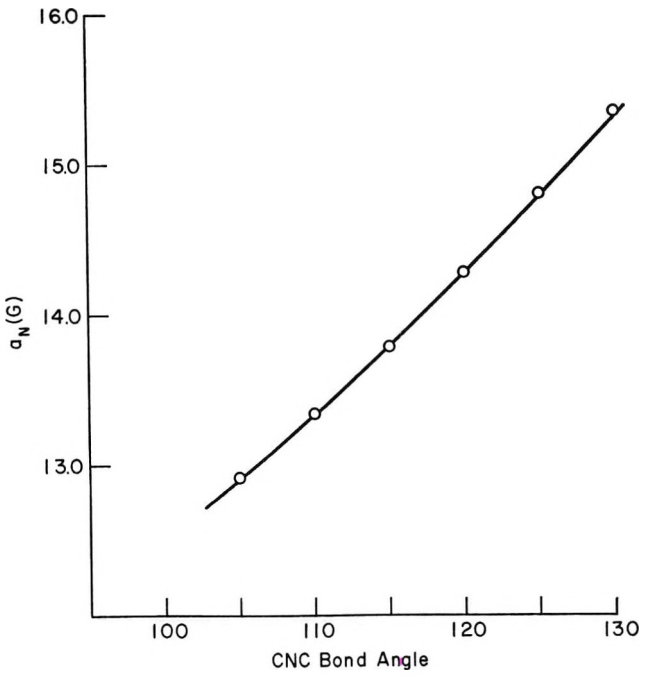

Figure 2. INDO coupling constant as a function of CNC bond angle for the eclipsed form of $(CH_3)_2N\cdot$ (r_{CN} = 1.40 Å, r_{CH} = 1.12 Å).

angles.[16] As the g values for the two groups of dialkylamino radicals are the same within experimental error, and since the CNC angle in the pyrrolidino and pyrrolino radicals is probably somewhat less than 120° because of the ring strain which would otherwise ensue, it seems reasonable to conclude that the CNC angle in the open-chain dialkylamino radicals is also less than 120°.

This proposal is supported by INDO calculations[12] on the dimethylamino radical. In these calculations, the optimum geometry was first determined by minimizing the energy of both the staggered and eclipsed conformations of $(CH_3)_2N\cdot$ with respect to the parameters r_{CH}, r_{CN}, and <CNC. The eclipsed form was found to be more stable; the resulting minimum energy parameters are shown in III. With r_{CH} and r_{CN} fixed at the

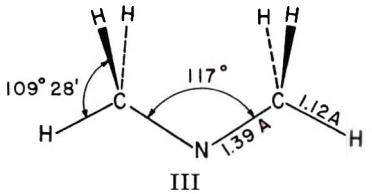

III

values shown, values of a_N were then calculated as a function of CNC bond angle. As can be seen from Figure 2, the calculated ^{14}N hfs of the eclipsed form increases monotonically from 12.9 G at 105° to 15.4 G at 130°. The value for the minimum energy geometry (<CNC = 117°) of the eclipsed form is 13.9 G, that for the lowest energy staggered form is 13.8 G. Comparison of these results with the experimental value of 14.78 G[11] for dimethylamino radical shows that they are within the error limits established by previous INDO calculations of this type.[12] Therefore, since the equilibrium bond angles calculated by INDO have been shown to have a mean absolute error of less than 2°,[17] it is concluded that the CNC bond angle in $(CH_3)_2N\cdot$ is *less* than 120°. Furthermore, since these calculations have shown the ^{14}N hfs in dimethylamino radical to be sensitive to the bond angle, the similarity of the ^{14}N hfs for all radicals in Table I again suggests that the CNC angle is essentially the same in all species.

This equilibrium bond angle is intermediate between that expected for two easily visualized limiting cases, namely CNC bond angles of 120 and 109°, respectively. In the first case, both the bonding orbitals and the lone-pair orbital on nitrogen are sp^2 hybrids and the unpaired electron occupies a p orbital. In the second, the bonding orbitals are sp^3 hybrids, the unpaired electron is again in a p orbital, and the lone pair occupies an sp hybrid on nitrogen. Since the nature of the lone-pair orbital is very different in these two limiting cases, we expect that more information about the hybridization around the nitrogen atom can be obtained by combining the results of optical studies on the $n \rightarrow \pi^*$ transitions in these radicals with the g values reported herein.[18] Experiments of this type are in progress, as are independent efforts to determine both the g and hyperfine tensors of the di-*tert*-butylamino radical.

The β-proton hyperfine splitting of 38.4 G calculated by INDO for a dihedral angle θ = 30° between the axis of the nitrogen p orbital and the CH bond for the dimethylamino radical[19] compares favorably with the experimental values for pyrrolidino and pyrrolino radicals. The fact that a_H^β for the pyrrolino radical is somewhat larger presumably reflects the extra stiffness given the pyrrolino ring by its double bond which, in turn, causes a larger average value for $\cos^2\theta$.[20] An absence of long-range interaction between the nitrogen and the double bond is indicated by the otherwise identical epr spectral parameters.

IV. Conclusions

Use of the adamantane matrix technique has made possible the preparation and characterization of cyclic dialkylamino radicals by epr spectroscopy. The ^{14}N hfs and g values of these radicals are quite similar to those obtained recently for several open-chain dialkylamino radicals including dimethylamino radical. INDO cal-

(16) B. E. Warren and R. L. Mozzi, *J. Appl. Cryst.*, 164 (1969).

(17) J. A. Pople, *Accounts Chem. Res.*, 3, 217 (1970).

(18) The use of adamantane as a matrix for optical experiments on free radicals is discussed in a recent publication. See D. E. Wood, R. V. Lloyd, and D. W. Pratt, *J. Amer. Chem. Soc.*, 92, 4115 (1970).

(19) The value calculated for free rotation of the methyl groups is 27.3 G, compared to the experimental value of 27.4 G.[11]

(20) A. Carrington and A. D. McLachlan, "Introduction to Magnetic Resonance," Harper and Row, New York, N. Y., 1967, p 109.

culations on $(CH_3)_2N\cdot$ indicate that the CNC bond angle in this radical is less than 120°; a similar angle is expected for the pyrrolidino and pyrrolino radicals from steric considerations. Since the INDO calculations also show that the ^{14}N hfs in $(CH_3)_2N\cdot$ is a strong function of the CNC bond angle and since the g values for both cyclic and open-chain dialkylamino radicals are essentially identical, it appears that the bond angle in all of these radicals is less than 120° and is not affected significantly by increasingly bulky alkyl groups.

Acknowledgment. D. W. P. thanks the Merck Company Foundation for the award of a Faculty Development grant.

Discussion

W. C. DANEN (Kansas State University). Do you believe the CNC bond angle in di-*tert*-butylamino radical is really *ca.* 117°? It was pointed out by you that a_N for this species is very similar to dimethylamino radical yet there are undoubtedly drastic differences in steric effects between these two radicals.

D. W. PRATT. Since both the g value and ^{14}N hfs for di-*tert*-butylamino radical are similar to those found for pyrrolidino radical, it appears that the CNC bond angles in the two radicals are nearly the same.

Electron Spin Resonance Study of X-Irradiated Long-Chain Alcohols Oriented in Urea Inclusion Crystals[1a]

by G. Bruce Birrell[1b] and O. Hayes Griffith*[1c]

Institute of Molecular Biology and Department of Chemistry, University of Oregon, Eugene, Oregon 97403
(Received January 15, 1971)

Publication costs assisted by The National Science Foundation

Single crystals of the 6-undecanol–urea and 1-decanol–urea inclusion compounds were X-irradiated at 77°K, and the resulting free radicals were examined using electron spin resonance techniques. In both cases the long-lived radicals were those formed by removal of a hydrogen atom from the carbon attached to the OH group.

The two preceding papers[2,3] have dealt with radiation damage to nitrogen-containing organic molecules which were trapped in an adamantane matrix. In this work we would like to discuss the formation of free radicals produced in long-chain alcohols which have been trapped in a different type of host: urea inclusion crystals. The motion of the trapped molecules in the two hosts is quite different. In adamantane the motion of the guest molecules is isotropic and a solution-like electron spin resonance (esr) spectrum results,[4] whereas in single crystals of urea there is free rotation only about the long axis of the guest molecule causing the esr spectra to be anisotropic except when the magnetic field is in the crystalline xy plane.[5] Urea is capable of forming inclusion crystals with many types of organic molecules,[6] and this technique has been used to examine radiation damage in a number of compounds, including most recently the dibutyl esters of oxalic and malonic acids[7] and an acetylenic compound, methyl-2-nonynoate.[8]

A number of studies of radicals produced in X-, γ-, and uv-irradiated alcohol glasses have been made.[9-12] Esr spectra from glasses of this type tend to be difficult to interpret and to date have not afforded accurate coupling constants. The present study represents the first examination of alcohol free radicals in an oriented matrix.

The sample preparation, X irradiation, and esr instrumentation have been previously described.[13] The

(1) (a) This work was supported by the National Science Foundation under Grant No. GP-16341; (b) NIH Postdoctoral Fellow (No. 5 FO3 CA42789-02); (c) Alfred P. Sloan Fellow.

(2) D. E. Wood, R. V. Lloyd, and W. A. Latham, *J. Amer. Chem. Soc.*, **93**, 4145 (1971).

(3) D. W. Pratt, J. J. Dillon, R. V. Lloyd, and D. E. Wood, *J. Phys. Chem.*, **75**, 3486 (1971).

(4) D. E. Wood and R. V. Lloyd, *J. Chem. Phys.*, **52**, 3840 (1970).

(5) O. H. Griffith, *ibid.*, **41**, 1093 (1964).

(6) W. Schlenk, Jr., *Fortsch. Chem. Forsch.*, **2**, 92 (1951).

(7) A. A. Lai, G. B. Birrell, and O. H. Griffith, *J. Chem. Phys.*, **53**, 4399 (1970).

(8) G. B. Birrell, A. A. Lai, and O. H. Griffith, *ibid.*, **54**, 1630 (1971).

(9) H. Zeldes and R. Livingston, *ibid.*, **30**, 40 (1959).

(10) C. Chachaty and E. Hayon, *J. Chim. Phys.*, **61**, 1115 (1964).

(11) P. J. Sullivan and W. S. Koski, *J. Amer. Chem. Soc.*, **85**, 384 (1963).

(12) H. S. Judeikis and S. Siegel, *J. Chem. Phys.*, **43**, 3625 (1965).

(13) E. E. Wedum and O. H. Griffith, *Trans. Faraday Soc.*, **63**, 819 (1967).

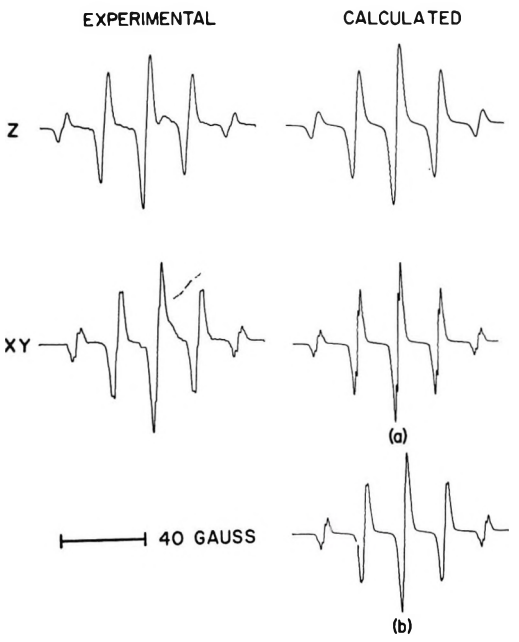

Figure 1. The 293°K esr spectra and computer simulations of X-irradiated 6-undecanol–urea inclusion crystals. Z and XY indicate the direction of the magnetic field to be parallel to the crystalline z axis and in the xy plane, respectively; (a) and (b) are spectral simulations of the XY experimental spectrum: (a) four equivalent β-proton coupling constants of 19.1 G plus four equivalent γ-proton coupling constants of 1.6 G; (b) four β-proton coupling constants—two of 19.4 G plus two of 18.8 G—and four equivalent γ-proton coupling constants of 1.6 G.

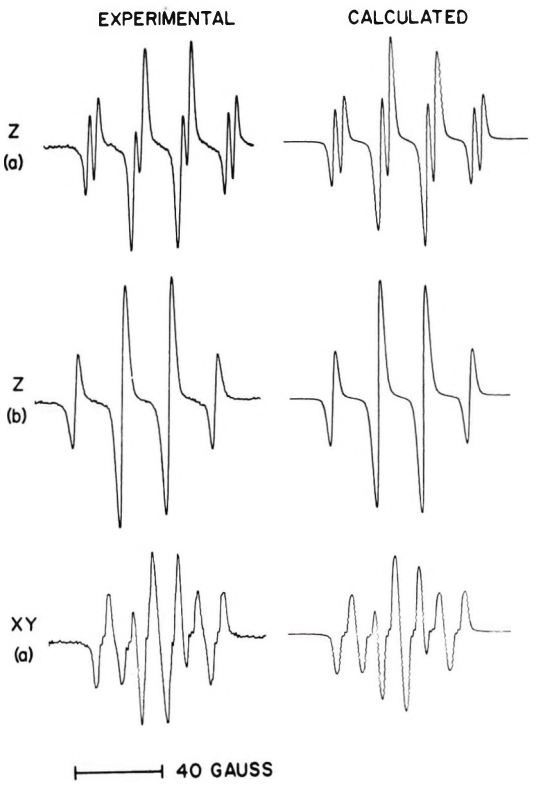

Figure 2. Experimental and computer-simulated 253°K esr spectra of X-irradiated 1-decanol–urea inclusion crystals. Top row: 1-decanol–urea with H $\|$ z. Center row: 1-decanol–urea with the OH hydrogen replaced by deuterium (H $\|$ z). Bottom row: 1-decanol–urea with H $\|$ xy.

inclusion crystals were X-irradiated at 77°K, and esr spectra were recorded on a Varian E-3 X-band esr spectrometer. Spectral simulations were performed on a Varian 620/i computer. The esr spectra obtained for X-irradiated 6-undecanol–urea and 1-decanol–urea inclusion crystals are shown in Figures 1 and 2. The esr hyperfine pattern of the 6-undecanol–urea crystal results from four large essentially equivalent proton coupling constants which are nearly isotropic and which are further split by four small proton coupling constants. The small splittings are resolved only when the magnetic field is aligned perpendicular to the crystalline z axis (needle axis). This is consistent with the following type of radical

$$\underset{\gamma\ \ \beta}{CH_3(CH_2)_2CH_2CH_2}—\overset{\cdot}{\underset{\text{OH}}{C}}—\underset{\beta\ \ \gamma}{CH_2CH_2(CH_2)_2CH_3}$$

The best computer fit for the xy orientation was obtained by using two slightly different β-proton coupling constants, each for two of the four protons. (The difference is presumably between the two protons in each β-CH_2 group rather than due to a difference between the two groups.) This implies that (in a given β-CH_2 group) there is a slight variation in angle (θ) between the C_β–H_β bonds and the p-orbital direction, projected perpendicular to the C_α–C_β bond.[5]

The esr spectra for 1-decanol–urea crystals arise from one large anisotropic proton coupling constant and two large equivalent and nearly isotropic proton coupling constants, which are further split by one small proton coupling constant when the magnetic field is parallel to the crystalline z axis and by three (two equivalent and one nonequivalent) small proton coupling constants when the magnetic field is perpendicular to the z axis. We conclude that the long-lived radical produced by X-irradiating 1-decanol–urea is

$$\underset{\gamma\ \ \beta\ \ \alpha\ \ \delta}{CH_3(CH_2)_6CH_2CH_2\dot{C}HOH}$$

The coupling constants and g values observed in the two principal directions for each radical are given in Table I. To identify the source of the 4-G splitting, inclusion crystals of the deuterated compound $CH_3(CH_2)_8CH_2OD$ were grown and X-irradiated. The esr spectrum obtained with the magnetic field in the z direction is shown in Figure 2b. The absence of a small splitting confirms that this splitting arises from the OH hydrogen.

The experimental spectra of the 1-decanol radical at the two principal orientations are not well resolved.

Table I: Proton Coupling Constants and g Values[a,b,c]

6-Undecanol	(4) $a_z^\beta = 19.7 \pm 0.4$	(2) $a_{xy_\beta}^\beta = 19.4 \pm 0.1$
		(2) $a_{xy_\beta}^\beta = 18.8 \pm 0.1$
		(4) $a_{xy}^\gamma = 1.6 \pm 0.1$
	$g_z = 2.0036$	$g_{xy} = 2.0027$
1-Decanol	(1) $a_z^\alpha = 20.0 \pm 0.2$	(1) $a_{xy_\beta}^\alpha = 11.6 \pm 0.2$
	(2) $a_{z_\beta}^\beta = 21.8 \pm 0.2$	(2) $a_{xy_\delta}^\beta = 20.4 \pm 0.2$
	(1) $a_{z_\delta}^\delta = 4.0 \pm 0.1$	(1) $a_{xy}^\gamma = 3.6 \pm 0.2$
		(2) $a_{xy}^\gamma = 1.7 \pm 0.1$
	$g_z = 2.0035$	$g_{xy} = 2.0029$

[a] a^α, a^β, a^γ, and a^δ are the coupling constants (in gauss) of the α, β, γ, and δ protons, respectively; z and xy indicate the direction of the magnetic field with respect to the crystalline axes. [b] The numbers in parentheses are the total number of protons with a given coupling constant. [c] The uncertainty in the g value measurements is ± 0.0002.

Trial parameters for the α- and β-proton coupling constants were obtained from plots of coupling constant *vs.* crystalline orientation, making use of the better resolution at intermediate orientations. An initial value for the OH proton splitting in the XY direction was obtained by observing a reduction of 3.6 G in the total splitting at that orientation on deuteration. The γ splittings were estimated from the experimental spectra. The coupling constants reported in Table I were obtained from best-fit computer simulations using experimental line widths. Spectral simulations for both the 6-undecanol radical and the 1-decanol radical were sensitive to small deviations (those indicated in Table I) from the coupling constants reported.

The hyperfine interaction due to the OH hydrogen is observed in 1-decanol and not in 6-undecanol, apparently because of orientation differences arising from the fact that in one case the hydroxyl group is at the end of the molecule and in the other it is at the center. A small coupling due to the OH hydrogen is observed in 6-undecanol at crystalline orientations intermediate to those reported in Table I and Figure 1. Hyperfine interactions of this type have been previously observed, primarily in radicals formed in α-hydroxy acids.[14,15] Interactions due to γ-hydrogens have been rarely reported for alcohol free radicals.[16]

The esr spectra of radicals formed in alcohol–urea inclusion crystals do not change with rotation of the laboratory magnetic field vector in the crystalline xy plane but are anisotropic (if the radicals contain α-hydrogen atoms) with respect to arbitrary rotations out of the xy plane. This behavior is characteristic of organic inclusion compounds and is a direct result of free radical motion in the tubular cavities formed by the urea molecules. An estimate of the isotropic component a_0 of the proton coupling constant can be obtained from the relation[5]

$$a_0 = (2a_{xy} + a_z)/3 \quad (1)$$

where a_{xy} and a_z are the values of the proton coupling constant measured with the magnetic field direction in the xy plane and parallel to the z axis, respectively. With this relationship the proton coupling constants listed in Table I can be compared to data obtained for similar radicals which have been previously reported. For example, Dixon and Norman[17] have examined the free radical produced by the reaction of ethanol with OH^- in aqueous acid and have found that the $CH_3\dot{C}HOH$ radical is formed with $a_0^\alpha = 15.0$ G and $a_0^\beta = 22.0$ G. Using (1) the corresponding values for 1 decanol are 14.4 and 20.8 G. The a_0^α are in good agreement. The small differences in a_0^β can result from slight differences in radical conformation.

(14) N. M. Atherton and D. H. Whiffen, *Mol. Phys.*, **3**, 1 (1960).
(15) G. C. Moulton and H. T. Crenshaw, *Radiat. Res.*, **25**, 139 (1965).
(16) R. Livingston and H. Zeldes, *J. Chem. Phys.*, **44**, 1245 (1966).
(17) W. T. Dixon and R. O. C. Norman, *J. Chem. Soc.*, 3119 (1963).

AMERICAN CHEMICAL SOCIETY

"Primary Publications on Microfilm"

Your Key to—

- Dramatic savings in archival space and dollars.
- Faster access to needed data.
- Unlimited distribution of copyrighted scientific data.

ACS publications in the program:

JOURNAL OF THE AMERICAN CHEMICAL SOCIETY
INDUSTRIAL & ENGINEERING CHEMISTRY
CHEMICAL TECHNOLOGY
CHEMICAL & ENGINEERING NEWS
CHEMICAL & ENGINEERING NEWS ANNUAL INDEXES
ANALYTICAL CHEMISTRY
JOURNAL OF PHYSICAL CHEMISTRY
JOURNAL OF AGRICULTURAL & FOOD CHEMISTRY
JOURNAL OF ORGANIC CHEMISTRY
JOURNAL OF CHEMICAL AND ENGINEERING DATA
CHEMICAL REVIEWS
JOURNAL OF CHEMICAL DOCUMENTATION
I&EC FUNDAMENTALS
I&EC PROCESS DESIGN AND DEVELOPMENT
I&EC PRODUCT RESEARCH AND DEVELOPMENT
BIOCHEMISTRY
INORGANIC CHEMISTRY
JOURNAL OF MEDICINAL CHEMISTRY
CHEMISTRY
ENVIRONMENTAL SCIENCE & TECHNOLOGY
ACCOUNTS OF CHEMICAL RESEARCH
MACROMOLECULES

For information on "ACS Primary Publications on Microfilm", write or call:

Mr. George Virvan
Special Issues Sales
American Chemical Society
1155 16th Street, N.W.
Washington, D.C. 20036
(202-737-3337)

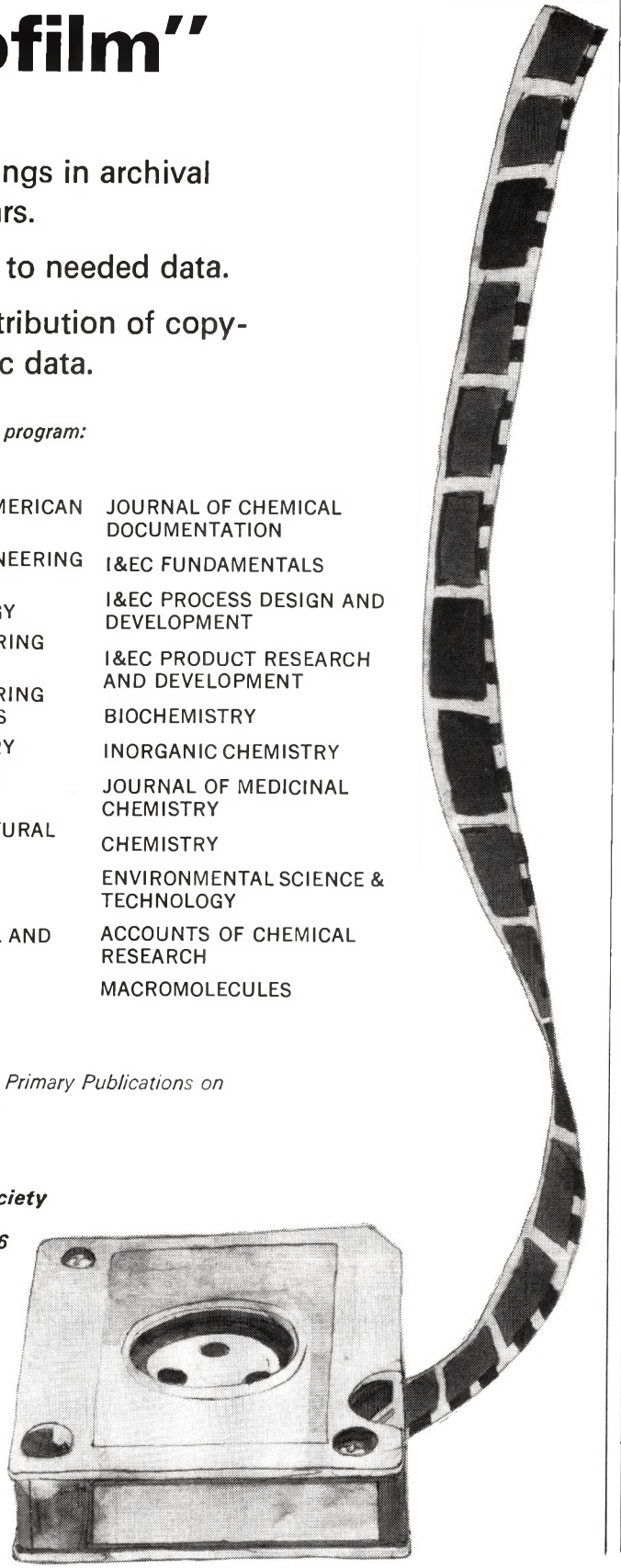

ESR SPOKEN HERE

Complete Low-Cost ESR SYSTEMS

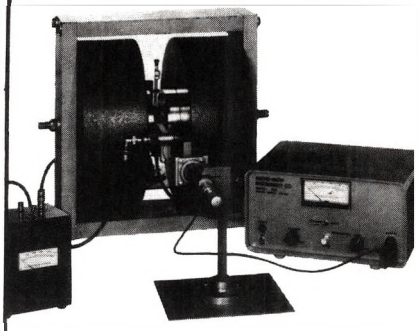

x-band Model 810B
Includes Lecture Materials

ESR COMPONENTS

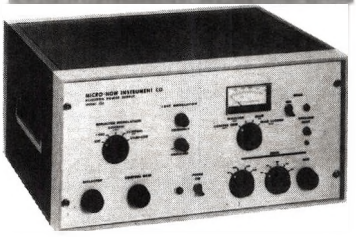

Model 756
3 kV Klystron Supply

NEW! Model 210 Cavity Referenced Stabilizer

Tailored to Your Needs & Budget

Microwave Instrumentation for Science and Industry

stabilizers
mm-wave sweepers
sources/mixers/multipliers

MICRO-NOW
INSTRUMENT CO., INC.
6104 North Pulaski Rd.,
Chicago, Illinois 60646
Area Code 312
478-1151

FIGHT FUZZINESS

WITH THE NEW REAL-TIME

256 POINT CORRELATOR

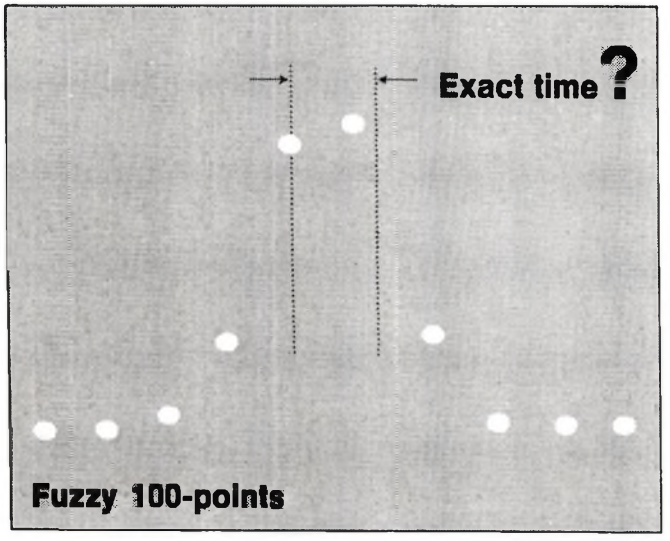

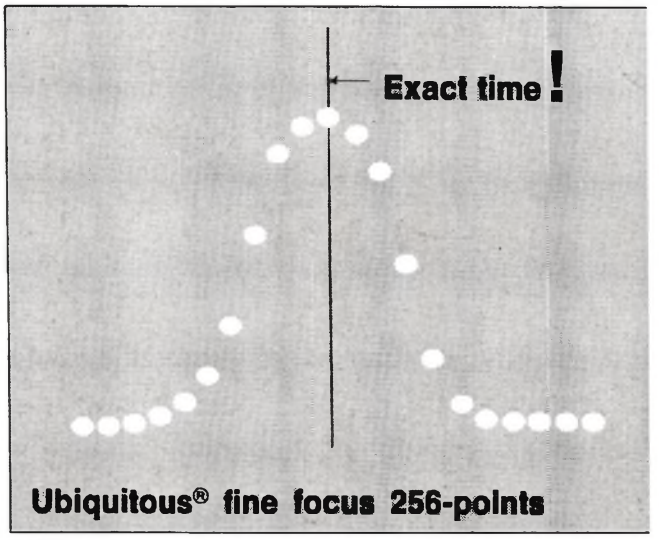

The new UC-201A Ubiquitous® Correlator is a complete time-domain measurement laboratory for real-time auto and cross-correlation • signal enhancement • probability

For underwater acoustics, fluid dynamics, medical research, vibration analysis, noise source identification, aerodynamics, radio astronomy, geophysics, hydrodynamics.

Features:

- exact time measurements with digital dial
- computes the integral and differential of any stored function (converts probability density to cumulative distribution without rerunning data)
- precomputational delay built-in (256 samples)
- sampling increments from ½ usec to 2 se
- complete external (computer) control plu digital outputs
- built-in test signals for all modes
- small, portable, easy use
- reasonably priced

Options:

- exponential (running) a eraging
- additional precomput tional delay (2048 samples)
- centering (128) dela switch

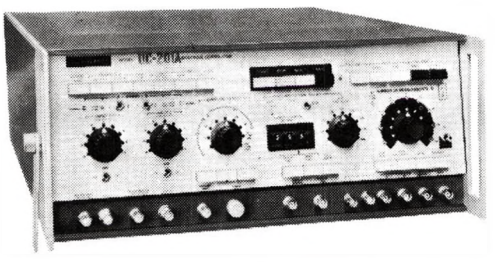

federal scientific

From FEDERAL SCIENTIFIC, originators of the Ubiquitous Spectrum Analyzer, the most widely used real-time unit of its type in the free world.

FEDERAL SCIENTIFIC CORPORATION, SUBSIDIARY OF ELGIN NATIONAL INDUSTRIES, INC.
615 W. 131st ST., N.Y., N.Y. 10027. TEL: (212) 286-4400